Alma Mater Studiorum - Università di Bologna

DOTTORATO DI RICERCA IN

INGEGNERIA BIOMEDICA, ELETTRICA E DEI SISTEMI

Ciclo 34

Settore Concorsuale: 09/G1 - AUTOMATICA

Settore Scientifico Disciplinare: ING-INF/04 - AUTOMATICA

ROBUST ADAPTIVE CONTROL WITH APPLICATIONS TO MULTI-AGENT
SYSTEMS AND MOBILE ROBOTICS

Presentata da: Ilario Antonio Azzollini

Coordinatore Dottorato

Michele Monaci

Supervisore

Lorenzo Marconi

Esame finale anno 2022

Abstract

This thesis deals with robust adaptive control and its applications, and it is divided into three main parts. The first part is about the design of robust estimation algorithms based on recursive least squares. First, we present an estimator for the frequencies of biased multi-harmonic signals, and then an algorithm for distributed estimation of an unknown parameter over a network of adaptive agents. In the second part of this thesis, we consider a cooperative control problem over uncertain networks of linear systems and Kuramoto systems, in which the agents have to track the reference generated by a leader exosystem. Since the reference signal is not available to each network node, novel distributed observers are designed so as to reconstruct the reference signal locally for each agent, and therefore decentralizing the problem. In the third and final part of this thesis, we consider robust estimation tasks for mobile robotics applications. In particular, we first consider the problem of slip estimation for agricultural tracked vehicles. Then, we consider a search and rescue application in which we need to drive an unmanned aerial vehicle as close as possible to the unknown (and to be estimated) position of a victim, who is buried under the snow after an avalanche event. In this thesis, robustness is intended as an input-to-state stability property of the proposed identifiers (sometimes referred to as adaptive laws), with respect to additive disturbances, and relative to a steady-state trajectory that is associated with a correct estimation of the unknown parameter to be found.

Sommario

Questa tesi riguarda il controllo adattativo robusto e le sue applicazioni ed è divisa in tre parti. Nella prima parte vengono presentati algoritmi di stima robusti basati su minimi quadrati ricorsivi. Innanzitutto, presentiamo uno stimatore per le frequenze di segnali multi-armonici e successivamente un algoritmo per la stima distribuita di parametri sconosciuti all'interno di una rete di agenti adattativi. Nella seconda parte di questa tesi, consideriamo un problema di controllo cooperativo su reti di sistemi lineari incerti e sistemi di Kuramoto, in cui gli agenti devono inseguire il riferimento generato da un esosistema leader. Poiché il segnale di riferimento non è disponibile per ciascun nodo della rete, nuovi osservatori distribuiti vengono progettati in modo da ricostruire localmente il segnale di riferimento per ciascun agente, e quindi decentralizzare il problema. Nella terza e ultima parte di questa tesi, consideriamo problemi di stima robusta per applicazioni di robotica mobile. In particolare, consideriamo innanzitutto il problema della stima dello slittamento per i veicoli cingolati agricoli. Quindi, consideriamo un'applicazione di ricerca e soccorso in cui dobbiamo guidare un drone il più vicino possibile alla posizione sconosciuta (e da stimare) di una vittima, sepolta sotto la neve in seguito ad una valanga. In questa tesi, la robustezza è intesa come una proprietà di stabilità input-to-state degli identificatori proposti, rispetto a disturbi additivi, e relativa a una traiettoria a regime associata a una stima corretta dei parametri sconosciuti da trovare.

Contents

II   Robust Adaptive Control of Multi-Agent Systems   41

3   A distributed indirect adaptive approach to cooperative tracking in networks of uncertain single-input single-output systems   43

4   Adaptive Hybrid Control for Robust Global Phase Synchronization of Kuramoto Oscillators   61

List of Figures

Introduction

To adapt means to change oneself so that one's behavior will conform to new or changed circumstances. This feature is what we would like to embed in our regulators, in a scenario where we are able to get a model of the system we want to control, but we lack (a precise) knowledge of its parameters. In fact, adaptive control does not deal with unknown systems/models, but rather with systems having a known "structure" (e.g. we know that the system can be described by a linear model, or by a Kuramoto model, etc.) but unknown parameters. In system identification literature, this is sometimes referred to as a grey box problem.

The design of autopilots for high-performance aircraft was one of the primary motivations for active research on adaptive control in the early 1950s. The lack of understanding of stability and robustness properties of the proposed adaptive control schemes coupled with a disaster in the well known Nasa X-15-3 flight test, in 1967. One of the factors that caused the 1967 crash was an electrical disturbance that degraded the controls. The take-home message was that adaptive control is not intrinsically robust, and sources of uncertainty should be included in the model, in order to design robust adaptive controllers (Dydek, Annaswamy, and Lavretsky, 2010). A lot of work was done in the field of robust adaptive control starting from 1979. In fact, many adaptive control schemes were redesigned as a byproduct of crucial discoveries as state-space techniques, stability theory based on Lyapunov, dynamic programming, stochastic control, system identification and parameter estimation (Ioannou and Sun, 2012).

The fact that a system is always different from the model that we mathematically develop to describe it, is a key concept in control theory. There will always be parametric uncertainties, unmodeled dynamics, or (bounded) disturbances affecting our model and thus making it an approximation for representing the system, with a certain degree of precision. For this fundamental reason, robustness should always be a requirement in control system design, and adaptive/learning control algorithms make no exception.

As often happens in science, theoretical results of independent interest arise from application-oriented studies. This thesis, in its own small way, is another proof of this phenomenon, within the vast world of adaptive control. This thesis is divided into three parts. The first part deals with the design of robust estimation algorithms based on recursive least squares. First, we present an estimator for the frequencies of biased multi-harmonic signals (Azzollini et al., 2021a), and then an algorithm for distributed estimation of an unknown parameter over a network of adaptive agents. In the second part of this thesis, we consider a cooperative control problem over uncertain networks of linear systems and Kuramoto systems, in which the agents have to track the reference generated by a leader exosystem (Baldi, Azzollini, and Ioannou, 2020; Bosso et al., 2021b). Since the reference signal is not available to each network node, novel distributed observers are designed so as to reconstruct the reference signal locally for each agent, and therefore decentralizing the problem. In the third and final part of this thesis, we consider robust estimation for mobile robotics applications. In particular, we first consider the problem of slip estimation

for agricultural tracked vehicles (Tazzari, Azzollini, and Marconi, 2021). Then, we consider a search and rescue application in which we need to drive a drone as close as possible to the unknown (and to be estimated) position of a victim, who is buried under the snow after an avalanche event (Azzollini, Mimmo, and Marconi, 2020; Azzollini et al., 2021b).

In this thesis, robustness is intended as an input-to-state stability property of the proposed identifiers (sometimes referred to as adaptive laws), with respect to additive disturbances, and relative to a steady-state trajectory that is associated with a correct estimation of the unknown parameter to be found. When dealing with linear time invariant systems, this is easily obtained by ensuring or requiring persistency of excitation. In fact, persistency of excitation property does not only guarantee convergence to the true parameters, but it also guarantees robustness for the (estimation or tracking) error system with respect to additive perturbations as it induces uniform global asymptotic stability (or even exponential in case of linear systems). In spite of this well known facts, we find that persistency of excitation is not necessary to obtain strong robustness properties. In this case, as expected, the estimated parameters will not converge to the true parameters. Nevertheless, it can be proven the existence and stability of an optimal steady state (where a cost function - being a function of the estimation or tracking error - is minimized), and robustness with respect to the disturbances in form of input-to-state and input-output stability relative to the unperturbed steady-state trajectories. This is found in three different works in this thesis: the first two dealing with recursive least squares estimation (Chapters 1 and 2), and the other one dealing with adaptive distributed control over a Kuramoto network (Chapter 4). This makes us conjecture that there is a common underlying principle linking the three works, possibly applicable to general adaptive estimation/control problems, which is briefly discussed in the concluding remarks.

Part I

Robust Estimation: Least Squares

Chapter 1

Robust Frequency Estimation of Multi-Harmonic Signals

In this chapter we propose a robust estimator for the frequencies of biased multi-harmonic signals in the presence of unknown additive disturbances. The estimator consists of a continuous-time stable linear system and a discrete-time recursive least-squares identifier. In absence of additive disturbances, the proposed design guarantees global exponential convergence to the optimal (in the least-squares sense) parameter estimates. In presence of disturbances, instead, an input-to-state stability property relative to such optimal estimates holds.

1.1 Introduction

The online frequency estimation problem has attracted considerable interest from the control community, and its applications span many engineering fields such as telecommunications and signal processing, power systems, health monitoring, and all those control applications in which this class of signals have to be tracked and/or rejected (Carnevale et al., 2016; Bodson, Jensen, and Douglas, 2001; Chen et al., 2014; Bin, Marconi, and Teel, 2019; Baldi, Azzollini, and Ioannou, 2020).

A wide variety of approaches exist in the literature, based on fast Fourier transform (Schoukens, Pintelon, and Van Hamme, 1992), extended Kalman filters (Hajimolahoseini, Taban, and Soltanian-Zadeh, 2012), adaptive notch filters (Hsu, Ortega, and Damm, 1999; Mojiri and Bakhshai, 2004), phase-locked loop (Karimi-Ghartemani and Ziarani, 2004; Wu and Bodson, 2003), second and third order generalized integrator-based orthogonal signal generators (Fedele and Ferrise, 2011; Fedele and Ferrise, 2014), nonlinear estimation algorithms (Pin et al., 2013; Na et al., 2015), and observer-based (adaptive (Marino and Tomei, 2002; Hou, 2011; Chen et al., 2017), nonlinear Luenberger (Praly, Isidori, and Marconi, 2006), and hybrid (Carnevale et al., 2016; Carnevale and Astolfi, 2009)). Discontinuous (sliding mode-based) estimation laws also exist (Na et al., 2015; Pin, Chen, and Parisini, 2017), ensuring finite-time convergence.

Initial research on this topic dealt with a single sinusoid (Hsu, Ortega, and Damm, 1999; Bodson, Jensen, and Douglas, 2001). Without disturbances or noise, adaptive approaches typically guarantee global convergence of the estimates (Marino and Tomei, 2002; Chen et al., 2017). Nevertheless, most works lack of a formal robustness analysis and only conjecture that their approaches are robust to noise by means of numerical simulations (Praly, Isidori, and Marconi, 2006). In this sense, only very recent works formally show robustness to quite general disturbances in an Input-to-State-Stability (ISS) (Pin et al., 2013; Pin, Chen, and Parisini, 2017; Chen et al., 2017) or Uniformly Ultimate Boundedness (UUB) (Na et al., 2015) sense.

The vast majority of existing observer-based methodologies rely on the fact that harmonic or multi-harmonic signals can be thought of as generated by a marginally stable autonomous linear system, which is completely observable, and whose eigenvalues are directly related to the frequencies to be estimated (Marino and Tomei, 2002; Hou, 2011; Chen et al., 2017). In particular, in (Chen et al., 2017) the signal generator is first augmented with a stable filter. Then, an adaptive observer is designed for this augmented system. This was the first estimator in literature establishing semiglobal stability properties and robustness (in an ISS sense) to disturbances, when the number of harmonics is possibly overestimated. In (Na et al., 2015), the signal is also first filtered via a stable filter, in order to obtain stable estimates of the signal derivatives. Then, a continuous-time online estimation algorithm processing the signal and its derivatives is proposed, guaranteeing global exponential stability and UUB properties.

It can be noticed how, both observer-based (Praly, Isidori, and Marconi, 2006; Chen et al., 2017) and online parameter estimation (Na et al., 2015) approaches share the need to design stable filters for the measured signal, usually with the purpose of estimating its derivatives (or some other signals equivalent to derivatives, up to a change of coordinates). This is in line with "classic" online parameter estimation approaches (Ioannou and Sun, 2012) and can be traced back to (Kreisselmeier, 1977). This common feature is justified in this chapter by means of well-known steady-state tools (Serrani, Isidori, and Marconi, 2001; Nikiforov, 1998; Isidori, 2017), which are instrumental in order to design the proposed estimator. Not surprisingly, our steady-state analysis is in line with the nonlinear analysis presented in (Afri et al., 2016), where the unknown parameters of parameterized linear systems are estimated thanks to a nonlinear Luenberger observer design strategy.

In this chapter, we propose a hybrid system able to robustly estimate the frequencies of a biased multi-harmonic signal in the presence of unknown additive disturbances. The proposed estimator consists of a continuous-time stable linear system and a discrete-time recursive least-squares identifier. The main contributions of this work are that (i) the proposed design is globally ISS with a guaranteed exponential rate of convergence; (ii) the discrete-time identifier can work at any sampling frequency (or with every aperiodic clock strategy ensuring uniform upper and lower bounds on successive sampling times); (iii) uniform continuity between the asymptotic disturbances size and the induced asymptotic deviation from the noiseless estimates is established.

1.2   Notation

We denote by $\mathbb{R}$ and $\mathbb{N}$ the set of real and natural numbers, respectively. We define $\mathbb{R}_{\geq 0} := [0, \infty)$. Given a set S, $\mathbb{K}(\mathbb{S})$ indicates the collection of nonempty, compact subsets of S. We use $|\cdot|$ to denote norms whenever the underlying normed space is clear. Let X and Y be two nonempty subsets of a metric space (M, d). We define the Hausdorff distance $d_{\mathrm{H}}(X, Y) = \max \left\{ \sup_{x \in X} \inf_{y \in Y} d(x, y), \sup_{y \in Y} \inf_{x \in X} d(x, y) \right\}$. On the set $\mathbb{K}(\mathbb{S})$ of all nonempty compact subsets of S, d_{H} is a metric. We use $\mathrm{minsv}(A)$ to denote the minimum singular value of a matrix A. A function $\gamma : \mathbb{R}_+ \to \mathbb{R}_+$ belongs to class-$\mathcal{K}$ ($\gamma \in \mathcal{K}$) if it is continuous, strictly increasing and $\gamma(0) = 0$. Moreover, if $\gamma(s) \to_{s \to \infty} \infty$, γ is said to belong to class-$\mathcal{K}_\infty$ ($\gamma \in \mathcal{K}_\infty$). A continuous function $\beta : \mathbb{R}_+ \times \mathbb{R}_+ \to \mathbb{R}_+$ belongs to class-$\mathcal{KL}$ ($\beta \in \mathcal{KL}$) if, for each $t \in \mathbb{R}_+$ $\beta(\cdot, t) \in \mathcal{K}$, and for each $s \in \mathbb{R}_+$, $\beta(s, \cdot)$ is decreasing and $\beta(s, t) \to_{t \to \infty} 0$. In this chapter we deal with hybrid dynamical systems (Goebel, Sanfelice, and Teel,

2012), described by equations of the form

$$\Sigma : \begin{cases} \dot{x} & = F(x,u) \qquad (x,u) \in C \\ x^+ & = G(x,u) \qquad (x,u) \in D \end{cases} \tag{1.1}$$

where x is the state, u is the input, C is the flow set, F is the flow map, D is the jump set, and G is the jump map. The state of the hybrid system can either flow according to the differential equation $\dot{x} = F$ (while $(x,u) \in C$), or jump according to the difference equation $x^+ = G$ (while $(x,u) \in D$). Solutions to (1.1) are defined over hybrid time domains. A compact hybrid time domain is a subset of $\mathbb{R}_+ \times \mathbb{N}$ of the form $\mathcal{T} = \cup_{j=0}^{J-1} [t_j, t_{j+1}] \times \{j\}$ for some finite $J \in \mathbb{N}$ and $0 = t_0 \le t_1 \le \cdots \le t_J \in \mathbb{R}_+$. A set $\mathcal{T} \subset \mathbb{R}_+ \times \mathbb{N}$ is called a hybrid time domain if for each $(T,J) \in \mathbb{R}_+ \times \mathbb{N}$, $\mathcal{T} \cap [0,T] \times \{1,\dots,J\}$ is a compact hybrid time domain. For any $(t,j) \in \mathcal{T}$, we let $t^j = \sup_{t\in\mathbb{R}}(t,j) \in \mathcal{T}$, $t_j = \inf_{t\in\mathbb{R}}(t,j) \in \mathcal{T}$ and we similarly define j^t and j_t. A function $x : \mathcal{T} \to \mathcal{X}$ is called an hybrid arc if $x(\cdot,j)$ is locally absolutely continuous for each j. A hybrid input u is a hybrid arc such that $u(\cdot,j)$ is locally essentially bounded and Lebesgue measurable for each j. A solution pair to (1.1) is a pair (x,u), with x a hybric arc and u a hybrid input satisfying those dynamical equations. We call a solution pair complete if its time domain is unbounded. For simplicity, if x is constant during flows (resp. jumps), we neglect the "t" (resp. "j") argument and we write $x(j)$ (resp. $x(t)$). With $u : \operatorname{dom} u \to \mathcal{U}$ a hybrid input, and $\Gamma(u) := \{(t,j) \in \operatorname{dom} u \mid (t,j+1) \in \operatorname{dom} u\}$, for $(t,j) \in \operatorname{dom} u$, we let $|u|_{(t,j)} := \max\{\sup_{(t,j)\in\Gamma(\operatorname{dom} u),(0,0)\preceq(s,i)\preceq(t,j)} |u(s,i)|, \operatorname{ess.} \sup_{(s,i)\in\operatorname{dom} u/\Gamma(\operatorname{dom} u),(0,0)\preceq(s,i)\preceq(t,j)} |u(s,i)|\}$. If u is constant during jumps (resp. flows), we write $|u|_t$ (resp. $|u|_j$) as short for $|u|_{(t,j)}$. The pseudoinverse operator is indicated by $\cdot^\dagger$. We denote by i the imaginary unit. We denote by $I_n \in \mathbb{R}^{n\times n}$ the identity matrix of order n.

1.3 Problem statement

We consider a signal of the form

$$y(t) = y_0(t) + v(t) \tag{1.2}$$

where $y_0(t) \in \mathbb{R}$ is the nominal signal, given by the sum of N harmonics and a bias, and $v(t) \in \mathbb{R}$ is an unknown additive disturbance term which may represent measurement noise, exogenous perturbations, or any other unmodeled component. The disturbance $v(t)$ is locally essentially bounded and integrable on each compact subset of its time domain. Without loss of generality, the nominal signal can be written as

$$y_0(t) = a_0 + \sum_{i=1}^{N} a_i \sin(\omega_i t + \phi_{0i}), \tag{1.3}$$

where a_0 is the unknown constant bias, and a_i and $\phi_i(t) = \omega_i t + \phi_{0i}$ are the unknown amplitude and phase of the i-th harmonic, respectively, with ϕ_{0i} the initial phases. In particular, the constants ω_i are the unknown frequencies we aim at estimating. Without loss of generality we can consider $\omega_i > 0$, and $\phi_{0i} \in [-\pi, \pi]$, for all $i = 1, 2, \dots, N$. We define the set of frequencies to be estimated as

$$\Omega = \{\omega_1, \omega_2, \dots, \omega_N\}.$$

The nominal output can be seen as generated by a continuous-time linear system of the form

$$\begin{aligned} \dot{x} &= Ax \\ y_0 &= Cx \end{aligned}$$
(1.4)

in which $A \in \mathbb{R}^{n \times n}$, $C \in \mathbb{R}^n$, with $n = 2N + 1$, and the pair (C, A) is *completely observable*. In particular, the matrix A has spectrum

$$\sigma(A) = \{\lambda_0, \lambda_{1,1}, \lambda_{1,2}, \ldots, \lambda_{N,1}, \lambda_{N,2}\}$$

in which

$$\begin{cases} \lambda_0 = 0 \\ \lambda_{i,1} = +\omega_i \mathrm{i}, \ \lambda_{i,2} = -\omega_i \mathrm{i}, \quad i \in \{1, 2, \ldots, N\}. \end{cases}$$
(1.5)

Then, we consider the following problem, under the following assumptions.

Problem 1.1. *Design a dynamical system with input y, producing as output a set of estimated frequencies $\hat{\Omega} = \{\hat{\omega}_1, \hat{\omega}_2, \ldots, \hat{\omega}_N\}$, where $\hat{\omega}_i$ is an estimate of ω_i in (1.5), such that the following properties are guaranteed:*

- ***Nominal convergence*** *- the estimates converge exactly/practically[1] to the true frequencies when disturbances are not present (i.e. $v = 0$);*

- ***Robustness*** *- when disturbances are present, the asymptotic amplitude of the disturbance maps continuously to the asymptotic deviation between the nominal estimates and the disturbed ones.*

Assumption 1.1. *There exists a known bound $\bar{y}_0$ on the nominal output (1.3), such that $|y_0(t)| \leq \bar{y}_0$.*

Assumption 1.2. *There exists a known bound $\bar{\omega}$ on the maximum frequency in (1.3), such that $\max_i \omega_i \leq \bar{\omega}$.*

1.4   The Estimator

The proposed estimator solving Problem 1.1 is

$$\begin{cases} \dot{\tau} = 1 \\ \dot{z} = Fz + Gy \\ \dot{\eta}_1 = 0, \dot{\eta}_2 = 0 \\ (\tau, z, \eta_1, \eta_2, y) \in [0, \overline{T}] \times \mathbb{R}^n \times \mathbb{R}^{n \times n} \times \mathbb{R}^n \times \mathbb{R} \\ \begin{cases} \tau^+ = 0, z^+ = z \\ \eta_1^+ = \mu\eta_1 + zz^\top \\ \eta_2^+ = \mu\eta_2 + zy \end{cases} \\ (\tau, z, \eta_1, \eta_2, y) \in [\underline{T}, \overline{T}] \times \mathbb{R}^n \times \mathbb{R}^{n \times n} \times \mathbb{R}^n \times \mathbb{R} \end{cases}$$
(1.6)

in which the matrices $(F, G) \in \mathbb{R}^{n \times n} \times \mathbb{R}^n$, as well as the scalar parameters μ, $\underline{T}$, $\overline{T}$, are degrees of freedom to be designed. The measured signal y is the only input to this hybrid system.

---

[1] practical convergence means convergence to a neighborhood of the actual frequencies, whose size can be reduced arbitrarily by tuning some design parameters accordingly.

We associate with (1.6) the output map

$$\hat{\Omega} = \Gamma(\hat{\theta}) \tag{1.7}$$

with $\hat{\theta} \in \mathbb{R}^n$ given by

$$\hat{\theta} = \text{sat}(\gamma(\eta)) = \text{sat}\left((\eta_1 + R)^\dagger \eta_2\right) \tag{1.8}$$

where $R \in \mathbb{R}^{n \times n}$ is yet another design parameter, and sat is a suitable saturation function to be chosen. The function $\Gamma : \mathbb{R}^n \to \mathbb{K}(\mathbb{R}_{\geq 0})$ maps the current estimate $\hat{\theta}$ to the set $\hat{\Omega}$ of estimated frequencies, where we recall that $\mathbb{K}(\mathbb{R}_{\geq 0})$ is the collection of nonempty, compact subsets of $\mathbb{R}_{\geq 0}$. As shown later in this section, at steady-state, the matrix $(F + G\theta)$ is similar to the signal generator matrix A, where θ indicates the vector of "true" parameters to be estimated by (1.6), (1.8) (we want that $\hat{\theta} \to \theta$). Therefore, considering the link between the eigenvalues and the frequencies in (1.5), the map Γ can be constructed by using the current estimate $\hat{\theta}$ to compute the eigenvalues of the matrix $(F + G\hat{\theta})$, then taking the absolute value of the imaginary part of each eigenvalue. In particular, we have

$$\Gamma(\hat{\theta}) = l \circ r(\hat{\theta}) = l(r(\hat{\theta}))$$

in which

$$r : \mathbb{R}^n \to \mathbb{K}(\mathbb{C}),$$
$$r(\hat{\theta}) = \{\lambda \in \mathbb{C} : \det(\lambda I_n - F - G\hat{\theta}) = 0\}$$
$$l : \mathbb{C} \to \mathbb{R}_{\geq 0}, \qquad l(\lambda) = |\text{Im}(\lambda)|,$$

and we give $\mathbb{K}(\mathbb{C})$ and $\mathbb{K}(\mathbb{R}_{\geq 0})$ the Hausdorff metric d_H.

System (1.6) can be conveniently decomposed into three subsystems: a clock, a continuous-time filter, and a discrete-time identifier.

1.4.1 The Clock

The clock is the hybrid system

$$\begin{cases} \dot{\tau} &= 1 & \tau \in [0, \overline{T}] \\ \tau^+ &= 0 & \tau \in [\underline{T}, \overline{T}] \end{cases} \tag{1.9}$$

in which $\underline{T}, \overline{T} \in \mathbb{R}$ satisfy $0 < \underline{T} \leq \overline{T} < \infty$. Jumps do not need to be periodic, and the only constraints on the time between two successive jumps are that it must be lower bounded by $\underline{T}$ and upper bounded by $\overline{T}$. Notice that we may also choose $\underline{T} = \overline{T} = T$, corresponding to a periodic clock with a sampling period of T seconds. In order to solve Problem 1.1, the Nyquist-Shannon Theorem suggests

$$\overline{T} < \frac{1}{2\overline{\omega}} \tag{1.10}$$

in which $\overline{\omega}$ comes from Assumption 1.2.

1.4.2　The Continuous-Time Filter

The measured signal (1.2) is filtered through the continuous-time linear system

$$\dot{z} = Fz + G(y_0 + v) \tag{1.11}$$

in which $z \in \mathbb{R}^n$, $F \in \mathbb{R}^{n \times n}$ is a *Hurwitz* matrix, $G \in \mathbb{R}^n$, and the pair (F, G) is *completely reachable*.

It is well known that any Globally Asymptotically Stable (GAS) linear system, subject to a harmonic input, exhibits a steady-state response which is itself a harmonic function of time oscillating at the same frequency of the input, while having different amplitude and phase (Isidori, 2017, Appendix A.5). Moreover, for linear systems GAS implies ISS. Formally we say that the filter has a unique steady-state which is ISS, as emphasized by the following lemma.

Lemma 1.1. *The cascade*

$$\begin{aligned}
\dot{x} &= Ax \\
\dot{z} &= Fz + GCx + Gv,
\end{aligned} \tag{1.12}$$

is ISS relative to the set

$$\mathcal{Z}^\star := \{(x, z) \in \mathbb{R}^n \times \mathbb{R}^n : z = Tx\} \tag{1.13}$$

with respect to the input v, where $T \in \mathbb{R}^{n \times n}$ is the unique and nonsingular solution to the Sylvester equation

$$TA = FT + GC. \tag{1.14}$$

Lemma 1.1 states that for $v = 0$ the "steady-state" set (1.13) is invariant and GAS (Serrani, Isidori, and Marconi, 2001; Nikiforov, 1998; Isidori, 2017). The state trajectory of the stable filter (1.11), in absence of disturbances, can be then written as the sum of a vanishing transient component $\tilde{z}$ and a steady-state component $z^\star$:

$$z(t) = \tilde{z}(t) + z^\star(t) \to_{t \to \infty} z^\star(t) = Tx(t).$$

In particular, at steady-state, we have

$$\dot{z}^\star = Fz^\star + Gy_0 = (F + GCT^{-1})z^\star = TAT^{-1}z^\star \tag{1.15}$$

in which we used (1.14) and nonsingularity of T. Thus, A is similar to $F + GCT^{-1}$. In fact, the row vector CT^{-1} is precisely the unique solution to the problem of assigning the eigenvalues of A to $F + GCT^{-1}$. Therefore, the model linking the output y_0 and the filter state at steady-state $z^\star$ is simply the *linear-in-the-parameter model*

$$y_0(t) = CT^{-1}z^\star(t) = \theta^\top z^\star(t) \tag{1.16}$$

with $\theta \in \mathbb{R}^n$ a vector of (unknown) "true" parameters to be estimated.

Under Assumption 1.1, the steady-state solution $z^\star$ of (1.15) satisfies the following bound

$$|z^\star(t)| \leq 2\sqrt{\frac{\lambda_{max}}{\lambda_{min}}} \frac{|P| |G|}{1 - \epsilon} \bar{y}_0 = \bar{z} \tag{1.17}$$

in which $0 < \epsilon < 1$, $P \in \mathbb{R}^{n \times n}$ is the solution to the Lyapunov equation

$$PF + F^\top P = -I_n \tag{1.18}$$

and λ_{max} and λ_{min} are the maximum and minimum eigenvalues of P, respectively.

1.4.3 The Discrete-Time Identifier

The identifier is a discrete-time system taking as input the signals y and z at jump times. It has state $\eta = (\eta_1, \eta_2) \in \mathcal{H}$ with $\eta_1 \in \mathbb{R}^{n \times n}$ symmetric and positive definite, and $\eta_2 \in \mathbb{R}^n$. We equip $\mathcal{H}$ with the norm $|\eta| = |\eta_1| + |\eta_2|$. The dynamics of the identifier is

$$\begin{aligned}
\eta_1^+ &= \mu\eta_1 + zz^\top \\
\eta_2^+ &= \mu\eta_2 + zy
\end{aligned} \tag{1.19}$$

with output (1.8), in which $\mu \in [0, 1)$ and $R = R^\top > 0 \in \mathbb{R}^{n \times n}$ are design parameters called *forgetting factor* and *regularization matrix*, respectively. The role of these two parameters will be discussed below. The map sat is constructed hereafter under the following *persistency of excitation* assumption.

Assumption 1.3. *There exist $j^\star \in \mathbb{N}$ and $\varepsilon > 0$ such that, for each solution $(\tau, z^\star)$ of* (1.9),(1.15), *the following holds*

$$\text{minsv}\left(R + \sum_{i=0}^{j-1} \mu^{j-i-1} z^\star(t^i) z^\star(t^i)^\top \right) \geq \varepsilon, \quad \forall j \geq j^\star.$$

With $\bar{y}_0$ given by Assumption 1.1, let

$$\mathcal{Y}^\star := \{y_0 \in \mathbb{R} : y_0 \leq \bar{y}_0\} \tag{1.20}$$

and define the constants

$$\begin{aligned}
c_1 &:= (1 - \mu)^{-1} \sup_{z \in \mathcal{Z}^\star} |z\, z^\top| \\
c_2 &:= (1 - \mu)^{-1} \sup_{(z,y_0) \in \mathcal{Z}^\star \times \mathcal{Y}^\star} |z\, y_0|.
\end{aligned} \tag{1.21}$$

With ε given in Assumption 1.3, define the compact set

$$\mathcal{H}^\star = \{\eta \in H \mid \text{minsv}(\eta_1 + R) \geq \varepsilon, |\eta_1| \leq c_1, |\eta_2| \leq c_2\}. \tag{1.22}$$

Then, sat in (1.8) is any continuous function $\mathbb{R}^n \to \mathbb{R}^n$ satisfying for some $c > 0$

$$\begin{cases} \text{sat}(\gamma(\eta)) &= (\eta_1 + R)^\dagger \eta_2, \quad \eta \in \mathcal{H}^\star \\ |\text{sat}(\gamma(\eta))| &\leq c, \quad\quad\quad\quad \text{otherwise.} \end{cases} \tag{1.23}$$

In view of (1.16), the multi-harmonic signal and the steady-state filter state $z^\star$ are related by a linear regression. The identifier (1.19) is designed so as to asymptotically find the "best" linear model fitting (1.16) to the measured samples. Formally, we have a prediction model

$$\hat{y}_0 = \hat{\theta}^\top z^\star \tag{1.24}$$

with the associated prediction error

$$e = y_0 - \hat{y}_0 = y_0 - \hat{\theta}^\top z^\star.$$

The estimate $\hat{\theta}(j)$, generated by (1.19)-(1.8), is such that at each j the model $\hat{\theta}^\top(j)z^\star$ is optimal with respect to the cost functional

$$\mathcal{J}_j(\hat{\theta}) = \sum_{i=0}^{j-1} \mu^{j-i-1} \left| y_0(t^i) - \hat{\theta}^\top z^\star(t^i) \right|^2 + \hat{\theta}^\top R\hat{\theta} \tag{1.25}$$

which is a weighted sum of the squares of the prediction errors. We associate with the cost functional, the (set-valued) map

$$\mathrm{Opt}(j) := \mathrm{argmin}_{\hat{\theta} \in \mathbb{R}^n} \mathcal{J}_j(\hat{\theta}) \tag{1.26}$$

which collects, at each j, the set of minima of $\mathcal{J}_j$. The intuition behind the design of the identifier (1.19)-(1.8), in relation to the chosen cost functional (1.25), resides in the fact that the optimal trajectory (1.26) can be proven to satisfy

$$\mathrm{Opt}(j) = \{\hat{\theta} \in \mathbb{R}^n \mid (\eta_1^\star(j) + R)\hat{\theta} = \eta_2^\star(j)\} \tag{1.27}$$

in which

$$\eta_1^\star(j) = \sum_{i=0}^{j-1} \mu^{j-i-1} z^\star(t^i) z^\star(t^i)^\top$$
$$\tag{1.28}$$
$$\eta_2^\star(j) = \sum_{i=0}^{j-1} \mu^{j-i-1} z^\star(t^i) y_0(t^i).$$

It can be proven that (1.28) is an asymptotically stable trajectory for system (1.19) when fed with the *ideal* inputs $(y_0, z^\star)$. Therefore we can say that the identifier (1.19)-(1.8) is designed so as to track the map of minima (1.27) when fed with $(y_0, z^\star)$. These ideal signals are clearly not available, thus the identifier processes the "proxy" variables $(y_0 + \nu, z^\star + \tilde{z})$. For this reason, (1.19)-(1.8) is required to be robust, relative to the optimal trajectory (1.27), with respect to the additive disturbances $(\nu, \tilde{z})$. In particular, robustness can be proven in an ISS sense. The required properties are precisely characterized by considering the system

$$\begin{cases} \dot{\tau} = 1 \\ \dot{z}^\star = TAT^{-1}z^\star \\ \dot{\eta}_1 = 0, \dot{\eta}_2 = 0 \end{cases}$$
$$(\tau, z^\star, \eta, y_0, \tilde{z}, \nu) \in [0, \overline{T}] \times \mathbb{R}^n \times \mathcal{H} \times \mathbb{R} \times \mathbb{R}^n \times \mathbb{R}$$
$$\begin{cases} \tau^+ = 0, z^+ = z \\ \eta_1^+ = \mu\eta_1 + (z^\star + \tilde{z})(z^\star + \tilde{z})^\top \\ \eta_2^+ = \mu\eta_2 + (z^\star + \tilde{z})(y_0 + \nu) \end{cases}$$
$$(\tau, z^\star, \eta, y_0, \tilde{z}, \nu) \in [\underline{T}, \overline{T}] \times \mathbb{R}^n \times \mathcal{H} \times \mathbb{R} \times \mathbb{R}^n \times \mathbb{R} \tag{1.29}$$

with output (1.8).

Lemma 1.2. *Under Assumptions 1.1, 1.2, and 1.3, there exist $j^\star \in \mathbb{N}$, two Lipschitz functions $\rho_\eta, \rho_\theta \in \mathcal{K}$, and for each solution $(\tau, z^\star)$ of (1.9),(1.15), a hybrid arc $\eta^\star : \mathrm{dom}(\tau, z^\star) \to \mathcal{H}$, such that $((\tau, z^\star, \eta^\star), (\tilde{z}, \nu))$ with $(\tilde{z}, \nu) = (0, 0)$ is a solution pair to (1.29) satisfying $\eta^\star(j) \in \mathcal{H}^\star$ for all $j \geq j^\star$, and the following properties, relative to $\mathcal{J}_j$ in (1.25), hold*

- *For all $j \geq j^\star$, the signal $\theta^\star := \mathrm{sat}(\gamma(\eta^\star))$ satisfies*

$$\theta^\star(j) \in \mathrm{Opt}(j).$$

- *For every solution pair $((\tau, z^\star, \eta), (\tilde{z}, \nu))$ to (1.29) with $(\tau, z^\star)$ the same as above, for each jump it holds*

$$|\eta(j) - \eta^\star(j)| \leq \mu^j |\eta(0) - \eta^\star(0)| + \rho_\eta(|(\tilde{z}, \nu)|_j).$$

- *The map $\mathrm{sat}(\gamma(\cdot))$ satisfies*

$$|\mathrm{sat}(\gamma(\eta)) - \mathrm{sat}(\gamma(\eta^\star))| \leq \rho_\theta(|\eta - \eta^\star|)$$

for all $(\eta, \eta^\star) \in \mathcal{H} \times \mathcal{H}^\star$.

Remark 1.1. *Assumption 1.3 always holds if R is positive definite. In fact, if this is the case, we have $\varepsilon \geq \mathrm{minsv}(R)$. Instead, if $R = 0$, Assumption 1.3 boils down to a canonical persistence of excitation condition on $z^\star(t^i)$ (Bin, Marconi, and Teel, 2019). However, it is important to remark that having a positive definite R introduces a bias on the parameter estimates. In fact, for any nonzero R, the optimal $\hat{\theta}$ minimizing (1.25) does not necessarily correspond to a zero prediction error, and the parameter estimates rather converge to a neighborhood of the true parameters, whose size is related to the eigenvalues of R and can be reduced arbitrarily. This is the reason why we distinguish between θ, which we called vector of "true" parameters, and $\theta^\star$ which are the optimal parameters according to (1.25) (see Lemma 2).*

The properties of the identifier can be summarized as follows. There exists a steady-state $\eta^\star$ with corresponding output $\theta^\star$, associated with the ideal signals $(y_0, z^\star)$, which is optimal with respect to the chosen cost functional (1.25), and ISS with respect to the "disturbance input" $(\tilde{z}, \nu)$. Finally, the map $\mathrm{sat}(\gamma(\cdot))$ is regular, which means that as η approaches $\eta^\star$, it is also guaranteed that $\hat{\theta}$ approaches $\theta^\star$ (Bin, Marconi, and Teel, 2019; Bin and Marconi, 2020).

1.4.4 Main Result

As shown in Figure 1.1, the proposed design (1.6)-(1.7)-(1.8) is a "cascade" of the filter and the identifier. There follows from Lemmas 1.1 and 1.2, that the overall system is ISS relative to the ideal and optimal steady state $(\tau, z^\star, \eta_1^\star, \eta_2^\star)$ with output $\theta^\star$, and with respect to the input ν. In particular, we can conclude that there exists $\rho_d \in \mathcal{K}$ such that the following asymptotic bound holds (Cai and Teel, 2009)

$$\limsup_{j \to \infty} |\theta^\star(j) - \hat{\theta}(j)| \leq \rho_d \left(\limsup_{t \to \infty} (|\nu(t)|) \right). \tag{1.30}$$

This result leads to the following theorem, which is the main result of this work.

Theorem 1.1. *Consider the estimator (1.6)-(1.7)-(1.8), and suppose that Assumptions 1.1, 1.2, and 1.3 hold. Let $\Omega^\star(j) = \Gamma(\theta^\star(j))$. Then, there exists a function $\rho_\omega \in \mathcal{K}$ such that*

$$\limsup_{j \to \infty} d_H\left(\Omega^\star(j), \hat{\Omega}(j)\right) \leq \rho_\omega \left(\limsup_{t \to \infty} (|\nu(t)|) \right). \tag{1.31}$$
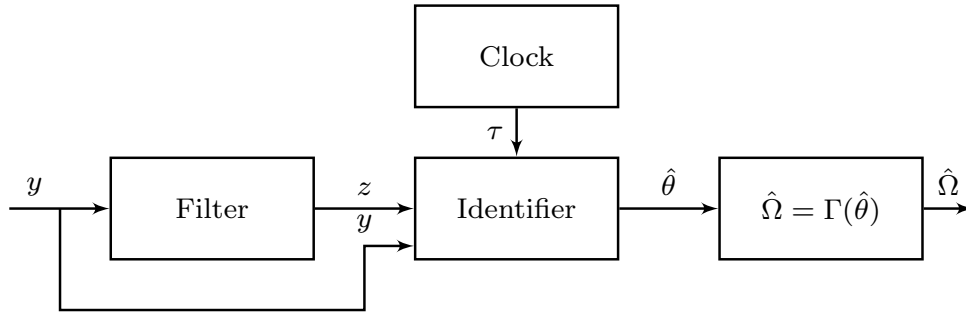
FIGURE 1.1: Overall system.

Remark 1.2. *Since $x(t)$ is persistently exciting in the continuous-time sense (see, e.g., (Ioannou and Sun, 2012, Definition 4.3.1) and (Ioannou and Sun, 2012, Section 5.2.1)), then it can be proven that so is $z^\star(t)$. Therefore, if (1.10) is satisfied, it can be proven that Assumption 1.3 holds with $R = 0$. Nevertheless, we chose to present this general framework anyway, as it is well-known in the pertinent literature that, in presence of disturbances ν, a nonzero regularization matrix R may play a beneficial role by smoothing the estimates and making ill-posed realizations numerically treatable (Sjöberg, McKelvey, and Ljung, 1993). Hence, in the ideal case with no disturbances, if we choose the sampling time sufficiently small (satisfying (1.10)), we can take $R = 0$ to obtain exact exponential convergence to the true parameters.*

1.5 Technical Proofs

1.5.1 Proof of Lemma 1

Being the spectra of A and F in (1.12) disjoint by construction, and being the pair (A, C) completely observable, and the pair (F, G) completely reachable, it is well-known in the literature that the solution T to the Sylvester equation (1.14) exists and it is unique and nonsingular (Isidori, 2017; Serrani, Isidori, and Marconi, 2001; Nikiforov, 1998). Consider the change of variables

$$\begin{bmatrix} x \\ z \end{bmatrix} \rightarrow \begin{bmatrix} x \\ \tilde{z} = z - Tx \end{bmatrix}$$

resulting in the cascade

$$
\begin{aligned}
\dot{x} &= Ax \\
\dot{\tilde{z}} &= \dot{z} - T\dot{x} \\
&= Fz + GCx + G\nu - TAx \\
&= F(\tilde{z} + Tx) + GCx + G\nu - TAx \\
&= F\tilde{z} + G\nu
\end{aligned}
\tag{1.32}
$$

where we used (1.14). Being F Hurwitz, the origin of the $\tilde{z}$-subsystem with $\nu = 0$ is GAS and, being (1.32) linear, it is ISS relative to the origin with respect to the input ν. In the original coordinates this means that the z-subsystem is ISS relative to the set (1.13) with respect to the input ν. Then we can write

$$TAT^{-1} = F + GCT^{-1} \tag{1.33}$$

therefore A is similar to $F + GCT^{-1}$. In fact, the row vector CT^{-1} is precisely the unique solution to the problem of assigning the eigenvalues of A to $F + GCT^{-1}$.

To conclude this part, we want to find a computable estimate of the asymptotic bound for the signal z when no disturbances are present. We consider the perturbation free system

$$\dot{z} = Fz + Gy_0 \tag{1.34}$$

which is a GAS system with input y_0. An asymptotic bound for the signal z corresponds, by definition of input-to-state stability, to the so-called *gain function*. We now prove ISS for system (1.34) in order to give an estimate of the gain function. We make use of Definition 10.4.1, Definition 10.4.2, and Theorem 10.4.1 from (Isidori, 1999). We take as ISS-Lyapunov function candidate

$$V(z) = z^\top P z \tag{1.35}$$

where P is the symmetric and positive definite solution to the Lyapunov equation (1.18), which is guaranteed to exist because F is Hurwitz. We call λ_{max} and λ_{min} the maximum and minimum eigenvalues of the matrix P, respectively, and we have

$$\lambda_{min} |z|^2 \le z^\top P z \le \lambda_{max} |z|^2 \tag{1.36}$$

where $\underline{\alpha} = \lambda_{min} |z|^2$ and $\bar{\alpha} = \lambda_{max} |z|^2$ are both class-$\mathcal{K}_\infty$ functions. The derivative of (1.35) along the system trajectories results in

$$\begin{aligned}
\frac{\partial V}{\partial z} f(x, u) &= 2z^\top P [Fz + Gy_0] \\
&= x^\top (PF + F^\top P)x + 2z^\top PGy_0 \\
&\le -|z|^2 + 2 |P| |G| |z| |y_0|
\end{aligned} \tag{1.37}$$

from which we conclude that the system with $y_0 = 0$ is GAS. Now we want to find a class class-$\mathcal{K}_\infty$ function $\alpha(\cdot)$ and a class-$\mathcal{K}$ function $\chi(\cdot)$ such that

$$\frac{\partial V}{\partial z} f(x, u) \le -\alpha(|z|), \quad \forall(z, y_0) : |z| \ge \chi(|z|). \tag{1.38}$$

We try to force

$$\frac{\partial V}{\partial z} f(x, u) \le -\varepsilon |z|^2$$

with $0 < \varepsilon < 1$, obtaining

$$\begin{aligned}
-|z|^2 + 2 |P| |G| |z| |y_0| &\le -\varepsilon |z|^2 \\
2 |P| |G| |z| |y_0| &\le (1 - \varepsilon) |z|^2 \\
\frac{2 |P| |G| |y_0|}{(1 - \varepsilon)} &\le |z|
\end{aligned} \tag{1.39}$$

from which we conclude

$$\chi(|z|) = \frac{2 |P| |G|}{(1 - \varepsilon)} |y_0|. \tag{1.40}$$

We can now compute an estimate of the gain function $\gamma(\cdot)$ as

$$
\begin{aligned}
\gamma(r) &= \underline{\alpha}^{-1} \circ \bar{\alpha} \circ \chi(r) \\
&= \sqrt{\frac{\lambda_{max}}{\lambda_{min}}} \frac{2 \, |P| \, |G|}{(1 - \varepsilon)} r
\end{aligned}
\tag{1.41}
$$

from which we obtain (1.17) by using Assumption 1.1.

1.5.2　Proof of Lemma 2

We refer to (Bin, Marconi, and Teel, 2019; Bin and Marconi, 2020) for the proof of the first and last items. We provide a proof for the second item. In the following, the argument t^i is almost always omitted for the sake of space and clarity.

We define the identifier ideal steady-state trajectory $\eta^\star(j) := (\eta_1^\star(j), \eta_2^\star(j))$ by taking $\eta^\star(0) = 0$ and

$$
\begin{aligned}
\eta_1^\star(j) &= \sum_{i=0}^{j-1} \mu^{j-i-1} z^\star(t^i) z^\star(t^i)^\top \\
\eta_2^\star(j) &= \sum_{i=0}^{j-1} \mu^{j-i-1} z^\star(t^i) y_0(t^i)
\end{aligned}
\tag{1.42}
$$

for $j \geq 1$. It is easy to see that $\eta^\star$ is a solution to (1.19) when $(z, y) = (z^\star, y_0)$.

By direct computation, we obtain

$$
\begin{aligned}
|\eta(j) - \eta^\star(j)| &\leq \mu^j |\eta(0) - \eta^\star(0)| \\
&+ \sum_{i=0}^{j-1} \mu^{j-i-1} \left(|(z^\star + \tilde{z})(z^\star + \tilde{z})^\top + (z^\star + \tilde{z})(y_0 + v)| \right) \\
&- \sum_{i=0}^{j-1} \mu^{j-i-1} \left(|z^\star z^{\star\top} + z^\star y_0| \right) \\
&= \mu^j |\eta(0) - \eta^\star(0)| \\
&+ \sum_{i=0}^{j-1} \mu^{j-i-1} \left(|z^\star \tilde{z}^\top + \tilde{z} z^{\star\top} + \tilde{z} \tilde{z}^\top + z^\star v + \tilde{z} y_0 + \tilde{z} v| \right) \\
&\leq \mu^j |\eta(0) - \eta^\star(0)| \\
&+ \sum_{i=0}^{j-1} \mu^{j-i-1} \left(|\tilde{z}|^2 + 2 |z^\star| \, |\tilde{z}| + |z^\star| \, |v| + |\tilde{z}| \, |y_0| + |\tilde{z}| \, |v| \right)
\end{aligned}
\tag{1.43}
$$

from where we can distinguish the required exponentially decaying-term $\mu^j |\eta(0) - \eta^\star(0)|$. An estimate of the gain function $\rho_\eta \in \mathcal{K}$ is given by what is left from (1.43). In particular, by using the bounds given by Assumption 1.1 and (1.17), and convergenge of the geometric series, we obtain

$$
\begin{aligned}
&\sum_{i=0}^{j-1} \mu^{j-i-1} \left(|\tilde{z}|^2 + 2 |z^\star| \, |\tilde{z}| + |z^\star| \, |v| + |\tilde{z}| \, |y_0| + |\tilde{z}| \, |v| \right) \\
&\leq (1 - \mu)^{-1} \left[|\tilde{z}|^2 + |\tilde{z}| \, (2\bar{z} + \bar{y}_0) + \bar{z} \, |v| + |\tilde{z}| \, |v| \right].
\end{aligned}
\tag{1.44}
$$

Now, considering that $|(\tilde{z},0)| \le |(\tilde{z},v)|$ and $|(v,0)| \le |(\tilde{z},v)|$, we obtain

$$\rho_\eta(|(\tilde{z},v)|) = (1-\mu)^{-1} \left[2\,|(\tilde{z},v)|^2 + (3\bar{z} + \bar{y}_0)\,|(\tilde{z},v)| \right] \tag{1.45}$$

which concludes the proof.

1.5.3 Proof of Theorem 1

In view of (1.23), both $\theta^\star$ and $\hat{\theta}$ belong to the ball B_c of radius c on $\mathbb{R}^n$. Since $\Gamma : \mathbb{R}^n \to \mathbb{K}(\mathbb{R}_{\ge 0})$ is continuous, then by (*Observer design for nonlinear systems*, Lemma A.2.1) we conclude the existence of a function $\rho_\Gamma \in \mathcal{K}$ such that

$$d_H[\Gamma(\theta^\star(j)), \Gamma(\hat{\theta}(j))] \le \rho_\Gamma[|\theta^\star(j) - \hat{\theta}(j)|] \tag{1.46}$$

for all $\theta^\star, \theta \in B_c$. This, together with (1.30), directly results in (1.31).

1.6 Numerical examples

The simulations presented in this section are obtained by means of the well-known HyEQ toolbox for Matlab&Simulink (Sanfelice, Copp, and Nanez, 2013). We consider the signal

$$y(t) = 1 + [2\sin(t+\pi) + \sin(3t - \pi/2)] + v(t) \tag{1.47}$$

in which $v(t)$ is a bounded realization of a zero-mean white noise. We assume that our prior knowledge corresponds to a maximum amplitude for the y signal of 10, and a maximum frequency of 4 rad/s. We thus select $\bar{y}_0 = 10$, $\bar{\omega} = 4$, relative to Assumptions 1.1 and 1.2.

We choose a periodic clock (1.9) with sampling period

$$T = 0.1 \le \frac{1}{2\bar{\omega}}.$$

The filter is taken as

$$\dot{z} = \begin{bmatrix} -1 & 1 & 0 & 0 & 0 \\ 0 & -1.1 & 1 & 0 & 0 \\ 0 & 0 & -1.2 & 1 & 0 \\ 0 & 0 & 0 & -1.3 & 1 \\ 0 & 0 & 0 & 0 & -1.4 \end{bmatrix} z + \begin{bmatrix} 0 \\ 0 \\ 0 \\ 0 \\ 1 \end{bmatrix} y$$

with zero initial conditions. Regarding the identifier, we choose $\mu = 0.99$, $R = 10^{-5} \cdot I_5$, $\eta_1(0) = 0.1 \cdot I_5$, $\eta_2(0) = 0_n$, and sat as the component-wise saturation function. In particular, we construct (1.23) as follows. Given the vector $(\eta_1 + R)^\dagger \eta_2 = [v_{1j}] \in \mathbb{R}^{1\times n}$, $j = (1, 2, \dots, n)$, and the constant $c > 0$, $\text{sat}((\eta_1 + R)^\dagger \eta_2) = [s_{1j}] \in \mathbb{R}^{1\times n}$ where each entry is given by $s_{1j} := \min\{\max\{v_{ij}, -c\}, c\}$. Now, in order to find c, we consider the Euclidian norm $|\cdot|_2$ as tool of choice, and from (1.23) we have $\left|(\eta_1 + R)^\dagger \eta_2\right|_2 \le c$, then we notice that

$$\left|(\eta_1 + R)^\dagger \eta_2\right|_2 \le \left|(\eta_1 + R)^\dagger\right|_2 |\eta_2|_2$$

$$\le \frac{1}{\text{minsv}(\eta_1 + R)} c_2 \le \frac{c_2}{\varepsilon}$$

for all $\eta \in \mathcal{H}^\star$, resulting in $c \geq c_2/\varepsilon$. Now, as already emphasized in Remark 2, we can choose $\varepsilon \geq \mathrm{minsv}(R) = 10^{-5}$, while, in order to find c_2, we have to use the a priori knowledge $\bar{y}_0$ as well as computing $\bar{z}$ as in (1.17). First, we solve the Lyapunov equation (1.18) from where we also compute λ_{min} and λ_{max}. Then we can compute (1.17) by choosing $\epsilon = 0.5$, obtaining $\bar{z} = 209.42$. Finally $c_2 = 2.1 \cdot 10^5$ from (1.21), and then $c = 2.1 \cdot 10^{10}$.

We consider three different experiments in order to test the performance of the proposed design:

- Disturbance-free experiment (experiment #1), shown in Figure 1.2. From the top to the bottom we see the signal y and the reconstructed signal $\hat{y} = \hat{\theta}^\top z$, the convergence of $\hat{\theta}$ to $\theta^\star$, and the convergence of the set $\hat{\Omega}$ which approaches the set $\Omega = \{1, 3\}$;

- Experiment #2 with a SNR of 15.5 dB, shown in Figure 1.3. On top we see the measurement, while at the bottom we see the convergence of the frequency estimates.

- Experiment #3 with a SNR of 6.4 dB, shown in Figure 1.4. On top we see the measurement, while at the bottom we see the convergence of the frequency estimates.

Finally, Figure 1.5 shows the good filtering capabilities of the proposed estimator relative to the reconstruction of y, which we did not discuss but could be appealing for some applications.
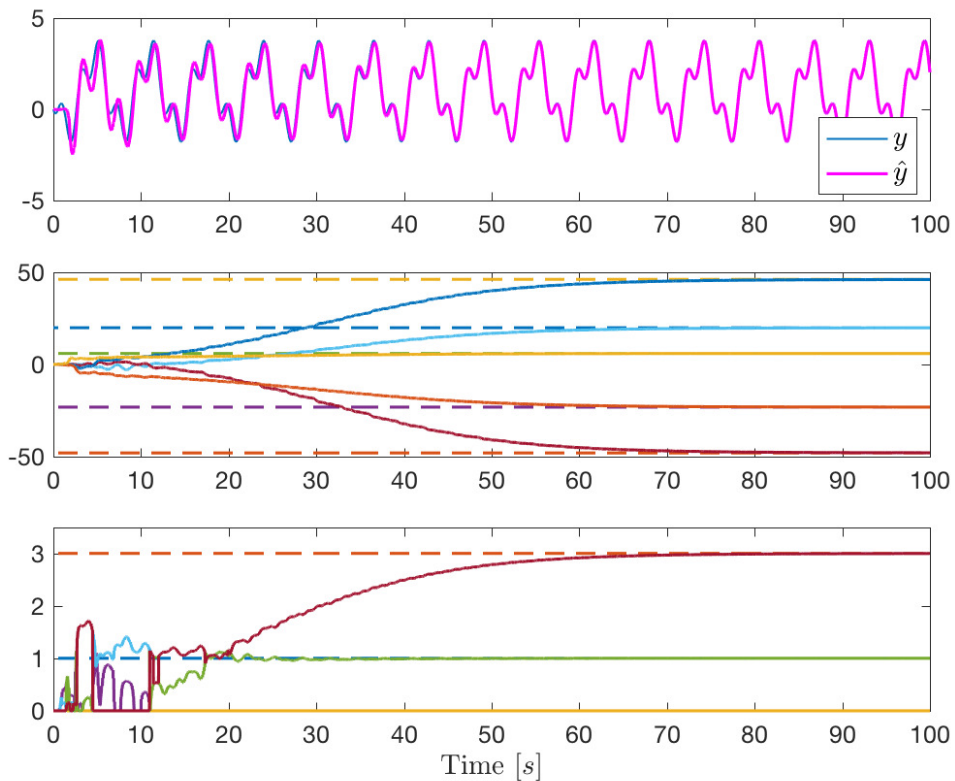
FIGURE 1.2: Disturbance-free experiment.
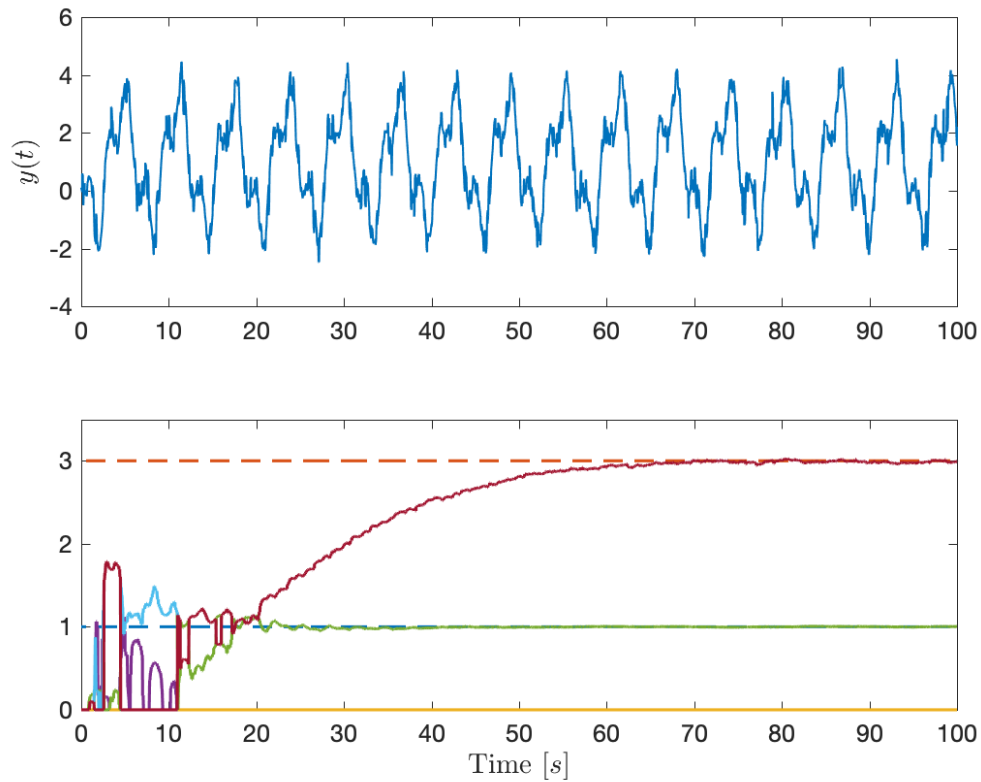
FIGURE 1.3: Experiment with a SNR of 15.5 dB.
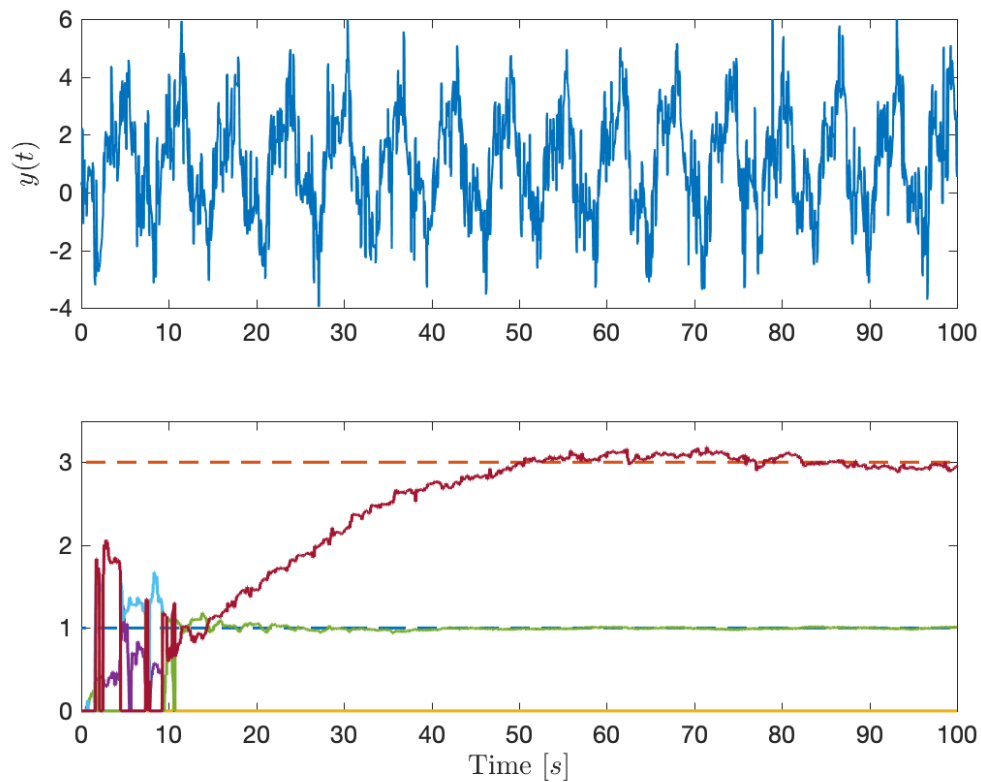
FIGURE 1.4: Experiment with a SNR of 6.4 dB.
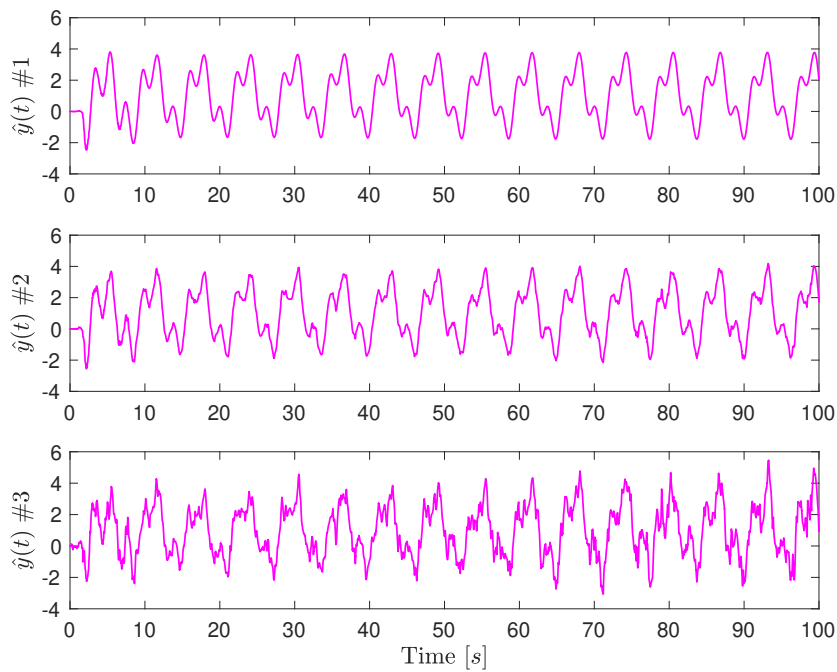
FIGURE 1.5: Signal reconstruction relative to the three different experiments.

1.7 Conclusions

The problem of robust estimation of the frequencies of biased multi-harmonic signals has been considered in this chapter. The proposed estimator consists of a stable linear filter and a discrete-time recursive least squares identifier. Using a discrete-time identifier better fits the needs of practical applications. Future work will be devoted to a precise characterization of the impact that the design parameters have on the performance (for instance, if we have some prior knowledge about the nature of the disturbance, we may choose a convenient form for the stable filter), as well as the important problems of overparameterization and underparameterization (i.e. when we underestimate or overestimate the number of harmonics present in y, respectively).

Chapter 2

Robust and Scalable Distributed Recursive Least Squares

In this chapter, we consider the problem of distributed estimation of an unknown parameter, over a network of discrete-time adaptive systems. Each system measures noisy samples of different pairs of signals related by a linear regression. As a consequence, we are in the so-called errors-in-variables context. The proposed estimator provides a robust stability result for the overall network trajectories, relative to a steady state that is associated with a correct estimation of the unknown parameter. Everything works under a cooperative excitation assumption, which is formally investigated and, not surprisingly, it is strictly weaker than (classic) persistence of excitation of the local data set.

2.1 Introduction

2.1.1 Problem Overview

We consider a set of $n \in \mathbb{N}$ agents. Each agent i measures noisy samples of a pair (y_i, ϕ_i) of signals related by a linear regression of the form

$$y_i(t) = \phi_i(t)^\top \theta, \tag{2.1}$$

in which θ is a *common* unknown parameter. Agents exchange information through a communication network, possibly disconnected and asymmetric. In this setting, we consider the problem of decentralized online asymptotic estimation of the unknown parameter θ.

While this is a problem that can be solved with n independent local algorithms, each one trying to estimate θ from the local samples, communication permits agents to benefit from the information gathered by the other agents, and thus ensures faster convergence under excitation conditions that are *strictly weaker* than persistence of excitation of the local data set. Thus, looking for a distributed design is well motivated in all those context where measurements are difficult or expensive, or when sensors are spatially distributed by construction, or in large-scale problems where the number of parameters is large, or simply when faster convergence is needed.

For ease of exposition, we focus on the "single-variable" case where, for some arbitrary $n_\theta \in \mathbb{N}$, $\theta \in \mathbb{R}^{n_\theta}$ and, for each $i = 1, \ldots, n$, $y_i : \mathbb{N} \to \mathbb{R}$ and $\phi_i : \mathbb{N} \to \mathbb{R}^{n_\theta}$. Nevertheless, we remark that the approach easily extends to a multi-variable setting, where $y_i(t) \in \mathbb{R}^m$, $\phi_i(t) \in \mathbb{R}^{n_\theta \times m}$ and $\theta \in \mathbb{R}^{n_\theta \times m}$ for some $m > 1$, by concatenating m single-variable solutions.

We assume that the collection of new samples, the communication, and the update of the local estimates are synchronous (while synchronicity is not necessary in

principle, it considerably simplifies the analysis.). At each step, every agent collects the new samples, exchanges its local state with a subset of other agents, and then updates its local estimate of θ. This is repeated in an infinite time horizon. We suppose that the measured samples are corrupted by additive disturbances on which we make no assumption other than local boundedness. These disturbances can model measurement noise, unmodeled dynamics/terms in (2.1), or any other sources of uncertainty in the measurement process. As disturbances affect both y_i and ϕ_i, we are in an *errors-in-variables* context (Söderström, 2007).

We propose a decentralized estimation law by which each agent can robustly estimate the common unknown parameter θ asymptotically. In particular, we provide a robust stability result of the aggregate trajectories relative to a steady state that, if a "cooperative persistence of excitation" condition holds, is associated with a correct estimation of θ. Robustness is meant in the sense of *input-output stability* with respect to the exogenous disturbances, and the main result of the chapter states that each agent's asymptotic estimation error of θ is bounded by a continuous function of the asymptotic size of the disturbances. In particular, when disturbances vanish, exact convergence is recovered.

2.1.2   Related Works

Multi-agent systems are well suited to model complex behaviors exhibited by biological, social, economic, and engineering networks. We want to focus on adaptive networks, which consist of spatially distributed agents having some learning capabilities. In this context, nature provides several examples of real-time learning and adaptation behaviors, emerging from highly localized interactions among agents having limited capabilities. Over the last decades, many distributed estimation algorithms have been developed to solve signal processing or control/optimization tasks by mimicking the aforementioned behaviors observed in natural networks (Sayed et al., 2013).

In particular, we focus our attention on distributed estimation over networks of systems locally sensing a pair of signals which are related by a linear regression. The vast majority of the approaches present in the literature are based on distributed versions of Least Squares (LS) (Mateos, Schizas, and Giannakis, 2009; Mateos and Giannakis, 2012; Yu et al., 2019; Breschi, Bemporad, and Kolmanovsky, 2020; Xie, Zhang, and Guo, 2020), Least Mean Squares (LMS) (Lopes and Sayed, 2008; Schizas, Mateos, and Giannakis, 2009; Xie and Guo, 2018a; Xie and Guo, 2018c; Xie and Guo, 2018b), or Total Least Squares (TLS) (Li, Zhao, and Lv, 2021).

In general, different cooperation strategies (imposed by the network topology or by what and how many information can be exchanged among neighbors) lead to different estimation algorithms. We can distinguish among 3 types of estimation strategies in the distributed RLS literature, namely *consensus* (Mateos, Schizas, and Giannakis, 2009; Schizas, Mateos, and Giannakis, 2009; Mateos and Giannakis, 2012; Xie and Guo, 2018a; Xie and Guo, 2018c; Breschi, Bemporad, and Kolmanovsky, 2020), *diffusion* (Lopes and Sayed, 2008; Cattivelli, Lopes, and Sayed, 2008; Chen and Sayed, 2012; Sayed et al., 2013; Xie and Guo, 2018b; Yu et al., 2019; Xie, Zhang, and Guo, 2020), and *incremental* (Lopes and Sayed, 2007; Cattivelli and Sayed, 2010).

Diffusion strategies introduce an aggregation step that helps to incorporate into the adaptation mechanism the local information collected from the neighbors. At each iteration, this aggregation step may either be performed before adaptation (combine then adapt) or after (adapt then combine). On the other hand, adaptive consensus-type strategies rely on the use of two-time scales: one for the collection of

the measurements across the nodes, and another one to perform a sufficient number of iterations such that the agreement on some variable of interest is reached, before the process is repeated. Recently, inspired by distributed optimization literature, single time-scale implementations for consensus strategies have been proposed as well.

Considering single time scale consensus strategies having also a constant step size (to enable continuous adaptation and learning), it can be noticed how they have the same computational complexity of diffusion-type strategies. However, diffusion strategies should be preferred over consensus strategies (Tu and Sayed, 2012; Sayed et al., 2013): diffusion networks converge faster and reach lower mean-square error deviations. Moreover, consensus-based adaptive networks may become unstable even if all individual nodes are stable, while this is not the case in diffusion-based adaptive networks.

Since those two strategies require all nodes to share data simultaneously with all their neighbors and process everything in real time, it is important to mention that other strategies exist (which are not conceptually different in terms of the local adaptation algorithms), having the goal of reducing the required overall computational complexity. In terms of reducing the communication burden, we find the aforementioned incremental (Lopes and Sayed, 2007; Cattivelli and Sayed, 2010) and the partial diffusion ones (Arablouei et al., 2014; Rastegarnia, 2019). For instance, in the incremental approach, a cyclic path is defined over the nodes and data are processed in a cyclic manner through the network until optimization is achieved. However, determining a cyclic path that covers all nodes is known to be an NP-hard problem and, in addition, cyclic trajectories are prone to link and node failures. On the other hand, in terms of targeting low computational complexity at each node, we could adopt sparse RLS (Liu, Liu, and Li, 2014) or RLS with data-adaptive censoring (Wang et al., 2018), which could be beneficial in large-scale networks.

Most approaches rely on the typical assumptions of independence, stationarity, or gaussian properties of the measured signals. Recently, both distributed LMS (Xie and Guo, 2018a; Xie and Guo, 2018c; Xie and Guo, 2018b) and LS (Xie, Zhang, and Guo, 2020) strategies have been developed, which do not need these assumptions and thus are potentially applicable to stochastic feedback systems. In addition, they formally discuss the concept of cooperative excitation. Finally, another recent work (Li, Zhao, and Lv, 2021) considers an errors-in-variables context, where it is allowed to have noise affecting both measured signals.

In terms of the literature just mentioned, our work could be categorized as a *combine then adapt diffusion RLS*. However, the main objective of this work is that of approaching the problem of estimating θ under a different control-oriented perspective. We consider that both y_i and ϕ_i are affected by generic disturbance terms, on which we make no statistical assumption, and we shift the focus from unbiasedness and consistency to robustness of the estimate with respect to the disturbance, formalized in terms of input-to-state stability (ISS) (Sontag and Wang, 1996). In this way, as in (Bin, Marconi, and Teel, 2019; Bin, Bernard, and Marconi, 2021), we enable the use of canonical nonlinear control techniques applying to ISS systems, such as small-gain methods (Jiang, Teel, and Praly, 1994), for the analysis of interconnections between controlled systems and identifiers. To the best of our knowledge, this is the first time that asymptotic stability and ISS properties are addressed in distributed RLS literature, while they constitute the main focus of this chapter.

2.1.3 Notation

We denote by $\mathbb{R}$ and $\mathbb{N}$ the set of real and natural numbers, respectively. If A is a set, A^n denotes the n-fold Cartesian product of A. If $(S, \geq)$ is a preordered set, for every $s \in S$ we let $S_{\geq s} := \{z \in S : z \geq s\}$. If $A_1, \ldots, A_n$ are matrices, we denote by $\mathrm{diag}(A_1, \ldots, A_n)$ their diagonal concatenation. By $\otimes$ we denote the Kronecker product and by $\sigma(A)$ the spectrum of a matrix A. For $p = 1, \ldots, \infty$, $|\cdot|_p$ denotes the vector, or matrix induced, p-norm. We denote by $\P_n$ the set of positive semi-definite symmetric operators on $\mathbb{R}^n$. We write $A \geq B$ if $A - B \in \P_n$. The n-dimensional identity matrix is denoted by I_n and the $n \times m$ zero matrix by $0_{n \times m}$. Dimensions are omitted when clear. A function $\gamma : \mathbb{R}_{\geq 0} \to \mathbb{R}_{\geq 0}$ is of class-$\mathcal{K}$ ($\gamma \in \mathcal{K}$) if it is continuous, strictly increasing, and $\gamma(0) = 0$. We denote by $\cdot^+$ the shift operator, i.e. $x^+(t) = x(t+1)$.

2.2 The Framework

2.2.1 Samples Acquisition

Let $\mathcal{N} := \{1, \ldots, n\}$ denote the set of agents. At each time $t \in \mathbb{N}$, each agent $i \in \mathcal{N}$ samples the signals (y_i, ϕ_i) of its regression (2.1) and obtains the samples

$$\begin{aligned}
\xi_i(t) &= y_i(t) + \delta_{y,i}(t), \\
\varphi_i(t) &= \phi_i(t) + \delta_{\phi,i}(t),
\end{aligned} \tag{2.2}$$

in which $\delta_i := (\delta_{y,i}, \delta_{\phi,i}) : \mathbb{N} \to \mathbb{R}^{n_\delta}$, $n_\delta := n_\theta + 1$, are the exogenous perturbations adding to the measurements of y_i and ϕ_i and representing, for example, noise affecting the measurement process and/or unmodeled dynamics or components in the case in which a non-ideal regression of the form

$$y_i(t) = (\phi_i(t) + w_i(t))^\top \theta + \varepsilon_i(t)$$

is sampled in place of (2.1). Due to the presence of δ_i affecting both the regressor ϕ_i and the regressand y_i, estimating θ is an *errors-in-variables* problem (Söderström, 2007). In the remainder of the chapter, we let $y := (y_i)_{i \in \mathcal{N}}$, $\phi := (\phi_i)_{i \in \mathcal{N}}$, $\delta := (\delta_i)_{i \in \mathcal{N}}$, $\xi := (\xi_i)_{i \in \mathcal{N}}$, $\varphi := (\varphi_i)_{i \in \mathcal{N}}$, and we make the following uniform boundedness assumption.

Assumption 2.1. *There exist $\bar{y}, \bar{\phi} > 0$, such that $|y_i(t)| \leq \bar{y}$ and $|\phi_i(t)|_\infty \leq \bar{\phi}$ for every $i \in \mathcal{N}$ and $t \in \mathbb{N}$.*

2.2.2 Communication

We assume that agents can exchange information over a communication network formally described by a family $\mathcal{C} = \{I_i\}_{i \in \mathcal{N}}$ of sets $I_i \subset \mathcal{N}$ satisfying $i \in I_i$. We call $\mathcal{C}$ the *communication network*, and the set I_i the *(inward) neighborhood* of i. Each agent can receive information by all the agents $k \in I_i$, and can send information to all the agents in the set $O_i := \{k \in \mathcal{N} : i \in I_k\}$. It is not required that $k \in I_i$ implies $i \in I_k$, so the network may be undirected. We denote by d_i the cardinality of I_i, and we associate with $\mathcal{C}$ the *adjacency matrix* $A \in \mathbb{R}^{n \times n}$, defined by letting $A_{ik} = 1$ if $k \in I_i$ and $A_{ik} = 0$ otherwise, where A_{ik} denotes the (i, k)-th entry of A. We stress that $A_{ii} = 1$ for all $i \in \mathcal{N}$. Finally, we define the matrix

$$\Lambda := \mathrm{diag}(d_1, \ldots, d_n)^{-1} A.$$

2.2.3 Problem Statement

With the previous definitions in mind, the problem we consider in this chapter is that of defining, for each agent $i \in \mathcal{N}$, a recursive procedure that exploits the samples acquired by (2.2) and the information coming from the neighboring agents to find, asymptotically, a "good" estimate $\hat{\theta}_i$ of the unknown common parameter θ in (2.1). The sought procedure must have the following properties:

1. *Regulation:* In absence of disturbances, i.e. when $\delta = 0$, $\lim \hat{\theta}_i(t) = \theta$ for all $i \in \mathcal{N}$.

2. *Robustness:* If $\delta \neq 0$, then the asymptotic estimation errors must be bounded continuously by the "asymptotic size" of δ. Specifically, there must exists $\kappa \in \mathcal{K}$ such that $\limsup |\hat{\theta}_i - \theta| \leq \kappa(\limsup |\delta|)$ for all $i \in \mathcal{N}$ and all bounded δ.

3. *Decentralization:* The update law of $\hat{\theta}_i$ and of all other state variables must depend only from the current samples produced by (2.2) and the values of the state variables communicated by the agents $j \in I_i$.

4. *Scalability:* The update laws must be independent, as far as possible, from "centralized" parameters or quantities.

2.3 Distributed Recursive Least Squares

2.3.1 The Update Laws

To approach the problem delineated in Section 2.2.3, for each agent $i \in \mathcal{N}$, we propose the following update law

$$
\begin{aligned}
\Psi_i^+ &= \frac{\mu_i}{d_i} \sum_{k \in I_i} \Psi_k + (1 - \mu_i) \varphi_i \varphi_i^\top, \\
\eta_i^+ &= \frac{\mu_i}{d_i} \sum_{k \in I_i} \eta_k + (1 - \mu_i) \varphi_i \xi_i,
\end{aligned}
\tag{2.3}
$$

with output

$$
\hat{\theta}_i = \gamma_i(\Psi_i, \eta_i),
\tag{2.4}
$$

in which Ψ_i and η_i are the state variables associated with Agent i and take their values in $\P_{n_\theta}$ and $\mathbb{R}^{n_\theta}$ respectively, $\Psi := (\Psi_i)_{i \in \mathcal{N}}$ and $\eta := (\eta_i)_{i \in \mathcal{N}}$, the output $\hat{\theta}_i$ is the estimate Agent i has on θ and it takes values in $\mathbb{R}^{n_\theta}$, φ_i and ξ_i are the samples produced by (2.2), the parameters $\mu_i \in (0, 1)$ are arbitrarily chosen, and the functions $\gamma_i : \P_{n_\theta} \times \mathbb{R}^{n_\theta} \to \mathbb{R}^{n_\theta}$ are degrees of freedom fixed later in Section 2.3.5.

2.3.2 The Aggregate System

Let $\Phi : (\mathbb{R}^{n_\theta})^n \to (\P_{n_\theta})^n$ and $\Xi : (\mathbb{R}^{n_\theta})^n \times \mathbb{R}^n \to (\mathbb{R}^{n_\theta})^n$ be functions mapping $\varphi = (\varphi_i)_{i \in \mathcal{N}} \in (\mathbb{R}^{n_\theta})^n$ and $(\varphi, \xi) = ((\varphi_i)_{i \in \mathcal{N}}, (\xi_i)_{i \in \mathcal{N}}) \in (\mathbb{R}^{n_\theta})^n \times \mathbb{R}^n$ respectively to

$$
\Phi(\varphi) := (\varphi_i \varphi_i^\top)_{i \in \mathcal{N}}, \qquad\qquad \Xi(\varphi, \xi) := (\varphi_i \xi_i)_{i \in \mathcal{N}}.
$$

Let $W := \operatorname{diag}(\mu_1, \dots, \mu_n)$, $F := W\Lambda \otimes I_{n_\theta}$, and $G := (I_n - W) \otimes I_{n_\theta}$. Then, the composition of (2.2) and (2.3) is a system with input (y, ϕ, δ), state variable $x :=$

(Ψ, η) ranging in the sate-space $\mathcal{X} := (\P_{n_\theta})^n \times (\mathbb{R}^{n_\theta})^n$, output $\hat{\theta} := (\hat{\theta}_i)_{i \in \mathcal{N}}$, and its dynamics is described by the following equation

$$x^+ = g(x, y, \phi, \delta) \tag{2.5}$$

in which

$$g(x, y, \phi, \delta) := (F\Psi, F\eta) + (G\Phi(\phi + \delta_\phi), G\Xi(\phi + \delta_\phi, y + \delta_y)) \tag{2.6}$$

where $\delta_\phi := (\delta_{\phi,i})_{i \in \mathcal{N}}$ and $\delta_y := (\delta_{y,i})_{i \in \mathcal{N}}$. We equip $\mathcal{X}$ with the norm

$$|x| := \max\{|\Psi|_\infty, |\eta|_\infty\}.$$

2.3.3   Existence and Robust Stability of a Steady State

Let $\bar{\mu} := \max_{i=1,\ldots,n} \mu_i$. Then, $\bar{\mu} < 1$ for every choice of $\mu_i \in (0,1)$, and the operator F is Schur stable as established by the following proposition.

Proposition 2.1. $|F|_\infty \leq \bar{\mu}$ and, for all $\lambda \in \sigma(F)$, $|\lambda| \leq \bar{\mu}$.

Proof. By definition of A in Section 2.2.2, $\sum_{k=1}^n A_{ik} = d_i$ for all $i = 1, \ldots, n$. Thus,

$$|F|_\infty = |W\Lambda|_\infty = \max_{i=1,\ldots,n} \sum_{k=1}^n \mu_i d_i^{-1} A_{ik} = \bar{\mu}.$$

As $|\cdot|_\infty$ is sub-multiplicative, then $\max_{\lambda \in \sigma(F)} |\lambda| \leq |F|_\infty \leq \bar{\mu}$, which concludes the proof $\square$

As in (Bin, 2020), with each solution pair $(x, (y, \phi, \delta))$ of (2.5), we associate a signal $x^\star = (\Psi^\star, \eta^\star) : \mathbb{N} \to \mathcal{X}$ defined as

$$\begin{aligned} \Psi^\star(t) &:= \sum_{s=0}^{t-1} F^{t-s-1} G\Phi(\phi(s)), \\ \eta^\star(t) &:= \sum_{s=0}^{t-1} F^{t-s-1} G\Xi(\phi(s), y(s)). \end{aligned} \tag{2.7}$$

Let $(\Psi_i^\star)_{i \in \mathcal{N}}$ be such that $\Psi^\star(t) = (\Psi_i^\star(t))_{i \in \mathcal{N}}$ for all $t \in \mathbb{N}$. Then, $\Psi_i^\star(t) \in \P_{n_\theta}$ for all $t \in \mathbb{N}$, since $0 \in \P_{n_\theta}$ and, by construction, $\phi_i(s)\phi_i(s)^\top \in \P_{n_\theta}$ for all $i \in \mathcal{N}$ and $s \in \mathbb{N}$. Moreover, we underline that $x^\star$ is defined only by the ideal unperturbed samples of (2.1), and does not depend on δ or on the aggregate state variable x. Finally, we also observe that $(x^\star, (y, \phi, 0))$ is the unique solution pair of (2.5) satisfying $x^\star(0) = 0$.

The forthcoming proposition establishes an input-to-state stability property of the motion $x^\star$ relative to the input δ. If $\delta = 0$, the result implies asymptotic convergence of x to $x^\star$. Thus, we refer to $x^\star$ as the *ideal steady state* of x. Let $\underline{\mu} := \min_{i \in \mathcal{N}} \mu_i$ and, with $\bar{y}$ and $\bar{\phi}$ given by Assumption 2.1, let

$$\omega(s) = (1 - \underline{\mu})(1 - \bar{\mu})^{-1}(2 \max\{\bar{\phi}, \bar{y}\} s + s^2). \tag{2.8}$$

Then, $\omega \in \mathcal{K}$ and the following holds.

Proposition 2.2. *Suppose that Assumption 2.1 holds. Then, there exists $\alpha > 0$ such that, for every solution pair $(x, (y, \phi, \delta))$ of (2.2), the following holds*

$$|x(t) - x^\star(t)| \le \alpha \bar{\mu}^t |x(0) - x^\star(0)| + \omega(\sup_{s \in \mathbb{N}_{\le t-1}} |\delta(s)|_\infty)$$

for all $t \in \mathbb{N}$.

The proof of the proposition is in Section 2.7.

Remark 2.1. *If the estimation scheme (2.2), (2.3) has to be used within a closed-loop control system, one may want to have a function ω which is sub-linear, as this is necessary to enforce small-gain like conditions with linear feedback (see, e.g. (Bin and Marconi, 2020; Bin, Bernard, and Marconi, 2021)). We remark that this can be achieved by "saturating" the terms $\varphi_i \varphi_i^\top$ and $\varphi_i \xi_i$ in (2.3) within a ball of radius larger than $\max\{\bar{y}, \bar{\phi}\}$. We refer to (Bin, 2020; Bin and Marconi, 2020; Bin, Bernard, and Marconi, 2021) for further details.*

Remark 2.2. *We underline that δ represents disturbances on all the variables. It is well-known that in this errors-in-variables setting, least-squares schemes are biased also if δ is a realization of a white noise (Söderström, 2007). We notice, however, that this is not in contrast with the claim of Proposition 2.2, which in turn implies that if a bias is present due to δ, then it vanishes continuously with δ. See also (Bin and Marconi, 2020, Remark 3 and Example 1).*

2.3.4 Cooperative Persistence of Excitation and Optimality of the Steady State

Existence and robust stability of the steady state $x^\star$ is always guaranteed if the signals y and ϕ are bounded. In this section we show that, under suitable persistence of excitation conditions, $x^\star$ is also associated with a correct estimate of θ for each agent. Let $(\Psi_i^\star)_{i \in \mathcal{N}}$ and $(\eta_i^\star)_{i \in \mathcal{N}}$ be such that $\Psi^\star$ and $\eta^\star$, defined in (2.7), satisfy $\Psi^\star(t) = (\Psi_i^\star(t))_{i \in \mathcal{N}}$ and $\eta^\star(t) = (\eta_i^\star(t))_{i \in \mathcal{N}}$ at each $t \in \mathbb{N}$. Then, the following holds.

Lemma 2.1. *For every solution pair $(x, (y, \phi, \delta))$ of (2.5)*

$$\Psi_i^\star(t)\theta = \eta_i^\star(t) \tag{2.9}$$

for all $i \in \mathcal{N}$ and $t \in \mathbb{N}$.

Lemma 2.1, proved in Section 2.8, guarantees that the sought parameter θ satisfies $\Psi_i(t)\theta = \eta_i(t)$ for all $t \in \mathbb{N}$ in the ideal steady state $x^\star$, which is attractive when $\delta = 0$. However, it does not guarantee that θ can be uniquely determined by $\Psi_i^\star(t)$ and $\eta_i^\star(t)$, as in general $\Psi_i^\star(t)$ may be singular or ill-conditioned. Identifiability of θ requires further conditions formalized in this chapter as a persistence of excitation property of the samples taken and exchanged by the agents.

Definition 2.1. *Let $(x, (y, \phi, \delta))$ be a solution pair of (2.5). The samples of Agent $i \in \mathcal{N}$ ar said to be* persistently exciting *with parameters $(\varepsilon_i, \tau_i) \in \mathbb{R}_{>0} \times \mathbb{N}$ if*

$$\Psi_i^\star(t) \ge \varepsilon_i I \tag{2.10}$$

holds for all $t \ge \tau_i$.

For ease of exposition we shall say that "Agent i is (ε_i, τ_i)-PE" to say that its samples are persistently exciting with parameters (ε_i, τ_i). We omit (ε_i, τ_i) if clear or unimportant. The following proposition follows directly from Lemma 2.1 and shows that persistence of excitation implies indentifiability of θ.

Proposition 2.3. *Let* $(x, (y, \phi, \delta))$ *be a solution pair to* (2.5). *If Agent* $i \in \mathcal{N}$ *is* (ε_i, τ_i)-*PE, then for all* $t \geq \tau_i$, $\Psi_i^\star(t)$ *is invertible and*

$$\theta = \Psi_i^\star(t)^{-1} \eta_i^\star(t). \tag{2.11}$$

In the remainder of the section, we further discuss the persistence of excitation condition of Definition 2.1. Let $(x, (y, \phi, \delta))$ be a solution pair of (2.5). In view of (2.7), for each $t \in \mathbb{N}$,

$$\Psi^\star(t) = \sum_{s=0}^{t-1} F^{t-s-1} G(\phi_i^\star(s)\phi_i^\star(s)^\top)_{i \in \mathcal{N}} \tag{2.12}$$

in which $(\phi_i(s))_{s=0,\dots,t-1}$ are samples of the regressor ϕ_i of (2.1), and $F = W\Lambda \otimes I$ incorporates the communication network. Therefore, each matrix $\Psi_i^\star(t)$ is an "aggregate" quantity obtained by summing terms of the kind $\phi_k(s)\phi_k(s)^\top$ obtained by mixing the local endogenous samples ($k = i$) and the ones accumulated and communicated by the other agents of the network ($k \in \mathcal{N} \setminus \{i\}$), all properly weighted by the factors μ_i and filtered. As a consequence, the persistence of excitation condition (2.10) is not just a property of the samples of Agent i, but depends on all the samples of all the other agents of the network. Hence, the name "cooperative persistence of excitation".

At this point, one may wonder if the contribution of communication in achieving PE does actually carry some advantages with respect to the case in which Agent i only uses its own samples to compute an estimate of θ. In our setting, this is a well-posed question, since the communication network has no connectivity requirements to satisfy (Proposition 2.1 holds for every row-stochastic adjacency matrix A). For every $i \in \mathcal{N}$, define $\Psi_i^L : \mathbb{N} \to \mathbb{1}_{n_\theta}$ by letting $\Psi_i^L(0) := 0$ and

$$\Psi_i^L(t+1) = \frac{\mu_i}{d_i}\Psi_i^L(t) + (1 - \mu_i)\phi_i(t)\phi_i(t)^\top \tag{2.13}$$

for $t \in \mathbb{N}$. Then, Ψ_i^L represents the ideal steady-state of Ψ in case the information coming from other agents is discarded in (2.3) (i.e. if $\sum_{k \in I_i} \Psi_k$ is substituted by Ψ_i). Therefore, the condition $\Psi_i^L(t) \geq \varepsilon_i I$ refers to a persistence of excitation property concerning only the local samples, hence called "local PE". Lemma 2.2 below, proved in Section 2.9, establishes that local PE always implies that Agent i is PE if the information coming from the neighboring agents is not discarded.

Lemma 2.2. *For every solution pair* $(x, (y, \phi, \delta))$ *of* (2.5), *every* $i \in \mathcal{N}$, *every* $t \in \mathbb{N}$, *and every* $\varepsilon_i > 0$,
$$\Psi_i^L(t, j) \geq \varepsilon_i I \implies \Psi_i^\star(t) \geq \varepsilon_i I.$$

The converse implication is instead false in general. Therefore, cooperative PE as defined in Definition 2.1 is *strictly weaker* than local PE.

Finally, we remark that the PE condition is not required if one uses regularization, as explained later in Section 2.5.2.

2.3.5 Input-to-Output Stability and Design of γ_i

The only degrees of freedom of (2.3)-(2.4) that remain to be fixed are the functions γ_i. In this section, we choose γ_i according to (Bin, 2020) (see also (Bin and Marconi, 2020; Bin, Bernard, and Marconi, 2021)) in order to force an input-to-output stability property (made precise by Lemma 2.3 below) that will be needed for the main convergence result later in Section 2.4. In particular, in view of Proposition 2.3, a reasonable choice for $\gamma_i(\Psi_i, \eta_i)$ would be $\gamma_i(\Psi_i, \eta_i) = \Psi_i^{-1}\eta_i$. This choice, however, is only valid at the ideal steady state where $\Psi_i = \Psi_i^\star$ and $\eta_i = \eta_i^\star$ and if Agent i is PE. During transitory, $\Psi_i(t)$ can be singular or of variable rank and, with such choice of γ_i, we would fail to establish a relation of the kind (2.14) below between the difference $\gamma_i(\Psi_i(t), \eta_i(t)) - \gamma_i(\Psi_i^\star(t), \eta_i^\star(t))$ and the deviation $x(t) - x^\star(t)$ from the ideal steady state, which is needed to bound $|\hat{\theta}_i - \theta|$ by using the stability result of Proposition 2.2.

To avoid these problems, in this section we use the construction of (Bin, 2020) as follows. With $\underline{\varepsilon}_i > 0$ arbitrary and $\bar{\phi}$, $\bar{y}$ given by Assumption 2.1, define the set

$$\Gamma_i := \{(\Psi_i, \eta_i) \in \mathbb{I}_{n_\theta} \times \mathbb{R}^{n_\theta} \ : \ |\Psi_i|_\infty \leq \left(\frac{1-\underline{\mu}}{1-\bar{\mu}}\right)\bar{\phi}^2 + 1$$

$$|\eta_i|_\infty \leq \left(\frac{1-\underline{\mu}}{1-\bar{\mu}}\right)\bar{\phi}\bar{y} + 1, \ \Psi_i \geq \frac{\varepsilon_i}{2}I\}.$$

Then, we pick $\gamma_i : \mathbb{I}_{n_\theta} \times \mathbb{R}^{n_\theta} \to \mathbb{R}^{n_\theta}$ in such a way that:

G1. γ_i is continuous and bounded.

G2. $\gamma_i(\Psi_i, \eta_i) = \Psi_i^{-1}\eta_i$ for all $(\Psi_i, \eta_i) \in \Gamma_i$ (notice that in this case Ψ_i is invertible).

Then, by means of the same arguments used in (Bin, 2020), the following property can be established.

Lemma 2.3. *For each $i \in \mathcal{N}$, let γ_i be chosen such that **G1** and **G2** hold. Then, there exists $\ell_i > 0$ such that*

$$|\gamma_i(\Psi_i, \eta_i) - \gamma_i(\Psi_i', \eta_i')|_\infty \leq \ell_i(|\Psi_i - \Psi_i'|_\infty + |\eta_i - \eta_i'|_\infty)$$

holds for all $(\Psi_i, \eta_i) \in \Gamma_i$ and all $(\Psi_i', \eta_i') \in \mathbb{I}_{n_\theta} \times \mathbb{R}^{n_\theta}$.

In view of Proposition 2.1, from (2.7) we obtain $|\Psi_i^\star(t)|_\infty \leq |\Psi^\star(t)|_\infty \leq (1-\underline{\mu})(1-\bar{\mu})^{-1}\bar{\phi}^2$ and $|\eta_i^\star(t)|_\infty \leq |\eta^\star(t)|_\infty \leq (1-\underline{\mu})(1-\bar{\mu})^{-1}\bar{\phi}\bar{y}$ for all $t \in \mathbb{N}$. Hence, if Agent i is (ε_i, τ_i)-PE with $\varepsilon_i \geq \underline{\varepsilon}_i$, then $(\Phi_i^\star(t), \eta_i^\star(t)) \in \Gamma_i$ for all $t \geq \tau_i$. Therefore, Lemma 2.3 implies that for every solution pair $(x, (y, \phi, \delta))$ of (2.5) such that Agent i is (ε_i, τ_i)-PE with $\varepsilon_i \geq \underline{\varepsilon}_i$, the input-to-output stability property

$$|\gamma_i(\Psi_i^\star(t), \eta_i^\star(t)) - \gamma_i(\Psi_i(t), \eta_i(t)| \leq 2\ell_i|x^\star(t) - x(t)| \tag{2.14}$$

holds for all $t \geq \tau_i$.

Remark 2.3 (Choice of γ_i). *A possible choice of γ_i satisfying the above properties consists in taking $\gamma_i(\Psi_i, \eta_i)$ as a vector with k-th component $\gamma_i(\Psi_i, \eta_i)_k := \mathrm{sat}_{\bar{\theta}_i}(u_{i,k})$, where $u_{i,k}$ is the k-th component of $\Psi_i^\dagger \eta_i$ ($\cdot^\dagger$ denotes the Moore-Penrose pseudoinverse), $\bar{\theta}_i := 2(\bar{\phi}\bar{y}(1-\underline{\mu})(1-\bar{\mu})^{-1} + 1)/\underline{\varepsilon}_i$, and $\mathrm{sat}_\star(\cdot) := \min\{\max\{\cdot, -\star\}, \star\}$ denotes the standard saturation function. See (Bin, 2020) for further details.*

2.4   Main Result

Let ω be the class-$\mathcal{K}$ function (2.8) for which Proposition 2.2 holds and, for each $i \in \mathcal{N}$, let $\varepsilon_i > 0$ be the constant used in the construction of the set Γ_i and $\ell_i > 0$ be such that Lemma 2.3 holds. Then, the following theorem establishes the main result of the chapter, which relates the asymptotic estimation error on θ to the asymptotic "size" of the disturbance δ.

Theorem 2.1. *Suppose that Assumption 2.1 holds. Then, every solution pair $(x, (y, \phi, \delta))$ of (2.5) with δ bounded is bounded. Moreover, if Agent $i \in \mathcal{N}$ is $(\varepsilon_i, \tau_i^\star)$-PE for some $\tau_i \in \mathbb{N}$ and with $\varepsilon_i \geq \underline{\varepsilon}_i$, then*

$$\limsup |\hat{\theta}_i - \theta|_\infty \leq 2\ell_i \omega(\limsup |\delta|_\infty). \tag{2.15}$$

Proof. In view of (2.7), under Assumption 2.1 $x^\star$ is bounded. Then, boundedness of x when δ is bounded follows by Proposition 2.2. Moreover, by means of standard ISS arguments (see, e.g. (Cai and Teel, 2009, Lemma 3.6)), one can deduce from Proposition 2.2 that

$$\limsup |x - x^\star| \leq \omega(\limsup |\delta|_\infty). \tag{2.16}$$

Finally, if Agent i is (ε_i, τ_i)-PE with $\varepsilon_i \geq \underline{\varepsilon}_i$ then, as shown at the end of Section 2.3.5, $(\Psi_i^\star(t), \eta_i^\star(t)) \in \Gamma_i$ for all $t \geq \tau_i$. Since in this case Propositions 2.3 implies $\theta = \Psi_i^\star(t)^{-1}\eta_i^\star(t) = \gamma_i(\Psi_i^\star(t), \eta_i^\star(t))$ for $t \geq \tau_i$, then the claim follows from (2.14) and (2.16). $\qquad\square$

2.5   Some Remarks on Convergence, Regularization and Scalability

2.5.1   Convergence Rate and Exact Convergence

For a given $i \in \mathcal{N}$, we say that the limit (2.15) holds uniformly if, for fixed δ, the following property holds: for every $\epsilon > 0$ and $r > 0$, there exists $\bar{t} > 0$, such that every solution pair $(x, (y, \phi, \delta))$ with $|x(0)| \leq r$ satisfies $|\hat{\theta}_i(t) - \theta|_\infty \leq 2\ell_i \omega(\limsup |\delta|_\infty) + \epsilon$ for all $t \geq \bar{t}$.

In general, (2.15) does not hold uniformly since (2.14) starts to hold only after time τ_i, which is the time after which Agent i is PE. However, after τ_i has passed, convergence is uniform and *exponential* with rate $\bar{\mu}$, in view of Proposition 2.2. Therefore, if one can guarantee that there exists $\bar{\tau} \in \mathbb{N}$ such that Agent i is $(\varepsilon_i, \bar{\tau})$-PE for every solution pair of (2.5) with $\varepsilon_i \geq \underline{\varepsilon}_i$, then (2.15) is uniform and an exponential convergence rate is guaranteed.

Finally, we stress that, if $\lim \delta = 0$, then (2.15) can be strengthen to

$$\lim \hat{\theta}_i(t) = \theta,$$

which is exact convergence.

2.5.2   On the Use of Regularizers

As the persistence of excitation condition of Definition 2.1 cannot be checked a priori in general, one may wonder whether such assumption can be eliminated. It turns out it is possible at the price, however, of introducing a bias in the estimates. In particular, by following (Bin, 2020), we can define a matrix $\Omega_i \in \P_{n_\theta}$ arbitrarily and choose γ_i such that the following property holds in place of Item **G2**:

G2′. $\gamma_i(\Psi_i, \eta_i) = (\Psi_i + \Omega_i)^{-1}\eta_i$ for all $(\Psi_i, \eta_i) \in \Gamma'_i$,

in which Γ'_i is defined by modifying Γ_i as follows

$$\Gamma'_i := \{(\Psi_i, \eta_i) \in \mathbb{I}_{n_\theta} \times \mathbb{R}^{n_\theta} : |\eta_i|_\infty \leq \left(\frac{1-\underline{\mu}}{1-\bar{\mu}}\right)\bar{\phi}\bar{y} + 1$$

$$|\Psi_i|_\infty \leq \left(\frac{1-\underline{\mu}}{1-\bar{\mu}}\right)\bar{\phi}^2 + |\Omega_i|_\infty + 1, \ \Psi_i \geq \frac{\varepsilon_i}{2}I\}.$$

If Ω_i is chosen such that $\Omega_i \geq \varepsilon_i I$, then $\Psi_i^\star(t) + \Omega_i \geq \varepsilon_i I$ for all $t \in \mathbb{N}$ and, hence, $\Psi_i^\star(t) + \Omega_i \in \Gamma'_i$ for all $t \in \mathbb{N}$. Therefore, the PE condition of Definition 2.1 *is not needed* anymore to conclude (2.14). Furthermore, in this case also the saturation of γ_i (Item **G1**) can be avoided. Indeed, $\Omega_i \geq \varepsilon_i I$ implies $\Psi_i(t) + \Omega_i \geq \varepsilon_i I$ for all $t \in \mathbb{N}$ and for all solution pairs $(x, (y, \phi, \delta))$ of (2.5), since $\Psi_i(t) \in \mathbb{I}_{n_\theta}$ for all $t \in \mathbb{N}$. Hence, one has[1]

$$|(\Psi_i^\star(t) + \Omega_i)^{-1}\eta_i^\star(t) - (\Psi_i(t) + \Omega_i)^{-1}\eta_i(t)|_\infty$$

$$\leq \frac{n(1-\underline{\mu})\bar{\phi}\bar{y}}{(1-\bar{\mu})\varepsilon^2}|\Psi_i^\star(t) - \Psi_i(t)|_\infty + \frac{\sqrt{n}}{\varepsilon}|\eta_i^\star(t) - \eta_i(t)|_\infty,$$

which implies (2.14) with $2\ell_i = n(1-\underline{\mu})\bar{\phi}\bar{y}(1-\bar{\mu})^{-1}\varepsilon^{-2} + \sqrt{n}\varepsilon^{-1}$. Thus, if $\Omega_i \geq \varepsilon_i I$, one can simply pick

$$\gamma_i(\Psi_i, \eta_i) := (\Psi_i + \Omega_i)^{-1}\eta_i. \tag{2.17}$$

Nevertheless, if $\Omega_i \neq 0$, one cannot conclude (2.15) anymore. Instead, one obtains the weaker inequality

$$\limsup |\hat{\theta}_i - \theta|_\infty \leq c_i(\Omega_i) + 2\ell_i \omega(\limsup |\delta|_\infty), \tag{2.18}$$

in which $c_i(\Omega_i) \geq 0$ is a bias vanishing with $|\Omega_i|$. For further details, we refer to (Bin, 2020).

2.5.3 Remarks on Scalability and Decentralization

The update laws (2.3) are decentralized, since the update of the state variables of each agent i depends only on the state variables of the neighboring agents $k \in I_i$. Moreover, the "gains" μ_i are arbitrary, and each agent can fix μ_i independently from the others. The construction of γ_i, however, uses centralized quantities since the set Γ_i relies on the knowledge of $\underline{\mu}$, $\bar{\mu}$, and the constants $\bar{\phi}$ and $\bar{y}$ given by Assumption 2.1. Nevertheless, we observe the following:

- The quantities $\underline{\mu}$, $\bar{\mu}$, $\bar{\phi}$, and $\bar{y}$ are only used to estimate an a priori upper bound on the norm of $\Psi_i^\star$ and $\eta_i^\star$. If such quantities are not available, an agent can either estimate the upper bound by looking at the local quantities $|\Psi_i(t)|_\infty$ and $|\eta_i(t)|_\infty$, or take a very large upper bound that is likely to be achieved.

- If Agent i uses a regularization matrix $\Omega_i \geq \varepsilon_i I$ then, as explained in previous Section 2.5.2, γ_i can be chosen as in (2.17), and thus no knowledge of $\underline{\mu}$, $\bar{\mu}$, $\bar{\phi}$, and $\bar{y}$ is required anymore.

---

[1] We used the fact that for every $A, B \in \mathbb{I}_{n_\theta}$ satisfying $A, B \geq \varepsilon I$, one has $|A^{-1} - B^{-1}| = |B^{-1}(B - A)A^{-1}| \leq |B^{-1}||A^{-1}||A - B|$ for every sub-multiplicative norm, and $|A^{-1}|_\infty \leq \sqrt{n}|A^{-1}|_2 \leq \sqrt{n}/\varepsilon$. Hence, for every $x, y \in \mathbb{R}^{n_\theta}$, $|A^{-1}x - B^{-1}y|_\infty = |(A^{-1} - B^{-1})x + B^{-1}(x - y)|_\infty \leq (n/\varepsilon^2)|x|_\infty|A - B|_\infty + (\sqrt{n}/\varepsilon)|x - y|_\infty$.

Overall, we can therefore conclude that (2.3) has good scalability properties for what concerns the definition of the update laws. Nevertheless, the update laws (2.3) are synchronous, and synchronization may be seen as a centralized feature. We remark, however, that synchronicity is not strictly necessary, as long as a stability property of the kind proved in Proposition 2.2 holds, and it has been assumed to simplify the forthcoming analysis. The same applies to the communication topology, which can be time-varying as far as stability is preserved.

Finally, we observe that the function ω, defined in (2.8), for which the claim of Proposition 2.2 holds is proportional to the factor $(1 - \underline{\mu})(1 - \bar{\mu})^{-1}$. Thus, while the choice of each gain μ_i is independent from the others, the more the gains are similar, the better it is from the standpoint of sensitivity to disturbances. In the limit case in which the gains satisfy $\mu_1 = \cdots = \mu_n$, then $(1 - \underline{\mu})(1 - \bar{\mu})^{-1} = 1$, and ω does not depend on them.

2.6 Numerical Example

Given a road network, represented by a directed graph $(\mathcal{V}, \mathcal{N})$ as in Figure 2.1, with $\mathcal{V}$ a set of vertices representing crossings and $\mathcal{N} \subset \mathcal{V}^2$ the set of roads, the problem of road pricing pertains the assignment of a toll τ_i to each road $i \in \mathcal{N}$ with the aim of mitigating congestion. Road pricing boasts a long academic history, especially in the economics community (Pigou, 1920; Walters, 1961; Small and Verhoef, 2007; Yang and Huang, 2005). The basic idea follows the principle of *marginal cost* (or Pigovian tax): Efficiency is obtained when each driver pays a toll balancing the externalities caused by their journey. Formally, if d_i denotes the density of vehicles on Road $i \in \mathcal{N}$, and $\ell(d_i)$ the corresponding *latency*[2] (the average travel time), then the marginal cost pricing theory suggests taking (Yang and Huang, 2005, Section 3.2)

$$\tau_i = \ell'(d_i)d_i, \tag{2.19}$$

where ℓ' denotes the derivative of ℓ.

In this section, we consider the problem of *adaptive decentralized marginal cost pricing* described hereafter. We assume that with each arc i there is associated a unique agent (labeled by i as the corresponding arc). Agents aim to implement the marginal cost policy (2.19) in a distributed way, with each agent responsible of deciding the toll levied on its arc. To implement (2.19), agents need the function ℓ', which is unknown a priori (the uncertain form of such functions is, indeed, one of the main obstacles for the implementation of marginal cost pricing, see e.g.(Yang, Meng, and Lee, 2004)). Hence, ℓ' must be estimated at run time. We approach this problem by applying the methodology developed in the previous sections. Specifically, we suppose that each agent i can measure (with the due approximation) the density $d_i(t)$ and the corresponding latency $\ell(d_i(t))$ on the associated road i at each time t. In terms of (2.2), we thus have $y_i(t) = \ell(d_i(t))$, $\phi_i(t) = (\psi_1(d_i(t)), \ldots, \psi_{n_\theta}(d_i(t)))$. Furthermore, we assume that agents can communicate with those associated with neighboring arcs. Namely, we assume that a communication network (Section 2.2.2) $\mathcal{C} = \{I_i\}_{i \in \mathcal{N}}$ is given with $I_i := \{j \in \mathcal{N} : j_1 = i_1 \vee j_1 = i_2 \vee j_2 = i_1 \vee j_2 = i_2\}$, where for an arc $k \in \mathcal{N}$ we let $k_1, k_2 \in \mathcal{V}$ be such that $k = (k_1, k_2)$. In this setting, we consider the approximation $\ell \approx \sum_{k=1}^{n_\theta} \theta_k \psi_k$ for some $\mathcal{C}^1$ basis-functions ψ_k,

---

[2]Here, we tacitly assume that the latency function ℓ is the same for each road. This assumption is justified when considering similar roads, as we do in the forthcoming simulations.
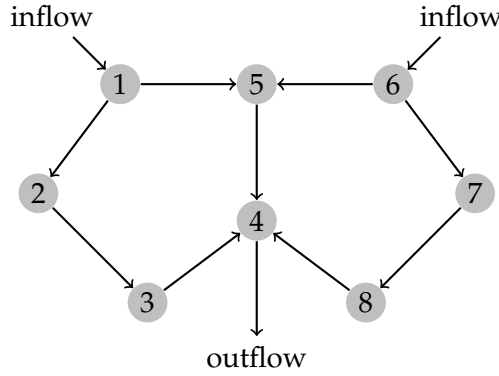
FIGURE 2.1: Road Network.

and we equip each agent with the distributed estimation scheme (2.3)-(2.4). Theorem 2.1 ensures robustness with respect to the unavoidable uncertainty in the measurements and in the approximation of ℓ. Finally, with $\hat{\theta}_i$ denoting the approximation of $\theta := (\theta_1, \ldots, \theta_{n_\theta})$ that Agent i obtains from (2.4), each agent approximates ℓ' by $\widehat{\ell}'_i := \hat{\theta}_i^\top \psi'$, with $\psi' := (\psi'_1, \ldots, \psi'_{n_\theta})$.

A similar problem has been considered in (Poveda et al., 2017) where, however, each agent estimates its own parameters alone without communicating with others. We stress that, in our context, estimating the parameters θ in a collective way has the advantage that each agent can exploit the information coming from the traffic data in other roads. This is particularly useful for agents controlling empty or very low congested roads, as otherwise they could not obtain a meaningful estimate from their own measurements and thus levy a proper toll.

In the forthcoming simulation, we consider a road network represented by the graph shown in Figure 2.1. The simulation setting is the following. Arcs represent one-way one-lane paths. Their length L_i is measured in cells (a cell is the discrete unit of space), and in the following is set to $L_i = 50$ for all $i \in \mathcal{N}$. Vehicles flows are simulated microscopically and in discrete-time. Each vehicle v enters the network with a given origin O_v and destination D_v, and has state variable $(\alpha_v, c_v) \in \mathcal{N} \times \mathbb{N}$, where α_v represents the current arc and c_v the current cell occupied by v. These variables are updated as follows

$$\alpha_v^+ = \begin{cases} \alpha_v & \text{if } c_v < L_{\alpha_v} \text{ or } (J(\alpha_v), 1) \text{ is occupied} \\ J(\alpha_v) & \text{otherwise} \end{cases}$$

$$c_v^+ = \begin{cases} c_v & \text{if } c_v = L_{\alpha_v} \text{ and } (J(\alpha_v), 1) \text{ is occupied} \\ 1 & \text{if } c_v = L_{\alpha_v} \text{ and } (J(\alpha_v), 1) \text{ is free} \\ c_v + K_v & \text{otherwise} \end{cases}$$

in which $K_v := \sup\{k \in \mathbb{N}_{\leq V} : c_v + k \leq L_{\alpha_v} \text{ and } (\alpha_v, c_v + h) \text{ is not occupied for all } h \in \mathbb{N}_{\leq k}\}$ denotes the maximal number of cells v can advance, where $V = 4$ denotes a common maximal speed (in cells per time units), and $J(\alpha_v)$ is the first arc produced by a shortest-path algorithm finding the shortest weighted path[3] between the current node to which α_v is incident and the vehicle's destination D_v. Here, the weights

---

[3]This corresponds to the simplifying (yet widespread) assumption of fully rational drivers with perfect knowledge of the network weights.

on each $i \in \mathcal{N}$ at each $t \in \mathbb{N}$ are given by

$$w_i(t) := L_i/V + \tau_i(t),$$

namely, by the sum of an expected travel time L_i/V when no congestion is present, and the time-equivalent of the toll levied on i at time t (here, we assume that all vehicles have a unitary value of time factor, so as we can measure $\tau_i(t)$ in time units). The order of update of the vehicles is chosen randomly at each time.

For the estimation phase, we pick $n_\theta = 6$ and choose the basis functions $\psi_1, \ldots, \psi_6$ as the elements of a biorthogonal spline basis[4] for $L_2([0,1])$ (Daubechies, 1992, Pages 271–280). Each agent is then equipped with the estimator (2.3)-(2.4). For simplicity, the update of the estimation law is synchronized with that of the vehicles. The density $d_i(t)$ and latency $y_i(t) = \ell(d_i(t))$ on Road i are estimated from microscopic observations as $d_i(t) = \text{card}\mathcal{V}_i^t/L_i$, and $y_i(t) = L_i \cdot (\sum_{v \in \mathcal{V}_i^t} s_v^t)^\dagger$, where $\mathcal{V}_i^t := \{v \in \mathcal{V} : \alpha_v(t) = i\}$ denotes the set of vehicles on Road i at time t, and s_i^t is the speed of vehicles v at time t, estimated as $s_i^t = c_v(t) - c_v(t-1)$ if $\alpha_v(t) = \alpha_v(t-1)$, or $s_i^t = 1$ otherwise. The parameters μ_i are chosen as $\mu_i = 0.99 + i_1 \cdot 10^{-3}$ (i_1 denotes the tail node of the arc i). Moreover, for each i, γ_i is chosen as in (2.17) with $\Omega_i = 10^{-3}I$.

Figures 2.2-2.5 show the results of a simulation running for $T = 1000$ units of time with the inflow form node 1 to node 4 at full capacity and that from 6 to 4 at 80%. Namely, at each time t, after the update of the vehicles' state variables, if the first cell of the first arc of the current shortest path connecting 1 and 4 (resp. 6 and 4) is free, then with probability 1 (resp. 0.8) a new vehicle v with origin-destination pair $(O_v, D_v) = (1,4)$ (resp. $(O_v, D_v) = (6,4)$) is added to the network.

In particular, Figure 2.2 shows that, without tolls, all drivers seek the path that would be the shortest in absence of congestion. Consequently, we observe a high congestion concentrated to few roads, which provokes a low traveling speed. Instead, Figure 2.3 shows a simulation where tolls are levied according to the adaptive methodology described previously. As the figure clearly shows, the levied tolls have the effect of distributing more equally the drivers over the networks' roads, with the consequence of a lower congestion on each road and a larger mean speed. Figure 2.4 shows a comparison between these two simulations in terms of mean congestion, mean speed, and mean travel time from the origin to the destinations. As shown by the figure, the developed adaptive pricing mechanism permits to more than double the mean speed while more than halving congestion and travel time. Finally, for the case where tolls are levied, Figure 2.5 shows the dynamics of the estimated parameters. As it can be seen from the figure, all agents estimate similar parameters thanks to the communication and the updates (2.3).

2.7   Proof of Proposition 2.2

Pick arbitrarily a solution pair $(x, (y, \phi, \delta))$ to (2.5), and let $x^\star$ be defined as in (2.7). By direct solution, (2.5) yields

$$\Psi(t) = F^t \Psi(0) + \sum_{s=0}^{t-1} F^{t-s-1} G\Phi(\phi(s) + \delta_\phi(s))$$

---

[4]Specifically, ψ_k can be obtained in MATLAB as $\psi_k(\cdot) := 2^{-s/2}\varphi(2^{-s} \cdot -k)$ with $s = -2$ and where φ is the dual scaling function obtained with the command *wavefun* of the Wavelet Toolbox with argument 'bior3.5'.
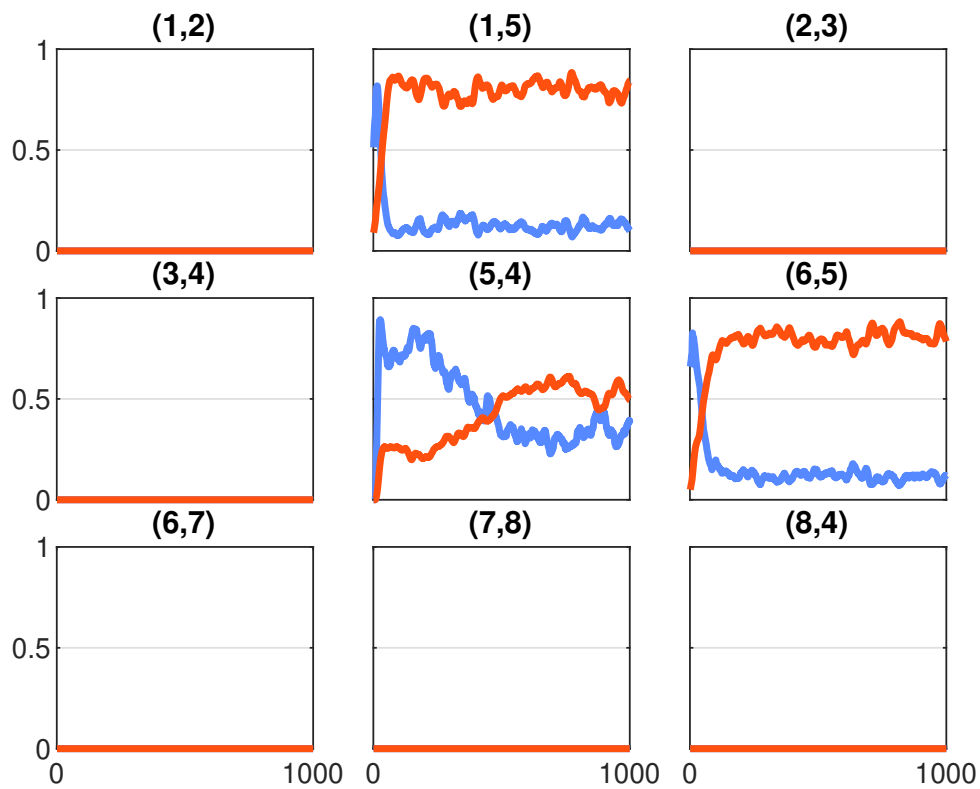
FIGURE 2.2: Time series of the congestion (red) and mean speed (blue) on each road in absence of tolls. The speed is normalized with respect to the maximum speed V. The time series are averaged on a moving window of size 15 time units. Label (i, j) denotes the arc (road) from Node i to Node j in the graph of Figure 2.1.
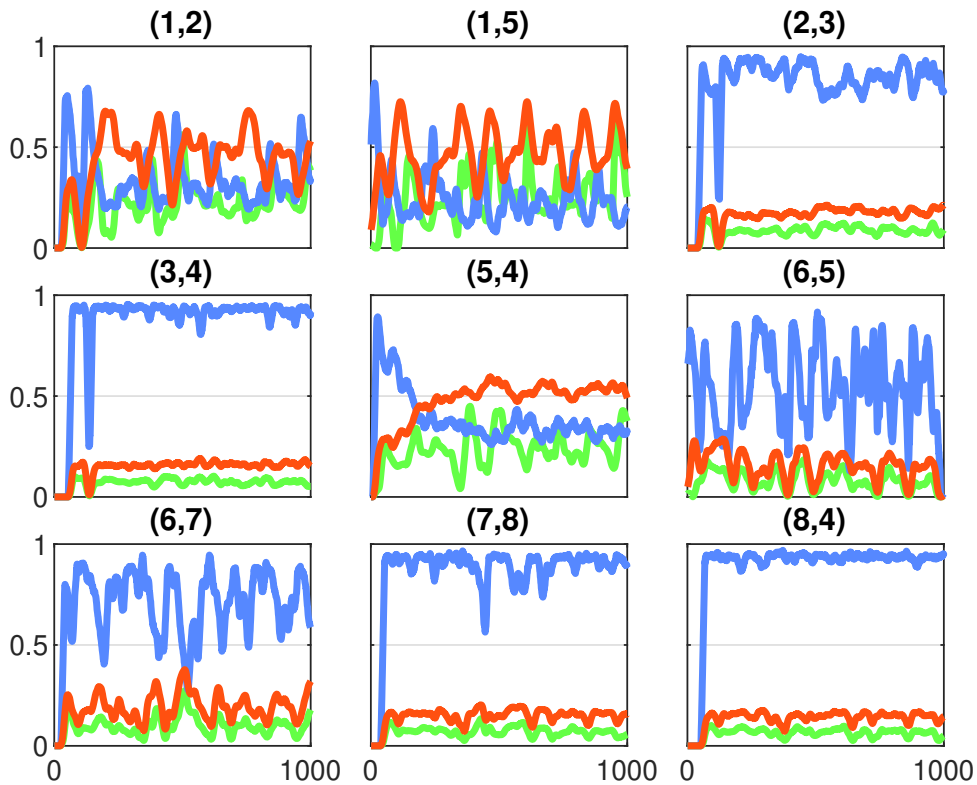
FIGURE 2.3: Time series of the congestion (red), mean speed (blue), and levied toll (green) on each road in presence of tolls. The speed is normalized with respect to the maximum speed V, the tolls are normalized with respect to the maximum toll levied. The time series are averaged on a moving window of size 15 time units. Label (i, j) denotes the arc (road) from Node i to Node j in the graph of Figure 2.1.
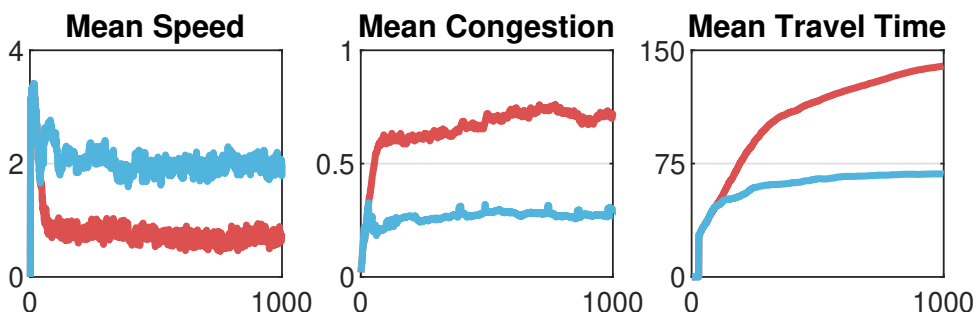
FIGURE 2.4: Comparison between performances when no tolls are levied (red) and when tolls are levied (blue). The mean speed an the mean congestion are computed by averaging the corresponding time series shown in Figures 2.2 and 2.3 over the roads with non-zero occupation. The mean travel time is the average of the time each driver takes to go from its origin to its destination.
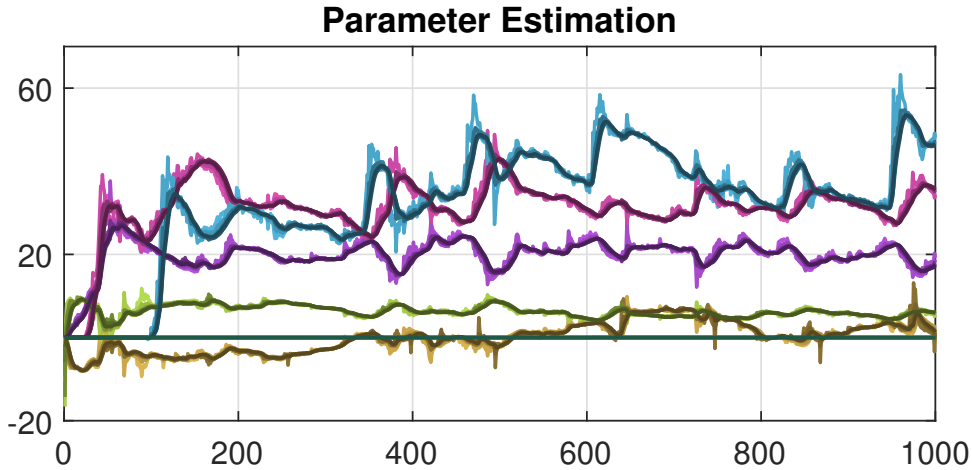
FIGURE 2.5: Estimated parameters when tolls are levied. Brighter and darker shades of the same color are used to plot the time series of the same parameter for different agents.

for all $t \in \mathbb{N}$. Define $\widetilde{\Psi} := \Psi - \Psi^\star$ and $\widetilde{\Phi}(\phi, \delta_\phi) := \Phi(\phi + \delta_\phi) - \Phi(\phi)$. In view of (2.7), we obtain

$$|\widetilde{\Psi}(t)|_\infty \leq \bar{\mu}^t |\widetilde{\Psi}(0)|_\infty + (1 - \underline{\mu}) \sum_{s=0}^{t-1} \bar{\mu}^{t-s-1} |\widetilde{\Phi}(\phi(s), \delta_\phi(s))|_\infty,$$

for all $t \in \mathbb{N}$, where we have used the fact that, by construction, $\Psi^\star(0) = 0$, $|G|_\infty = 1 - \underline{\mu}$, and that, in view of of Proposition 2.1, $|F|_\infty \leq \bar{\mu}$.

Similar arguments show that, with $\tilde{\eta} := \eta - \eta^\star$ and $\widetilde{\Xi}(\phi, y, d) := \Xi(\phi + \delta_\phi, y + \delta_y) - \Xi(\phi, y)$, we have

$$|\tilde{\eta}(t)|_\infty \leq \bar{\mu}^t |\tilde{\eta}(0)|_\infty + (1 - \underline{\mu}) \sum_{s=0}^{t-1} \bar{\mu}^{t-s-1} |\widetilde{\Xi}(\phi(s), y(s), \delta(s))|_\infty$$

for all $t \in \mathbb{N}$.

Next, observe that, for all $a, b \in \mathbb{R}^{n_\theta}$ and $c, d \in \mathbb{R}$

$$|aa^\top - bb^\top|_\infty \leq 2|a|_\infty |a - b|_\infty + |a - b|_\infty^2$$
$$|ac - bd|_\infty \leq |a|_\infty |c - d|_\infty + |c|_\infty |a - b|_\infty$$
$$+ |a - b|_\infty |c - d|_\infty.$$

By using these relations with $a = \phi(s)$, $b = \phi(s) + \delta_\phi(s)$, $c = y(s)$, and $d = y(s) + \delta_y(s)$, we obtain

$$\max \left\{ |\widetilde{\Phi}(\phi(s), \delta_\phi(s))|_\infty, |\widetilde{\Xi}(\phi(s), y(s), \delta(s))|_\infty \right\}$$
$$\leq 2 \max\{\bar{\phi}, \bar{y}\} |\delta(s)| + |\delta(s)|^2$$

for all $s \in \mathbb{N}$. Hence, $\tilde{x} := x - x^\star$ satisfies

$$|\tilde{x}(t)| = \max \left\{ |\widetilde{\Psi}(t)|_\infty, |\tilde{\eta}(t)|_\infty \right\}$$
$$\leq \bar{\mu}^t |\tilde{x}(0)| + \left(\frac{1 - \underline{\mu}}{1 - \bar{\mu}} \right) \left(2 \max\{\bar{\phi}, \bar{y}\} |\delta|_{\infty,t} + |\delta|_{\infty,t}^2 \right),$$

where we let $|\delta|_{\infty,t} := \sup_{s \in \mathbb{N}_{\leq t-1}} |\delta(s)|_\infty$ and we used the fact that $\sum_{s=0}^{t} \bar{\mu}^{t-s-1} \leq \sum_{s=0}^{\infty} \bar{\mu}^s = (1 - \bar{\mu})^{-1}$. $\qquad\square$

2.8   Proof of Lemma 2.1

For every $t \in \mathbb{N}$, we have $\Psi_i^\star(t)\theta = \eta_i^\star(t)$ for all $i \in \mathcal{N}$ if and only if

$$\Psi^\star(t)\theta = \eta^\star(t). \tag{2.20}$$

It thus suffices to prove that (2.20) holds for all $t \in \mathbb{N}$. We proceed by induction. Suppose that at some $t \in \mathbb{N}$, (2.20) holds. Then, and at $t + 1$ we have

$$\begin{aligned}
\Psi^\star(t&+1)\theta - \eta^\star(t+1) \\
&= F(\Psi^\star(t)\theta - \eta^\star(t)) + G(\Phi(\phi(t))\theta - \Xi(\phi(t), y(t))) \\
&= G(\Phi(\phi(t))\theta - \Xi(\phi(t), y(t))).
\end{aligned}$$

By definition of Φ and Ξ, and using (2.1), we obtain $\Phi(\phi(t))\theta = (\phi_i(t)\phi_i(t)\theta)_{i \in \mathcal{N}} = (\phi_i(t)y_i(t))_{i \in \mathcal{N}} = \Xi(\phi(t), y(t))$, and thus we conclude that $\Phi(t+1)\theta - \eta(t+1) = 0$, which implies $\Psi^\star(t+1)\theta = \eta^\star(t+1)$.

Since $\Psi^\star(0) = 0$ and $\eta^\star(0) = 0$, then (2.20) holds at $t = 0$. Therefore, the claim follows by induction on t. $\qquad\square$

2.9   Proof of Lemma 2.2

The proof is by induction. Pick a solution pair $(x, (y, \phi, \delta))$ to (2.5), and assume that $\Psi_i^\star(t) \geq \Psi_i^L(t)$ for some $t \in \mathbb{N}$, then in view of (2.7) and (2.13), we obtain

$$\begin{aligned}
\Psi_i^\star(t+1) &= \frac{\mu_i}{d_i} \sum_{k \in I_i} \Psi_k^\star(t) + (1 - \mu_i)\phi_i^\star(t)\phi_i^\star(t)^\top \\
&= \Psi_i^L(t+1) + \frac{\mu_i}{d_i}\left(\Psi_i^\star(t) - \Psi_i^L(t)\right) + \frac{\mu_i}{d_i} \sum_{k \in I_i \setminus \{i\}} \Psi_k^\star(t) \\
&\geq \Psi_i^L(t+1),
\end{aligned}$$

where we used the fact that $\Psi_k^\star(t) \geq 0$ for all $i, k \in \mathcal{N}$ and, by assumption, $\Psi_i^\star(t) \geq \Psi_i^L(t)$.

By arbitrariness of $t \in \mathbb{N}$, and since $\Psi_i^\star(0) = 0 \geq 0 = \Psi_i^L(0)$, then we conclude that $\Psi_i^\star(t) \geq \Psi_i^L(t)$ holds for all $t \in \mathbb{N}$. Thus, for all $t \in \mathbb{N}$, $\Psi_i^L(t) \geq \varepsilon_i I$ implies $\Psi_i(t) \geq \Psi_i^L(t) \geq \varepsilon_i I$. $\qquad\square$

2.10   Conclusions

We proposed a distributed recursive least squares algorithm for the estimation of an unknown parameter over a network. The main feature and novelty of this work consists in robustness to general bounded disturbances in an ISS sense, considering an errors-in-variables context. In addition to robustness and cooperative excitation, also convergence rate and scalability were discussed. Finally, a road pricing example was discussed and simulated.

The most important concept to be stressed is that this distributed identifier could be easily used in control problems like, for instance, cooperative adaptive output

regulation. Indeed, the ISS property of the identifier (usually not investigated in other works in distributed estimation literature) enables the use of canonical nonlinear control techniques such as small-gain methods for the analysis of the interconnection between controlled systems and identifiers.

Part II

Robust Adaptive Control of Multi-Agent Systems

Chapter 3

A distributed indirect adaptive approach to cooperative tracking in networks of uncertain single-input single-output systems

Current approaches to the cooperative control of network systems are based on a priori knowledge about the (follower) system dynamics: either the dynamics are known, or assumed to be minimum phase, or initial stabilizing controllers are available for each system. The purpose of this chapter is to show that for single-input single-output systems the above assumptions can be relaxed. We propose an indirect adaptive methodology that does not require the knowledge of the parameters of the systems, or the systems to be minimum phase, or initial stabilizing controllers, in order to guarantee asymptotic tracking.

3.1 Introduction

Cooperative output tracking refers to the problem of making a network of follower systems (hereafter referred to simply as systems) to track the behavior of a leader exosystem (hereafter referred to simply as exosystem). This problem can be viewed as a special case of cooperative output regulation, where tracking and disturbance rejection can be treated in a unified way, even for Multi-Input Multi-Output (MIMO) systems (Su and Huang, 2012a). Cooperation arises from solving the problem in a distributed way when not all systems in the network can access the signals of the exosystem: the main idea is that the systems not directly connected to the exosystem reconstruct the exosystem signals through communication with neighbors (Xiang, Wei, and Li, 2009). In the traditional formulations of cooperative tracking (see (Wang et al., 2010) for a linear example and (Isidori, Marconi, and Casadei, 2014) for a nonlinear one), the dynamics of the systems are considered to be perfectly known or belonging to a sufficiently small uncertainty set, and the exosystem dynamics are assumed to be globally known in the network. For example, in the linear case, the exosystem dynamics correspond to a multi-dimensional harmonic oscillator (Wieland, Sepulchre, and Allgöwer, 2011), whose frequencies are traditionally considered to be globally known in the network (Su, Hong, and Huang, 2013). However, in real-life networked environments, information is partial or not available. Therefore, it is desirable to consider cooperative tracking problems in which: (a) the dynamics of the systems involve large parametric uncertainties, and (b) the exosystem dynamics are not globally known. Different distributed observer designs with adaptive

gains have been used to reconstruct the state of the exosystem not only for homogeneous (Li et al., 2013) and heterogeneous (Li, Chen, and Ding, 2016) known system dynamics, but also for special classes of heterogeneous uncertain system dynamics (e.g. harmonic oscillators (Baldi and Frasca, 2019), Euler-Lagrange dynamics (Abdessameud, Tayebi, and Polushin, 2017; Feng et al., 2018), dynamics in model reference form (Harfouch, Yuan, and Baldi, 2018) or observer canonical form (Ding, 2017)).

When the leader exosystem dynamics are not globally known, it has been assumed in (Cai et al., 2017) that the systems connected to the exosystem know the leader state matrix and share it across the network through consensus dynamics. Communicating such matrices in addition to the observer states requires extra communication. To avoid the use of extra communication, estimation techniques for the exosystem dynamics have been combined with: robust designs where the dynamics of the (follower) systems belong to a sufficiently small uncertainty set (Wu et al., 2017); learning-based designs where the dynamics of the (follower) systems are unknown but an initial stabilizing controller is assumed to be available for each system(Modares et al., 2016); cooperative output regulation designs with asymptotic (Wang and Huang, 2019) or exponential (Wang and Huang, 2019) leader estimation, with known follower systems dynamics; and adaptive designs where the dynamics of the follower systems are unknown but with unitary relative degree and strongly minimum phase properties (Su and Huang, 2013).

The main contribution of this chapter is to show that, for Single-Input Single-Output (SISO) linear time-invariant systems, the cooperative tracking problem can be solved without any a priori knowledge about both the exosystem and system dynamics. In addition, the system dynamics are allowed to be non-minimum phase. Our approach is an adaptive methodology consisting of three steps. The first step involves an on-line fully-distributed estimation of the unknown exosystem frequencies. The second step involves the on-line estimation of the unknown parameters of a minimum state-space realization, considered without loss of generality, of the systems in the network. Finally, in the third step, all the estimated parameters are used on-line to solve a set of regulator equations, i.e. the resulting controller is an adaptive version of the so-called feedforward approach to distributed tracking (Su and Huang, 2012b; Lv et al., 2016).

The novelty of this work is to show analytically that the distributed exosystem (leader) estimator can work in synergy with local estimators, that estimate in real time the unknown parameters of the (follower) systems. Even though the methodology is developed for SISO systems by using a rich library of tools from (Ioannou and Sun, 2012), it is a starting point for extending the approach to more general MIMO systems.

3.2 Notation and Basic Concepts of Graph Theory

The transpose of a matrix or of a vector is indicated with X^T and x^T respectively. The $q-$th element of a vector v is indicated by v_q. The $n \times n$ identity matrix is denoted by I_n. If $A \in \mathbb{R}^{m \times n}$ and $B \in \mathbb{R}^{p \times q}$, then their Kronecker product is the $mp \times nq$ block matrix

$$A \otimes B = \begin{bmatrix} a_{11}B & \cdots & a_{1n}B \\ \vdots & \ddots & \vdots \\ a_{m1}B & \cdots & a_{mn}B \end{bmatrix}$$

where a_{ij} are the entries of matrix A. A diagonal matrix $\Delta = \text{diag}(\delta_1, \delta_2, \dots, \delta_n)$ is denoted as $\text{diag}(\delta_k)_{\overline{n}}$; a block-diagonal matrix is denoted as $\Delta = \text{bdiag}(\Delta_k)_{\overline{n}}$. A matrix $M \in \mathbb{R}^{n \times n}$ is said to be negative definite if, for every non-zero vector $x \in \mathbb{R}^n$, it results $x^T M x < 0$. A vector signal $x(\cdot)$ is said to belong to $\mathcal{L}_2$ ($x \in \mathcal{L}_2$) if $\int_0^\infty \|x(\tau)\|^2 \, d\tau < \infty$. A vector signal $x(\cdot)$ is said to belong to $\mathcal{L}_\infty$ ($x \in \mathcal{L}_\infty$) if $\max\limits_{t \geq 0} \|x(t)\| < \infty$.

We consider networks of dynamical systems (also referred to as nodes), which are linked to each other via a *communication graph*, that describes the allowed information flow. In other words, we say that system *i* has a *directed* connection to system *j* if the second can receive information from the first. When the information can flow in both directions, the connection is said to be *undirected*. In a communication graph, a special role is played by the *leader* node, which is a system (typically indicated as system 0) that does not receive information from any other system in the network. The communication graph describing the allowed information flow between all the systems, *leader excluded*, is completely defined by the pair $\mathcal{G} = (\mathcal{V}, \mathcal{E})$, where $\mathcal{V} = \{1, \dots, N\}$ is a finite nonempty set of nodes, and $\mathcal{E} \subseteq \mathcal{V} \times \mathcal{V}$ is a set of pairs of nodes, called edges. To include the presence of the leader in the network we define $\bar{\mathcal{G}} = \{\mathcal{V}, \mathcal{E}, \mathcal{T}\}$, where $\mathcal{T} \subseteq \mathcal{V}$ is the set of those nodes, called *target nodes*, which receive information from the leader. Figure 3.1 provides a simple example of how $\mathcal{V}$, $\mathcal{E}$, and $\mathcal{T}$ can be defined. Two square matrices are instrumental to find many

$$\mathcal{G} = \{\mathcal{V}, \mathcal{E}\} \qquad \bar{\mathcal{G}} = \{\mathcal{V}, \mathcal{E}, \mathcal{T}\}$$
$$\mathcal{V} = \{1, 2, 3, 4\} \qquad \mathcal{T} = \{1\}$$
$$\mathcal{E} = \{(1,2), (2,1), (1,3), (3,1),$$
$$(3,2), (2,3), (3,4), (4,3)\}$$
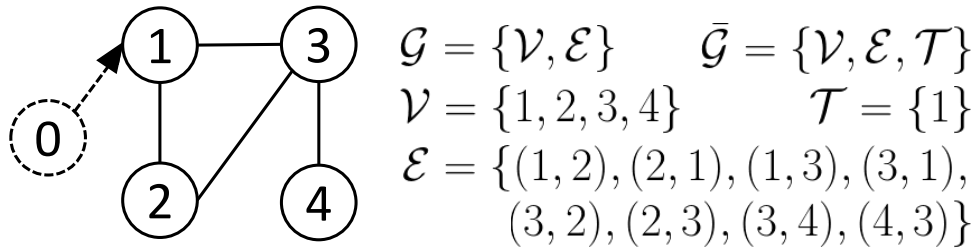
FIGURE 3.1: Example of communication graph.

useful properties of a communication graph: the *adjacency matrix* $\mathcal{A} = [a_{ij}] \in \mathbb{R}^{N \times N}$ and the *Laplacian matrix* $\mathcal{L} = [l_{ij}] \in \mathbb{R}^{N \times N}$. Specifically, the adjacency matrix of an undirected communication graph is defined as $a_{ii} = 0$ and $a_{ij} = a_{ji} = 1$ if $(i, j) \in \mathcal{E}$, where $i \neq j$; the Laplacian matrix is defined as $l_{ii} = \sum_j a_{ij}$ and $l_{ij} = -a_{ij}$, if $i \neq j$. The adjacency and Laplacian matrices corresponding to the example in Figure 3.1 are

$$\mathcal{A} = \begin{bmatrix} 0 & 1 & 1 & 0 \\ 1 & 0 & 1 & 0 \\ 1 & 1 & 0 & 1 \\ 0 & 0 & 1 & 0 \end{bmatrix}, \quad \mathcal{L} = \begin{bmatrix} 2 & -1 & -1 & 0 \\ -1 & 2 & -1 & 0 \\ -1 & -1 & 3 & -1 \\ 0 & 0 & -1 & 1 \end{bmatrix}.$$

In addition, we use a square diagonal matrix, the *target matrix* $\mathcal{M} = [m_{ij}] \in \mathbb{R}^{N \times N}$, to describe the directed communication of the leader with the target nodes. The target matrix is defined as $m_{ii} = 1$ if $i \in \mathcal{T}$ and $m_{ii} = 0$ otherwise. In the example of Figure 3.1, we have $\mathcal{M} = \text{diag}(1,0,0,0)$. An undirected graph $\mathcal{G}$ is said to be *connected* if, taken any arbitrary pair of nodes (i, j) where $i, j \in \mathcal{V}$, there is a path that leads from i to j (the graph $\mathcal{G}$ in Figure 3.1 is undirected and connected). Finally, let us define the *leader-follower topology matrix* as $\mathcal{B} = \mathcal{L} + \mathcal{M}$. When $\mathcal{L}$ is the Laplacian matrix of an undirected and connected graph, $\mathcal{B}$ is positive definite by construction.

3.3   Problem formulation

The following network of N heterogeneous uncertain SISO systems is considered

$$
y_i = \frac{b_{i,1}s^{n_i-1} + \ldots + b_{i,n_i-1}s + b_{i,n_i}}{s^{n_i} + a_{i,1}s^{n_i-1} + \ldots + a_{i,n_i-1}s + a_{i,n_i}} u_i
$$

$$
i \in \mathcal{V} = \{1, 2, \ldots, N\}
$$

(3.1)

whose minimal state-space realization in the observable form is given, without loss of generality, as:

$$
\dot{x}_i = \underbrace{\begin{bmatrix} -a_{i,1} & & \\ \vdots & & I_{n_i-1} \\ -a_{i,n_i} & 0 \cdots 0 \end{bmatrix}}_{A_i} x_i + \underbrace{\begin{bmatrix} b_{i,1} \\ \vdots \\ b_{i,n_i} \end{bmatrix}}_{b_i} u_i
$$

$$
y_i = \underbrace{\begin{bmatrix} 1 & 0 & \cdots & 0 \end{bmatrix}}_{c_i^T} x_i , \quad i \in \mathcal{V}
$$

(3.2)

where $x_i \in \mathbb{R}^{n_i}$, $u_i \in \mathbb{R}$, $y_i \in \mathbb{R}$ are the state, the control input, and the output of the i-th system, respectively. The coefficients of the numerator and denominator polynomials in (3.1) which appear as entries of $A_i \in \mathbb{R}^{n_i \times n_i}$ and $b_i \in \mathbb{R}^{n_i}$, are *unknown* constants.

The control objective is to design, for every system (3.2), a distributed control strategy for u_i, that makes each y_i track the output of an exosystem, or leader system. The exosystem is a multi-dimensional harmonic oscillator described by the following equations

$$
\dot{v} = \underbrace{\mathrm{bdiag}\left(\begin{bmatrix} 0 & \omega_k \\ -\omega_k & 0 \end{bmatrix} \right)_{\overleftarrow{q/2}}}_{S} v , \quad v(0) = \begin{bmatrix} v_1(0) \\ \vdots \\ v_q(0) \end{bmatrix}
$$

$$
r = \underbrace{\begin{bmatrix} \overbrace{0\ 1}^{q/2 \text{ times}} & 0\ 1 & \cdots & 0\ 1 \end{bmatrix}}_{c_0^T} v
$$

$$
e_i = y_i - r = c_i^T x_i - c_0^T v
$$

(3.3)

where $\omega_k > 0$, $k = 1, \ldots, q/2$, are the frequencies of the leader system, which are distinct and assumed to be *unknown* to all systems in the network. The exosystem is marginally stable, because the frequencies ω_k are assumed to be distinct. Each pair k of initial conditions $[v_{2k-1}(0)\ v_{2k}(0)]^T$, $k = 1, \ldots, q/2$, in (3.3) should be nonzero (in order to generate harmonics with nonzero amplitude). In (3.3), $v \in \mathbb{R}^q$ is the leader state, $r \in \mathbb{R}$ is the reference signal to be tracked, and $e_i \in \mathbb{R}$ is the tracking error to be driven to zero. It is worth remarking that, when the state of the exosystem is fully measurable and available to the target nodes, the structure of the exosystem is in practice completely determined by the user (Su and Huang, 2012a; Su and Huang, 2012b; Lv et al., 2016). In this work we consider the exosystem structure (3.3) (generator of harmonics), with unknown parameters.

A scalar integrator $\dot{v}_{q+1} = 0$, $v_{q+1}(0) \neq 0$, $c_{0\,q+1}^T = 1$, can be added to the blocks of (3.3) to generate as output r a sum of harmonics with nonzero offset. In such

case the results of this chapter follow accordingly with minor modifications since no additional unknown parameters need to be estimated.

The following standard assumptions are made.

Assumption 3.1. *The pairs (A_i, b_i) are controllable, the pairs (c_i, A_i) are observable, and n_i is known, $\forall\, i \in \mathcal{V}$.*

Assumption 3.2. *The zeros of (3.1) do not coincide with the eigenvalues of S.*

Assumption 3.3. *The order q of the exosystem is known and satisfies $\frac{q}{2} \geq \bar{n} = \max_i n_i$.*

Assumption 3.4. *The graph $\mathcal{G}$ of the leaderless network is undirected and connected, and the leader interacts with at least one system ($\mathcal{T} \neq \varnothing$).*

Remark 3.1. *Assumption 2 is sufficient to guarantee the existence of solution pairs (X_i, p_i), $\forall\, i \in \mathcal{V}$ to the linear regulator equations (Francis, 1977)*

$$\begin{aligned} X_i S &= A_i X_i + b_i p_i^T \\ 0 &= c_i^T X_i - c_0^T \ . \end{aligned} \tag{3.4}$$

Equations (3.4), whose solutions are used to solve the tracking problem, can be expressed in the compact form

$$Q_i \xi_i = \beta_i \tag{3.5}$$

where

$$\xi_i = \vec{2}\left(\begin{bmatrix} X_i \\ p_i^T \end{bmatrix}\right), \quad \beta_i = \vec{2}\left(\begin{bmatrix} 0 \\ -c_0^T \end{bmatrix}\right), \tag{3.6}$$

$$Q_i = S^T \otimes \begin{bmatrix} I_{n_i} & 0 \\ 0 & 0 \end{bmatrix} - I_q \otimes \begin{bmatrix} A_i & b_i \\ c_i^T & 0 \end{bmatrix}. \tag{3.7}$$

Assumption 3 guarantees the correct identification of all parameters in (3.1) and, as later explained in Remark 5, provides a less restrictive external probing as compared to existing approaches (Modares et al., 2016).

We are now ready to give the problem formulation.

Problem 3.1. *Under Assumptions 1-4, given the network of uncertain systems (3.2) with uncertain exosystem (3.3), design distributed adaptive control laws u_i such that the signals of the closed-loop network system are bounded, and the tracking errors e_i satisfy*

$$\lim_{t \to \infty} e_i(t) = 0, \quad \forall\, i \in \mathcal{V}.$$

Remark 3.2. *Solving Problem 3.1 in a distributed way presents at least three challenges: (a) the exosystem frequencies are unknown to all systems; (b) the parameters in (3.2) are unknown; (c) the solutions to the regulator equations (3.4) are unknown as they depend on unknown parameters. In our approach to be presented in the subsequent sections we use on-line parameter estimators and adaptive control techniques (Ioannou and Sun, 2012) to deal with the unknown parameters.*

3.4 Distributed exosystem estimator

The first step for solving Problem 3.1 is the design of a distributed exosystem estimator. The task of such estimator, as sketched in Figure 3.2, is to estimate S for all systems, and to reconstruct the state v for the non-target nodes (the exosystem state v
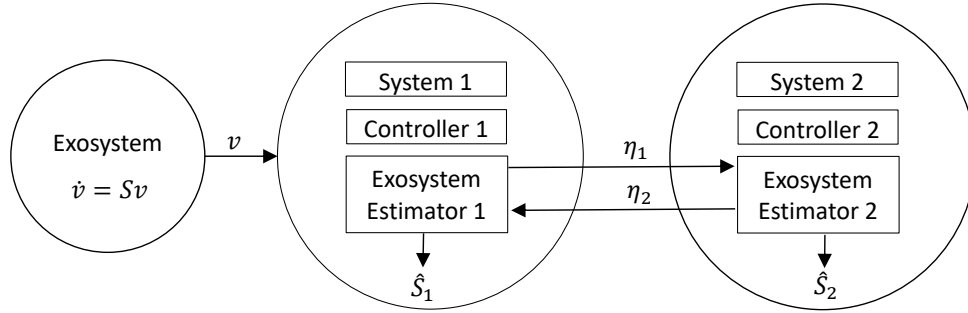
FIGURE 3.2: To reconstruct the exosystem state, non-target nodes exchange auxiliary variables according to the communication graph.

is available only to the target nodes through m_{ii}). In the following, time dependence is omitted whenever obvious.

Let us start by defining the local observation error for system i:

$$\epsilon_i = \sum_{j=1}^{N} a_{ij}(\eta_i - \eta_j) + m_{ii}(\eta_i - v), \tag{3.8}$$

where a_{ij} and m_{ii} come from the adjacency and the target matrices, and η_i represents the locally reconstructed exosystem state for system i. Note that the error in (3.8) represents a *consensus* error over the variable of interest v; in other words, $\epsilon_i \to 0 \; \forall i \in \mathcal{V}$ implies the local reconstruction of the exosystem state, $\eta_i \to v \; \forall i \in \mathcal{V}$.

To represent the variables for the overall network in a compact form, we use the Kronecker product. After defining $\eta = [\eta_1^T, \eta_2^T, \ldots, \eta_N^T]^T \in \mathbb{R}^{Nq}$ and $v_m = [v^T, v^T, \ldots, v^T]^T \in \mathbb{R}^{Nq}$, it is easy to write the overall observation error $\epsilon = [\epsilon_1^T, \epsilon_2^T, \ldots, \epsilon_N^T]^T$, stemming from (3.8), as

$$\epsilon = (\mathcal{L} \otimes I_q)\eta + (\mathcal{M} \otimes I_q)(\eta - v_m).$$

Exploiting the fact that $(\mathcal{L} \otimes I_q)v_m = 0$ (Gibson, 2016), we can write

$$\epsilon = (\mathcal{B} \otimes I_q)(\eta - v_m).$$

The design of the distributed exosystem estimator is provided by the following theorem.

Theorem 3.1. *Under Assumption 4, consider the following distributed dynamics for η_i*

$$\dot{\eta}_i = \hat{S}_i \eta_i + (A_m - \hat{S}_i)\epsilon_i \tag{3.9}$$

with the following Hurwitz diagonal matrix $A_m \in \mathbb{R}^{q \times q}$

$$A_m = -\, bdiag\, (a_k \cdot I_2)_{\overleftarrow{q/2}}, \quad a_k > 0, \; k = 1, \ldots, q/2. \tag{3.10}$$

Furthermore, let us write η_i and ϵ_i component-wise as

$$\eta_i = \begin{bmatrix} \eta_{i,1} \\ \vdots \\ \eta_{i,q} \end{bmatrix}, \quad \epsilon_i = \begin{bmatrix} \epsilon_{i,1} \\ \vdots \\ \epsilon_{i,q} \end{bmatrix}, \tag{3.11}$$

and let $\hat{S}_i$ in (3.9) be

$$\hat{S}_i = bdiag\left(\begin{bmatrix} 0 & (\hat{\omega}_k)_i \\ -(\hat{\omega}_k)_i & 0 \end{bmatrix}\right)_{\overleftarrow{q/2}} \tag{3.12}$$

with $(\hat{\omega}_k)_i$ being the estimate of ω_k for system i, generated by

$$(\dot{\hat{\omega}}_k)_i = \kappa_k(\eta_{i,(2k-1)}\epsilon_{i,(2k)} - \eta_{i,(2k)}\epsilon_{i,(2k-1)}), \tag{3.13}$$

with initial conditions $(\hat{\omega}_k)_i(0)$ and where $\kappa_k > 0$ is a constant design gain.
Then, the adaptation laws (3.13) guarantee that $\eta_i \rightarrow v$ and $\hat{S}_i \rightarrow S$ as $t \rightarrow \infty$, $\forall i \in \mathcal{V}$.

Proof. The dynamics (3.9) can be equivalently written as a function of the local error (3.8) and of the estimation error $\tilde{S}_i = \hat{S}_i - S$

$$\dot{\eta}_i = S\eta_i + (A_m - S)\epsilon_i + \tilde{S}_i(\eta_i - \epsilon_i). \tag{3.14}$$

Moreover, by defining

$$\tilde{S}_d(t) = \text{diag}(\tilde{S}_1(t), \tilde{S}_2(t), \dots, \tilde{S}_N(t))$$

we can write (3.14) for the overall network as

$$\dot{\eta} = (I_N \otimes S)\eta + [I_N \otimes (A_m - S)]\epsilon + \tilde{S}_d(\eta - \epsilon). \tag{3.15}$$

Let us write the overall error dynamics, using (3.8) and (3.15) as

$$\begin{aligned} \dot{\epsilon} =& (\mathcal{B} \otimes I_q)(I_N \otimes S)(\eta - v_m) \\ &+ (\mathcal{B} \otimes I_q)[I_N \otimes (A_m - S)]\epsilon + (\mathcal{B} \otimes I_q)\tilde{S}_d(\eta - \epsilon) \\ =& [(I_N \otimes S) + (\mathcal{B} \otimes (A_m - S))]\epsilon + (\mathcal{B} \otimes I_q)\tilde{S}_d(\eta - \epsilon). \end{aligned} \tag{3.16}$$

Positive-definiteness of $\mathcal{B}$ leads to the existence of a unitary matrix $\mathcal{U} \in \mathbb{R}^{N \times N}$ such that $\mathcal{U}^T \mathcal{B}^{-1} \mathcal{U} = \text{diag}(\delta_1, \delta_2, \dots, \delta_N) \triangleq \Delta$, where δ_i, $i = 1, \dots, N$, are the eigenvalues of $\mathcal{B}$. This can be used to define the transformation $\epsilon = (\mathcal{U} \otimes I_n)\bar{\epsilon}$ with $\bar{\epsilon} = [\bar{\epsilon}_1^T, \bar{\epsilon}_2^T, \dots, \bar{\epsilon}_N^T]^T$ (Li et al., 2010). Consider the positive definite Lyapunov function candidate

$$V = \frac{1}{2}\epsilon^T(\mathcal{B}^{-1} \otimes I_q)\epsilon + \frac{1}{2}\sum_{i=1}^{N}\sum_{k=1}^{q/2}\frac{(\tilde{\omega}_k)_i^2}{\kappa_k} \tag{3.17}$$

where $(\tilde{\omega}_k)_i = (\hat{\omega}_k)_i - \omega_k$ is the estimation error on the k-th harmonic frequency for system i. Using (3.13), we have

$$
\begin{aligned}
\dot{V} =& \epsilon^T (\mathcal{B}^{-1} \otimes I_q) \left[(I_N \otimes S) + (\mathcal{B} \otimes (A_m - S)) \right] \epsilon \\
& + \epsilon^T (\mathcal{B}^{-1} \otimes I_q)(\mathcal{B} \otimes I_q)\tilde{S}_d(\eta - \epsilon) + \sum_{i=1}^{N} \sum_{k=1}^{q/2} \frac{(\tilde{\omega}_k)_i}{\kappa_k}(\dot{\hat{\omega}}_k)_i \\
=& \epsilon^T \left[(\mathcal{B}^{-1} \otimes S) + (I_N \otimes (A_m - S)) \right] \epsilon + \epsilon^T \tilde{S}_d(\eta - \epsilon) \\
& + \sum_{i=1}^{N} \sum_{k=1}^{q/2} \frac{(\tilde{\omega}_k)_i}{\kappa_k}(\dot{\hat{\omega}}_k)_i \\
=& \sum_{i=1}^{N} \bar{\epsilon}_i^T (\delta_i S + A_m - S)\bar{\epsilon}_i + \sum_{i=1}^{N} \epsilon_i^T \tilde{S}_i(\eta_i - \epsilon_i) \\
& + \sum_{i=1}^{N} \sum_{k=1}^{q/2} (\tilde{\omega}_k)_i (\eta_{i,(2k-1)}\epsilon_{i,(2k)} - \eta_{i,(2k)}\epsilon_{i,(2k-1)}).
\end{aligned}
\tag{3.18}
$$

Considering the first summation in the last equation of (3.18), we have that each matrix $\delta_i S - S + A_m$ is always negative definite for each i, since, for any non-zero vector $s \in \mathbb{R}^q$ we obtain

$$
\begin{aligned}
& \begin{bmatrix} s_1 & \cdots & s_q \end{bmatrix} \operatorname{bdiag}\left(\begin{bmatrix} -a_k & \omega_k(\delta_i - 1) \\ -\omega_k(\delta_i - 1) & -a_k \end{bmatrix} \right)_{\overleftarrow{q/2}} \begin{bmatrix} s_1 \\ \vdots \\ s_q \end{bmatrix} \\
& = - \sum_{j=0}^{(q/2)-1} \sum_{k=1}^{q/2} a_k \left(s_{2j+1}^2 + s_{2j+2}^2 \right).
\end{aligned}
\tag{3.19}
$$

Considering now the second summation in the last equation of (3.18), we can write for system i

$$
\begin{aligned}
& \begin{bmatrix} \epsilon_{i,1} & \cdots & \epsilon_{i,q} \end{bmatrix} \operatorname{bdiag}\left(\begin{bmatrix} 0 & (\tilde{\omega}_k)_i \\ -(\tilde{\omega}_k)_i & 0 \end{bmatrix} \right)_{\overleftarrow{q/2}} \begin{bmatrix} \eta_{i,1} - \epsilon_{i,1} \\ \vdots \\ \eta_{i,q} - \epsilon_{i,q} \end{bmatrix} \\
& = \sum_{i=1}^{N} \sum_{k=1}^{q/2} (\tilde{\omega}_k)_i (\eta_{i,(2k-1)}\epsilon_{i,(2k)} - \eta_{i,(2k)}\epsilon_{i,(2k-1)}).
\end{aligned}
$$

Therefore, we have

$$
\dot{V} = \sum_{i=1}^{N} \bar{\epsilon}_i^T (\delta_i S + A_m - S)\bar{\epsilon}_i
\tag{3.20}
$$

which is negative semi-definite in view of (3.19). Since $V > 0$ and $\dot{V} \leq 0$, $V(t)$ is non-increasing and bounded from below by zero, which implies the existence of a limit

$$
\lim_{t \to \infty} V(\epsilon(t), \tilde{\Omega}(t)) = V_\infty < \infty
\tag{3.21}
$$

where $\tilde{\Omega} = [(\tilde{\omega}_1)_1...(\tilde{\omega}_{q/2})_1...(\tilde{\omega}_1)_N...(\tilde{\omega}_{q/2})_N]$ collects all the parametric errors. Boundedness of $V(t)$ implies that the error ϵ and the estimates $\tilde{\Omega}_k$ are bounded functions of time. Furthermore, we derive that $\dot{V}(t)$ is a uniformly continuous function of time

because $\ddot{V}(t)$ is a uniformly bounded function of time. In fact

$$\ddot{V} = 2 \sum_{i=1}^{N} \bar{\epsilon}_i^T (\delta_i S + A_m - S)\dot{\bar{\epsilon}}_i \tag{3.22}$$

where boundedness of $\dot{\bar{\epsilon}}_i$ follows by using (3.16), after noticing that: the homogeneous part of (3.16) leads to an exponentially stable system; the input term in (3.16) is a bounded function of time because ϵ and $\tilde{\Omega}_k$ are bounded. From Barbalat's lemma (Ioannou and Sun, 2012, Lemma 3.2.6), we conclude that $\dot{V} \to 0$ as $t \to \infty$ and hence $\epsilon \to 0$. Therefore $\eta_i \to v$ is derived, $\forall i \in \mathcal{V}$.

The fact that $\hat{S}_i$ converges to S is derived as follows. Since v is the state of a harmonic oscillator with distinct frequencies, it is persistently exciting, i.e. it satisfies the property

$$\int_t^{t+T_0} v(\tau)v^T(\tau)\mathrm{d}\tau \geq \alpha_0 T_0 I$$

for some $T_0, \alpha_0 > 0$ and for all $t > 0$ (Ljung, 1999, Definition 13.1),(Wang and Huang, 2019, Lemma 3). By considering (3.16) and applying convergence properties of adaptive systems (Jenkins et al., 2018, Theorem 4), that $(\hat{\omega}_k)_i \to \omega_k$, i.e. $\hat{S}_i \to S$ (see also (Yuan, De Schutter, and Baldi, 2017, Theorem 2) and (Wang and Huang, 2019, Lemma 3) for analogous convergence properties). This concludes the proof. □

Remark 3.3. *It is interesting to notice that the term $\hat{S}_i\epsilon_i$ in (3.9) could be in principle omitted due to the fact that $x^T S x = 0$ for any vector x and matrix S with structure as in (3.3). This would make the proposed Theorem 3.1 consistent with Lemma 1 in (Wang and Huang, 2019), albeit obtained using a different Lyapunov function. The result in (Wang and Huang, 2019) was extended in (Wang and Huang, 2019) to show exponential convergence to the true exosystem parameters. However, compared to these works, two observations follow. The first one is that, making the distributed exosystem estimator work in sinergy with local estimators (so as to consider also unknown parameters for the systems in (3.1)) is an open problem in (Wang and Huang, 2019; Wang and Huang, 2019) which is solved in this chapter as described by Theorem 3.2 below. The second observation is that the observer structure (3.9), is consistent with the standard full-state measurement adaptive Luenberger observer in (Ioannou and Sun, 2012, Sect. 5.2.2). This structure can be applied even if skew-symmetry in (3.3) is lost. For instance, consider*

$$\dot{v} = \underbrace{bdiag\left(\begin{bmatrix} 0 & \bar{\omega}_k \\ -\omega_k & 0 \end{bmatrix}\right)_{\overleftarrow{q/2}}}_{S} v \tag{3.23}$$

with $\bar{\omega}_k, \omega_k > 0$, which is also able to generate distinct harmonics provided that the products $\omega_k\bar{\omega}_k$ are distinct for all k. Note that $x^T S x = 0$ does not hold anymore for (3.23). Nevertheless, using (3.9), the following estimators can be derived in place of (3.13):

$$(\dot{\hat{\bar{\omega}}}_k)_i = \kappa_k \epsilon_{i,(2k)} \big(\eta_{i,(2k-1)} - \epsilon_{i,(2k-1)}\big)$$
$$(\dot{\hat{\omega}}_k)_i = \kappa_k \epsilon_{i,(2k-1)} \big(\eta_{i,(2k)} - \epsilon_{i,(2k)}\big)$$

(derived along similar lines as the proof of Theorem 3.1). In this case, in place of (3.19) we have

$$-\sum_{j=0}^{(q/2)-1} \sum_{k=1}^{q/2} a_k \left(s_{2j+1}^2 + s_{2j+2}^2\right) + (\bar{\omega}_k - \omega_k)(\delta_i - 1)s_{2j+1}s_{2j+2}$$

which, using the necessary and sufficient Sylvester criterion, is negative definite if and only if $4a_k^2 - (\bar{\omega}_k - \omega_k)^2(\delta_i - 1)^2 > 0$, i.e. for an a_k large enough (call it a_k^*). To retain the fully distributed nature of Theorem 3.1 (convergence not requiring the knowledge of structural parameters of the communication graph), each system can adapt its own gain a_k in (3.10) (call such gain $(\hat{a}_k)_i$) according to the monotonically increasing law

$$(\dot{\hat{a}}_k)_i = \bar{\kappa}_\kappa \epsilon_i^T \epsilon_i$$

where $\bar{\kappa}_\kappa > 0$: convergence of η_i to v can be proven via the Lyapunov function candidate

$$V = \frac{1}{2}\epsilon^T(\mathcal{B}^{-1} \otimes I_q)\epsilon + \frac{1}{2}\sum_{i=1}^{N}\sum_{k=1}^{q/2}\left(\frac{(\tilde{\omega}_k)_i^2}{\kappa_k} + \frac{(\tilde{\bar{\omega}}_k)_i^2}{\kappa_k} + \frac{(\tilde{a}_k)_i^2}{\bar{\kappa}_\kappa}\right)$$

where $(\tilde{\omega}_k)_i = (\hat{\omega}_k)_i - \omega_k$, $(\tilde{\bar{\omega}}_k)_i = (\hat{\bar{\omega}}_k)_i - \bar{\omega}_k$, and $(\tilde{a}_k)_i = (\hat{a}_k)_i - a_k^*$. The details follow according to the proof of Theorem 3.1.

3.5 Adaptive observer and regulator equations

Since the states x_i are not measurable and the parameters in (3.2) are unknown, it is necessary to estimate them on-line simultaneously using an adaptive observer. We adopt a Luenberger observer where A_i, b_i are replaced with their estimates $\hat{A}_i$ and $\hat{b}_i$, that is

$$\dot{\hat{x}}_i = \underbrace{\begin{bmatrix} -\hat{a}_{i,1} & \\ \vdots & I_{n_i-1} \\ -\hat{a}_{i,n_i} & 0\cdots 0 \end{bmatrix}}_{\hat{A}_i}\hat{x}_i + \underbrace{\begin{bmatrix} \hat{b}_{i,1} \\ \vdots \\ \hat{b}_{i,n_i} \end{bmatrix}}_{\hat{b}_i}u_i + l_i(y_i - \hat{y}_i)$$

$$\hat{y}_i = \underbrace{[1\ 0\ \cdots\ 0]}_{c_i^T}\hat{x}_i$$

(3.24)

where $\hat{x}_i$ is the observed state and the time-varying observer gain $l_i(t)$ is

$$l_i(t) = \begin{bmatrix} a_{i,1}^* - \hat{a}_{i,1}(t) \\ \vdots \\ a_{i,n_i}^* - \hat{a}_{i,n_i}(t) \end{bmatrix}$$

and $a_{i,1}^*, \ldots, a_{i,n_i}^*$ are chosen as the coefficients of a stable polynomial. Several methods can be used to generate the parameter estimates $\hat{a}_{i,1}, \ldots, \hat{a}_{i,n_i}$ and $\hat{b}_{i,1}, \ldots, \hat{b}_{i,n_i}$ at each time t. The methods rely on expressing the system equation (3.1) in the form of a linear-in-the-parameter model (Ioannou and Sun, 2012, Sect. 2.4.1)

$$z_i = \theta_i^{*T}\phi_i$$

(3.25)

where z_i and ϕ_i are measurable from (filtered) input/output data as

$$z_i = \frac{s^{n_i}}{\Lambda_i(s)} y_i = y_i + \lambda_i^T \phi_{2_i}$$

$$\phi_i = \left[\frac{\alpha_{n_i-1}^T(s)}{\Lambda_i(s)} u_i, -\frac{\alpha_{n_i-1}^T(s)}{\Lambda_i(s)} y_i \right]^T = \left[\phi_{1_i}^T, \phi_{2_i}^T \right]^T$$

$$\Lambda_i(s) = s^{n_i} + \lambda_i^T \alpha_{n_i-1}(s)$$

$$\lambda_i = [\lambda_{n_i-1} \ \lambda_{n_i-2} \ \ldots \ \lambda_1 \ \lambda_0]^T$$

$$\alpha_{n_i-1}(s) = [s^{n_i-1} \ s^{n_i-2} \ \ldots \ s \ 1]^T$$

and the unknown coefficients of (3.1) are in the unknown vector

$$\theta_i^* = [b_{i,1} \ \ldots \ b_{i,n_i} \ a_{i,1} \ \ldots \ a_{i,n_i}]^T$$

with $\Lambda_i(s)$ a Hurwitz polynomial of degree n_i chosen by the designer. In view of (3.25), a possible adaptive law to estimate on-line θ_i^* is a gradient algorithm based on integral cost (Ioannou and Sun, 2012, Chap. 4.3.5)

$$\dot{\theta}_i = -\Gamma_i(\Psi_i \theta_i + \rho_i)$$

$$\dot{\Psi}_i = -\gamma_i \Psi_i + \frac{\phi_i \phi_i^T}{m_i^2}, \quad \Psi_i(0) = 0$$

$$\dot{\rho}_i = -\gamma_i \rho_i - \frac{z_i \phi_i^T}{m_i^2}, \quad \rho_i(0) = 0$$

(3.26)

with the following choices for the design parameters: $m_i^2 = 1 + n_{s_i}^2$, with n_{s_i} chosen so that $\phi_i/m_i \in \mathcal{L}_\infty$ (e.g., $n_{s_i}^2 = \alpha_i \phi_i^T \phi_i, \alpha_i > 0$); $\gamma_i > 0$; $\Gamma_i = \Gamma_i^T > 0$. The following convergence properties apply to (3.26).

Lemma 3.1. *(Ioannou and Sun, 2012, Theorem 4.3.3) The adaptive observer formed by combining the observer equation (3.24) and the adaptive law (3.26) based on the parametric model (3.25) guarantees that:*

   (i) all signals are uniformly bounded;

  (ii) $\dot{\theta}_i \in \mathcal{L}_2 \cap \mathcal{L}_\infty$ and $\theta_i \in \mathcal{L}_\infty$;

 (iii) the output observation error $\tilde{y}_i = y_i - \hat{y}_i$ converges to zero as $t \to \infty$;

 (iv) if u_i is sufficiently rich of order $2n_i$, then the state observation error $\tilde{x}_i = x_i - \hat{x}_i$ and the parameter error $\tilde{\theta}_i = \theta_i - \theta_i^*$ converge to zero with exponential rate of convergence.

In the following we show how to solve the regulator equations (3.4) on-line. Let us replace ξ_i and Q_i in (3.6) and (3.7) with

$$\hat{\xi}_i(t) = \text{vec}\left(\begin{bmatrix} \hat{X}_i(t) \\ \hat{p}_i^T(t) \end{bmatrix} \right),$$

$$\hat{Q}_i(t) = \hat{S}_i^T(t) \otimes \begin{bmatrix} I_{n_i} & 0 \\ 0 & 0 \end{bmatrix} - I_q \otimes \begin{bmatrix} \hat{A}_i(t) & \hat{b}_i(t) \\ c_i^T & 0 \end{bmatrix}$$

where $\hat{S}_i$ is provided by (3.13), $\hat{A}_i, \hat{b}_i$ are provided by (3.26), and $\hat{\xi}_i(t)$ collects the estimates $(\hat{X}_i, \hat{p}_i)$ of the solution to the regulator equations. Based on these estimates,

the regulator equations can be solved on-line via the systems of linear equations

$$\hat{Q}_i \hat{\xi}_i = \beta_i, \qquad \forall i \in \mathcal{V}. \tag{3.27}$$

The system of linear equations (3.27) can be regarded as a pointwise solution to the regulator equations. As known in indirect adaptive control literature (Ioannou and Sun, 2012, Chap. 7), from the properties of systems of linear equations we have that if $\hat{A}_i, \hat{b}_i$ converge to A_i, b_i, then $\hat{X}_i, \hat{p}_i$ converge to the actual solutions X_i, p_i, respectively. The existence and uniqueness of a solution to (3.27) is guaranteed provided that the estimates are controllable and observable, having zeros that do not coincide with the eigenvalues of S. As later explained in Remark 6, Assumption 3 guarantees that the estimates converge exponentially fast to a set in which the solution exists and is unique (which is in line with (Ioannou and Sun, 2012, Thm. 7.4.2, Sect. 7.6)).

Remark 3.4. *On-line solutions to the regulator equations are also proposed in (Cai et al., 2017; Wang and Huang, 2019) using estimates of the exosystem dynamics. The on-line solution (3.27) presented in this work involves the estimated dynamics of both the exosystem and the follower systems. The benefits of coping with such uncertainties are demonstrated by the simulations of Section VII.*

3.6 Main result

The solution to Problem 3.1 is obtained by combining the distributed exosystem estimators of Theorem 3.1 with the adaptive observers and the on-line solution to the regulator equations.

Theorem 3.2. *The control law composed of: the distributed exosystem estimators (3.9) with adaptive laws (3.13), the adaptive observers (3.26), the adaptive solutions of the regulator equations (3.27), and the output-feedback control input*

$$u_i(t) = -k_i^T(t)\hat{x}_i(t) + f_i^T(t)\eta_i(t) \tag{3.28}$$

where

$$f_i^T(t) = \hat{p}_i^T(t) + k_i^T(t)\hat{X}_i(t) \tag{3.29}$$

solves Problem 3.1 provided that the gains k_i, l_i are chosen such that

$$\hat{A}_i(t) - \hat{b}_i(t)k_i^T(t), \qquad \hat{A}_i(t) - l_i(t)c_i^T(t) \tag{3.30}$$

are Hurwitz[1].

Proof. First, we will prove persistency of excitation of the control input (3.28), that can be rewritten as

$$u_i(t) = -k_i^T(t)(\hat{x}_i(t) - \hat{X}_i\eta_i) + \hat{p}_i^T\eta_i. \tag{3.31}$$

Let us write the dynamics of $\hat{x}_i - \hat{X}_i\eta_i$

$$\begin{aligned}
\dot{\hat{x}}_i - \dot{\hat{X}}_i\eta_i - \hat{X}_i\dot{\eta}_i =& (\hat{A}_i - \hat{b}_i k_i^T)(\hat{x}_i - \hat{X}_i\eta_i) + l_i c_i^T(x_i - \hat{x}_i) \\
& - \dot{\hat{X}}_i\eta_i - \hat{X}_i(A_m - \hat{S}_i)\epsilon_i,
\end{aligned} \tag{3.32}$$

---

[1] Two strategies for choosing k_i, l_i are possible: (i) the eigenvalues in (3.30) are placed at fixed locations, in line with adaptive pole placement (Ioannou and Sun, 2012, Chap. 7); (ii) non-fixed locations are allowed, provided that the eigenvalues in (3.30) are slowly time-varying (i.e. their time variation is in $\mathcal{L}_2$ (Ioannou and Sun, 2012, Thm. 3.4.11)).

where we have substituted the regulator equation $\hat{X}_i \hat{S}_i = \hat{A}_i \hat{X}_i + \hat{b}_i \hat{p}_i^T$. By observing the terms on the right-hand side in (3.32), we have that $c_i^T(x_i - \hat{x}_i) \to 0$, $\epsilon_i \to 0$ (from Lemma 3.1 and Theorem 3.1, respectively). In addition, since $\dot{\hat{A}}_i, \dot{\hat{b}}_i \in \mathcal{L}_2 \cap \mathcal{L}_\infty$ from the properties of the estimator, the system of linear equations (3.27) allows us to conclude that $\dot{\hat{X}}_i \in \mathcal{L}_2 \cap \mathcal{L}_\infty$. Therefore, with $\hat{A}_i - \hat{b}_i k_i^T$ Hurwitz at every time instant and eventually slowly time-varying, using notions of input/output stability (Ioannou and Sun, 2012, Lemma 3.3.3), we obtain that $\hat{x}_i - \hat{X}_i \eta_i \in \mathcal{L}_2 \cap \mathcal{L}_\infty$. Therefore, using standard properties of persistently exciting signals (Ioannou and Sun, 2012, Lemma 4.8.3), we have that u_i is sufficiently rich of order $2\bar{n}$.

Now, define $\tilde{\chi}_i = x_i - X_i v$, $\tilde{u}_i = u_i - p_i^T v$, $\tilde{\eta}_i = \eta_i - v$, $f_i^{*T} = p_i^T + k_i^T X_i$, $\tilde{f}_i = f_i - f_i^{*T}$, and $\tilde{\zeta}_i = \hat{x}_i - X_i v$. By making use of the regulator equations, we obtain the closed-loop system

$$
\begin{aligned}
\dot{\tilde{\chi}}_i &= A_i \tilde{\chi}_i + b_i \tilde{u}_i \\
\dot{\tilde{\zeta}}_i &= \hat{A}_i \tilde{\zeta}_i + \hat{b}_i \tilde{u}_i + l_i c_i^T(\tilde{\chi}_i - \tilde{\zeta}_i) + \tilde{A}_i X_i v + \tilde{b}_i p_i^T v \\
e_i &= c_i^T \tilde{\chi}_i \\
\tilde{u}_i &= k_i^T(\tilde{\chi}_i - \tilde{\zeta}_i) - k_i^T \tilde{\chi}_i + \tilde{f}_i^T v + f_i^T \tilde{\eta}_i
\end{aligned}
\tag{3.33}
$$

which leads to the dynamics

$$
\begin{bmatrix} \dot{\tilde{\chi}}_i \\ \dot{\tilde{\chi}}_i - \dot{\tilde{\zeta}}_i \end{bmatrix} = \begin{bmatrix} \hat{A}_i - \hat{b}_i k_i^T & b_i k_i^T \\ 0 & \hat{A}_i - l_i c_i^T \end{bmatrix} \begin{bmatrix} \tilde{\chi}_i \\ \tilde{\chi}_i - \tilde{\zeta}_i \end{bmatrix}
$$
$$
+ \begin{bmatrix} -(\tilde{A}_i - \tilde{b}_i k_i^T)\tilde{\chi}_i + b_i \tilde{f}_i^T v + b_i f_i^T \tilde{\eta}_i \\ -\tilde{A}_i x_i - \tilde{b}_i u_i \end{bmatrix}.
\tag{3.34}
$$

Since the control input u_i is sufficiently rich of order $2\bar{n}$, we can conclude that the terms $\tilde{A}_i$ and $\tilde{b}_i$ in (3.34) converge to zero exponentially fast. Moreover, from Theorem 3.1 we know that $\tilde{\eta}_i \to 0$ and $\hat{S}_i \to S$ also exponentially fast. Now, we can conclude $\hat{X}_i \to X_i$ and $\hat{p}_i \to p_i$, which imply that $\tilde{f}_i \to 0$. Then, the Hurwitz and slowly time-varying properties of $\hat{A}_i - \hat{b}_i k_i^T$ and $\hat{A}_i - l_i c_i^T$ (that converge to $A_i - b_i k_i^T$ and $A_i - l_i c_i^T$, respectively) guarantee that $\tilde{\zeta}_i \to \tilde{\chi}_i \to 0$ exponentially, from which we obtain convergence of e_i to zero. This concludes the proof. $\square$

The following remarks apply to Theorem 3.2.

Remark 3.5. *In contrast to past approaches based on fixed-gain robust control (Wu et al., 2017), in Theorem 3.2 no assumption is made on the size of the parameter uncertainty set. Also, differently from the learning-based approach of (Modares et al., 2016), no initially stabilizing feedback is required. Note that learning-based solutions require injecting an external probing signal in the input to induce persistency of excitation (an input sufficiently rich of order $\frac{\bar{n}(\bar{n}+1)}{2} + \bar{n} + 1$ is required in (Modares et al., 2016) to estimate both the Lyapunov function and the control gains). In our case, the adaptive closed loop (3.34) reduces the requirements on the sufficiently richness of the input, which is only of order $2\bar{n}$.*

Remark 3.6. *Theorem 3.2 requires the estimated pairs $(\hat{A}_i, \hat{b}_i)$, $(c_i, \hat{A}_i)$ to be controllable and observable at every time instant (necessary and sufficient to have $\hat{A}_i - \hat{b}_i f_i^T$ and $\hat{A}_i - l_i c_i^T$ Hurwitz). Similarly, the zeros of the estimated system should not coincide with the eigenvalues of the estimated exosystem, which would guarantee Assumption 1 and 2 to be satisfied (and (3.27) to be solvable) for the estimated dynamics. This is in line with the*

well-known 'loss-of-controllability/observability' situation of indirect pole-placement adaptive control (Ioannou and Sun, 2012, Chap. 7), where the calculation of the controller parameters is performed based on estimated dynamics that must be controllable/observable at every time instant. In our case, a sufficiently rich input of order $2\bar{n}$ guarantees exponential convergence of the estimated parameters to their true values. Since the true parameters correspond to a controllable and observable system, it is implied by continuity that the estimated dynamics will enter in finite time a set where (3.27) is solvable (Ioannou and Sun, 2012; Elliott, Cristi, and Das, 1985; Bai and Sastry, 1987). If (3.27) is not solvable at a given time, it suffices to freeze the controller parameters to their previous values; then, exponential convergence guarantees that any loss-of-controllability/observability issue is removed in finite time.

3.7 Simulations

Four systems connected as in the communication graph of Figure 3.1 are used as numerical validation of the proposed approach. The exosystem, represented as system 0, is given by (3.3) with $\omega_1 = 3$ and $\omega_2 = 2$. The heterogeneous followers are given by (3.2) with:

$$
A_1 = \begin{bmatrix} -10.1 & 1 \\ -24.1 & 0 \end{bmatrix}, b_1 = \begin{bmatrix} 2.1 \\ 3.1 \end{bmatrix}, A_2 = \begin{bmatrix} -12.1 & 1 \\ -11.1 & 0 \end{bmatrix}, b_2 = \begin{bmatrix} 2.1 \\ 1.1 \end{bmatrix},
$$
$$
A_3 = \begin{bmatrix} 3.1 & 1 \\ -1.1 & 0 \end{bmatrix}, b_3 = \begin{bmatrix} 1.1 \\ 1.1 \end{bmatrix}, A_4 = \begin{bmatrix} 2.1 & 1 \\ -2.1 & 0 \end{bmatrix}, b_4 = \begin{bmatrix} 3.1 \\ 1.1 \end{bmatrix}.
$$

(3.35)

As in practice there is always some degree of uncertainty in the knowledge of the actual matrices (3.35), let us consider a case with good a priori knowledge, i.e. the initial estimates for the parameters of the systems are close to the actual parameters:

$$
\hat{A}_1 = \begin{bmatrix} -10 & 1 \\ -24 & 0 \end{bmatrix}, \hat{b}_1 = \begin{bmatrix} 2 \\ 3 \end{bmatrix}, \hat{A}_2 = \begin{bmatrix} -12 & 1 \\ -11 & 0 \end{bmatrix}, \hat{b}_2 = \begin{bmatrix} 2 \\ 1 \end{bmatrix},
$$
$$
\hat{A}_3 = \begin{bmatrix} 3 & 1 \\ -1 & 0 \end{bmatrix}, \hat{b}_3 = \begin{bmatrix} 1 \\ 1 \end{bmatrix}, \hat{A}_4 = \begin{bmatrix} 2 & 1 \\ -2 & 0 \end{bmatrix}, \hat{b}_4 = \begin{bmatrix} 3 \\ 1 \end{bmatrix}.
$$

(3.36)

Let us now consider three different settings of uncertainty:

- *Experiment 1.* The exosystem is perfectly known to system 1, and the a priori knowledge of the dynamics of the systems is given by (3.36). This corresponds to the setting in (Cai et al., 2017), after adding some small uncertainty to the dynamics of the systems;

- *Experiment 2.* The a priori knowledge of the dynamics of the systems is given by (3.36), and the exosystem frequencies are unknown to all systems, including system 1. No a priori knowledge of the frequencies is considered, i.e. the initial estimates are set to zero. This setting will be handled by the proposed method;

- *Experiment 3.* No a priori knowledge is available both for the exosystem (whose estimated frequencies are initialized to zero) and for the systems (whose estimated parameters are initialized to some quite arbitrary values). This large uncertainty setting will also be handled by the proposed method.

In all experiments, the initial state of the exosystem is $v(0) = [1, 0.2, 0.5, 1]^T$ and the states of the systems are initialized to zero.

For *Experiment 1*, we use the algorithm in (Cai et al., 2017) with gains $\mu_1 = \mu_2 = 10$ (gains for consensus over S and v) and $\mu_3 = 40$ (gain for the on-line solution to the regulator equations). The tracking errors are shown in Figure 3.3 and the consensus over S is shown in Figure 3.4. It can be noted that the algorithm in (Cai et al., 2017) contains a feedforward term which relies on the perfect knowledge of the dynamics of the systems. It is well known that, whenever a possibly small uncertainty in such dynamics is present as in the case of this experiment, asymptotic tracking will inevitably be lost (due to lack of robustness of the feedforward (Isidori, Marconi, and Serrani, 2012, Sect. 1.4),(Huang, 2004, Sect. 1.3)).

For *Experiment 2*, the matrices in (3.36) are used as initial conditions for the estimators (3.26). For the estimators made of (3.24) and (3.26), we choose the parameters $\alpha_i = 0.1$, $\gamma_i = 0.1$, $\Gamma_i = 180I_4$, $a^* = \begin{bmatrix} 15 & 56 \end{bmatrix}^T$ and $\Lambda_i(s) = s^2 + 2s + 1$. In addition, the proposed distributed exosystem estimator (3.9) has $A_m = -15I_4$, $\kappa_1 = \kappa_2 = 60$, and zero initial conditions for (3.13). Because the regulator equations (3.27) are solved on-line using the estimates of the parameters of the systems, the robustness issue highlighted in (Isidori, Marconi, and Serrani, 2012, Sect. 1.4) can be overcome, and the tracking errors in Figure 3.5 exhibit asymptotic convergence. Also, a transient comparable to that of Figure 3.3 can be noted. This can be explained by the fact, well known in adaptive control, that good initial estimates positively affect the transient performance. The estimates of the parameters of the systems start so close to their actual values that no plot is shown for compactness. It is also of interest to see the estimates of the exosystem in Figure 3.6, which show a different transient as compared to Figure 3.4: this is because the systems are not allowed to use an extra communication channel to do consensus over their estimates of S, but they can perform the estimation only by communicating η_i.
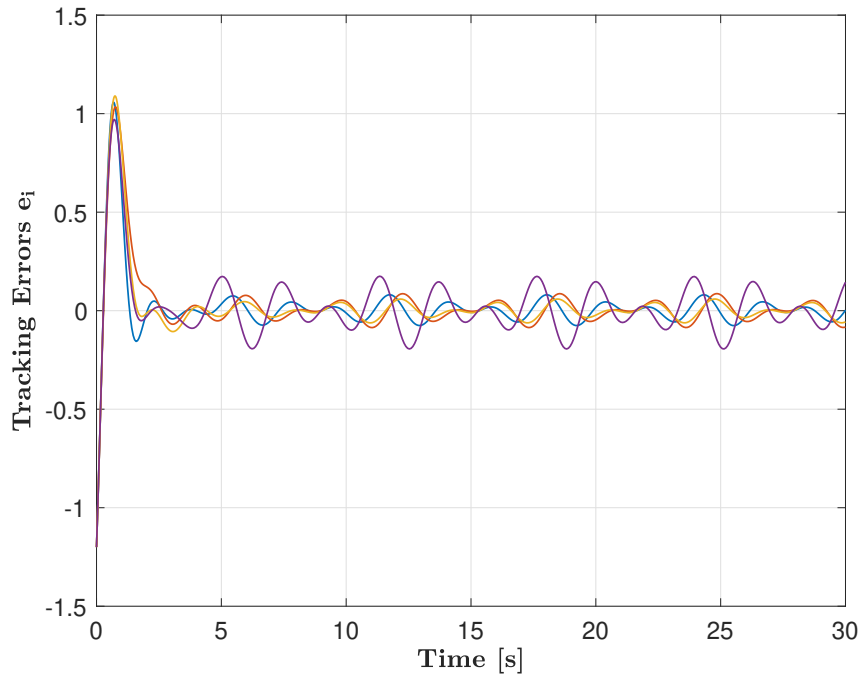
FIGURE 3.3: Experiment 1: tracking errors using the algorithm in (Cai et al., 2017).

Finally, for *Experiment 3*, the estimators (3.26) are initialized to $\theta_i(0) = [1, 1, 1, 1]^T$,
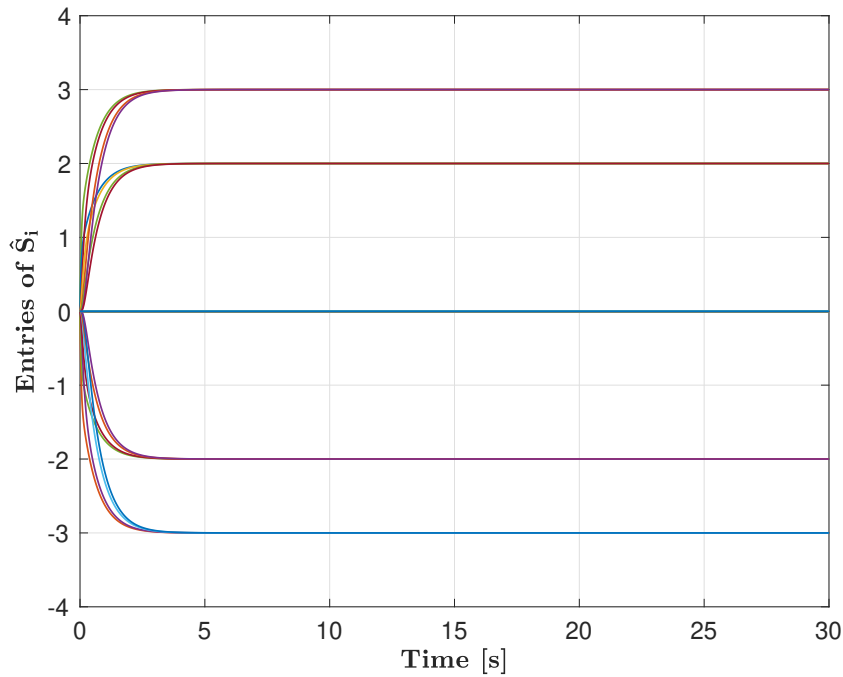
FIGURE 3.4: Experiment 1: estimates of the entries of the exosystem using the algorithm in (Cai et al., 2017).

$\forall i \in \mathcal{V}$ to represent poor a priori knowledge. This naturally results in a longer transient for the tracking errors in Figure 3.7, as compared to the one of Figure 3.5. On the other hand, the estimation of S is identical to Figure 3.6, and therefore not shown for compactness. Rather, in Figure 3.8 we show, for system 1, the convergence of the estimates $\hat{A}_1$, $\hat{b}_1$ to the actual A_1, b_1.

3.8 Conclusions

This chapter considers the problem of cooperative tracking in networks of linear SISO systems with unknown parameters, where the reference signal is generated by a linear exosystem with unknown harmonic frequencies. A stable fully-distributed indirect adaptive methodology consisting of three steps has been proposed, comprising: (i) distributed adaptation for estimating the exosystem dynamics; (ii) adaptive estimation of the parameters of each SISO system; (iii) on-line solution of the regulator equations using all the estimates.
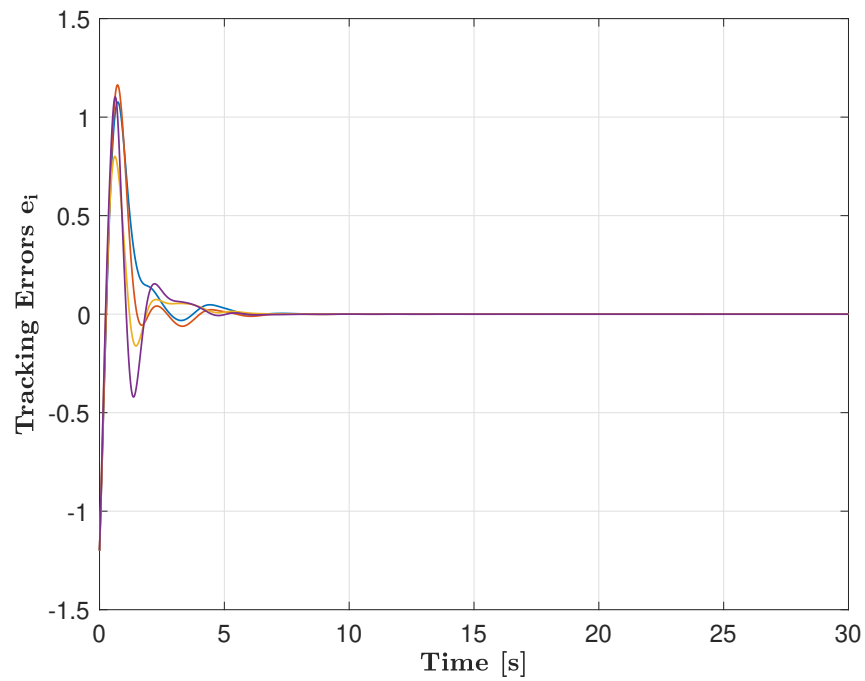
FIGURE 3.5: Experiment 2: tracking errors using the proposed approach.
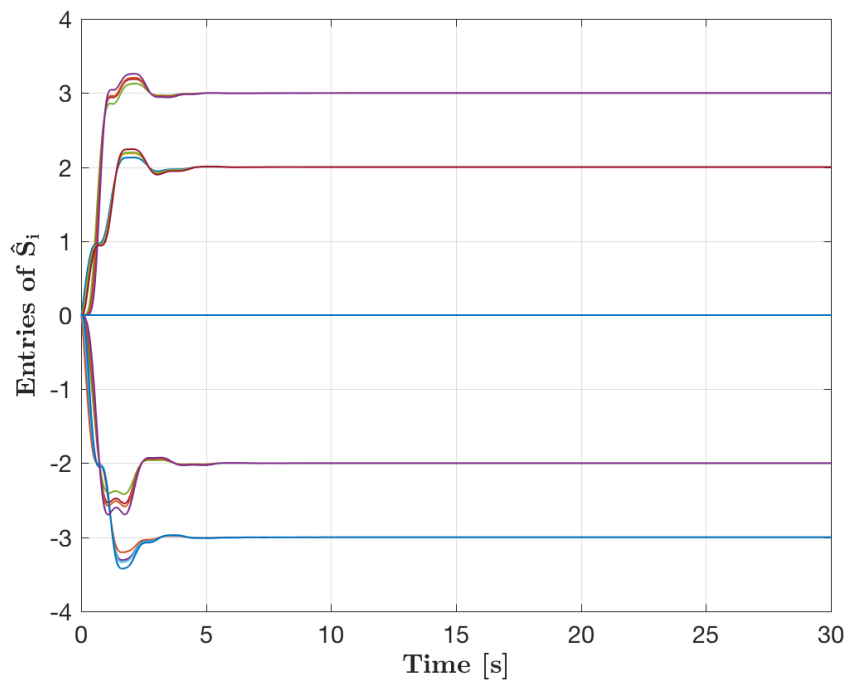
FIGURE 3.6: Experiment 2: estimates of the entries of the exosystem using the proposed approach.
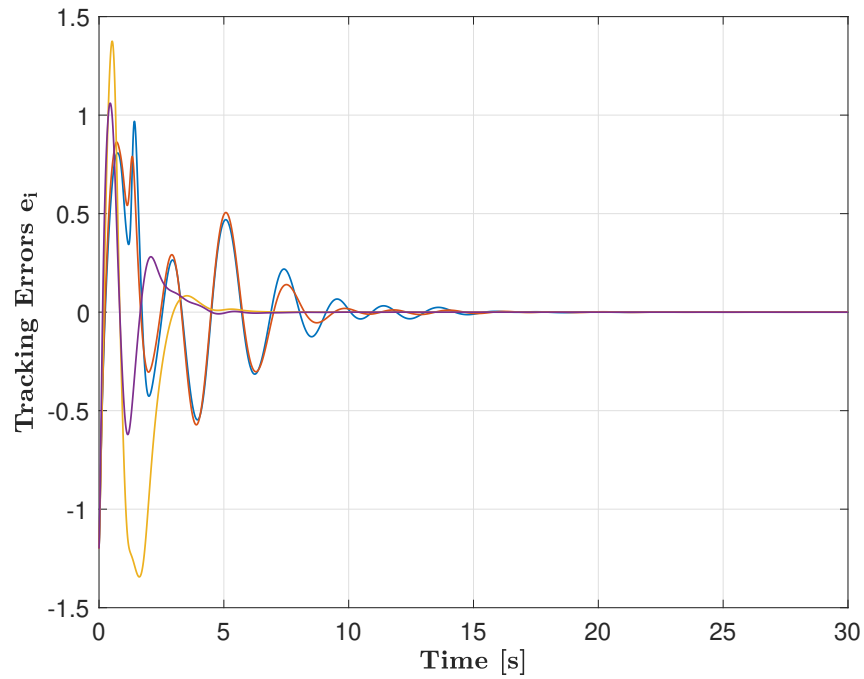
FIGURE 3.7: Experiment 3: tracking errors using the proposed approach.
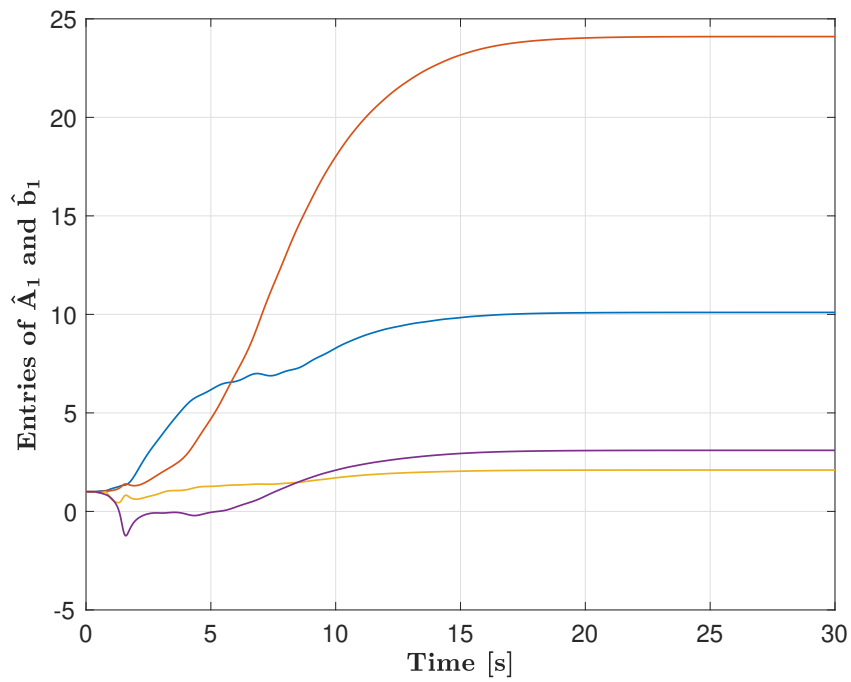
FIGURE 3.8: Experiment 3: estimates of A_1 and b_1 using the proposed approach.

Chapter 4

Adaptive Hybrid Control for Robust Global Phase Synchronization of Kuramoto Oscillators

In this chapter, a distributed controller is designed for robust global phase synchronization of a network of uncertain second-order Kuramoto oscillators with a leader system, modeled as a nonlinear autonomous exosystem. The phase angles being elements of the unit circle, we propose an adaptive hybrid strategy based on a hysteresis mechanism to obtain global results despite the well-known topological obstructions. Only an upper bound on the unknown parameters of the oscillators is required to keep the adaptive estimates in a compact set. Since the reference signal is not available to each network node, we design a distributed observer of the leader exosystem. Leveraging the results of hybrid systems theory, including reduction theorems, Lyapunov techniques, and properties of ω-limit sets, we prove robust global asymptotic stability of the closed-loop dynamics, despite the presence of an adaptive control law.

4.1 Introduction

Synchronization and coordination phenomena are ubiquitous in several application domains, including physics, engineering, biology, and social sciences. Particularly studied, in this context, are the dynamical behaviors arising from networks of interacting oscillators. To describe these behaviors, the Kuramoto model (Kuramoto, 1984) is certainly the most popular model due to its ability to capture complex nonlinear phenomena with appealing mathematical simplicity. The study of power networks (Guo et al., 2021; Dorfler and Bullo, 2012) or of connectivity patterns in the human brain (Menara et al., 2019; Qin et al., 2021) are just some examples where Kuramoto oscillators have been adopted.

In general, synchronization of Kuramoto oscillators may occur with or without a control input affecting the network. Concerning the uncontrolled scenario, significant efforts have been dedicated to studying the impact of couplings (either the network topology or the intensity of connections) on the synchronization properties of the trajectories (Ha, Ha, and Kim, 2010; Zhang and Xiao, 2014; Schmidt et al., 2012; Zhang and Zhu, 2019; Chopra and Spong, 2009; Dörfler and Bullo, 2011). In the controlled scenario, the emphasis is on finding an appropriate input to achieve synchronization (Moreira and Aguiar, 2019; Zhu and Hill, 2020). In this context, the

objective of leader-follower synchronization, also known as pacemaker-based synchronization (Wang and Doyle, 2013), becomes particularly relevant. The typical challenge in achieving leader-follower synchronization is that the controller of each node should employ only locally available quantities and variables shared according to a communication topology.

This work considers a second-order version of the original first-order Kuramoto model, where each oscillator has its own inertia (Dorfler and Bullo, 2012; Choi, Ha, and Yun, 2011) and is characterized by a phase angle and an angular frequency. We remark that further extensions have been recently proposed, including the third-order Kuramoto model (Wu and Chen, 2020), inspired by the transient behavior of power networks, or the generalization of the phase state space given by the Kuramoto model on Stiefel manifolds (Ha, Kang, and Kim, 2021), capable of including in a unified framework both the classical model and more complex structures such as the Lohe model (Markdahl, Proverbio, and Goncalves, 2020).

The focus of this work is to achieve *global* leader-follower phase synchronization in a network of second-order Kuramoto oscillators, without precise information of the model parameters. In the following, we review some representative results in the field, which clarify the motivations for our study.

4.1.1   Related works

It has been well recognized in the literature that the non-Euclidean nature of the state space of a Kuramoto model is the main obstruction for achieving global asymptotic convergence to the leader's phase reference. Several strategies have been proposed to deal with this obstruction. For example, a natural approach is to represent the phase of each oscillator as an element of the unit circle. It follows that the ensemble of the phase angles is an element of the N-torus (Scardovi, Sarlette, and Sepulchre, 2007).

One of the main advantages of employing the unit circle formalism is that phase synchronization can be reformulated as the attractivity of a compact set. Although this property is beneficial for control design, the N-torus is a non-Euclidean set, meaning that synchronization cannot be handled with the same tools used in linear consensus. In particular, the topological properties of a non-contractible space (i.e., not diffeomorphic to any Euclidean space) pose significant obstacles to *global stabilization through continuous feedback*. For instance, the continuous-time algorithms in (Scardovi, Sarlette, and Sepulchre, 2007) (and their corresponding discrete-time versions) lead to multiple equilibria in the state space, where only one of them corresponds to the desired configuration. The same issue is shared by several applications involving rotations. In the context of rigid body dynamics, only *almost global* results can be achieved with continuous laws for control (De Marco et al., 2016) and observation (Mahony, Hamel, and Pflimlin, 2008).

In recent years, it has been shown that robust global stabilization can be achieved on non-contractible spaces through dynamic *hybrid* (instead of continuous) feedback (Mayhew, Sanfelice, and Teel, 2011). Meaningful results have been proposed, e.g., for unit quaternions (Mayhew, Sanfelice, and Teel, 2011) through hysteresis-based techniques and for the N-sphere (Casau et al., 2019) via synergistic potential functions. Some efforts have also been dedicated to the unit circle (Mayhew and Teel, 2010). However, all of the above solutions have been developed in a single-agent scenario and in the absence of uncertain dynamics. One of the first attempts to present hybrid feedback in a multi-agent setting can be found in (Mayhew et al., 2011), for the special case of acyclic communication graphs.

Despite the progress in the field, some additional vital elements are needed for achieving global leader-follower synchronization of uncertain Kuramoto oscillators. Since no specific communication topology is imposed for the network, while the reference is not assumed to be globally available, it is necessary to ensure that each node reconstructs the leader signals. Additionally, the above-cited works have been developed under the assumption of complete knowledge of the parameters. The presence of model uncertainties complicates the asymptotic synchronization goal. Therefore, specific control solutions are needed to ensure robust asymptotic stability of the synchronization set.

4.1.2   Main contribution of this work

Motivated by the previous overview, we propose here a distributed scheme that solves the leader-follower problem by combining three components: (i) a distributed observer, used to reconstruct the reference in the nodes not directly connected to the leader; (ii) a hybrid stabilizer used to track the locally estimated reference and ensure, under parametric uncertainties, phase synchronization in a global sense; (iii) an adaptive mechanism to suitably handle the parametric uncertainties. Besides the technological interest of the synchronization problem at stake, for each one of the above components, we provide a solution of independent interest, whose novelty is highlighted next.

(i) About the distributed observer, we follow the idea that the unit circle, used to represent the phase angles, can be naturally embedded in $\mathbb{R}^2$. With this embedding, since the estimates are designed without being constrained on the unit circle, consensus techniques for Euclidean spaces can be employed to achieve global estimation of the leader signals. As compared with other solutions in the literature that follow the embedding approach (Cai and Huang, 2016; Gui and Ruiter, 2018), here we allow for more general structures of the exosystem: in particular, we consider exosystems admitting a feedback interconnection between the phase and frequency subsystems, whereas the literature in this field only handles cascaded interconnections. Exploiting input-to-state stability (ISS) and small-gain arguments, we prove global asymptotic reconstruction of the reference for a fairly general class of exosystems, which is a contribution of independent interest.

(ii) About the hybrid stabilizers at each node, to ensure compatibility with the adaptive mechanism, we revisit and extend the hysteresis-based hybrid solution originally proposed in (Mayhew, Sanfelice, and Teel, 2011) to deal with the topological obstructions associated with the unit circle. In particular, we augment the hybrid feedback with a first-order filter, so that the stabilizing input does not change across jumps, a key property for interlacing the hybrid stabilizer with the continuous-time adaptation commented below. Due to the simplicity of the condition on the filter time constant under which we prove stability, this dynamic extension is of independent interest and can be exploited in future works.

(iii) Finally, about our hybrid adaptation mechanism, we show that, with an appropriate robust modification of the adaptive law, it is possible to ensure the existence of a *robustly globally asymptotically stable attractor* for the tracking error system, without requiring any persistency of excitation. This result, which may sound atypical as compared to standard results in the adaptive control literature, represents a notable by-product of this work. Specifically, the powerful characterization of ω-limit sets of well-posed hybrid systems given in the hybrid systems formalism (Goebel,

Sanfelice, and Teel, 2012), together with a simple dead-zone-based projection mechanism for keeping the parameter estimates in a compact set, enables proving the existence of such a compact globally asymptotically stable attractor.

To conclude, we emphasize that the closed-loop asymptotic stability of the overall control scheme is analyzed through reduction theorems for hybrid systems. In particular, we prove that global phase synchronization is well represented as robust global asymptotic stabilization of a suitable compact set. We remark that the robustness of asymptotic stability is guaranteed in this context by the regularity properties of the feedback law and compactness of the characterized attractor. With respect to this point, let us comment on the interesting distributed quaternion synchronization in (Gui and Ruiter, 2018), achieved by combining a sliding-mode distributed observer and a hybrid stabilizer. In that work, unfortunately, the presence of static discontinuities makes it impossible to ensure the robustness properties established in this work.

A preliminary version of this study is given by (Bosso et al., 2021a). In this chapter we improve the work (Bosso et al., 2021a) in several directions. First of all, (Bosso et al., 2021a) considers the simplified case of known parameters of the Kuramoto oscillators. Therefore, several challenges related to including adaptation laws in a hybrid setting are addressed and solved here for the first time. Moreover, (Bosso et al., 2021a) only considers a simplified cascaded exosystem structure as in (Cai and Huang, 2016; Gui and Ruiter, 2018), whereas in this chapter we address nontrivial challenges emerging from feedback interconnections, requiring suitable small-gain approaches not present in (Bosso et al., 2021a). For example, the results of (Bosso et al., 2021a) cannot be applied to our simulation example.

4.2 Notation

$\mathbb{R}$ and $\mathbb{Z}$ denote the sets of real and integer numbers, while $\mathbb{R}_{\geq 0} := [0, \infty)$. The transpose of real-valued vectors and matrices is denoted with $(\cdot)^\top$, while $\otimes$ indicates the Kronecker matrix product. For any integer $n \geq 1$, I_n is the identity matrix of dimension n and $\mathbf{1}_n \in \mathbb{R}^n$ is the vector of all ones. With column vectors v and w, the notation (v, w) indicates the concatenated vector $[v^\top \ w^\top]^\top$. Finally, $\operatorname{diag}(a_1, \ldots, a_n)$ denotes the block-diagonal matrix with diagonal elements a_i, $i \in \{1, \ldots, n\}$.

Graph Theory

An undirected graph of order N is defined as $\mathcal{G} := \{\mathcal{V}, \mathcal{E}\}$, where $\mathcal{V} := \{1, \ldots, N\}$ is a finite non-empty set of nodes and $\mathcal{E} \subseteq \mathcal{V} \times \mathcal{V}$ is a set of non-ordered pairs of nodes, called edges. For each $i \in \mathcal{V}$, $\mathcal{N}_i := \{j \in \mathcal{V} : (i, j) \in \mathcal{E}\}$ is the set of neighbors of i. An undirected graph $\mathcal{G}$ is connected if, taken any arbitrary pair of nodes (i, j), $i, j \in \mathcal{V}$, there is a path from i to j. Given a leader node not included in $\mathcal{V}$, we denote with $\mathcal{T} \subseteq \mathcal{V}$ the set of target nodes, i.e., the set of nodes that receive information from the leader. For an undirected graph $\mathcal{G}$ with target nodes $\mathcal{T}$, the adjacency matrix $A = [a_{ij}] \in \mathbb{R}^{N \times N}$ is defined as $a_{ij} = a_{ji} = 1$ if $(i, j) \in \mathcal{E}$, $i \neq j$, and $a_{ij} = 0$ otherwise; the Laplacian matrix $L = [l_{ij}] \in \mathbb{R}^{N \times N}$ is defined as $l_{ii} = \sum_j a_{ij}$ and $l_{ij} = -a_{ij}$ if $i \neq j$, while the target matrix $T = [\tau_{ij}] \in \mathbb{R}^{N \times N}$ is a diagonal matrix such that $\tau_{ii} = 1$ if $i \in \mathcal{T}$ and $\tau_{ii} = 0$ otherwise. Finally, the matrix $B := L + T$ is denoted leader-follower matrix. For an undirected and connected graph $\mathcal{G}$ with $\mathcal{T} \neq 0$ (equivalently, such that $T \neq 0$), B is positive definite (Zhang and Lewis, 2012).

Hybrid Dynamical Systems

A hybrid dynamical system can be compactly described as (Goebel, Sanfelice, and Teel, 2012):

$$\mathcal{H} : \begin{cases} \dot{x} \in F(x), & x \in C \\ x^+ \in G(x), & x \in D \end{cases} \tag{4.1}$$

where $x \in \mathbb{R}^n$ is the state, $C \subset \mathbb{R}^n$ is the flow set, $F : \mathbb{R}^n \rightrightarrows \mathbb{R}^n$ is the flow map, $D \subset \mathbb{R}^n$ is the jump set, and $G : \mathbb{R}^n \rightrightarrows \mathbb{R}^n$ is the jump map. A solution of (4.1) can either flow according to the differential inclusion $\dot{x} \in F(x)$ when $x \in C$, or jump according to the difference inclusion $x^+ \in G(x)$ when $x \in D$. We refer to (Goebel, Sanfelice, and Teel, 2012; Goebel, Sanfelice, and Teel, 2009) for the main definitions and tools for the analysis of hybrid systems.

4.3 Model description

4.3.1 Second-Order Kuramoto Network

In this chapter, we consider a generalization of the celebrated Kuramoto model (Kuramoto, 1984), based on the *swing equations* described in (Dorfler and Bullo, 2012). More specifically, the *second-order Kuramoto network* is a system of N nonlinear oscillators, coupled through an undirected and connected graph $\mathcal{G} = \{\mathcal{V}, \mathcal{E}\}$:

$$\begin{aligned} \dot{\theta}_i &= \omega_i, & i \in \mathcal{V} \\ m_i \dot{\omega}_i &= -d_i \omega_i + \omega_{\text{n}i} + u_i - \sum_{j \in \mathcal{N}_i} k_{ij} \sin(\theta_i - \theta_j - \varphi_{ij}), \end{aligned} \tag{4.2}$$

where, for each $i \in \mathcal{V}$, $\theta_i \in \mathbb{R}$ and $\omega_i \in \mathbb{R}$ are the phase and the frequency, respectively, u_i is the control input, $m_i > 0$ is the oscillator's inertia, $d_i > 0$ is a damping constant, and $\omega_{\text{n}i}$ is the oscillator's natural frequency. In addition, $k_{ij} = k_{ji} > 0$ and $\varphi_{ij} = \varphi_{ji} \in [0, 2\pi)$ are, respectively, the coupling weight and the phase shift between oscillators i and j. Suppose that the graph $\mathcal{G}$, associated with the physical couplings in (4.2), also defines the communication topology among the nodes.

Define $\theta := \begin{bmatrix} \theta_1 & \dots & \theta_N \end{bmatrix}^\top \in \mathbb{R}^N$ and $\omega := \begin{bmatrix} \omega_1 & \dots & \omega_N \end{bmatrix}^\top \in \mathbb{R}^N$, then denote by $(\theta(\cdot), \omega(\cdot)) : \mathbb{R}_{\geq 0} \to \mathbb{R}^{2N}$ a solution of system (4.2), for some input signals $u_i(\cdot)$, $i \in \mathcal{V}$, and with initial conditions $(\theta(0), \omega(0))$. We say that $(\theta(\cdot), \omega(\cdot))$ achieves *phase synchronization* if

$$\lim_{t \to +\infty} \theta_i(t) - \theta_j(t) \in \left\{ \tilde{\theta} : \tilde{\theta} = 2k\pi, k \in \mathbb{Z} \right\}, \quad \forall i, j \in \mathcal{V}. \tag{4.3}$$

Similarly, the solution $(\theta(\cdot), \omega(\cdot))$ is said to achieve *frequency synchronization* if

$$\lim_{t \to +\infty} \omega_i(t) - \omega_j(t) = 0, \qquad \forall i, j \in \mathcal{V}. \tag{4.4}$$

For the network (4.2), our objective is to design a distributed strategy that ensures robust global phase synchronization to a reference trajectory. Namely, our aim is to define feedback laws for the inputs u_i based only on local information and network communication such that, for any initialization of system (4.2), the corresponding solution $(\theta(\cdot), \omega(\cdot))$ robustly achieves phase synchronization and convergence to the reference. When we refer to robust synchronization, we mean that (4.3) is obtained through asymptotic stability of a compact set, with appropriate robustness

to perturbations of the closed-loop dynamics. A precise definition of this concept is presented in Section 4.4.

Because we do not assume exact knowledge of the local parameters m_i, d_i, $\omega_{\mathrm{n}i}$, k_{ij}, and φ_{ij}, we design adaptive controllers that ensure asymptotic convergence in the presence of parametric uncertainties. At the same time, it is well known that the sensitivity of adaptive techniques to non-parametric (unmodeled) perturbations of the dynamics calls for a robust design of the adaptive law and some known bounds of the parametric uncertainty (see, e.g., (Ioannou and Sun, 2012, Chapters 8 and 9)). Accordingly, we impose the following assumption.

Assumption 4.1. *There exists a scalar $\rho > 0$, known to each node $i \in \mathcal{V}$, such that:*

$$
\begin{aligned}
m_i \leq \rho, \ d_i \leq \rho, \ |\omega_{\mathrm{n}i}| \leq \rho, &\qquad \forall i \in \mathcal{V}, \\
k_{ij} \leq \rho, &\qquad \forall i \in \mathcal{V}, \forall j \in \mathcal{N}_i,
\end{aligned}
\tag{4.5}
$$

where the bound ρ is taken to be the same for all parameters for simplicity of notation.

4.3.2 Quaternion-Inspired Representation

For control design, we propose to rewrite system (4.2) in a more convenient form. Motivated by the equivalence modulo 2π of the phases θ_i, also reflected in the phase synchronization condition (4.3), we choose to represent θ_i on the unit circle $\mathbb{S}^1 := \left\{ \begin{bmatrix} \alpha & \beta \end{bmatrix}^\top \in \mathbb{R}^2 : \alpha^2 + \beta^2 = 1 \right\}$. Recall that the compact set $\mathbb{S}^1$ has Lie group structure that is isomorphic to the group of planar rotations $\mathrm{SO}(2) := \{R \in \mathbb{R}^{2\times 2} : R^\top R = I_2, \det(R) = 1\}$. In view of such an isomorphism, we define the function $\mathcal{R} : \mathbb{S}^1 \to \mathrm{SO}(2)$, which maps any $\begin{bmatrix} \alpha & \beta \end{bmatrix}^\top \in \mathbb{S}^1$ into the corresponding rotation matrix:

$$
\mathcal{R}\left(\begin{bmatrix} \alpha \\ \beta \end{bmatrix} \right) := \begin{bmatrix} \alpha & -\beta \\ \beta & \alpha \end{bmatrix}.
\tag{4.6}
$$

Function $\mathcal{R}(\cdot)$ is useful to define the group multiplication between any $\xi, \hat{\xi} \in \mathbb{S}^1$ as $\mathcal{R}(\xi)\hat{\xi} = \mathcal{R}(\hat{\xi})\xi$ (note that $\mathbb{S}^1$ is Abelian, i.e., the group operation is commutative), where the identity element is given by

$$
e := \begin{bmatrix} 1 & 0 \end{bmatrix}^\top.
\tag{4.7}
$$

From the above definitions, we introduce the following representation for θ_i:

$$
\zeta_i := \begin{bmatrix} \eta_i & \epsilon_i \end{bmatrix}^\top := \begin{bmatrix} \cos(\theta_i/2) & \sin(\theta_i/2) \end{bmatrix}^\top \in \mathbb{S}^1,
\tag{4.8}
$$

corresponding to a unit quaternion for planar rotations (cf. (Mayhew, Sanfelice, and Teel, 2011) for the parameterization adopted for 3D rotations). We refer to (Bosso et al., 2021a) for a detailed discussion on representation (4.8) and its relation with the choices in (Bosso, Azzollini, and Baldi, 2019) and (Goebel, Sanfelice, and Teel, 2009, Example 34). Using (4.6) and (4.8), the phase dynamics on $\mathrm{SO}(2)$ and $\mathbb{S}^1$ is obtained as

$$
\frac{d}{dt}\mathcal{R}(\zeta_i) = \frac{1}{2}\omega_i J \mathcal{R}(\zeta_i), \quad \dot{\zeta}_i = \frac{1}{2}\omega_i J \zeta_i, \qquad i \in \mathcal{V},
\tag{4.9}
$$

where $J := \begin{bmatrix} 0 & -1 \\ 1 & 0 \end{bmatrix} \in SO(2)$. Let $\mathbb{T}^N := \prod_{i=1}^N \mathbb{S}^1$ denote the N-torus. The network dynamics (4.2) can be conveniently rewritten on $\mathbb{T}^N \times \mathbb{R}^N$ as follows:

$$
\begin{aligned}
\dot{\zeta}_i &= \frac{1}{2}\omega_i J \zeta_i \\
m_i\dot{\omega}_i &= -d_i\omega_i + \omega_{\mathrm{ni}} + u_i - \sum_{j\in\mathcal{N}_i} k_{ij}\phi(\zeta_i)^\top J\phi(\zeta_j)\cos(\varphi_{ij}) \\
&\quad + \sum_{j\in\mathcal{N}_i} k_{ij}\phi(\zeta_i)^\top \phi(\zeta_j)\sin(\varphi_{ij}), \qquad i \in \mathcal{V},
\end{aligned} \tag{4.10}
$$

where $\phi : \mathbb{S}^1 \to \mathbb{S}^1$ is defined as

$$
\phi(\zeta_i) := \mathcal{R}(\zeta_i)\zeta_i = \begin{bmatrix} \eta_i^2 - \epsilon_i^2 \\ 2\eta_i\epsilon_i \end{bmatrix}, \quad \zeta_i := \begin{bmatrix} \eta_i \\ \epsilon_i \end{bmatrix} \tag{4.11}
$$

and corresponds to the double angle formula from $\zeta_i := [\cos(\theta_i/2) \ \sin(\theta_i/2)]^\top$ to $[\cos(\theta_i) \ \sin(\theta_i)]^\top$. Note that, with the proposed representation (4.8), the condition (4.3) corresponding to phase synchronization coincides with

$$
\lim_{t\to+\infty} \mathcal{R}(\zeta_i(t))^\top \zeta_j(t) \in \{-e, e\}, \quad \forall i, j \in \mathcal{V}. \tag{4.12}
$$

Remark 4.1. *In some applications, such as those involving rotary encoders, θ_i is provided by sensors that "wrap" the angles in $[0, 2\pi)$ (equivalently, in $[-\pi, \pi)$). In this scenario, if (4.8) is used to compute ζ_i from the available sensor measurement, call it θ_i^{s}, special care must be taken to ensure that a continuous trajectory of the vector $[\cos(\theta_i^{\mathrm{s}}) \ \sin(\theta_i^{\mathrm{s}})]^\top$ (uniquely corresponding to any $\theta_i^{\mathrm{s}} \in [0, 2\pi)$) be mapped into a continuous trajectory of ζ_i. More specifically, for any $\theta_i^{\mathrm{s}} \in [0, 2\pi)$, there are two possible values of ζ_i, expressed through the half-angle formula:*

$$
\zeta_i \in \{-\zeta_i^*, \zeta_i^*\}, \qquad \zeta_i^* := \begin{bmatrix} \sqrt{\frac{1+\cos(\theta_i^{\mathrm{s}})}{2}} \\ \sqrt{\frac{1-\cos(\theta_i^{\mathrm{s}})}{2}} \end{bmatrix}. \tag{4.13}
$$

The same issue arises for unit quaternions. In that context, a path-lifting mechanism has been proposed in (Mayhew, Sanfelice, and Teel, 2012) to ensure that a continuous selection of the two quaternions is obtained for a "measured" rotation matrix. For simplicity, we avoid embedding a similar mechanism as (Mayhew, Sanfelice, and Teel, 2012) by considering ζ_i available for measurement. Including the path-lifting mechanism does not affect the results of this chapter.

4.4 Problem statement

4.4.1 Leader Exosystem

Since our objective involves the synchronization of the network to a reference signal, we consider a formulation of the tracking problem based on a pacemaker (see, e.g., (Wang and Doyle, 2013; Bosso, Azzollini, and Baldi, 2019)). Specifically, the graph $\mathcal{G}$ is augmented with an additional node, named *leader system*, which delivers to the network some reference signals. The references are generated through an
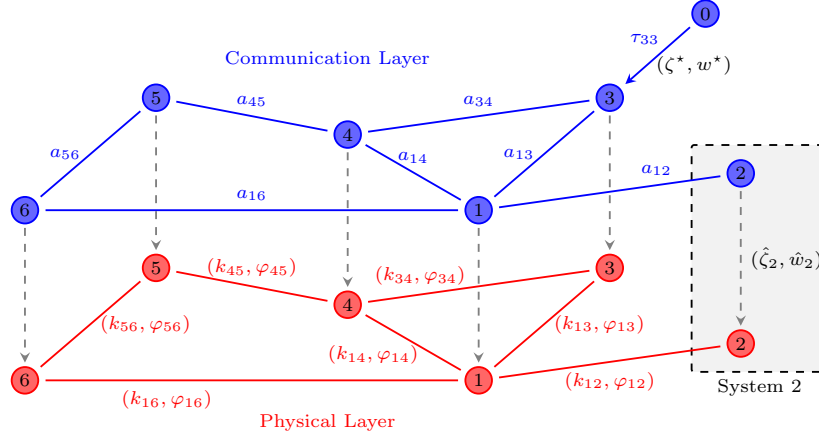
FIGURE 4.1: Interaction and communication scheme. The same graph will be employed for the numerical example in Section 4.8.

autonomous exosystem of the form

$$
\left.\begin{aligned}
\dot{\zeta}^\star &= \frac{1}{2} c^\top w^\star J \zeta^\star \\
\dot{w}^\star &= s(\zeta^\star, w^\star)
\end{aligned}\right\} \quad (\zeta^\star, w^\star) \in \mathcal{K}^\star \subset \mathbb{S}^1 \times \mathbb{R}^n,
\tag{4.14}
$$

where $\zeta^\star \in \mathbb{S}^1$ is the phase reference, $w^\star \in \mathbb{R}^n$, $n \in \mathbb{Z}_{\geq 1}$, is a state such that the frequency reference is given by $c^\top w^\star \in \mathbb{R}$, while $c \in \mathbb{R}^n$ is a constant vector and $s(\cdot) : \mathbb{S}^1 \times \mathbb{R}^n \to \mathbb{R}^n$ is a nonlinear function. Furthermore, $\mathcal{K}^\star$ is a compact set of admissible initial conditions $(\zeta^\star(0), w^\star(0))$.

The feedback structure in (4.14) suggests that, different from the solutions using unit quaternions (such as (Gui and Ruiter, 2018; Cai and Huang, 2016)), we do not restrict the structure of exosystem (4.14) to a cascade between the $w^\star$-subsystem and the $\zeta^\star$-subsystem. The following assumption describes the properties related to (4.14).

Assumption 4.2. *For system* (4.14)*, it holds that:*

1. *the compact set $\mathcal{K}^\star$ is forward invariant;*

2. *the map $s(\cdot)$ is globally Lipschitz, with Lipschitz constant $\ell_s \geq 0$;*

3. *c and $s(\cdot)$ are known to each node $i \in \mathcal{V}$.*

The global Lipschitz condition in Assumption 4.2 is instrumental in achieving global asymptotic stability, cf. (Isidori, Marconi, and Casadei, 2014). As we shall see in Section 4.5, this Lipschitz continuity property allows designing the controllers for each node $i \in \mathcal{V}$ without the explicit knowledge of the compact set $\mathcal{K}^\star$, even though the knowledge of ℓ_s is required for tuning the controller gains.

As a final requirement for our design, we impose a standard assumption describing the communication topology among the leader (4.14) and the network (4.10).

Assumption 4.3. *System* (4.14) *interacts, by communicating the reference* $(\zeta^\star, w^\star)$*, with at least one node of graph $\mathcal{G}$, which defines both the physical couplings and the communication topology. More specifically, it holds that $\mathcal{T} \neq \varnothing$ (equivalently, $T \neq 0$).*

Remark 4.2. *Since $\mathcal{G}$ is undirected and connected, Assumption 4.3 implies that the leader-follower matrix $B := L + T$ is positive definite.*

Figure 4.1 shows a scheme of the interaction and communication pattern underlying our distributed architecture.

The control problem of this work, stated in the following, aims at ensuring global asymptotic stability of a compact set corresponding to phase synchronization as in (4.12) and convergence to $\zeta^\star$, i.e.:

$$\lim_{t \to +\infty} \mathcal{R}(\zeta_i(t))^\top \zeta^\star \in \{-e, e\}, \quad \forall i \in \mathcal{V}. \tag{4.15}$$

In particular, we seek for a hybrid adaptive controller whose data satisfy the so-called hybrid basic conditions of (Goebel, Sanfelice, and Teel, 2012, Assumption 6.5). As a consequence, global asymptotic stability of a compact set is equivalent to the existence of a uniform class $\mathcal{KL}$ bound (Goebel, Sanfelice, and Teel, 2012, Theorem 7.12). Following the robustness results in (Goebel, Sanfelice, and Teel, 2012, Section 7.3), this also implies robust $\mathcal{KL}$ asymptotic stability in the presence of fairly general perturbations of the dynamics.

Problem 4.1. *Under Assumptions 4.1, 4.2, and 4.3, consider the following synchronization set to the reference $\zeta^\star$:*

$$\begin{aligned} \mathcal{A}_\mathrm{s} := \{ (\zeta^\star, w^\star), (\zeta_i, \omega_i), i \in \mathcal{V} : \\ \mathcal{R}(\zeta_i)^\top \zeta^\star \in \{-e, e\}, \omega_i = c^\top w^\star \}, \end{aligned} \tag{4.16}$$

where e is defined in (4.7), and note that $\mathcal{A}_\mathrm{s}$ is compact because (4.14) evolves in the compact set $\mathcal{K}^\star$. Then, design a distributed adaptive strategy, only based on the local measurements (ζ_i, ω_i) and the information exchange according to graph $\mathcal{G}$, such that the second-order Kuramoto network (4.10) achieves robust global phase synchronization to the reference $\zeta^\star$. Namely, the closed-loop dynamics is such that there exists a robustly globally $\mathcal{KL}$ asymptotically stable compact set (in the sense of (Goebel, Sanfelice, and Teel, 2012, Definition 7.18)), whose projection in the plant-exosystem direction coincides with the compact set $\mathcal{A}_\mathrm{s}$ in (4.16).

4.4.2 Control Architecture

Through the parametrization (4.8), (4.10), (4.11), Problem 4.1 addresses the synchronization goal in (4.3), (4.4), in a convenient scenario wherein the set to be stabilized is compact. Topological obstructions associated to the non-Euclidean nature of the phase dynamics make Problem 4.1 challenging. In fact, the N-torus is non-contractible, i.e., it is not diffeomorphic to any Euclidean space, and convergence to (4.16) requires convergence to a disconnected set of points. Two main issues arise in this context.

- If the control laws u_i are designed to stabilize only one of the points of (4.16), the trajectories in the coordinates θ_i display the so-called *unwinding phenomenon* (Mayhew, Sanfelice, and Teel, 2012), which causes unnecessary motion in cases where the system is initialized close to synchronization.

- If a static discontinuous feedback is employed, it is not possible to ensure robust $\mathcal{KL}$ asymptotic stability because the closed-loop system does not satisfy the hybrid basic assumptions. This fact, in practice, translates into chattering and high disturbance sensitivity (Mayhew, Sanfelice, and Teel, 2011).

In view of these considerations, we employ a hybrid dynamic feedback to robustly globally asymptotically stabilize a compact set comprising $\mathcal{A}_\mathrm{s}$ in (4.16). As discussed

in the introduction, the proposed control strategy is built upon the interconnection of a distributed observer for exosystem (4.14), a hybrid stabilizer for globally tracking the observer estimates, and an adaptive law to handle parametric uncertainties under Assumption 4.1. More specifically, our design is based on the following steps.

- A distributed observer is designed so that certain local estimates $(\hat{\zeta}_i, \hat{w}_i)$ of $(\zeta^\star, w^\star) \in \mathcal{K}^\star$ are defined as elements of $\mathbb{R}^{2+n}$. The ensuing estimation error dynamics is described by two feedback-interconnected subsystems, associated with the phase and the frequency estimation errors, respectively. These subsystems are proven to be ISS and then combined through small-gain arguments. The design and the stability analysis of the observer are discussed in Section 4.5.

- For each agent i, we implement an adaptive hybrid mechanism to ensure $\mathcal{R}(\zeta_i)^\top \hat{\zeta}_i \to \{-e, e\}$, $\omega_i \to c^\top \hat{w}_i$, for all $i \in \mathcal{V}$. The design is first performed assuming global knowledge of the leader signals (Section 4.6). Supposing that ω_i can be assigned as a virtual input ω_{vi}, a hysteresis-based controller is used to show global phase synchronization while ensuring that ω_{vi} is constant across jumps. Then, a backstepping-based adaptive controller is designed to guarantee $\omega_i \to \omega_{vi}$. Finally, exploiting the cascade structure between the estimation error subsystem and the tracking subsystem, the effectiveness of the overall control solution is proven through reduction theorems (Section 4.7).

4.5 Distributed observer

In order to solve Problem 4.1, we propose the following distributed observer:

$$
\begin{aligned}
\dot{\hat{\zeta}}_i &= \frac{1}{2} c^\top \hat{w}_i J \hat{\zeta}_i - k_\zeta e_{\zeta i} \\
\dot{\hat{w}}_i &= s(\hat{\zeta}_i, \hat{w}_i) - k_w e_{w_i}
\end{aligned}
\qquad i \in \mathcal{V},
\tag{4.17}
$$

where $\hat{\zeta}_i \in \mathbb{R}^2$, $\hat{w}_i \in \mathbb{R}^n$ are the local estimates of $(\zeta^\star, w^\star)$ (4.14) at node i, k_ζ and $k_w \in \mathbb{R}$ are gains to be designed, while

$$
\begin{aligned}
e_{\zeta i} &:= \sum_{j \in \mathcal{N}_i} a_{ij}(\hat{\zeta}_i - \hat{\zeta}_j) + \tau_{ii}(\hat{\zeta}_i - \zeta^\star) \\
e_{w_i} &:= \sum_{j \in \mathcal{N}_i} a_{ij}(\hat{w}_i - \hat{w}_j) + \tau_{ii}(\hat{w}_i - w^\star)
\end{aligned}
\qquad i \in \mathcal{V},
\tag{4.18}
$$

are the *local estimation errors*, in which a_{ij} and τ_{ii} are the entries of the adjacency matrix A and the target matrix T, respectively.

Observer (4.17) is distributed as it is only driven by locally available quantities (4.18). To represent the variables for the overall network in a compact form, it is convenient to use the Kronecker product. In particular, define the overall states $\hat{\zeta} := [\hat{\zeta}_1^\top \ \dots \ \hat{\zeta}_N^\top]^\top \in \mathbb{R}^{2N}$ and $\hat{w} := [\hat{w}_1^\top \ \dots \ \hat{w}_N^\top]^\top \in \mathbb{R}^{Nn}$, so that the overall estimation errors are $\tilde{\zeta} := \hat{\zeta} - \mathbf{1}_N \otimes \zeta^\star$ and $\tilde{w} := \hat{w} - \mathbf{1}_N \otimes w^\star$. Furthermore, define $e_\zeta := [e_{\zeta_1}^\top \ \dots \ e_{\zeta_N}^\top]^\top \in \mathbb{R}^{2N}$ and $e_w := [e_{w_1}^\top \ \dots \ e_{w_N}^\top]^\top \in \mathbb{R}^{Nn}$, which from (4.18) can be written as (Azzollini et al., 2020):

$$
e_\zeta = (B \otimes I_2)\tilde{\zeta}, \qquad e_w = (B \otimes I_n)\tilde{w},
\tag{4.19}
$$

where $B := L + T$ is the leader-follower matrix, which satisfies $B = B^\top > 0$ as discussed in Remark 4.2. In the following, denote with $\underline{\sigma}(B) > 0$ the smallest singular value of B.

4.5.1 Phase Subnetwork

We start by analyzing the $(\zeta^\star, \hat{\zeta})$-subsystem (referred to as phase subnetwork) and the phase estimation error $\tilde{\zeta}$. From (4.14), (4.17), the phase subnetwork obeys dynamics

$$\dot{\zeta}^\star = \frac{1}{2} c^\top w^\star J \zeta^\star$$

$$\dot{\hat{\zeta}}_i = \frac{1}{2} c^\top w^\star J \hat{\zeta}_i + \frac{1}{2} c^\top \tilde{w}_i J \hat{\zeta}_i - k_\zeta e_{\zeta_i}, \quad i \in \mathcal{V}. \tag{4.20}$$

For notational convenience, define

$$\mathbb{W} := \operatorname{diag}(c^\top \tilde{w}_1, \dots, c^\top \tilde{w}_N) = \operatorname{diag}((I_N \otimes c^\top)\tilde{w}), \tag{4.21}$$

which allows writing the dynamics of $\hat{\zeta}$ in compact form as follows

$$\dot{\hat{\zeta}} = \frac{1}{2} \left(c^\top w^\star (I_N \otimes J) + (\mathbb{W} \otimes J) \right) \hat{\zeta} - k_\zeta e_\zeta. \tag{4.22}$$

As a consequence, the dynamics of the phase estimation error $\tilde{\zeta} := \hat{\zeta} - \mathbf{1}_N \otimes \zeta^\star$, can be computed from (4.19), (4.20), and (4.22) as:

$$\dot{\tilde{\zeta}} = \left(\frac{1}{2} c^\top w^\star (I_N \otimes J) - k_\zeta (B \otimes I_2) + \frac{1}{2} (\mathbb{W} \otimes J) \right) \tilde{\zeta}$$

$$+ \frac{1}{2} (\mathbb{W} \otimes J)(\mathbf{1}_N \otimes \zeta^\star), \tag{4.23}$$

with inputs given by $\zeta^\star$, $w^\star$, and $\tilde{w}$ (through $\tilde{\Omega}$ in (4.21)). The next proposition provides an ISS characterization for system (4.23).

Proposition 4.1. *For any scalar gain $k_\zeta > 0$, system (4.23) is finite-gain exponentially input-to-state stable with respect to the input $\tilde{w}$, uniformly in the inputs $(\zeta^\star, w^\star)$. Namely, for any solution $(\zeta^\star(\cdot), w^\star(\cdot))$ of the exosystem (4.14) and any $\tilde{w}(\cdot) \in \mathcal{L}_\infty$, the solutions of (4.23) satisfy, for all $t \geq 0$:*

$$|\tilde{\zeta}(t)| \leq \max \left\{ e^{-\frac{1}{2}\underline{\sigma}(B)k_\zeta t} |\tilde{\zeta}(0)|, \frac{|c| \|\tilde{w}(\cdot)\|_\infty}{\underline{\sigma}(B)k_\zeta} \right\}. \tag{4.24}$$

Proof. For any solution $(\zeta^\star(\cdot), w^\star(\cdot))$ of the exosystem (4.14), system (4.23) can be regarded as a time-varying system with input $\tilde{w}$. It is convenient to rewrite the last term of (4.23) as

$$(\mathbb{W} \otimes J)(\mathbf{1}_N \otimes \zeta^\star) = \mathbb{W}\mathbf{1}_N \otimes J\zeta^\star$$

$$= \operatorname{diag}((I_N \otimes c^\top)\tilde{w})\mathbf{1}_N \otimes J\zeta^\star$$

$$= \operatorname{diag}(\mathbf{1}_N)(I_N \otimes c^\top)\tilde{w} \otimes J\zeta^\star \tag{4.25}$$

$$= \underbrace{\left(I_N \otimes J\zeta^\star c^\top\right)}_{:=Z^\star} \tilde{w} = Z^\star \tilde{w},$$

where we used the identity $((I_N \otimes c^\top)w) \otimes v = (I_N \otimes vc^\top)w$, which holds for any vectors $c^\top$, w, v, of compatible dimensions. Consider the Lyapunov function candidate

$$V_\zeta := \frac{1}{2}|\tilde\zeta|^2 \tag{4.26}$$

whose derivative along the system trajectories results in

$$\begin{aligned}
\dot V_\zeta = {} & -k_\zeta \tilde\zeta^\top (B \otimes I_2)\tilde\zeta + \frac{1}{2}\tilde\zeta^\top Z^\star \tilde w \\
& + \frac{1}{2}\tilde\zeta^\top \left(c^\top w^\star (I_N \otimes J) + (\mathbb{W} \otimes J) \right)\tilde\zeta, \\
= {} & -k_\zeta \tilde\zeta^\top (B \otimes I_2)\tilde\zeta + \frac{1}{2}\tilde\zeta^\top Z^\star \tilde w,
\end{aligned} \tag{4.27}$$

where we employed the fact that $I_N \otimes J$ and $\mathbb{W} \otimes J$ are skew symmetric. Since $k_\zeta > 0$, we obtain

$$\dot V_\zeta \leq -\underline\sigma(B)k_\zeta|\tilde\zeta|^2 + \frac{1}{2}|Z^\star||\tilde\zeta||\tilde w|. \tag{4.28}$$

The following computations yield $|Z^\star| = |c|$:

$$\begin{aligned}
|Z^\star| &= |I_N||J\zeta^\star c^\top| = |J\zeta^\star c^\top| \\
&= |J\zeta^\star c^\top|_F = \sqrt{\mathrm{Tr}(c\zeta^{\star\top}J^\top J\zeta^\star c^\top)} \\
&= \sqrt{\mathrm{Tr}(cc^\top)} = |c|,
\end{aligned} \tag{4.29}$$

where $|J\zeta^\star c^\top| = |J\zeta^\star c^\top|_F$ since the rank of $J\zeta^\star c^\top$ is 1 by construction. Applying (4.28) and (4.29) yields

$$|\tilde\zeta| \geq \frac{|c|}{\underline\sigma(B)k_\zeta}|\tilde w| \implies \dot V_\zeta \leq -\frac{\underline\sigma(B)k_\zeta}{2}|\tilde\zeta|^2, \tag{4.30}$$

which leads to (4.24) via standard ISS calculations (Isidori, 1999, Theorem 10.4.1).
□

4.5.2 Frequency Subnetwork

Starting again from (4.14), (4.17), the frequency subnetwork obeys dynamics

$$\begin{aligned}
w^\star &= s(\zeta^\star, w^\star) \\
\dot{\hat w}_i &= s(\hat\zeta_i, \hat w_i) - k_w e_{w_i}, \quad i \in \mathcal{V}.
\end{aligned} \tag{4.31}$$

We can then write the dynamics of $\hat w$ as

$$\dot{\hat w} = S(\hat\zeta, \hat w) - k_w e_w, \tag{4.32}$$

where

$$S(\hat\zeta, \hat w) := \begin{bmatrix} s(\hat\zeta_1, \hat w_1) \\ \vdots \\ s(\hat\zeta_N, \hat w_N) \end{bmatrix}. \tag{4.33}$$

Therefore, using (4.19), the dynamics of the frequency estimation error $\tilde{w} := \hat{w} - (\mathbf{1}_N \otimes w^\star)$ is given by

$$\dot{\tilde{w}} = S(\hat{\zeta}, \hat{w}) - \mathbf{1}_N \otimes s(\zeta^\star, w^\star) - k_w(B \otimes I_n)\tilde{w}, \tag{4.34}$$

which, in view of $\hat{\zeta} = \tilde{\zeta} + \mathbf{1}_N \otimes \zeta^\star$, $\hat{w} = \tilde{w} + \mathbf{1}_N \otimes w^\star$, is a non-autonomous system with inputs given by $\zeta^\star$, $w^\star$, and $\tilde{\zeta}$. In the following, we present a result that follows the same structure as Proposition 4.1, now applied to the frequency subnetwork.

Proposition 4.2. *For any scalar gain $k_w > \ell_s/\underline{\sigma}(B)$, system (4.34) is finite-gain exponentially input-to-state stable with respect to the input $\tilde{\zeta}$, uniformly in the inputs $(\zeta^\star, w^\star)$. Namely, for any solution $(\zeta^\star(\cdot), w^\star(\cdot))$ of the exosystem (4.14) and any $\tilde{\zeta}(\cdot) \in \mathcal{L}_\infty$, the solutions of system (4.34) satisfy, for all $t \geq 0$:*

$$|\tilde{w}(t)| \leq \max\left\{e^{-\frac{1}{2}(\underline{\sigma}(B)k_w - \ell_s)t}|\tilde{w}(0)|, \frac{2\ell_s\|\tilde{\zeta}(\cdot)\|_\infty}{\underline{\sigma}(B)k_w - \ell_s}\right\}. \tag{4.35}$$

Proof. For any solution $(\zeta^\star(\cdot), w^\star(\cdot))$ of the exosystem (4.14), system (4.34) can be regarded as a time-varying system with input $\tilde{\zeta}$. Consider the Lyapunov function candidate

$$V_w := \frac{1}{2}|\tilde{w}|^2, \tag{4.36}$$

whose derivative along (4.34) is

$$\begin{aligned}\dot{V}_w &= -k_w\tilde{w}^\top(B \otimes I_n)\tilde{w} + \tilde{w}^\top\left(S(\hat{\zeta}, \hat{w}) - \mathbf{1}_N \otimes s(\zeta^\star, w^\star)\right) \\ &= -k_w\tilde{w}^\top(B \otimes I_n)\tilde{w} + \sum_{i=1}^N \tilde{w}_i^\top\left(s(\hat{\zeta}_i, \hat{w}_i) - s(\zeta^\star, w^\star)\right).\end{aligned} \tag{4.37}$$

By Assumption 4.2, it holds that

$$|s(\hat{\zeta}_i, \hat{w}_i) - s(\zeta^\star, w^\star)| \leq \ell_s(|\tilde{\zeta}_i| + |\tilde{w}_i|), \tag{4.38}$$

therefore we conclude that

$$\begin{aligned}\dot{V}_w &\leq -\underline{\sigma}(B)k_w|\tilde{w}|^2 + \ell_s\sum_{i=1}^N\left(|\tilde{w}_i|^2 + |\tilde{w}_i||\tilde{\zeta}_i|\right) \\ &\leq -\left(\underline{\sigma}(B)k_w - \ell_s\right)|\tilde{w}|^2 + \ell_s|\tilde{w}||\tilde{\zeta}|.\end{aligned} \tag{4.39}$$

Finally, from (4.39) we obtain the following ISS characterization:

$$|\tilde{w}| \geq \frac{2\ell_s}{\underline{\sigma}(B)k_w - \ell_s}|\tilde{\zeta}| \implies \dot{V}_w \leq -\frac{\underline{\sigma}(B)k_w - \ell_s}{2}|\tilde{w}|^2, \tag{4.40}$$

which proves the finite-gain exponential ISS bound (4.35) through (Isidori, 1999, Theorem 10.4.1). $\square$

4.5.3 Overall Observer Analysis

We conclude the section with a stability result for the feedback interconnection between the phase estimation error dynamics (4.23) and the frequency estimation error dynamics (4.34).

Theorem 4.1. *For any choice of the scalar gains k_ζ and k_w such that*

$$k_\zeta > 0, \qquad k_w > \ell_s / \underline{\sigma}(B),$$
$$k_\zeta \underline{\sigma}(B)(k_w \underline{\sigma}(B) - \ell_s) - 2\ell_s |c| > 0, \tag{4.41}$$

the zero-equilibrium $(\tilde{\zeta}, \tilde{w}) = 0$ of the overall estimation error system (4.23), (4.34) is globally exponentially stable.

Proof. From Proposition 4.1, which holds for $k_\zeta > 0$, and Proposition 4.2, valid for $k_w \underline{\sigma}(B) > \ell_s$, we obtain that both (4.23) and (4.34) are finite-gain exponentially ISS. Therefore, global exponential stability is ensured from (4.24), (4.35), and (Isidori, 1999, Theorem 10.6.1), through the following small-gain condition:

$$\frac{2\ell_s |c|}{k_\zeta \underline{\sigma}(B)(k_w \underline{\sigma}(B) - \ell_s)} < 1, \tag{4.42}$$

which is ensured by (4.41). □

Remark 4.3. *In the special case where exosystem (4.14) is a cascade, i.e., $s = s(w^\star)$, conditions (4.41) collapse to $k_\zeta > 0$, $k_w > \ell_s / \underline{\sigma}(B)$. Additionally, if $s(w^\star) = S_w w^\star$, where S_w is a Poisson stable matrix as in (Gui and Ruiter, 2018; Bosso et al., 2021a; Cai and Huang, 2016), (4.37) becomes $\dot{V}_w = -k_w \tilde{w}^\top (B \otimes I_n) \tilde{w}$, therefore conditions (4.41) become $k_\zeta > 0$, $k_w > 0$.*

4.6 Synchronization with global knowledge of the leader signals

In this section, we design a tracking controller for the simplified setup where the observer estimation errors are zero. This approach will be motivated in Section 4.7 by the reduction arguments of the stability analysis.

Firstly, we compute the local tracking error dynamics. Define the phase and frequency tracking errors as

$$\begin{aligned} \bar{\zeta}_i &:= \begin{bmatrix} \bar{\eta}_i & \bar{\epsilon}_i \end{bmatrix}^\top := \mathcal{R}(\zeta_i)^\top \hat{\zeta}_i \in \mathbb{R}^2 \\ \bar{\omega}_i &:= c^\top \hat{w}_i - \omega_i \in \mathbb{R} \end{aligned} \qquad i \in \mathcal{V}. \tag{4.43}$$

In these coordinates, the control objective in Problem 4.1 corresponds to imposing $\bar{\epsilon}_i \to 0$, for all $i \in \mathcal{V}$. From (4.10), (4.17), and $\mathcal{R}(\zeta_i)^\top J = J\mathcal{R}(\zeta_i)^\top$, we can compute the phase error dynamics as

$$\begin{aligned} \dot{\bar{\zeta}}_i &= \frac{d}{dt}\left(\mathcal{R}(\zeta_i)^\top\right)\hat{\zeta}_i + \mathcal{R}(\zeta_i)^\top \dot{\hat{\zeta}}_i \\ &= -\mathcal{R}(\zeta_i)^\top \frac{d\mathcal{R}(\zeta_i)}{dt}\mathcal{R}(\zeta_i)^\top \hat{\zeta}_i + \mathcal{R}(\zeta_i)^\top \dot{\hat{\zeta}}_i \quad i \in \mathcal{V} \\ &= \frac{1}{2}\bar{\omega}_i J\bar{\zeta}_i - k_\zeta \mathcal{R}(\zeta_i)^\top e_{\zeta_i}. \end{aligned} \tag{4.44}$$

Similarly, the dynamics of the frequency error $\bar{\omega}_i$ is computed from (4.10), (4.14), and (4.17) as

$$m_i \dot{\bar{\omega}}_i = \psi_i - u_i - m_i k_w c^\top e_{w_i}, \qquad i \in \mathcal{V}, \tag{4.45}$$

where we defined

$$
\begin{aligned}
\psi_i := \; & m_i c^\top s(\hat{\zeta}_i, \hat{w}_i) + d_i \omega_i - \omega_{\mathrm{n}i} \\
& + \sum_{j \in \mathcal{N}_i} k_{ij} \phi(\zeta_i)^\top J \phi(\zeta_j) \cos(\varphi_{ij}) \\
& - \sum_{j \in \mathcal{N}_i} k_{ij} \phi(\zeta_i)^\top \phi(\zeta_j) \sin(\varphi_{ij}).
\end{aligned}
\tag{4.46}
$$

Observe that, with $\hat{\zeta}_i = \zeta^\star$ and $\hat{w}_i = w^\star$ (i.e., $\tilde{\zeta} = 0$, $\tilde{w} = 0$, equivalently, $e_\zeta = 0$, $e_w = 0$), the quantities in (4.43) become $\bar{\zeta}_i = \mathcal{R}(\zeta_i)^\top \zeta^\star \in \mathbb{S}^1$ and $\bar{\omega}_i = c^\top w^\star - \omega_i \in \mathbb{R}$. In view of this reduction argument, we begin the design by assuming that the exosystem signals $(\zeta^\star, w^\star)$ are globally known for feedback. This scenario corresponds to the requirement $\mathcal{T} = \mathcal{V}$, which will be removed in Section 4.7.

4.6.1 Phase Synchronization

Assume initially that ω_i can be arbitrarily assigned by the feedback controller as a virtual input $\omega_{\mathrm{v}i}$. With $e_\zeta = 0$, the dynamics (4.44) thus reduces to

$$
\dot{\bar{\zeta}}_i = \frac{1}{2}(c^\top \hat{w}_i - \omega_{\mathrm{v}i}) J \bar{\zeta}_i, \qquad i \in \mathcal{V},
\tag{4.47}
$$

where $\omega_{\mathrm{v}i}$ is the virtual input that should ensure $\bar{e}_i \to 0$. We refer to this objective as *phase synchronization* with the reference $\zeta^\star$.

Define $\mathcal{Q} := \{-1, 1\}$ and choose any gain $k > 0$ and a hysteresis margin $\delta \in (0, 1)$. For each $i \in \mathcal{V}$, a hysteresis-based hybrid dynamic controller that achieves global phase synchronization is given by

$$
\begin{cases}
\dot{q}_i = 0, & (\bar{\zeta}_i, q_i) \in C_\kappa \\
q_i^+ = -q_i, & (\bar{\zeta}_i, q_i) \in D_\kappa
\end{cases} \qquad i \in \mathcal{V}
\tag{4.48}
$$
$$
\omega_{\mathrm{v}i} = c^\top \hat{w}_i + k q_i \bar{e}_i,
$$

where $q_i \in \mathcal{Q}$ is the controller state and

$$
\begin{aligned}
C_\kappa &:= \{(\bar{\zeta}_i, q_i) \in \mathbb{S}^1 \times \mathcal{Q} : \bar{\eta}_i q_i \geq -\delta\} \\
D_\kappa &:= \{(\bar{\zeta}_i, q_i) \in \mathbb{S}^1 \times \mathcal{Q} : \bar{\eta}_i q_i \leq -\delta\}.
\end{aligned}
\tag{4.49}
$$

The closed-loop error dynamics then corresponds to

$$
\begin{cases}
\dot{\bar{\zeta}}_i = -\frac{1}{2} k q_i \bar{e}_i J \bar{\zeta}_i \\
\dot{q}_i = 0,
\end{cases}
\begin{bmatrix} \bar{\zeta}_i \\ q_i \end{bmatrix} \in C_\kappa,
\begin{cases}
\bar{\zeta}_i^+ = \bar{\zeta}_i \\
q_i^+ = -q_i,
\end{cases}
\begin{bmatrix} \bar{\zeta}_i \\ q_i \end{bmatrix} \in D_\kappa,
\tag{4.50}
$$

which provides an autonomous hybrid dynamics having state $(\bar{\zeta}_i, q_i) = ((\bar{\eta}_i, \bar{e}_i), q_i) \in \mathbb{S}^1 \times \mathcal{Q}$ and such that $q_i \bar{\eta}_i = -1$ is not included in the flow set C_κ (because $\delta < 1$). The next lemma is a straightforward generalization of (Mayhew, Sanfelice, and Teel, 2011).

Lemma 4.1. *The attractor $\mathcal{A}_\kappa := \{(\zeta, q) \in \mathbb{S}^1 \times \mathcal{Q} : \zeta = q\boldsymbol{e}\}$ is uniformly globally asymptotically stable for* (4.50).

Proof. Choose the Lyapunov function

$$
V_\kappa(\bar{\zeta}_i, q_i) := 2(1 - q_i \bar{\eta}_i),
\tag{4.51}
$$

which is positive definite and radially unbounded with respect to $\mathcal{A}_\kappa$. Denoting $\dot{V}_\kappa = \left\langle \nabla V_\kappa, [\dot{\bar{\zeta}}_i \; \dot{q}_i]^\top \right\rangle$ and $\Delta V_\kappa = V_\kappa(\bar{\zeta}_i^+, q_i^+) - V_\kappa(\bar{\zeta}_i, q_i)$, straightforward calculations yield

$$
\begin{aligned}
\dot{V}_\kappa &= -k\bar{\epsilon}_i^2 < 0, & \forall (\bar{\zeta}_i, q_i) \in C_\kappa \backslash \mathcal{A}_\kappa \\
\Delta V_\kappa &= 4q_i\bar{\eta}_i \leq -4\delta < 0, & \forall (\bar{\zeta}_i, q_i) \in D_\kappa,
\end{aligned}
\tag{4.52}
$$

implying UGAS from standard hybrid Lyapunov theory. $\qquad \square$

For a convenient design of the backstepping-based adaptive controller defined in the next subsection, we propose now a dynamically extended version of (4.48) to ensure that ω_{vi} remains constant across jumps. Specifically, we augment the controller with a first-order filter of the feedback $kq_i\bar{\epsilon}_i$:

$$
\begin{cases}
\begin{cases} \dot{q}_i = 0 \\ \dot{\lambda}_i = -h(\lambda_i - kq_i\bar{\epsilon}_i) \end{cases} & (\bar{\zeta}_i, q_i, \lambda_i) \in C_\lambda \\
\begin{cases} q^+ = -q_i \\ \lambda_i^+ = \lambda_i \end{cases} & (\bar{\zeta}_i, q_i, \lambda_i) \in D_\lambda
\end{cases}
\qquad i \in \mathcal{V},
\tag{4.53}
$$

where h is a positive gain and the sets C_λ, D_λ are defined as the next generalization of (4.49):

$$
\begin{aligned}
C_\lambda &:= \left\{ (\bar{\zeta}_i, q_i, \lambda_i) \in \mathsf{S}^1 \times \mathcal{Q} \times \mathbb{R} : \left(\bar{\eta}_i + \frac{\lambda_i\bar{\epsilon}_i}{k} \right) q_i \geq -\delta \right\} \\
D_\lambda &:= \left\{ (\bar{\zeta}_i, q_i, \lambda_i) \in \mathsf{S}^1 \times \mathcal{Q} \times \mathbb{R} : \left(\bar{\eta}_i + \frac{\lambda_i\bar{\epsilon}_i}{k} \right) q_i \leq -\delta \right\}.
\end{aligned}
\tag{4.54}
$$

We can then replace by λ_i the term $kq_i\bar{\epsilon}_i$ in the selection of ω_{vi} of (4.48), namely we choose:

$$
\omega_{vi} = c^\top \hat{w}_i + \lambda_i, \qquad i \in \mathcal{V},
\tag{4.55}
$$

which remains constant across jumps. The closed-loop error dynamics for each node i, obtained from the interconnection of (4.47), (4.53), and (4.55), is described by:

$$
\begin{cases}
\dot{\bar{\zeta}}_i = -\frac{1}{2}\lambda_i J\bar{\zeta}_i \\
\dot{q}_i = 0 \\
\dot{\lambda}_i = -h(\lambda_i - kq_i\bar{\epsilon}_i)
\end{cases}
\begin{bmatrix} \bar{\zeta}_i \\ q_i \\ \lambda_i \end{bmatrix} \in C_\lambda,
\quad
\begin{cases}
\bar{\zeta}_i^+ = \bar{\zeta}_i \\
q_i^+ = -q_i \\
\lambda_i^+ = \lambda_i
\end{cases}
\begin{bmatrix} \bar{\zeta}_i \\ q_i \\ \lambda_i \end{bmatrix} \in D_\lambda.
\tag{4.56}
$$

The next result generalizes the argument of Lemma 4.1.

Proposition 4.3. *For any $h > k$, the attractor $\mathcal{A}_\lambda := \{(\zeta, q, \lambda) \in \mathsf{S}^1 \times \mathcal{Q} \times \mathbb{R} : \zeta = qe, \lambda = 0\}$ is uniformly globally asymptotically stable for the hybrid system (4.56).*

Proof. Define $\tilde{\lambda}_i := \lambda_i - kq_i\bar{\epsilon}_i$, then consider the Lyapunov function

$$
V_\lambda(\bar{\zeta}_i, q_i, \lambda_i) := 2k^2(1 - q_i\bar{\eta}_i) + \tilde{\lambda}_i^2.
\tag{4.57}
$$

Note that V_λ is positive definite with respect to $\mathcal{A}_\lambda$ and radially unbounded relative to $\mathbb{S}^1 \times \mathcal{Q} \times \mathbb{R}$. Denote $\dot{V}_\lambda = \left\langle \nabla V_\lambda, [\dot{\bar{\zeta}}_i \; \dot{q}_i \; \dot{\lambda}_i]^\top \right\rangle$. For all $(\bar{\zeta}_i, q_i, \lambda_i) \in C_\lambda$, it holds that

$$
\begin{aligned}
\dot{V}_\lambda &= -k^2 q_i \lambda_i \bar{\epsilon}_i + \tilde{\lambda}_i (-2h\tilde{\lambda}_i + kq_i \lambda_i \bar{\eta}_i) \\
&= -k^3 \bar{\epsilon}_i^2 + k^2 \tilde{\lambda}_i \bar{\epsilon}_i (\bar{\eta}_i - q_i) - (2h - kq_i \bar{\eta}_i) \tilde{\lambda}_i^2 \\
&\leq - \begin{bmatrix} |\bar{\epsilon}_i| \\ |\tilde{\lambda}_i| \end{bmatrix}^\top \begin{bmatrix} k^3 & -k^2 \\ -k^2 & 2h - k \end{bmatrix} \begin{bmatrix} |\bar{\epsilon}_i| \\ |\tilde{\lambda}_i| \end{bmatrix}.
\end{aligned}
\tag{4.58}
$$

From $\delta < 1$, for any point in C_λ we have that $\tilde{\lambda}_i = 0$ and $\bar{\epsilon}_i = 0$ implies that $(\bar{\zeta}_i, q_i, \lambda_i) \in \mathcal{A}$ (in particular, the point with $\lambda_i = 0$ and $q_i = -\bar{\eta}_i$ does not belong to C_λ), then $\dot{V}_\lambda < 0$, for all $(\bar{\zeta}_i, q_i, \lambda_i) \in C_\lambda \backslash \mathcal{A}_\lambda$, if $k^3(2h - k) - k^4 = 2k^3(h - k) > 0$, i.e., $h > k$. On the other hand, denote $\Delta V_\lambda = V_\lambda(\bar{\zeta}_i^+, q_i^+, \lambda_i^+) - V_\kappa(\bar{\zeta}_i, q_i, \lambda_i)$, then for all $(\bar{\zeta}_i, q_i, \lambda_i) \in D_\lambda$ we have:

$$
\begin{aligned}
\Delta V_\lambda &= 4k^2 q_i \bar{\eta}_i + (\tilde{\lambda}_i + 2kq_i \bar{\epsilon}_i)^2 - \tilde{\lambda}_i^2 \\
&= 4k^2 q_i \left(\bar{\eta}_i + \frac{\lambda_i \bar{\epsilon}_i}{k} \right) \leq -4k^2 \delta < 0,
\end{aligned}
\tag{4.59}
$$

thus concluding UGAS for the attractor $\mathcal{A}_\lambda$. $\qquad \square$

4.6.2 Global Adaptive Synchronization

Taking advantage of the hybrid system defined in (4.53), we propose to achieve global synchronization to the reference $\zeta^\star$ using an adaptive backstepping controller where, in place of the feedback $\omega_{vi} = c^\top \hat{w}_i + \lambda_i$ in (4.55), we ensure $\omega_i \to \omega_{vi}$ by design of the control input u_i.

In place of the frequency tracking error $\bar{\omega}_i$ in (4.43), consider the error variable

$$
z_i := c^\top \hat{w}_i + \lambda_i - \omega_i = \bar{\omega}_i + \lambda_i \in \mathbb{R}, \qquad i \in \mathcal{V}.
\tag{4.60}
$$

We can rewrite the error dynamics (4.44) and (4.45) using variables z_i as follows:

$$
\begin{aligned}
\dot{\bar{\zeta}}_i &= \frac{1}{2}(z_i - \lambda_i) J\bar{\zeta}_i - k_\zeta \mathcal{R}(\zeta_i)^\top e_{\zeta_i} \\
m_i \dot{z}_i &= \psi_i - u_i - m_i \left(k_w c^\top e_{w_i} + h(\lambda_i - kq_i \bar{\epsilon}_i) \right)
\end{aligned}
\qquad i \in \mathcal{V}.
\tag{4.61}
$$

Using (4.46), the second equation can also be rewritten as follows

$$
m_i \dot{z}_i = \Psi_i^\top p_i - u_i - m_i k_w c^\top e_{w_i}, \qquad i \in \mathcal{V},
\tag{4.62}
$$

with regressor Ψ_i and parameter vector $p_i \in \mathbb{R}^{3+2|\mathcal{N}_i|}$ given by:

$$
\Psi_i := \begin{bmatrix} c^\top s(\hat{\zeta}_i, \hat{w}_i) - h(\lambda_i - kq_i\bar{\epsilon}_i) \\ \omega_i \\ 1 \\ \phi(\zeta_i)^\top J\phi(\zeta_{j_1}) \\ \vdots \\ \phi(\zeta_i)^\top J\phi(\zeta_{j_{|\mathcal{N}_i|}}) \\ \phi(\zeta_i)^\top \phi(\zeta_{j_1}) \\ \vdots \\ \phi(\zeta_i)^\top \phi(\zeta_{j_{|\mathcal{N}_i|}}) \end{bmatrix}, \quad p_i := \begin{bmatrix} m_i \\ d_i \\ -\omega_{ni} \\ k_{ij_1}\cos(\varphi_{ij_1}) \\ \vdots \\ k_{ij_{N_i}}\cos(\varphi_{ij_{|\mathcal{N}_i|}}) \\ -k_{ij_1}\sin(\varphi_{ij_1}) \\ \vdots \\ -k_{ij_{N_i}}\sin(\varphi_{ij_{|\mathcal{N}_i|}}) \end{bmatrix} \tag{4.63}
$$

where we denoted $\mathcal{N}_i = \{j_1, \ldots, j_{|\mathcal{N}_i|}\}$. By Assumption 4.1, it follows that

$$
|p_i|_\infty = \max\{|p_{i1}|, \ldots, |p_{i(3+2|\mathcal{N}_i|)}|\} \leq \rho. \tag{4.64}
$$

The control of system (4.61) is based on the augmentation of control law (4.53) with the following adaptive state-input selections:

$$
\begin{aligned}
u_i &= \Psi_i^\top \hat{p}_i + k_z z_i \\
\dot{\hat{p}}_i &= \gamma \Psi_i z_i - \gamma \nu \, \mathrm{dz}(\hat{p}_i) \qquad i \in \mathcal{V}, \\
\hat{p}_i^+ &= \hat{p}_i,
\end{aligned} \tag{4.65}
$$

where k_z, γ, and ν are positive gains, while $\mathrm{dz} : \mathbb{R}^{3+2|\mathcal{N}_i|} \to \mathbb{R}^{3+2|\mathcal{N}_i|}$ is a decentralized dead-zone function defined as (Isidori, Marconi, and Serrani, 2012, Section 3.4):

$$
\mathrm{dz}(\xi) := \begin{bmatrix} \xi_1 - \rho \mathrm{sat}\left(\frac{\xi_1}{\rho}\right) \\ \vdots \\ \xi_{3+2|\mathcal{N}_i|} - \rho \mathrm{sat}\left(\frac{\xi_{3+2|\mathcal{N}_i|}}{\rho}\right) \end{bmatrix}, \tag{4.66}
$$

where $\mathrm{sat}(y) := \max\{-1, \min\{1, y\}\}$. Exploiting (4.64), it can be verified that, for all p_i and all $\xi \in \mathbb{R}^{3+2|\mathcal{N}_i|}$:

$$
(\xi - p_i)^\top \mathrm{dz}(\xi) \geq 0. \tag{4.67}
$$

Moreover, there exist positive scalars r and μ such that, for all p_i and all $\xi \in \mathbb{R}^{3+2|\mathcal{N}_i|}$:

$$
|\xi| \geq r \implies (\xi - p_i)^\top \mathrm{dz}(\xi) \geq \mu |\xi|^2. \tag{4.68}
$$

In view of our reduction arguments ($e_{\zeta_i} = 0$ and $e_{w_i} = 0$ in (4.61)), the closed-loop dynamics obtained from the interconnection of (4.61), (4.62), (4.53), and (4.65), having state $x_i := (\bar{\zeta}_i, q_i, \lambda_i, z_i, \hat{p}_i)$, is expressed, for each $i \in \mathcal{V}$, as follows:

$$
\begin{cases} \dot{\bar{\zeta}}_i = \dfrac{1}{2}(z_i - \lambda_i)J\bar{\zeta}_i \\ \dot{q}_i = 0 \\ \dot{\lambda}_i = -h(\lambda_i - kq_i\bar{\epsilon}_i) \qquad x_i \in C_i, \\ m_i\dot{z}_i = -k_z z_i - \Psi_i^\top(\hat{p}_i - p_i) \\ \dot{\hat{p}}_i = \gamma \Psi_i z_i - \gamma \nu \, \mathrm{dz}(\hat{p}_i) \end{cases} \begin{cases} \bar{\zeta}_i^+ = \bar{\zeta}_i \\ q_i^+ = -q_i \\ \lambda_i^+ = \lambda_i \quad x_i \in D_i, \\ z_i^+ = z_i \\ \hat{p}_i^+ = \hat{p}_i \end{cases} \tag{4.69}
$$

where $C_i := C_\lambda \times \mathbb{R}^{4+2|\mathcal{N}_i|}$ and $D_i := C_z \times \mathbb{R}^{4+2|\mathcal{N}_i|}$. In the following, we focus on the stability properties of the closed-loop system obtained through the interconnection of the exosystem (4.14) and the local error dynamics (4.69). For this interconnection, we are going to show that there exists a globally asymptotically stable compact attractor wherein all oscillators are synchronized with the reference $\zeta^\star$. More specifically, this compact attractor, named $\mathcal{A}_0$, is a set wherein $\bar{\zeta}_i = q_i e, z_i = 0$, for all $i \in \mathcal{V}$, and satisfying $\mathcal{A}_0 \subset \mathcal{K}_0$, with $\mathcal{K}_0$ compact, defined as:

$$
\mathcal{K}_0 := \{(\zeta^\star, w^\star, x_1, \dots, x_N) \in \mathcal{K}^\star \times \prod_{i \in \mathcal{V}} (\mathbb{S}^1 \times \mathcal{Q} \times \mathbb{R}^{5+2|\mathcal{N}_i|}): \\
\bar{\zeta}_i = q_i e, \lambda_i = 0, z_i = 0, |\hat{p}_i| \le r, \forall i \in \mathcal{V}\},
$$
(4.70)

where $r > 0$ as per (4.68). In the sequel, we call $\mathcal{K}_0$ *synchronization set*.

Remark 4.4. *The set $\mathcal{K}_0$ is compact. Indeed, $(\zeta^\star, w^\star) \in \mathcal{K}^\star$ is in a compact by assumption, while the only components of $x_i := (\bar{\zeta}_i, q_i, \lambda_i, z_i, \hat{p}_i)$ that are possibly unbounded are λ_i, z_i, and $\hat{p}_i$. Therefore, from the conditions in (4.70), compactness follows immediately.*

Remark 4.5. *Since no persistency of excitation is necessarily satisfied by the regressor Ψ_i in (4.63), it might be surprising that a globally asymptotically stable attractor can be found with the considered adaptive controller. This result is possible because we make use of the analysis tools in (Goebel, Sanfelice, and Teel, 2012, Chapter 6.10) instead of the standard tools for adaptive control (see, e.g., (Khalil, 2002, Section 8.3)). In particular, we leverage the result (Goebel, Sanfelice, and Teel, 2012, Corollary 7.7), which states that, under some regularity properties including-well posedness, the ω-limit set from a compact set of initial conditions is locally asymptotically stable.*

Theorem 4.2. *For any selection of the tuning parameters $k > 0, \delta \in (0, 1), h > k, k_z > 0$, $\gamma > 0$, and $\nu > 0$, there exists a compact set $\mathcal{A}_0$, contained in the synchronization set $\mathcal{K}_0$ of (4.70), that is robustly globally $\mathcal{KL}$ asymptotically stable in the sense of (Goebel, Sanfelice, and Teel, 2012, Definition 7.18) for the interconnection among (4.14) and (4.69).*

Robustness of our stability result follows from compactness of $\mathcal{A}_0$ and well posedness of the considered hybrid dynamics.

Proof. First, we prove that the closed-loop solutions are bounded and forward complete. The state $(\zeta^\star, w^\star)$ of the exosystem (4.14) evolves in the bounded forward invariant set $\mathcal{K}^\star$, thus it is bounded. Moreover, q_i is bounded by construction. In the scenario with known leader signals considered in this section, it holds that $\bar{\zeta}_i := \mathcal{R}(\zeta_i)^\top \hat{\zeta}_i = \mathcal{R}(\zeta_i)^\top \zeta_i \in \mathbb{S}^1$, thus $\bar{\zeta}_i$ is bounded. Since $|kq_i\bar{e}_i| \le k$ we obtain, for $|\lambda_i| \ge k$:

$$
\begin{aligned}
\frac{d}{dt}|\lambda_i| &= -h\frac{\lambda_i}{|\lambda_i|}(\lambda_i - kq_i\bar{e}_i) \qquad \forall i \in \mathcal{V} \\
&\le -h(|\lambda_i| - k) \le 0,
\end{aligned}
$$
(4.71)

therefore λ_i is bounded. Boundedness of $(z_i, \hat{p}_i)$ is established by using the following Lyapunov function

$$
V_i(z_i, \hat{p}_i) := \frac{1}{2}m_i z_i^2 + \frac{1}{2\gamma}|\hat{p}_i - p_i|^2, \qquad \forall i \in \mathcal{V}.
$$
(4.72)

Along the closed-loop solutions, we obtain from (4.69),

$$
\begin{aligned}
\dot{V}_i &= -k_z z_i^2 - z_i \Psi_i^\top (\hat{p}_i - p_i) + (\hat{p}_i - p_i)^\top \left[\Psi_i z_i - \nu\, dz(\hat{p}_i) \right] \\
&= -k_z z_i^2 - \nu(\hat{p}_i - p_i)^\top dz(\hat{p}_i), \qquad \forall i \in \mathcal{V}
\end{aligned}
\tag{4.73}
$$

Therefore, using (4.68) and the properties of the dead-zone function, we obtain, for all $i \in \mathcal{V}$,

$$
\begin{aligned}
\dot{V}_i &\leq -k_z z_i^2 \leq 0, && \text{if } |\hat{p}_i| \leq r, \\
\dot{V}_i &\leq -k_z z_i^2 - \nu\mu |\hat{p}_i|^2 < 0, && \text{if } |\hat{p}_i| \geq r.
\end{aligned}
\tag{4.74}
$$

Property (4.74) shows forward invariance of the sublevel sets of V_i, $i \in \mathcal{V}$, thus $(z_i, \hat{p}_i)$ is contained in a compact set, for all $i \in \mathcal{V}$. Exploiting boundedness of the components of x_i, $i \in \mathcal{V}$, established above, we also conclude by (Goebel, Sanfelice, and Teel, 2012, Proposition 6.10) that solutions are forward complete, thus they are precompact.

From (4.72)–(4.74) and using the fact that z_i and $\hat{p}_i$ do not change across jumps, we can apply (Goebel, Sanfelice, and Teel, 2012, Corollary 8.4) to obtain that all solutions approach the largest weakly invariant subset of the set

$$
\begin{aligned}
\mathcal{U} := \Big\{ (\zeta^\star, w^\star, x_1, \ldots, x_N) \in \mathcal{K}^\star \times \prod_{i \in \mathcal{V}} (\mathbb{S}^1 \times \mathcal{Q} \times \mathbb{R}^{5+2|\mathcal{N}_i|}) : \\
z_i = 0, |\hat{p}_i| \leq r, \forall i \in \mathcal{V} \Big\}.
\end{aligned}
\tag{4.75}
$$

The closed-loop dynamics restricted to the set $\mathcal{U}$ in (4.75) is given, for all $i \in \mathcal{V}$, by $z_i = 0$, $\dot{\hat{p}}_i = 0$, and (4.56). In view of Proposition 4.3, the solutions globally approach $\mathcal{K}_0 \subset \mathcal{U}$ as per (4.70) and (4.75).

For a set of initial conditions of the form $\mathcal{K}_\varepsilon := \mathcal{K}_0 + \varepsilon\mathbb{B}$, where $\varepsilon > 0$ is arbitrary, it holds that $\mathcal{A}_0 := \Omega(\mathcal{K}_\varepsilon) \subset \mathcal{K}_0 \subset \mathrm{Int}(\mathcal{K}_\varepsilon)$, where $\Omega(\mathcal{K}_\varepsilon)$ denotes the ω-limit set of $\mathcal{K}_\varepsilon$. By (Goebel, Sanfelice, and Teel, 2012, Corollary 7.7), $\mathcal{A}_0$ is asymptotically stable (therefore Lyapunov stable) with basin of attraction containing $\mathcal{K}_\varepsilon$. From the previous arguments, $\mathcal{A}_0$ is globally attractive, which, together with its Lyapunov stability, gives GAS. Since the hybrid dynamics satisfies the hybrid basic conditions of (Goebel, Sanfelice, and Teel, 2012, Assumption 6.5) and $\mathcal{A}_0$ is compact, then GAS of $\mathcal{A}_0$ implies robust global $\mathcal{KL}$ asymptotic stability from (Goebel, Sanfelice, and Teel, 2012, Theorem 7.21). □

As customary in adaptive control, convergence of the estimated parameters $\hat{p}_i$ to the true parameters p_i cannot be guaranteed. This in turn makes it difficult, if at all possible, to give an explicit representation of the attractor $\mathcal{A}_0$. Even without its explicit representation, the mere existence of $\mathcal{A}_0$ is sufficient to complete the design through reduction theorems in the next section.

4.7 Main Result

We finally present the complete hybrid observer-based controller for each node i, obtained by combining the distributed observer (4.17) and the local hysteresis-based controller (4.53), and the local adaptive controller (4.65). Note that, in this context, we no longer assume $\tilde{\zeta} = 0$, $\tilde{w} = 0$ (equivalently, $e_\zeta = 0$, $e_w = 0$), thus the dynamics of the tracking errors $(\bar{\zeta}_i, z_i)$ in (4.61) is not simplified as in the scenario with known leader signals. The robustness property established in Theorem 4.2 is naturally inherited here due to well posedness of the hybrid dynamics.
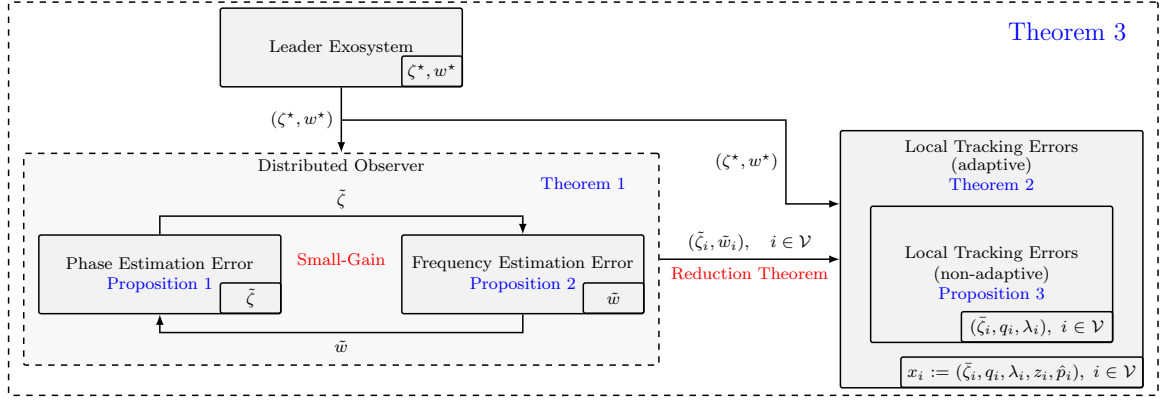
FIGURE 4.2: Sketch of the closed-loop error subsystems, with their interconnections and the related stability results.

Define the overall state at node i as

$$\chi_i := (\hat{\zeta}_i, \hat{w}_i, \underbrace{\bar{\zeta}_i, q_i, \lambda_i, z_i, \hat{p}_i}_{x_i}) \in \mathbb{R}^{n+4} \times \mathcal{Q} \times \mathbb{R}^{5+2|\mathcal{N}_i|}, \qquad (4.76)$$

then the local controllers that solve Problem 4.1 are given as follows, for each $i \in \mathcal{V}$:

$$\begin{cases} \dot{\hat{\zeta}}_i = \frac{1}{2} c^\top \hat{w}_i J \hat{\zeta}_i - k_\zeta e_{\zeta_i} \\ \dot{\hat{w}}_i = s(\hat{\zeta}_i, \hat{w}_i) - k_w e_{w_i} \\ \dot{q}_i = 0 \\ \dot{\lambda}_i = -h(\lambda_i - kq_i \bar{\epsilon}_i) \\ \dot{\hat{p}}_i = \gamma \Psi_i z_i - \gamma \nu \, \mathrm{dz}(\hat{p}_i) \end{cases} \chi_i \in C_{\chi i}, \qquad \begin{cases} \hat{\zeta}_i^+ = \hat{\zeta}_i \\ \hat{w}_i^+ = \hat{w}_i \\ q_i^+ = -q_i \\ \lambda_i^+ = \lambda_i \\ \hat{p}_i^+ = \hat{p}_i \end{cases} \chi_i \in D_{\chi i},$$

with: $C_{\chi i} := \Big\{ \chi_i \in \mathbb{R}^{n+4} \times \mathcal{Q} \times \mathbb{R}^{5+2|\mathcal{N}_i|} :$

$$\left(\bar{\eta}_i + \frac{\lambda_i \bar{\epsilon}_i}{k} \right) q_i \geq -\delta \Big\}, \qquad (4.77)$$

$$D_{\chi i} := \Big\{ \chi_i \in \mathbb{R}^{n+4} \times \mathcal{Q} \times \mathbb{R}^{5+2|\mathcal{N}_i|} :$$

$$\left(\bar{\eta}_i + \frac{\lambda_i \bar{\epsilon}_i}{k} \right) q_i \leq -\delta \Big\},$$

and: $u_i = \Psi_i^\top \hat{p}_i + k_z z_i,$

where e_{ζ_i}, e_{w_i} are given in (4.19), $\bar{\eta}_i$, $\bar{\epsilon}_i$ are defined in (4.43), z_i is defined in (4.60), Ψ_i is given in (4.63), dz is given in (4.66), while the tuning parameters are the stabilizer gains k, h, k_z, γ, ν, the observer gains k_ζ, k_w, and the hysteresis margin δ.

The closed-loop system is given by the interconnection of the second-order Kuramoto network (4.10), the exosytem (4.14), and the local controllers (4.77). For such system, we exploit reduction theorems to show that there exists a compact attractor $\mathcal{A}$ that is robustly globally $\mathcal{KL}$ asymptotically stable. As for Theorem 4.2, we show that $\mathcal{A}$ is a subset of a compact set $\mathcal{K}$ that we may call again *synchronization set*, with a slight abuse of notation, because its elements enjoy phase synchronization to the

reference $\zeta^\star$:

$$\mathcal{K} := \{(\zeta^\star, w^\star, \chi_1, \dots, \chi_N) \in \mathcal{K}^\star \times \prod_{i \in \mathcal{V}} (\mathbb{R}^{n+4} \times \mathcal{Q} \times \mathbb{R}^{5+2|\mathcal{N}_i|}):$$

$$\hat{\zeta}_i = \zeta^\star, \hat{w}_i = w^\star, \bar{\zeta}_i = q_i \mathbf{e}, \lambda_i = z_i = 0, |\hat{p}_i| \le r, \forall i \in \mathcal{V}\}. \tag{4.78}$$

Note that the projection of $\mathcal{K}$ in the direction of $(\zeta^\star, w^\star, x_1, \dots, x_N)$ corresponds to $\mathcal{K}_0$ in (4.70).

The main result of this work is given by the following statement, which provides formal guarantees for the effectiveness of the controllers (4.77).

Theorem 4.3. *For any selection of the tuning parameters $k > 0$, $\delta \in (0,1)$, $h > k$, $k_z > 0$, $\gamma > 0$, $\nu > 0$ and k_ζ, k_w satisfying (4.41), there exists a compact set $\mathcal{A}$, contained in $\mathcal{K}$ of (4.78), that is robustly globally $\mathcal{KL}$ asymptotically stable for the interconnection among (4.10), (4.14), and (4.77).*

Proof. We begin by highlighting the cascade-structure of the closed-loop error dynamics. As shown in Section 4.5, the distributed observer dynamics is collected in the estimation error subsystems (4.23) and (4.34). We can establish a cascade interconnection between the system (4.23), (4.34), (4.14), with output $(\zeta^\star, w^\star, \tilde{\zeta}, \tilde{w})$, and the tracking error dynamics (4.69). We highlight that whenever $(\tilde{\zeta}, \tilde{w}) = 0$ the closed-loop system is described by the dynamics with known leader signals (4.14), (4.69). The overall interconnection of these subsystems is shown in Figure 4.2.

Asymptotic stability of the attractor $\mathcal{A}$ is proven through reduction theorems. By Theorem 4.1, we showed that the closed (but not compact) attractor

$$\hat{\mathcal{A}} := \{(\zeta^\star, w^\star, \chi_1, \dots, \chi_N) \in \mathcal{K}^\star \times \prod_{i \in \mathcal{V}} (\mathbb{R}^{n+4} \times \mathcal{Q} \times \mathbb{R}^{5+2|\mathcal{N}_i|}):$$

$$\hat{\zeta}_i = \zeta^\star, \hat{w}_i = w^\star, \forall i \in \mathcal{V}\},$$

corresponding to the scenario with known leader signals, is UGAS. On the set $\hat{\mathcal{A}}$, we recover the dynamics (4.69), thus by Theorem 4.2 there exists an attractor $\mathcal{A} \subset \mathcal{K}$ that is UGAS relative to $\hat{\mathcal{A}}$. By (Maggiore, Sassano, and Zaccarian, 2018, Corollary 4.8), $\mathcal{A}$ is uniformly asymptotically stable for the overall closed-loop system, with basin of attraction given by all the initial conditions generating bounded solutions.

We conclude the proof by showing that all solutions of the closed-loop system are bounded, which then implies UGAS and then robust global $\mathcal{KL}$ asymptotic stability from (Goebel, Sanfelice, and Teel, 2012, Theorem 7.21). First note that the state $(\zeta^\star, w^\star)$ of the exosystem (4.14) evolves in the bounded forward invariant set $\mathcal{K}^\star$, thus it is bounded. Similarly, q_i is bounded by construction. Due to Theorem 4.1, $(\tilde{\zeta}, \tilde{w})$ converge to zero, therefore $(\hat{\zeta}_i, \hat{w}_i)$ are bounded for all $i \in \mathcal{V}$. It remains to show that $\bar{\zeta}_i$, λ_i, z_i, and $\hat{p}_i$ are bounded, for all $i \in \mathcal{V}$. Concerning $\bar{\zeta}_i$, recall that $\bar{\zeta}_i := \mathcal{R}(\zeta_i)^\top \hat{\zeta}_i$, where $\zeta_i \in \mathbb{S}^1$, therefore $\bar{\zeta}_i$ is bounded because $|\bar{\zeta}_i| \le |\hat{\zeta}_i|$. Since $\bar{\zeta}_i$ is bounded, so is $kq_i\bar{e}_i$. Indicate with $\bar{k}_i$ the upper bound of $kq_i\bar{e}_i$, for a given set of initial conditions, and boundedness of λ_i is proven by parallel derivations to (4.71). To analyze $(z_i, \hat{p}_i)$, as in the proof of Theorem 4.2, consider the Lyapunov function

$$V_i(z_i, \hat{p}_i) := \frac{1}{2} m_i z_i^2 + \frac{1}{2\gamma} |\hat{p}_i - p_i|^2, \qquad i \in \mathcal{V}. \tag{4.79}$$

From (4.67) and (4.68), respectively for each $i \in \mathcal{V}$, similar steps to those in (4.73), (4.74) yield:

$$
\begin{aligned}
\dot{V}_i &= -k_z z_i^2 - \nu(\hat{p}_i - p_i)^\top \mathrm{dz}(\hat{p}_i) - m_i k_w z_i c^\top e_{w_i} \\
&\leq -\frac{k_z}{2} z_i^2 + \frac{1}{2k_z}|m_i k_w c^\top e_{w_i}|^2, \\
|\hat{p}_i| \geq r &\implies \dot{V}_i \leq -\frac{k_z}{2} z_i^2 - \nu\mu|\hat{p}_i|^2 + \frac{1}{2k_z}|m_i k_w c^\top e_{w_i}|^2.
\end{aligned}
\tag{4.80}
$$

These two bounds provide, respectively,

$$
\begin{aligned}
|z_i| &> \frac{m_i k_w|c|}{k_z}|e_{w_i}| \implies \dot{V}_i(z_i, \hat{p}_i) < 0, \\
|\hat{p}_i| &> \max\left\{ r, \frac{m_i k_w|c|}{\sqrt{2k_z \nu\mu}}|e_{w_i}| \right\} \implies \dot{V}_i(z_i, \hat{p}_i) < 0.
\end{aligned}
\tag{4.81}
$$

The two implications above prove that neither z_i nor $\hat{p}_i$ can grow unbounded because $e_w = (B \otimes I_n)\tilde{w}$ is bounded. Therefore, we conclude global boundedness of solutions. □

4.8 Numerical example

For the numerical analysis, we consider a Kuramoto model composed of six oscillators, whose parameters and initial conditions are reported in Table 4.1. In particular, the graph of the network is depicted in Figure 4.1, where the coupling parameters have been assigned as $k_{12} = 0.5$, $k_{13} = 3$, $k_{14} = 1$, $k_{16} = 1.5$, $k_{34} = 2$, $k_{45} = 2.5$, $k_{56} = 2$, $\varphi_{12} = \pi/2$, $\varphi_{13} = \pi/3$, $\varphi_{14} = \pi/4$, $\varphi_{16} = \pi/3$, $\varphi_{34} = \pi/5$, $\varphi_{45} = \pi/4$, $\varphi_{56} = \pi/2$. We suppose to have a rough knowledge of the parameter bounds by letting $\rho = 25$ in (4.5). It follows that Assumptions 4.1 and 4.3 hold. The leader exosystem (4.14) has been chosen as

$$
\begin{aligned}
\frac{d}{dt}\begin{bmatrix} \zeta_1^\star \\ \zeta_2^\star \end{bmatrix} &= \frac{1}{2}(w_1^\star + w_3^\star)J\begin{bmatrix} \zeta_1^\star \\ \zeta_2^\star \end{bmatrix} \\
\frac{d}{dt}\begin{bmatrix} w_1^\star \\ w_2^\star \\ w_3^\star \end{bmatrix} &= \begin{bmatrix} 0 \\ w_3^\star \\ -w_2^\star + \left(1 - \frac{1}{2}|w_3^\star|\right)\tanh(w_3^\star) + \frac{3}{2}\zeta_2^\star \end{bmatrix},
\end{aligned}
\tag{4.82}
$$

with initial conditions $\zeta^\star(0) = [1 \ 0]^\top$ and $w^\star(0) = [2 \ 0 \ 0]^\top$. For completeness, we briefly prove that Assumption 4.2 is satisfied. The existence of $\mathcal{K}^\star$ is guaranteed by proving boundedness of solutions of (4.82). Note that $(\zeta_1^\star, \zeta_2^\star, w_1^\star)$ are bounded by construction. On the other hand, boundedness of $(w_2^\star, w_3^\star)$ is proven by direct application of (Arcak and Teel, 2002, Theorem 2). We remark that, from the chosen initial conditions, the solution converges to a periodic orbit as depicted in Figures 4.3, 4.4. It can be easily shown that $s(\hat{\zeta}^\star, w^\star)$ is globally Lipschitz, since the derivative of the nonlinear term is bounded for all $w_3^\star$. From the numerical evaluation of the differential of s over the values of $(\zeta^\star, w^\star)$, we established a Lipschitz constant $\ell_s = 2.129$.

The Kuramoto model has been implemented according to (4.2), with the angles θ_i wrapped between -2π and 2π in order to ensure boundedness of the simulation variables. Then, for the computation of the feedback laws, the variables ζ_i have been
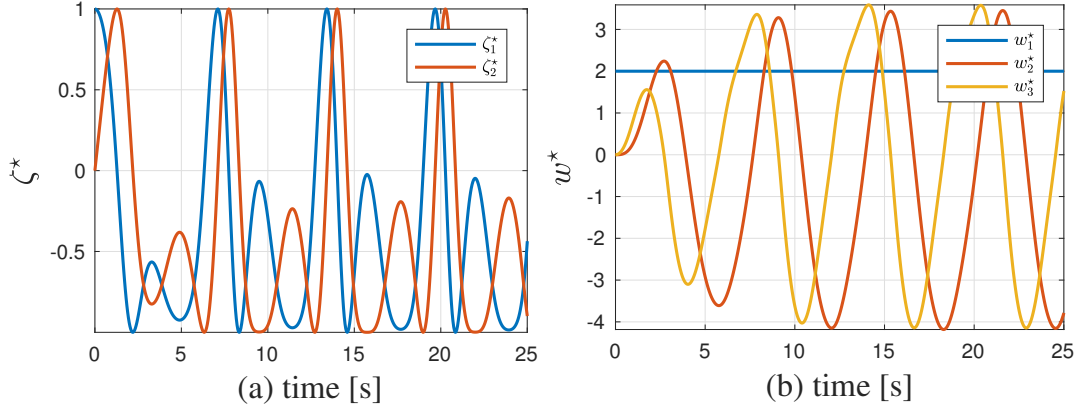
FIGURE 4.3: Response of exosystem (4.82) initialized in $\zeta^\star(0) = [1\ 0]^\top$, $w^\star(0) = [2\ 0\ 0]^\top$.
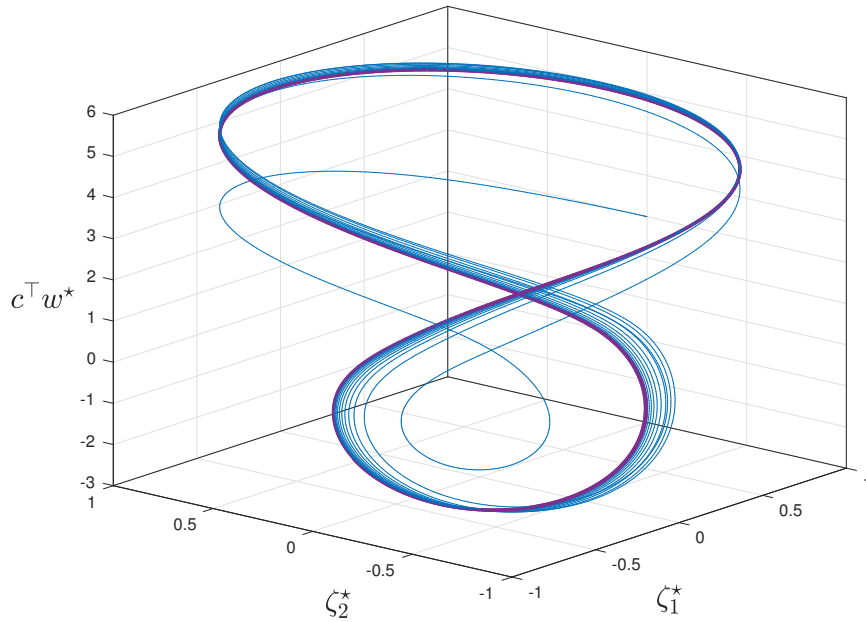
FIGURE 4.4: Response of exosystem (4.82) (in blue) and corresponding asymptotic behavior (in violet).

computed according to (4.8). The tuning parameters have been selected as $k_\zeta = 50$, $k_w = 50$, $\delta = 0.5$, $k = 1$, $k_z = 5$, $h = 2$, $\gamma = 1$, $\nu = 1$. Note that (4.41) is verified since $\underline{\sigma}(B) = 0.1136$. The initial conditions for controller (4.77) have been randomly chosen, where in particular the logic variables q_i have been initialized in the set $\mathcal{Q} := \{-1, 1\}$.

In Figures 4.5, 4.6 we report the results of a simulation run. Figure 4.5 shows the behavior of the distributed observer, which rapidly converges to the exosystem signals. On the other hand, Figure 4.6 depicts the tracking performance. In Figure 4.6-(e), we also report the evolution of $\hat{p}_1$, showing that the parameters of the adaptive controllers converge to constant values. Finally, we employ wrapped angles to depict the phase tracking performance in Figures 4.6-(f), 4.6-(g). In particular, we define

$$
\begin{aligned}
\vartheta^\star &:= 2\text{atan2}\left(\zeta_2^\star, \zeta_1^\star\right), \\
\vartheta_i &:= \text{mod}\left(\theta_i + \pi, 2\pi\right) - \pi, \qquad i \in \mathcal{V},
\end{aligned}
\tag{4.83}
$$

TABLE 4.1: Parameters and initial conditions of the oscillators

	m_i	d_i	ω_{ni}	$\theta_i(0)$	$\omega_i(0)$
oscillator #1	1.1	0.1	5	$-\pi$	2
oscillator #2	1.3	0.15	10	π	0.5
oscillator #3	1.2	0.2	15	$\pi/2$	1
oscillator #4	1.6	0.21	20	$-\pi/2$	0.3
oscillator #5	1.4	0.18	8	$\pi/3$	1.5
oscillator #6	1.5	0.13	18	$-\pi/3$	0.8
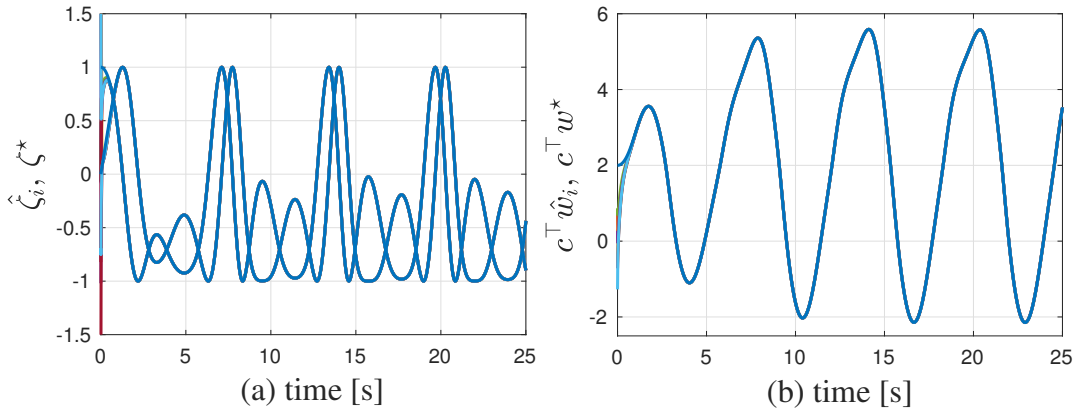
FIGURE 4.5: Closed-loop simulation results. (a): distributed observer phase estimation (reference in blue); (b): distributed observer frequency estimation (reference in blue).

where $\vartheta^\star$ is the angular reference corresponding to $\zeta^\star$, while ϑ_i is θ_i wrapped in the interval $[-\pi, \pi)$.

4.9 Conclusions

We introduced an adaptive hybrid control strategy for the robust global phase synchronization of second-order Kuramoto oscillators. The objective of phase synchronization was cast into a leader-follower tracking problem, where the leader system is modeled as an autonomous nonlinear exosystem. Under fairly mild assumptions on the network topology and the exosystem dynamics, we proved that our design, which comprises a distributed observer and an adaptive hybrid stabilizer, ensures robust global stability of a compact synchronization set. In particular, robust adaptive stabilization was ensured without requiring persistency of excitation conditions. Future efforts will be dedicated to relaxing the information requirements (e.g., by removing the frequency measurements) and the connectivity properties of the network. Furthermore, it will be worth generalizing the approach to a broader class of nonlinear oscillators.
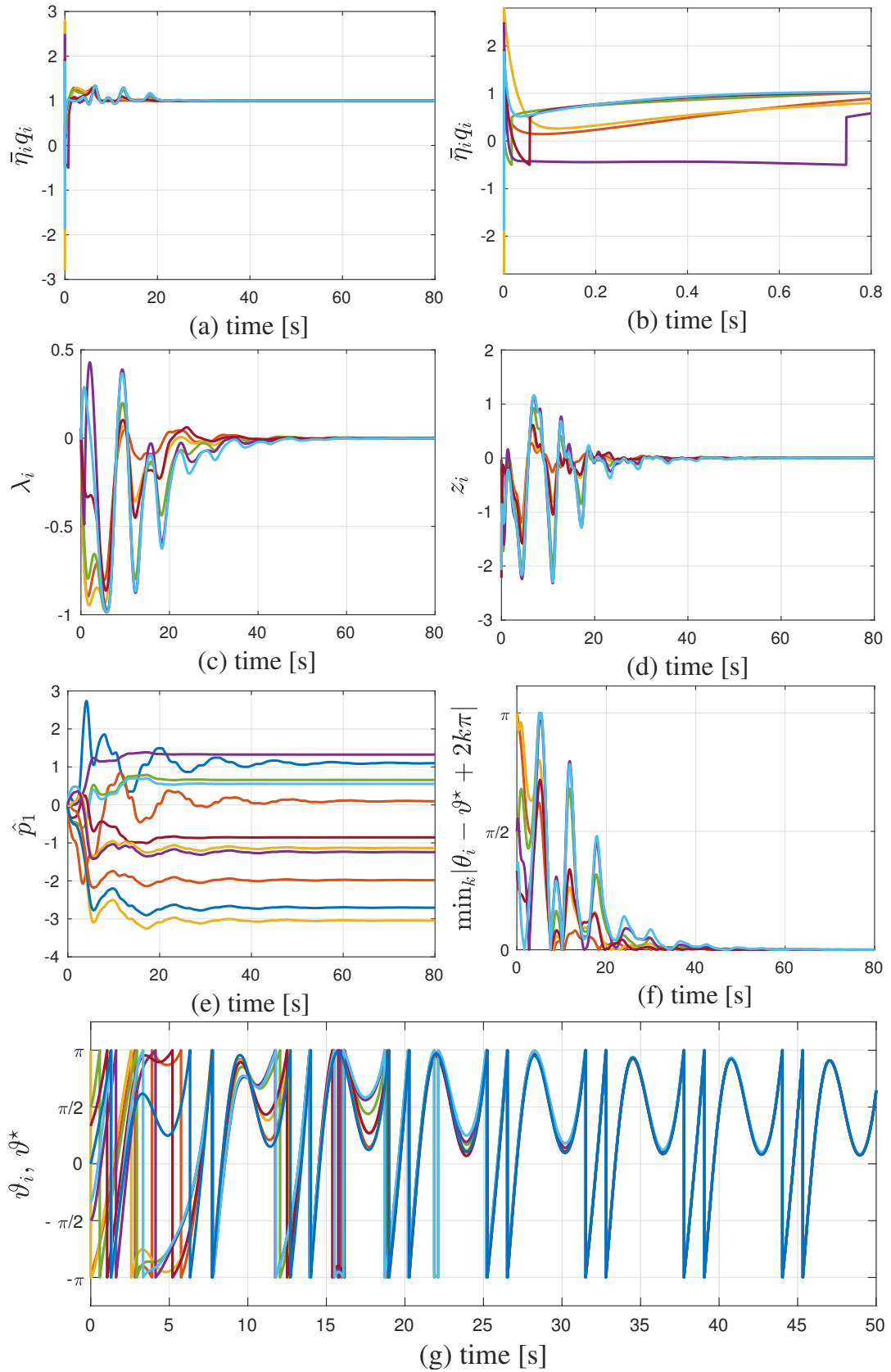
FIGURE 4.6: Closed-loop simulation results. (a): phase tracking errors; (b): phase tracking errors, zoomed in $[0, 0.8]$s to highlight the jumps during the initial transient; (c): filtered inputs λ_i; (d): frequency tracking errors z_i; (e): evolution of $\hat{p}_1$; (f): arc distance between θ_i and $\vartheta^\star$; (g): phase angles, wrapped in the interval $[-\pi, \pi)$ (reference in blue).

Part III

Robust Estimation for Mobile Robotics Applications

Chapter 5

An Adaptive Observer approach to Slip Estimation for Agricultural Tracked Vehicles

The chapter deals with autonomous Unmanned Ground Vehicles developed for precision agriculture contexts. The focus of this work is on the design of an adaptive observer for slip estimation ensuring exponential convergence to the real slip coefficients. Uniform global exponential stability of the origin of the error system is shown via Lyapunov analysis and persistency of excitation arguments. Furthermore, robustness to additive perturbations is shown in terms of Input-to-State Stability. Experimental results validate the effectiveness of the proposed estimator even in presence of noisy measurements.

5.1 Introduction

Mobile robotics in outdoor applications is already widespread in several fields (Delmerico et al., 2019; Azzollini, Mimmo, and Marconi, 2020; Chun and Papanikolopoulos, 2016; Yoshida, 2009). Recently, also agriculture, namely Precision Agriculture (PA), is merging farming techniques with data science and robotics to optimize farming processes (Haverkort, A.J. Ancha Srinivasan (ed), 2007; Slaughter, Giles, and Downey, 2008) and to support farmer decisions.

Currently, PA autonomous platforms are mostly deployed in *open-field* farming, while for Orchard PA (OPA) they are still at research level. The main difference between the two lies in the navigation. In open field, GPS data are enough to reliably navigate, while trees canopy and orchard structure can obstruct GPS signals requiring GPS-free navigation strategies. This work frames within the latter scenario and, in line with (Bergerman et al., 2015; Costley and Christensen, 2020; Mengoli, Tazzari, and Marconi, 2020), robot localization is achieved by leveraging odometry, LiDAR, and Inertia Measurement Unit (IMU).

Caterpillars feature a wider contact surface with the ground if compared to wheels, with a higher level of traction and stability. Therefore, they are the ideal choice for Unmanned Ground Vehicle (UGV) designed for rough terrains (Wong and Huang, 2006).

The main drawback of this locomotion system lies in the turning mechanism. In fact, the two tracks are actuated with different velocities causing the robot to skid over the ground - from here the name Skid-Steering Vehicles (SSVs) - shearing the terrain as in Figure 5.1. This slip reduces the reliability of odometry, making slip estimation even more relevant for localization and navigation purposes. Accurate slip estimation is also relevant for OPA tasks, as a good estimate of the vehicle velocity

FIGURE 5.1: Terrain shearing during turning maneuvers.

and position increases the capability of keeping a constant working speed, which is a key requirement in most of orchard operations, e.g. spraying.

Ideally, a SSV should behave as a Differential Wheeled Robot (DWR) but the presence of slip creates a mismatch between the two systems. This difference makes the problem of path following for tracked vehicles more complex and motivated several research activities aiming to design algorithms for estimating/compensating this effect. In particular, the kinematic slip has been modeled as a constant plus an additive zero-mean stochastic process and then estimated using Kalman filters as in (Zhou, Peng, and Han, 2007; Dar and Longoria, 2010; Rogers-Marcovitz, Seegmiller, and Kelly, 2012; Sebastian and Ben-Tzvi, 2019) or adaptively (Burke, 2012). On the other hand, (Nagatani, Endo, and Yoshida, 2007; Endo et al., 2007) studied the relation between the slip and track speeds, remarking the dependence of the slip on track velocities, turning radius and soil properties. However, these relations work only when the turning radius is kept small enough. Differently from all the other approaches, (Moosavian and Kalantari, 2008), (Rajagopalan, Meriçli, and Kelly, 2016) were driven by data fitting, leading to the definition of ad hoc slip models tailored for the specific platform-terrain combination considered.

Focusing on adaptive approaches, (Burke, 2012) models the slip as a random walk, estimating it through a recursive least squares and then using it to adapt the control action considering a DWR-based reference model, following a direct model reference adaptive control approach. Instead, (Yi et al., 2007) designs an adaptive feedback linearization control for the dynamic model of a wheeled SSV. We observe that, in line with classic adaptive control literature, both (Burke, 2012) and (Yi et al., 2007) share the need of Persistency of Excitation (PE) conditions in order to have convergence of the slip estimates to the true slip coefficients, without discussing in details what this would mean in terms of mobile robot trajectories.

In this chapter, we propose an adaptive observer which robustly estimates the slip coefficients with an exponential convergence rate, assuming the UGV moves at constant linear and angular velocities. This assumption is in line with the typical navigation trajectories required to be performed by an orchard agriculture robot. In particular, we design our estimator by mixing an identity observer with classic

adaptive laws, the latter found via a Lyapunov analysis. The design choice is convenient to bring the error system in a standard form (Panteley, Loria, and Teel, 2001). Moreover, in contrast to existing adaptive approaches (Burke, 2012; Yi et al., 2007), we formally prove how the considered trajectories are persistently exciting for our estimator, resulting in a globally uniformly exponentially stable origin for the estimation error system.

5.2 Notation

We denote by $\mathbb{R}$ the set of real numbers and we define $\mathbb{R}_{\geq 0} := [0, \infty)$. $|\cdot|$ denotes the Euclidian norm of vectors and induced norm of matrices, while $|\cdot|_p$, with $p \in [1, \infty]$, indicates the $\mathcal{L}_p$ norm of time signals. In particular, for a measurable function $\phi : \mathbb{R}_{\geq 0} \to \mathbb{R}^n$, $|\phi|_p := (\int_{t_0}^{\infty} |\phi(t)|^p \ dt)^{1/p}$ for $p \in [1, \infty)$, and $|\phi|_\infty := \text{ess sup}_{t \geq t_0} |\phi(t)|$. For $c_r > 0$, B_{c_r} denotes the open ball $B_{c_r} := \{x \in \mathbb{R}^n : |x| < c_r\}$. A function $\gamma : \mathbb{R}_{\geq 0} \to \mathbb{R}_{\geq 0}$ belongs to *class-$\mathcal{K}$* ($\gamma \in \mathcal{K}$) if it is continuous, strictly increasing and $\gamma(0) = 0$. Moreover, if in addition $\gamma(s) \to_{s \to \infty} \infty$, γ is said to belong to *class-$\mathcal{K}_\infty$* ($\gamma \in \mathcal{K}_\infty$). A solution to the differential equation $\dot{x} = f(t, x)$ at time t with initial conditions $(t_0, x_0) \in \mathbb{R}_{\geq 0} \times \mathbb{R}^n$ is denoted as $(x(t, t_0, x_0))$, or simply $x(t)$. For the function $V : \mathbb{R}_{\geq 0} \times \mathbb{R}^n \to \mathbb{R}$, we define $\dot{V}_{(\#)}(t, x) := (\partial V / \partial t) + (\partial V / \partial x) f(t, x)$ where (#) denotes the equation number that labels equation $\dot{x} = f(t, x)$.

5.3 Models

SSV kinematic model

Under the main assumption of planar motion, we consider the following kinematic model, described with respect to an inertial reference frame $\mathcal{F}_i(O_i, x, y, z)$, as

$$
\begin{aligned}
\dot{x} &= V_G \cos \theta \\
\dot{y} &= V_G \sin \theta \\
\dot{\theta} &= \Omega_z
\end{aligned}
\tag{5.1}
$$

where V_G is the linear velocity of the Center of Gravity (CoG) in body coordinates, $\mathcal{F}_b(O_b, x_b, y_b, z_b)$, and Ω_z represents the angular velocity of the vehicle around the axis normal to the motion plane. The main quantities of interest are also presented in Figure 5.2. Both SSVs and DWRs kinematics can be described using (5.1), due to their nonholonomic nature. The main difference lies in the expressions of V_G and Ω_z. In fact, for DWRs they can be computed as

$$
\begin{aligned}
V_G &= \frac{v_R + v_L}{2} = \frac{r}{2}(\omega_R + \omega_L) \\
\Omega_z &= \frac{v_R - v_L}{2d} = \frac{r}{2d}(\omega_R - \omega_L)
\end{aligned}
\tag{5.2}
$$
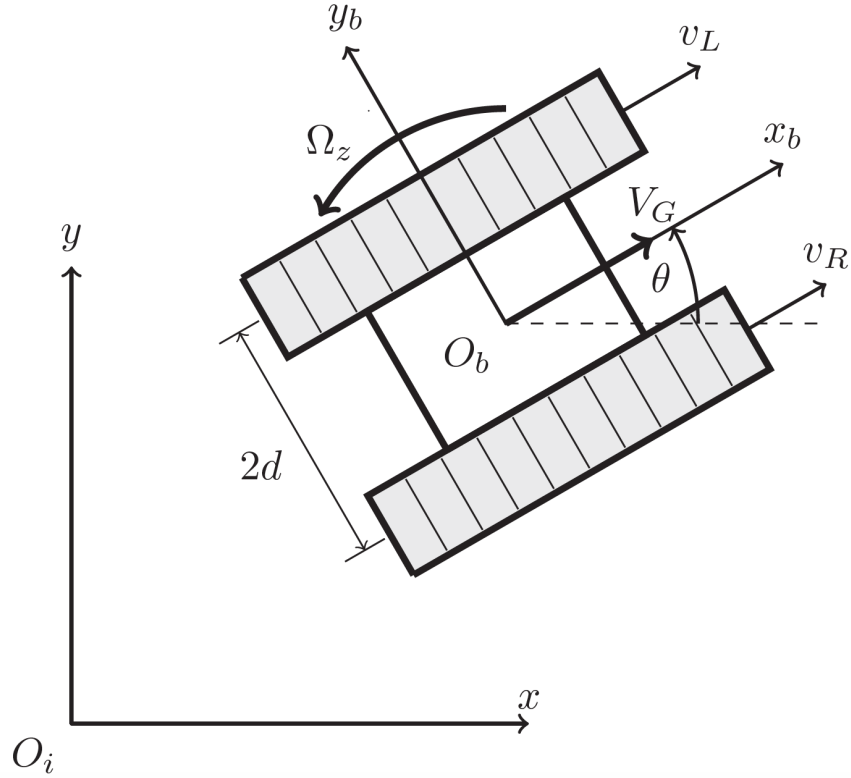
FIGURE 5.2: Planar motion of a tracked vehicle.

while for SSVs the same quantities are expressed as

$$
\begin{aligned}
V_G &= \frac{v_R(1 - i_R(t)) + v_L(1 - i_L(t))}{2} \\
&= \frac{r}{2}(\omega_R(1 - i_R(t)) + \omega_L(1 - i_L(t))) \\
\Omega_z &= \frac{v_R(1 - i_R(t)) - v_L(1 - i_L(t))}{2d} \\
&= \frac{r}{2d}(\omega_R(1 - i_R(t)) - \omega_L(1 - i_L(t))).
\end{aligned}
\tag{5.3}
$$

The quantities ω_R, ω_L are the right and left angular motor speeds, respectively, and similarly, v_R, v_L represent the linear velocities of the right and left wheel (or track). The quantity r is the wheel (or track sprocket) radius, while d is half the distance between the center lines passing through the two wheels (or tracks), also shown in Figure 5.2. The difference between (5.2) and (5.3) is given by the presence of $i_R(t), i_L(t) \in (-1, 1)$ that are the time-varying slip coefficients associated with the right and left track, respectively. Notice that in (5.3), the real inputs driving the system are $(1 - i_R)v_R$ and $(1 - i_L)v_L$, resulting in a variation of the efficiency of the control inputs v_L, v_R. By letting

$$
\begin{cases}
\eta_R := 1 - i_R, & 0 < \eta_R < 2 \\
\eta_L := 1 - i_L, & 0 < \eta_L < 2
\end{cases}
\tag{5.4}
$$

the overall kinematic model (5.1) is rewritten as

$$\dot{x} = \frac{\eta_R \cos\theta}{2} v_R + \frac{\eta_L \cos\theta}{2} v_L$$
$$\dot{y} = \frac{\eta_R \sin\theta}{2} v_R + \frac{\eta_L \sin\theta}{2} v_L \qquad (5.5)$$
$$\dot{\theta} = \frac{\eta_R}{2d} v_R - \frac{\eta_L}{2d} v_L \ ,$$

which is a system with control inputs v_R, v_L, and exogenous (uncontrollable) inputs η_R, η_L.

Slip coefficients model

While it is a well-known fact (Bekker, 1960; Wong, 2008; Nagatani, Endo, and Yoshida, 2007; Endo et al., 2007) that i_R, i_L depend on the soil type as well as on the track velocities (both absolute and relative to each other), to the best of authors' knowledge, a mathematical model capturing the underlying complex relation is not available in literature. In (Nagatani, Endo, and Yoshida, 2007) and (Endo et al., 2007), it is observed that there is a nonlinear relation between the ratio $i_R(t)/i_L(t)$ and v_R, v_L but this result is limited to small turning radii, and a complete relation also including soil dependency is still missing.

In general, track slip coefficients are expressed as

$$i = 1 - \frac{V_t}{v_i} = 1 - \frac{V_t}{\omega r} \qquad (5.6)$$

where i is the slip coefficient of a track, v_i is the ideal velocity of the track given by the product of the driving sprocket rotational speed ω and its radius r, and V_t is the actual speed of the track-ground contact point (which is hardly measurable). Equation (5.6) shows the relation between the value of the slip coefficient and the track velocity, but it does not show any dependency on soil-related parameters.

On the other hand, (Bekker, 1960) and (Wong, 2008) report a relation between slip coefficients and the traction force of the track to the ground, which depends on the physical properties of the terrain according to

$$F = F_{max} \left[1 - \frac{K}{il} \left(1 - e^{-\frac{il}{K}} \right) \right] \qquad (5.7)$$

where l is the length of the contact surface between the track and the ground, K represents the soil shear deformation modulus and F_{max} is the maximum traction force developed by a track. The latter can be expressed as

$$F_{max} = S_c \tau_{max} = S_c \left(c + p \tan\varphi \right) = S_c c + \frac{W}{2} \tan\varphi$$

in which S_c is the track-ground contact surface, τ_{max} the maximum shear strength of the terrain, c the apparent cohesion of the terrain and φ the angle of internal shearing resistance of the soil, p is the normal pressure acting on the track and W the total weight of the vehicle. Inverting (5.7) it is then possible to retrieve the slip coefficient of the track, given soil parameters and the traction forces applied by each of them, as done in (Zou, Angeles, and Hassani, 2018). Once again, the relation found is incomplete, as it does not relate both track velocities and soil features in a single equation.

In conclusion, both (5.6) and (5.7) are incomplete and therefore there is no advantage in considering the dynamic model over the kinematic one for problems of slip estimation.

5.4   Problem statement

The following general problem is considered.

Problem 5.1. *Considering system* (5.5), *the problem at hand is to design a dynamical system with inputs* x, y, θ, v_R, v_L, *producing as output the estimates* $\hat{\eta}_R$, $\hat{\eta}_L$ *asymptotically converging to the true coefficients* η_R *and* η_L, *respectively.*

As emphasized previously, the general problem is hard to be solved as it would require a model relating the intrinsically time-varying slip coefficients to the system states and inputs, as well as to the time-varying (and practically impossible to be modeled or measured) terrain parameters. The application framework given by OPA leads to simplifying assumptions making the problem more tractable, as most of the farming tasks require to navigate the orchard at a constant speed.

Orchard works feature a repetitive pattern in which one has to travel along the field lane, then switch to the following one, and so on. Therefore, it is possible to define two different navigation scenarios:

- *Straight motion* - navigating the current orchard row at a constant speed;

- *Turning motion* - switching from the current row to the next one at constant speed and turning radius.

While for straight motion constant speed is required by the tasks themselves (e.g to uniformly spray pesticides), for turning motion it is simply the most efficient trajectory for SSVs. In (Bergerman et al., 2015), where car-like vehicles are considered, it is shown that particular techniques have to be adopted for lane-switching manoeuvres, being turning radii bounded by their steering capabilities. Differently, SSVs allow one to perform turning manoeuvres with small turning radius (even zero).

Notice that each scenario requires the robot to move at a constant V_G and Ω_Z, which are obtained, according to (5.2), from constant values of v_R, v_L. From (5.6), it is possible to claim that when v_i is constant, i is constant as well. On the other hand, provided that constant track velocities are given by constant track forces, (5.7) requires the terrain to be homogeneous in order to obtain constant coefficients, which is a reasonable assumption in OPA. Then, this application framework allows one to rewrite the coefficients $i_R(t)$ and $i_L(t)$ as constants, namely $i_R(t) = i_R$ and $i_L(t) = i_L$. We want to comment already at this point that these considerations are validated by all the experimental results we performed on the field (as described in Section 5.6). Formally, the problem is considered under the following assumption.

Assumption 5.1. *The linear velocities* v_R, v_L *in* (5.5) *are constant and positive. Moreover, the soil is homogeneous, therefore also* i_R, i_L *are constant.*

5.5 Main result

Assuming that x, y, θ, v_R, v_L can be measured, the proposed estimator is the *adaptive identity observer*:

$$
\begin{bmatrix} \dot{\hat{x}} \\ \dot{\hat{y}} \\ \dot{\hat{\theta}} \end{bmatrix} = \begin{bmatrix} \dfrac{\cos\theta}{2}v_R & \dfrac{\cos\theta}{2}v_L \\ \dfrac{\sin\theta}{2}v_R & \dfrac{\sin\theta}{2}v_L \\ \dfrac{1}{2d}v_R & -\dfrac{1}{2d}v_L \end{bmatrix} \begin{bmatrix} \hat{\eta}_R \\ \hat{\eta}_L \end{bmatrix} + \underbrace{\begin{bmatrix} l_1 & 0 & 0 \\ 0 & l_2 & 0 \\ 0 & 0 & l_3 \end{bmatrix}}_{L} \begin{bmatrix} e_x \\ e_y \\ e_\theta \end{bmatrix}
$$

$$
\begin{bmatrix} \dot{\hat{\eta}}_R \\ \dot{\hat{\eta}}_L \end{bmatrix} = \underbrace{\begin{bmatrix} \lambda_1 & 0 \\ 0 & \lambda_2 \end{bmatrix}}_{\Lambda} \begin{bmatrix} \dfrac{\cos\theta}{2}v_R & \dfrac{\sin\theta}{2}v_R & \dfrac{1}{2d}v_R \\ \dfrac{\cos\theta}{2}v_L & \dfrac{\sin\theta}{2}v_L & -\dfrac{1}{2d}v_L \end{bmatrix} \begin{bmatrix} e_x \\ e_y \\ e_\theta \end{bmatrix}
\tag{5.8}
$$

where the state $\begin{bmatrix} \hat{x} & \hat{y} & \hat{\theta} & \hat{\eta}_R & \hat{\eta}_L \end{bmatrix}^\top \in \mathbb{R}^5$ contains the estimates of $x, y, \theta, \eta_R, \eta_L$ in (5.5), the output-injection matrix $L \in \mathbb{R}^{3\times3}$ and the adaptive-gain matrix $\Lambda \in \mathbb{R}^{2\times2}$ are design parameters to be chosen, and we define the *observation error*

$$
e = \begin{bmatrix} e_x \\ e_y \\ e_\theta \end{bmatrix} = \begin{bmatrix} x - \hat{x} \\ y - \hat{y} \\ \theta - \hat{\theta} \end{bmatrix}.
\tag{5.9}
$$

The properties of the estimator are presented in the following theorem, which represents the main result of this work.

Theorem 5.1. *Under Assumption 5.1, the problem of slip coefficients estimation is solved by the adaptive observer (5.8) with arbitrary initial conditions, and with L and Λ positive definite. In particular, the estimator guarantees uniform exponential convergence of the estimates to the true slip coefficients as time goes to infinity: $\hat{\eta}_R \to \eta_R, \hat{\eta}_L \to \eta_L$.*

Proof. We change coordinates by considering the observation error, (5.9), along with the *estimation error*

$$
\tilde{\eta} = \begin{bmatrix} \tilde{\eta}_R \\ \tilde{\eta}_L \end{bmatrix} = \begin{bmatrix} \hat{\eta}_R - \eta_R \\ \hat{\eta}_L - \eta_L \end{bmatrix}.
$$

Thus, system (5.8) in the new error coordinates becomes

$$
\dot{\varepsilon} = \begin{bmatrix} \dot{e} \\ \dot{\tilde{\eta}} \end{bmatrix} = \begin{bmatrix} -L & \Phi^\top(t) \\ -\Lambda\Phi(t) & 0 \end{bmatrix} \begin{bmatrix} e \\ \tilde{\eta} \end{bmatrix} = A(t, \varepsilon)
\tag{5.10}
$$

where, we call *regressor* the matrix

$$
\Phi(t) = \begin{bmatrix} -\dfrac{\cos\theta(t)}{2}v_R & -\dfrac{\sin\theta(t)}{2}v_R & -\dfrac{1}{2d}v_R \\ -\dfrac{\cos\theta(t)}{2}v_L & -\dfrac{\sin\theta(t)}{2}v_L & \dfrac{1}{2d}v_L \end{bmatrix}.
\tag{5.11}
$$

System (5.10) is almost standard in adaptive control literature, with the peculiarity of having a matrix regressor, instead of just a vector.

Solving our problem is equivalent to conclude uniform global asymptotic stability of the origin for the error system (error system 0-UGAS). To treat our problem we rely on Corollary 1 and Theorem 2 of (Panteley, Loria, and Teel, 2001). These results

require two assumptions (A1, A2) to hold, as well as requiring the pair (Φ, A) to be uniformly persistently exciting (u-PE).

A1 (Panteley, Loria, and Teel, 2001) *There exist $\gamma_1 \in \mathcal{K}_\infty$, a locally bounded function $\gamma_2 : \mathbb{R}_{\geq 0} \to \mathbb{R}_{\geq 0}$ and a positive definite continuous function $\gamma_3 : \mathbb{R}_{\geq 0} \to \mathbb{R}_{\geq 0}$, such that for all (t_0, ε_0), all corresponding solutions of* (5.10) *satisfy*

$$|\varepsilon|_\infty \leq \gamma_1(|\varepsilon_0|)$$
$$|\gamma_3(|e|)|_1 \leq \gamma_2(|\varepsilon_0|). \tag{5.12}$$

From (Panteley, Loria, and Teel, 2001, Remark 4) we know that A1 is satisfied if, for instance, there exist a locally Lipschitz function V and two functions $\underline{\alpha}, \bar{\alpha} \in \mathcal{K}_\infty$ such that

$$\underline{\alpha}(|\varepsilon|) \leq V(t, \varepsilon) \leq \bar{\alpha}(|\varepsilon|)$$
$$\dot{V}_{(5.10)}(t, \varepsilon) \leq -\gamma_3(|e|).$$

To prove this, we consider the Lyapunov function candidate

$$V(\varepsilon) = \frac{1}{2} \left(e^\top L^{-1} e + \tilde{\eta}^\top \Lambda^{-1} \tilde{\eta} \right)$$

which is a valid candidate by choosing $l_1 > 0$, $l_2 > 0$, $l_3 > 0$, $\lambda_1 > 0$, $\lambda_2 > 0$, as stated in Theorem 5.1. Now, its time derivative along the error system trajectories is

$$\dot{V}_{(5.10)}(\varepsilon) = -e^\top e + e^\top \Phi^\top \tilde{\eta} - \tilde{\eta}^\top \Phi e$$
$$= - |e(t)|^2 = -\gamma_3(|e|) \tag{5.13}$$

which is negative semidefinite. In addition, each entry of the regressor $\Phi(t)$ is bounded and globally Lipschitz. Therefore, by La Salle/Yoshizawa (Khalil, 2002, Theorem 8.4), system (5.10) is 0-UGS and

$$\lim_{t \to \infty} |e(t)|^2 = 0$$

resulting in $e(t) \to 0$, satisfying A1. In fact, we can introduce $c_m, c_M > 0$ such that

$$\underline{\alpha}(|\varepsilon|) = c_m^2 |\varepsilon|^2 \leq V(\varepsilon) \leq c_M^2 |\varepsilon|^2 = \bar{\alpha}(|\varepsilon|).$$

Moreover, being $V(\varepsilon)$ a positive nonincreasing function bounded from below by 0, we conclude that it has a limit

$$\lim_{t \to \infty} V(t) = V_\infty.$$

Integrating (5.13) from t_0 to ∞, it results

$$\int_{t_0}^\infty |e(\tau)|^2 \, d\tau = - \int_{t_0}^\infty \dot{V}(\tau) \, d\tau = V(\varepsilon_0) - V_\infty$$

and we have

$$V(\varepsilon_0) - V_\infty \leq V(\varepsilon_0) \leq c_M^2 |\varepsilon_0|^2 = \gamma_2(|\varepsilon_0|).$$

Also,

$$c_m^2 |\varepsilon|_\infty^2 \leq c_m^2 |\varepsilon(t)|^2 \leq V(\varepsilon(t)) \leq V(\varepsilon_0) \leq c_M^2 |\varepsilon_0|^2$$

from which $|\varepsilon|_\infty \le (c_M/c_m)\,|\varepsilon_0|$. Thus (5.12) holds with $\gamma_1(s) = (c_M/c_m)s$, $\gamma_2(s) = c_M^2 s^2$ and $\gamma_3(s) = s^2$.

A2 (Panteley, Loria, and Teel, 2001) *Each entry of Φ is locally Lipschitz, and there exist nondecreasing functions $\rho_i : \mathbb{R}_{\ge 0} \to \mathbb{R}_{\ge 0}$, $(i = 1,2,3)$ such that, for almost all $(t, \varepsilon) \in \mathbb{R}_{\ge 0} \times \mathbb{R}^5$*

$$\max\{|Le|\,,|\Lambda\Phi e|\} \le \rho_1(|\varepsilon|)\,|e|$$
$$|\Phi| \le \rho_2(|\varepsilon|)$$
$$\left|\frac{\partial\Phi}{\partial t}\right| \le \rho_3(|\varepsilon|).$$

Being the entries of our regressor bounded and globally Lipschitz, A2 trivially holds with some constants ρ_1, ρ_2, ρ_3.

Definition: u-PE (Panteley, Loria, and Teel, 2001) *The pair (Φ, A) is called uniformly persistently exciting (u-PE) if, for each $c_r > 0$, there exist $\mu, T > 0$, such that, for all $(t_0, \varepsilon_0) \in \mathbb{R}_{\ge 0} \times B_{c_r}$, all corresponding solutions satisfy*

$$\int_t^{t+T} \Phi(\tau)\Phi^\top(\tau)\,d\tau \ge \mu I \quad \forall t \ge t_0. \tag{5.14}$$

In general it is difficult to check the u-PE condition since it must be valid for all possible solutions, clearly impossible to be known a priori. However, the proposed design leads to

$$\Phi\Phi^T = \begin{bmatrix} \dfrac{v_R^2}{4}\left(1 + \dfrac{1}{d^2}\right) & \dfrac{v_R v_L}{4}\left(1 - \dfrac{1}{d^2}\right) \\[2ex] \dfrac{v_R v_L}{4}\left(1 - \dfrac{1}{d^2}\right) & \dfrac{v_L^2}{4}\left(1 + \dfrac{1}{d^2}\right) \end{bmatrix}$$

which is positive definite for any positive v_R, v_L. In particular, it is even constant and positive definite under Assumption 5.1, and, as a consequence, (5.14) is directly satisfied in both scenarios. Under A1, A2 and having u-PE, we conclude that the error system (5.10) is 0-UGAS (Panteley, Loria, and Teel, 2001, Corollary 1).

Moreover, by Panteley, Loria, and Teel, 2001, Theorem 2 we conclude 0-UGES as: (i) $\Phi(t)$ is independent of ε; (ii) $\gamma_1(s)$, $\gamma_2(s)$, $\gamma_3(s)$ are proportional to s, s^2, and s^2, respectively, for all s. $\qquad\square$

Remark 5.1. *The extra requirement given by the u-PE property does not only guarantee convergence to the true parameters, but it also guarantees robustness for the error system (5.10) with respect to additive perturbations (i.e. considering $\dot\varepsilon = A(t, \varepsilon) + d(t)$). In particular, when the u-PE contributes to conclude uniform global asymptotic stability, the error system is "totally stable", which means it is robust against "small" nonvanishing perturbations (Panteley, Loria, and Teel, 2001, Equation (13)). In our case, u-PE induces uniform global exponential stability, so the error system is robust with respect to arbitrarily large nonvanishing perturbations as the system is globally input-to-state stable (Khalil, 2002, Lemma 4.6). This property derives from a converse Lyapunov theorem (Khalil, 2002, Theorem 4.14). Robustness of the proposed adaptive observer is shown in Section 5.6 as we have real noisy measurements.*

The vast majority of other designs present in the literature, explicitly or implicitly assume the slip coefficients to be constant (resulting in a zero-error result) or slowly time-varying (resulting in a small-error "practical" result). Our work is perfectly in line with these results and, in addition: (i) we discuss how only with constant track velocities and homogeneous soil

it makes sense to consider constant slip coefficients; (ii) we formally prove that for any positive constant track velocities we have u-PE and related robustness. Notice that with other design choices the straight motion could result to be not u-PE (Burke, 2012).

Remark 5.2. *Oftentimes, adaptive approaches are not appealing for robotics applications as, in order to have robustness (which is induced by the u-PE property), the robot needs to perform some kind of oscillatory trajectories in order to obtain sufficiently rich signals. In contrast to this, with our design we have u-PE even for constant inputs v_R, v_L, resulting in smooth trajectories, which makes the designed estimator appealing for OPA applications.*

Remark 5.3. *The design of an identity observer on top of the adaptive laws may seem redundant as we are measuring the whole state. The intuition behind the proposed design comes from noticing that* (5.5) *is linear in the parameters to be found:*

$$\begin{bmatrix} \dot{x} & \dot{y} & \dot{\theta} \end{bmatrix}^\top = -\Phi^\top \begin{bmatrix} \eta_R & \eta_L \end{bmatrix}^\top$$

where, as already emphasized by Assumption 5.1, the unknown parameters η_R, η_L are constant. This is a desirable scenario for designing adaptive laws. However, as we do not have direct measurements of $\dot{x}, \dot{y}, \dot{\theta}$, we cannot design estimation laws for the unknown parameters without designing any extra dynamical system. This reasoning is what justified our choice to design an identity observer to be combined with the estimation laws. This choice resulted to be very convenient both in order to bring the error system in the standard form (5.10), *and in terms of u-PE requirement.*

5.6 Experimental results

Experimental tests were performed using the agricultural tracked UGV described in details in (Mengoli, Tazzari, and Marconi, 2020) and (Tazzari, Mengoli, and Marconi, 2020). In particular, the state measurements were provided by the onboard sensor suite. Namely, we measured x, y, θ using a high precision GNSS sensor with an embedded compass. Notice that we used raw-data measurements, without any filtering, to highlight robustness of the proposed design.

To compare the estimates of slip coefficients coming from (5.8) with ground truth values, we used (5.6) as follows:

$$
\begin{aligned}
i_R &= 1 - \frac{V_{t,R}}{v_R} = 1 - \frac{V_{G,m} + d\Omega_{z,m}}{v_{R,m}} \\
i_L &= 1 - \frac{V_{t,L}}{v_L} = 1 - \frac{V_{G,m} - d\Omega_{z,m}}{v_{L,m}}
\end{aligned}
\tag{5.15}
$$

in which, $V_{t,R}, V_{t,L}$ are the right and left track true velocities, respectively. The subscript m identifies the measured quantities: $V_{G,m}$ from the GNSS, $\Omega_{z,m}$ from IMU data (gyroscope) and $v_{R,m}, v_{R,m}$ collected from motor encoders. For ground truth sake, we performed the experiments in open-field and not inside orchard rows, in order to obtain more accurate and reliable GNSS data.

To test the performance of (5.8) in both the navigation scenarios described above, we carried out experiments in which the robot negotiated: (i) a circular trajectory, as shown in Figure 5.3.a with constant turning radius and angular velocity, in fact, Figure 5.3.b shows noisy but constant values of v_L, v_R; (ii) a straight linear trajectory, as shown in Figure 5.3.c, with constant linear body velocity, indeed, Figure 5.3.d shows constant values of the two tracks velocities, highlighting the noisy nature of measurements collected.
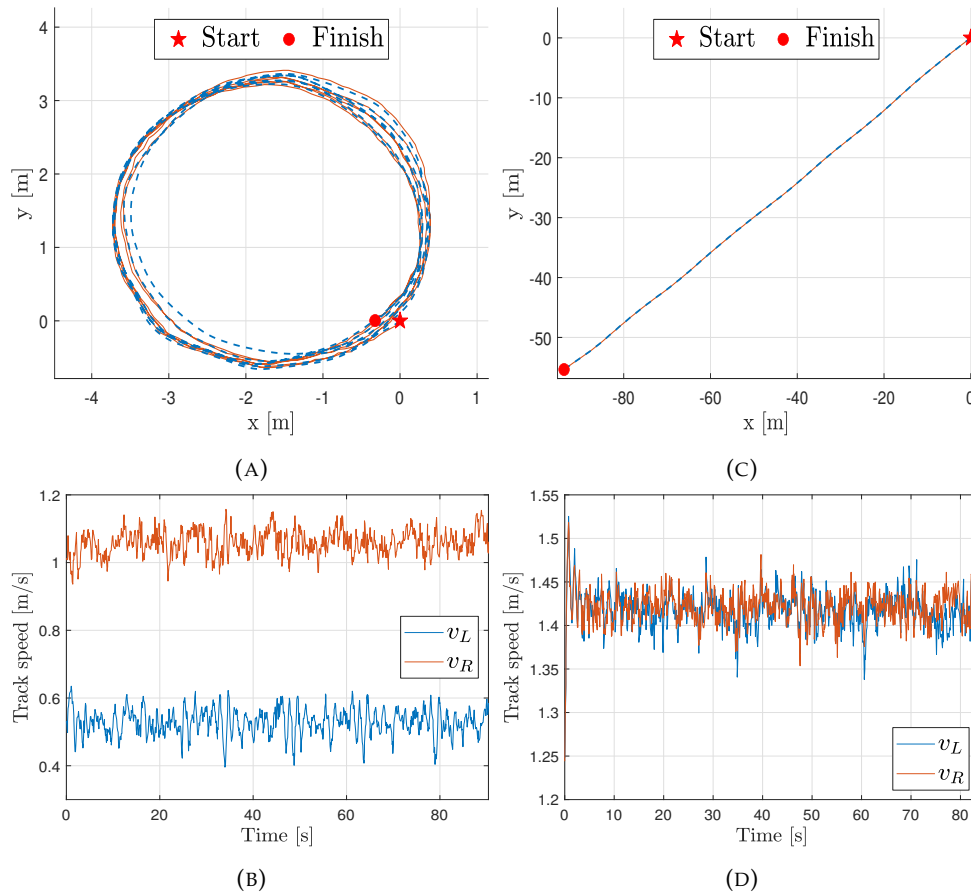
(A)

(C)

(B)

(D)

FIGURE 5.3: Circular and straight motion experiments. (a),(c): Measured (continuous) and estimated position (dashed) trajectories. (b),(d): Corresponding track velocities.
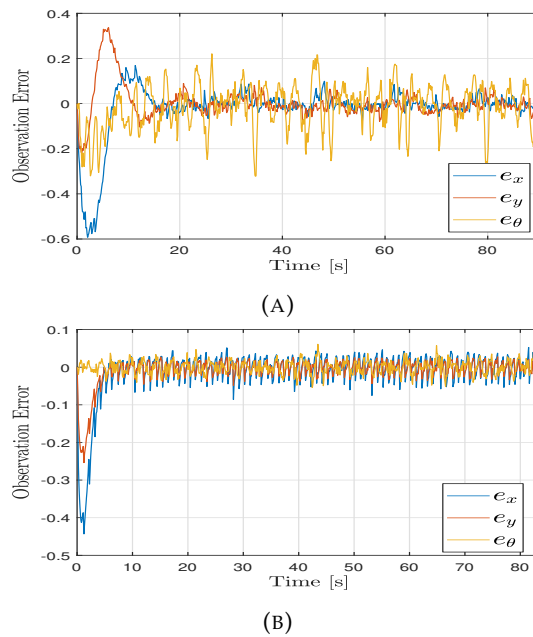

(A)

(B)

FIGURE 5.4: Observation error (5.9): (a) circular and (b) straight motion.

While Figure 5.3.a and Figure 5.3.c qualitatively show how the observed trajectory and the real ones tend to overlap, Figure 5.4.a and Figure 5.4.b give proper values of the observation errors e_x, e_y, e_θ, respectively for circular and straight motion tests.

As expected from Remark 5.1, Figure 5.5 shows the robust convergence of the estimated slip coefficients $\hat{\eta}_L, \hat{\eta}_R$, to the real ones, η_L, η_R, approximated using (5.4) and (5.15).
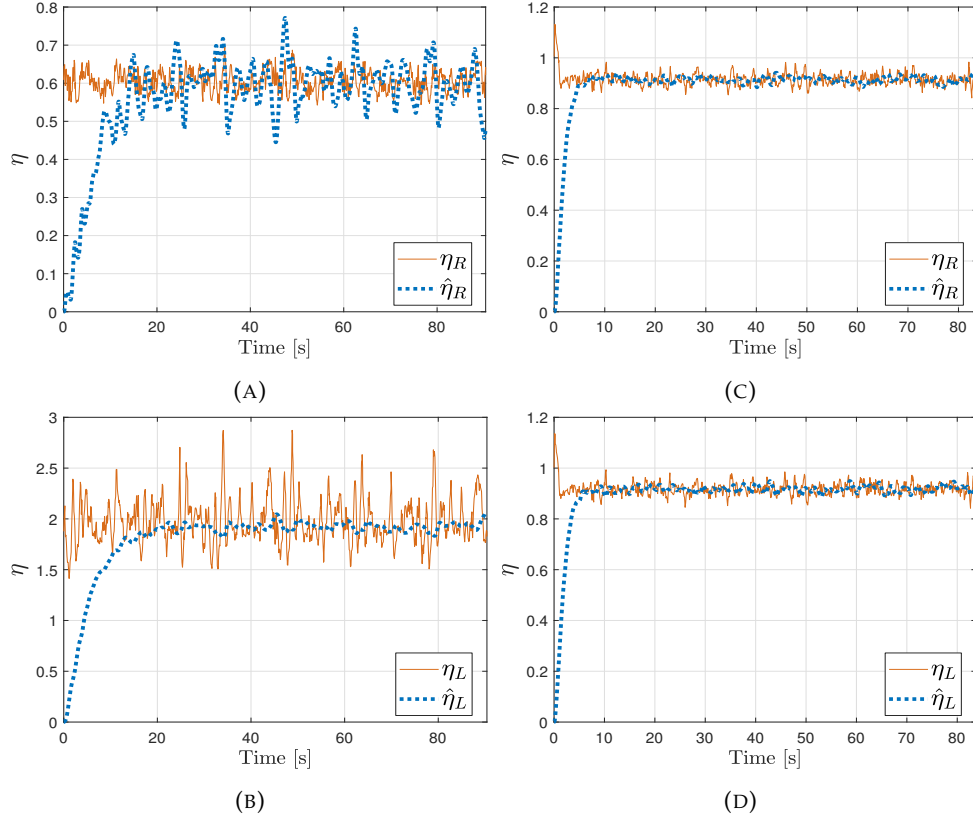
FIGURE 5.5: Slip estimation: (a),(b) circular and (c),(d) straight motion.

It is also important to mention that the good performance obtained during experimental tests are not given by specifically-tuned observer parameters, but rather by the structural properties described and proved in Sec. 5.5. In fact, both L, Λ have been considered as identity matrices (this also explains the convergence time), since the focus of this chapter is to show the effectiveness of the proposed approach rather than fine tuning parameters for a particular application. In the end, Figure 5.6 and Figure 5.7 point out what said in Remark 5.2, in noise-free cases. The convergence of the slip coefficients to real values is asymptotic and not just practical as before, remarking once again u-PE of the trajectories. To show this, we fed the observer with mean values obtained by the tests shown in the cases above, achieving asymptotic convergence both in turning and straight motion scenarios.

5.7 Conclusions

In this work, we presented an adaptive observer for slip estimation for tracked skid-steering vehicles. We formally proved uniform global exponential stability of the error system, resulting in robustness with respect to additive perturbations in terms
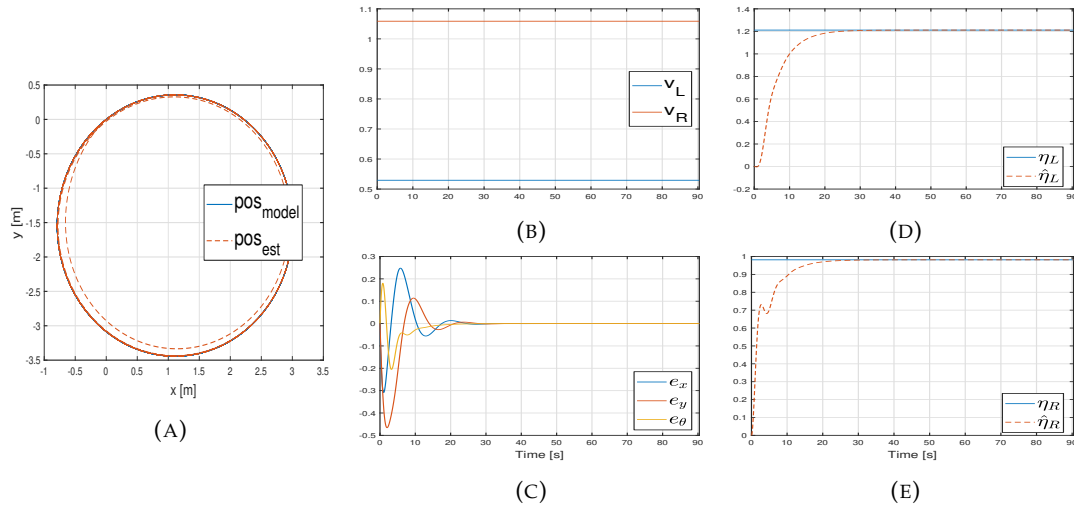
FIGURE 5.6: Results of the numerical simulation for turning motion.
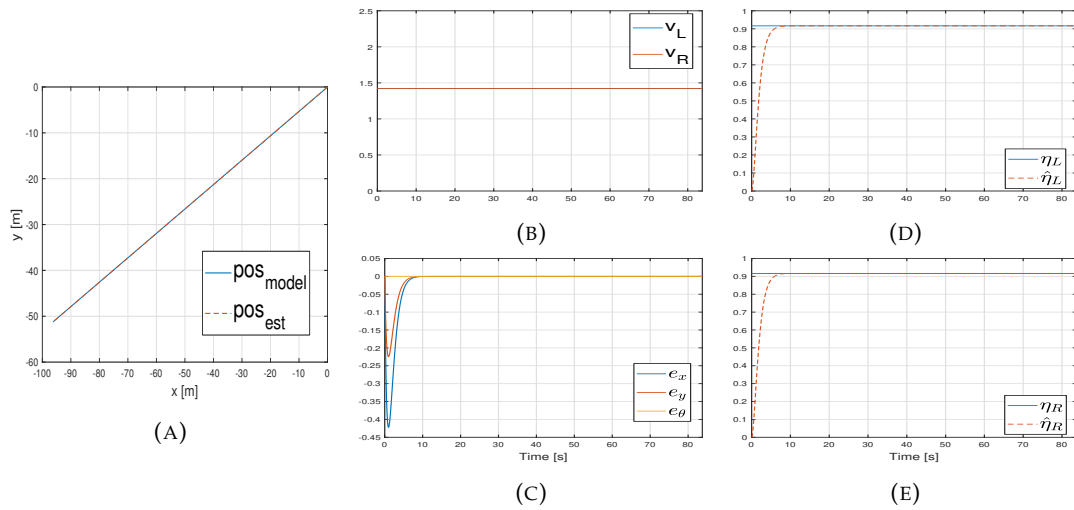
FIGURE 5.7: Results of the numerical simulation for straight motion.

of input-to-state stability. Through two different experimental tests, straight and turning motion, we validated the claims obtained via analytical methods, showing the good performance of the proposed approach. Future work will be devoted to use this estimator in synergy with a controller in an *indirect* adaptive control fashion. The main challenge will reside in having an overall controller guaranteeing slowly time-varying track velocities, to which correspond slowly time-varying slip coefficients, in order to preserve all the considerations we made in this work. In this direction, the reference trajectories required for OPA application, together with the robustness of the proposed estimator, are really promising.

Chapter 6

UAV-Based Search and Rescue in Avalanches using ARVA: An Extremum Seeking Approach

This work deals with the problem of localizing a victim buried by an avalanche by means of a drone equipped with an ARVA (Appareil de Recherche de Victimes d'Avalanche) sensor. The proposed control solution is based on a "model-free" extremum seeking strategy which is shown to succeed in steering the drone in a neighborhood of the victim position. The effectiveness and robustness of the proposed algorithm is tested in Gazebo simulation environment, where a new flight mode and a new controller module have been implemented as an extension of the well-known PX4 open source flight stack. Finally, to test usability, we present hardware-in-the-loop simulations on a Pixhawk 2 Cube board.

6.1 Introduction

6.1.1 The Search & Rescue avalanche application context

Nowadays, disasters due to avalanches are even more frequent because of the changing environmental conditions and the even more marked attitude of people to live extreme mountain experiences, often without the appropriate experience and preparation. Even focusing only on rescuing operations on the Italian and Swiss side of the Alps, 2988 people were rescued in alpine accidents due to avalanches in the last 15 years with 883 fatalities (source AINEVA and SLF).

Rescue missions in avalanches are characterized by specific peculiarities that make them quite demanding. One of the challenging aspects is the tight constraint imposed on the rescue time. In fact, survival chances of people buried under the snow decreases rapidly with burial time due to hypothermia. Furthermore, the rescue scenes are typically quite harsh because of irregular and unstable snow blocks, typically on steep slopes, which make the human intervention complicated, slow and, very often, risky. In fact, it is not rare that the rescuers may trigger a second avalanche event during the S&R mission. A further critical element is represented by the limited range of sensors that can be used to localize a person buried under meters of snow (Ferrara, 2015). One of the most common equipments used in avalanche setting is represented by the ARVA system.

The ARVA equipment has two easily switchable operating modes, which are the *transmitter* and the *receiver* mode. Before starting their activities, experienced skiers switch the worn sensor to the transmitter mode, thus emitting an electromagnetic

signal. In case of an accident, companions not buried by the avalanche, or rescuers who reach the disaster area, switch their devices to the receiver mode and start searching the victim by following well-established ARVA-based search strategy (Azzollini, Mimmo, and Marconi, 2020). The receiver provides information about the electromagnetic field generated by the transmitter sensed at the receiver location. The rescuers are trained to interpret these data to move towards the victim.

The aforementioned tight requirements of the mission, naturally lead to imagine the development of an aerial robotic platform carrying the ARVA receiver and accomplishing the localization of the ARVA transmitter autonomously. Drones, in fact, represent a valid support for humans since they can fly autonomously above the snow to find the transmitter location, thus resulting in a faster and safer search.

The specific application of S&R in avalanche settings already attracted the interest of the scientific community. Activities were conducted in the context of the European project *SHERPA* (Marconi, 2012) where the development of specific robotic technologies to support professional alpine rescue teams in avalanche scenarios were proposed, and now with the H2020 European project AirBorne (*AerIal RoBotic technologies for professiOnal seaRch aNd rescuE, https://www.airborne-project.eu* 2018), motivating the present work, whose objective is to develop (at TRL8) a drone equipped with sensor technologies typically used for quick localization of victims. In this context, the works (Cacace et al., 2016; Cacace, Finzi, and Lippiello, 2016; Bevacqua et al., 2015) already showed how S&R operations can greatly benefit from the use of UAVs to survey the environment and collect evidences about the position of people buried under the snow.

6.1.2 State-of-the-art in source seeking algorithms

The applicative scenario illustrated before frames in a broader research area that is the one referred to as *source seeking control*. In the framework of source seeking, a robotic agent (or a fleet of agents) is able to sense the signal emitted by an omnidirectional source located at an unknown position, with the signal strength having an extremum at the source location. The control problem then consists of processing the signal field measurements, *possibly using a model of it*, to steer the agent (or agents) towards the source. In source seeking the vector field underlying the signal strength is dealt with as the "map" to be optimized. Several approaches have been proposed in literature to solve this class of control problems. Among the existing ones, a central role for this chapter is played by Extremum Seeking (ES). ES is a real-time model-free optimization approach, which can be used to optimize input-output maps having a *global extremum* (either a minimum or a maximum). It is referred to as model free as no explicit knowledge about this map is required (Ariyur and Krstic, 2003). ES could be dated back to 1922 (Tan et al., 2010) but it has seen a renewed growth in the control community during the last two decades, starting with the proof of local stability in (Krstic and Wang, 2000) and the extension to semiglobal stability in (Tan, Nešić, and Mareels, 2006). ES schemes are intrinsically robust and thus appealing for several applications. In particular, talking about control of mobile robots, ES has been used extensively over the last decade for solving source seeking problems *where the model of the source vector field is not available*: the robot has to autonomously find the unknown position of the source, without having any explicit mathematical knowledge of its vector field, therefore by only sensing the source power at the current robot location (Zhang et al., 2007).

Because ES can deal with unknown systems by design, it has been proven to be a powerful tool for steering mobile robots towards a source even in GPS-denied

environments (Cochran et al., 2009; Cochran and Krstic, 2009). Recently, in (Poveda et al., 2021), a class of novel hybrid model-free controllers achieving robust source seeking and obstacle avoidance has been proposed, also in a multi-vehicle scenario. In fact, even with a single agent trying to locate a source, smooth time-invariant feedback controllers based on navigation or barrier functions have been shown to be highly susceptible to arbitrarily small jamming signals that can induce instability in the closed-loop system. Moreover, the problem is not trivial mainly because of the topological obstructions induced by the obstacle.

Besides ES, all the other existing approaches still rely on the intuition that a source localization problem can be formulated as an optimization problem. Inspired by ES, (Ghadiri-Modarres, Mojiri, and Zangeneh, 2017) shows how the motion limitations arising from using a high-frequency dither signal can be overcome when the typical sinusoidal functions usually employed in ES, already exist in the plant model. In particular, considering a unicycle, they show how ES-like controllers can be developed without adding any external excitation signals, because of the trigonometric nonlinearities of the unicycle model.

Another family of interesting approaches are the *line minimization-based algorithms* (Mayhew, Sanfelice, and Teel, 2008). In these approaches the receiver finds, on a search line, the location of minimum/maximum signal strength. Then, the receiver changes its search path (which belongs to a set of directions that span the whole search space) and iterates the procedure to find the transmitter.

On the other hand, if the radiation pattern is known, the source location could be also obtained via state observers (Salaris et al., 2019). Here the main challenge is that of designing sufficiently exciting but also feasible receiver trajectories which ensure the stability of the estimator.

A problem related to the source seeking is the *boundary tracking problem* (Menon et al., 2014). In this context it is assumed that the signal iso-strength lines enclose a region of the search domain which contains the source. Then, the receiver may locate the transmitter by exploiting the geometry of these boundary lines.

Finally, (Jiang et al., 2020) and references therein, deal with bio-inspired optimization techniques. In particular, (Jiang et al., 2020) presents a planner able to drive an underactuated robot towards the odor source, whose control law is inspired by two prominent behaviors widely observed in biology, namely, chemotaxis and anemotaxis.

6.1.3 Contributions of the work

In this work, we develop an innovative ES-based control solution able to steer an autonomous ARVA-equipped UAV, as close as possible to the victim position. By leveraging on the main properties of ES, the proposed algorithm is not relying on an exact knowledge of the ARVA signal, which is quite uncertain and noisy, but rather on the main features of the ARVA signal in terms of convexity and existence of a unique maximum. In particular, among all the existing ES algorithms, we rely on (Scheinker and Krstić, 2014), which is an optimal choice for this application.

The presented control framework is general for solving source seeking problems by means of mobile robots, where ES control can be chosen as reference position generator. In particular, it is shown how the proposed ES scheme can be easily tuned so as to produce smooth position reference signals to be tracked by the robot, taking into account the maximum allowed robot speed and acceleration. Then, we discuss how to guarantee the needed time scale separation between the reference generator and the low-level controller, so as to have the two units working in synergy in

a stable way. The proposed low-level controller leverages on the fact that typically, in many ES control schemes like the one we propose, the needed excitation/exploration is provided by having sinusoidal signals to be followed. Thus, we propose an internal model-based controller, leveraging on the fact that the model of the reference signals to be tracked is known.

The specific choices of both the ES algorithm and the low-level controller, are driven by the need of having a complete control scheme which is efficient in terms of computational resources used. In this direction, in order to prove its effectiveness and robustness, the proposed control algorithm has been extensively tested and evaluated through realistic Software-In-The-Loop (SITL) Gazebo simulations. Then, prototyping of the code with Hardware-In-The-Loop (HITL) simulations on a resource constrained microcontroller was performed. In particular, the proposed control algorithm has been implemented as an extension of the open source PX4 flight stack and tested on a Pixhawk 2 Cube board.

Our previous work (Azzollini, Mimmo, and Marconi, 2020) was a proof of concept presentation, where we showed how ES could be the tool of choice to solve the ARVA-based S&R problem after conditioning the ARVA map. Unlike (Azzollini, Mimmo, and Marconi, 2020), here: (i) we choose the most convenient ES algorithm for searching on a 2D plane with smooth trajectories that could be easily followed by the drone; (ii) we do not assume that the search plane is simply at a certain height with respect to the inertial frame, but rather we take into account the mountain slope; (iii) we develop an internal model-based controller, working in synergy with the ES unit; (iv) we discuss how to add a low-pass filter and tune the parameters so as to guarantee a dynamically feasible trajectory, given the maximum allowed speed and acceleration of the robot; (v) we perform simulations using a realistic drone model and simulation environment, and we also test the code/algorithm performance on a low-cost microcontroller.

6.2 Notation

$I_n \in \mathbb{R}^{n \times n}$ is used to denote the n-dimensional identity matrix, while $0_{n \times m}$ denotes a $n \times m$ matrix of zeros. With $SO(3)$ it is denoted the *special orthogonal group* of 3D rotation matrices, i.e. $SO(3) = \{R \in \mathbb{R}^{3 \times 3} : R^\top R = RR^\top = I_3, \det R = 1\}$, while $SE(3) = \{H \in \mathbb{R}^{4 \times 4} : H = \begin{bmatrix} R & o \\ 0_{1 \times 3} & 1 \end{bmatrix}$, s.t. $R \in SO(3)$, $o \in \mathbb{R}^3\}$. For a differentiable function g, its gradient is denoted by ∇g.

In this chapter, four Cartesian coordinate frames are defined (see Figure 6.1): $\mathcal{F}_i = (O_i, x_i, y_i, z_i)$ denotes the right-handed static inertial frame, with origin O_i, with the axis x_i oriented toward geographic north, z_i oriented opposite to the local gravity vector and y_i oriented to create a right-handed frame (i.e. North-East-Down, or simply NED), while $\mathcal{F}_t = (O_t, x_t, y_t, z_t)$ and $\mathcal{F}_r = (O_r, x_r, y_r, z_r)$ are the right-handed frames associated to the static transmitter worn by the victim and to the receiver installed on the moving drone, respectively. Moreover, $\mathcal{F}_p = (O_p, x_p, y_p, z_p)$ defines the reference frame for the search plane description. In more details, z_p is orthogonal to the search plane whereas O_p lives on the search plane. For the sake of simplicity we assume that the body frame, attached to the centre of gravity of the drone, coincides with $\mathcal{F}_r$. The positions of O_r and O_t relative to O_p are indicated by the vectors $p_r \in \mathbb{R}^3$ and $p_t \in \mathbb{R}^3$, respectively. Given that O_t and O_p are static reference frames, p_t is a constant. The position of O_r relative to O_t is indicated by

the vector $p \in \mathbb{R}^3$, with $p = p_r - p_t$. Throughout the chapter, we shall use the superscripts i, p, t and r on the left of the vectors p, p_t, p_r to denote the representation of the previous vectors in the reference frames $\mathcal{F}_i$, $\mathcal{F}_p$, $\mathcal{F}_t$ and $\mathcal{F}_r$, respectively (for instance, ${}^p p$ denotes a representation of p in $\mathcal{F}_p$). Finally $e_3 = [0\,0\,1]^\top$ and $S(x)$, with $x = [x_1\,x_2\,x_3]^\top \in \mathbb{R}^3$, denotes the skew-symmetric matrix

$$S(x) = \begin{bmatrix} 0 & -x_3 & x_2 \\ x_3 & 0 & -x_1 \\ -x_2 & x_1 & 0 \end{bmatrix}.$$

Considering a static reference frame and a moving frame attached to a body, *intrinsic* rotations are elementary rotations that occur about the axes of the coordinate system attached to a moving body, which changes its orientation after each elemental rotation. The orientation of the moving frame $\mathcal{F}_\#$ with respect to the inertial frame $\mathcal{F}_i$ can be expressed by means of the sequence of intrinsic elementary rotations denoted by yaw $\psi_\#$ (about the z-axis), pitch $\theta_\#$ (about the y-axis), and roll $\phi_\#$ (about the x-axis). In particular, starting from the inertial frame, we perform an elementary rotation about the z-axis (which is z_i) of an angle $\psi_\#$. This rotation brings us to the first intermediate frame we call $\mathcal{F}_1$, and can be represented by means of the rotation matrix ${}^1 R_i$ (from the i-frame to the 1-frame). For instance, considering the relative position p we have

$$\underbrace{{}^1 p = \begin{bmatrix} \cos \psi_\# & \sin \psi_\# & 0 \\ -\sin \psi_\# & \cos \psi_\# & 0 \\ 0 & 0 & 1 \end{bmatrix}}_{{}^1 R_i} {}^i p. \tag{6.1}$$

Now, starting from the frame $\mathcal{F}_1$ we perform a rotation about the *current* y-axis (which is y_1) of an angle $\theta_\#$, which brings us to a second intermediate frame that we call $\mathcal{F}_2$. The rotation matrix associated to this transformation is

$$\underbrace{{}^2 p = \begin{bmatrix} \cos \theta_\# & 0 & -\sin \theta_\# \\ 0 & 1 & 0 \\ \sin \theta_\# & 0 & \cos \theta_\# \end{bmatrix}}_{{}^2 R_1} {}^1 p. \tag{6.2}$$

The last rotation starting from the frame $\mathcal{F}_2$, has to be performed about the current x-axis (which is x_2) of an angle $\phi_\#$. This rotation brings us from the frame $\mathcal{F}_2$ to the final moving frame $\mathcal{F}_\#$, with the associated rotation matrix given by

$$\underbrace{{}^\# p = \begin{bmatrix} 1 & 0 & 0 \\ 0 & \cos \phi_\# & \sin \phi_\# \\ 0 & -\sin \phi_\# & \cos \phi_\# \end{bmatrix}}_{{}^\# R_2} {}^2 p. \tag{6.3}$$

The overall rotation matrix ${}^\# R_i \in SO(3)$ (from the inertial frame to the #-frame) is given by

$${}^\# R_i = {}^\# R_2 \, {}^2 R_1 \, {}^1 R_i = R_x(\phi_\#) R_y(\theta_\#) R_z(\psi_\#) \tag{6.4}$$

and, as a consequence, the overall rotation matrix from the moving #-frame to the inertial frame is given by

$${}^i R_\#(\psi_\#, \theta_\#, \phi_\#) = R_z^\top(\psi_\#) R_y^\top(\theta_\#) R_x^\top(\phi_\#). \tag{6.5}$$
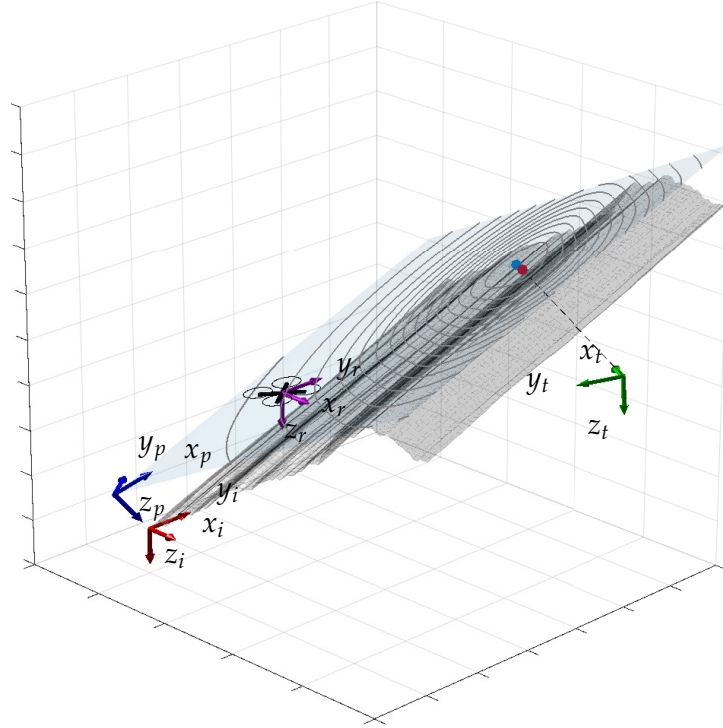
FIGURE 6.1: Reference frames: one to identify the inertial space, one
to describe the search plane, and two to denote the transmitter and
the receiver pose, respectively.

Note that the resulting rotation matrix (6.5) is the same as in (Siciliano et al., 2010,
Section 2.4.2). In fact, the ordered sequence of rotations ZYX about axes of the cur-
rent frame (intrinsic), which we just considered, is equivalent to the sequence XYZ
about axes of the fixed frame (extrinsic).

6.3   The ARVA system

In this section, we first go through the main physical principles of the ARVA system
with the final goal to derive a model of the signal vector field. Then, we present the
related search strategy and we describe the problem we want to solve.

6.3.1   Modeling

The transceivers commercially available have two operating modes, namely they
can work as receivers or as transmitters, with a manual switch used to commute
between the two. In *transmission* mode the ARVA generates a magnetic field that is
modeled as a dipole aligned with the x_t axis of $\mathcal{F}_t$. The electromagnetic vector field,
described in $\mathcal{F}_p$, is indicated by ${}^p h \in \mathbb{R}^3$. By letting ${}^p p = {}^p p_r - {}^p p_t = [x\ y\ z]^\top$, it
turns out that a mathematical model of the magnetic vector field is given by (Piniés
and Tardós, 2006)

$$
{}^p h({}^p p, {}^p R_t) = \frac{1}{4\pi \| {}^p p \|^5} \, \mathrm{A}({}^p p) \, {}^p R_t e_1 \tag{6.6}
$$

where

$$
A(^pp) := \begin{bmatrix} 2x^2 - y^2 - z^2 & 3xy & 3xz \\ 3xy & 2y^2 - x^2 - z^2 & 3yz \\ 3xz & 3yz & 2z^2 - x^2 - y^2 \end{bmatrix}
$$

and $e_1 = [1 \; 0 \; 0]^\top$. The flux lines described by the previous model are symmetric with respect to the transmitter x_t axis. The intensity of the magnetic field can be then obtained by the previous relation as (see (Piniés and Tardós, 2006))

$$
\| {}^ph \| = \frac{1}{4\pi \| {}^pp \|^3} \sqrt{1 + 3\frac{{}^pp^\top M {}^pp}{\| {}^pp \|^2}} \tag{6.7}
$$

where $M = {}^tR_p^\top e_1 e_1^\top {}^tR_p \geq 0$ with minimum and maximum singular values given by $\underline{\sigma}(M) = 0$ and $\overline{\sigma}(M) = 1$, respectively. It turns out that $\| {}^ph \|$ is radially unbounded with $1/\| {}^pp \|$, namely the intensity of the magnetic field is infinity when $p_r = p_t$. Furthermore, (6.7) can be exploited to compute the iso-power lines, that are also symmetric with respect to the transmitter x_t axis.

In the context of this S&R application, what is relevant is the projection of the flux and iso-power fields onto the so-called *search plane*, conveniently identified as the $x_p y_p$-plane, (see Figure 6.1). The search plane is the plane on which the drone is required to operate, and it is chosen to be parallel to the snow surface, at a safe distance from the ground. This distance should be kept as small as possible, with a minimum imposed by the irregularities of the terrain and the presence of possible rescuers on the avalanche scene. The overall distance between the victim-transmitter and the chosen search plane is denoted by d_t. Therefore, we can simply write the position of the transmitter with respect to the search plane frame $\mathcal{F}_p$, as ${}^pp_t = [t_x \; t_y \; d_t]^\top$. Ideally, we would like to drive the drone on the geometric projection of O_t on the search plane, that is simply given by ${}^pp_{t/\text{proj}} = [t_x \; t_y \; 0]^\top$, as this is clearly the closest admissible position to the transmitter location.

However, the projection of the iso-power field onto the search plane is affected by the distance d_t and by the rotation matrix ${}^pR_t$, parameterizing the orientation of the transmitter with respect to the search plane frame. In fact, the optimal position $p^\star$, corresponding to the maximum intensity of the magnetic field that we can sense on the plane, usually differs from $p_{t/\text{proj}}$. As a first example, in Figure 6.1, the distance d_t is indicated by the dashed line, the geometric projection position $p_{t/\text{proj}}$ is given by the red dot, while the optimal position $p^\star$ is indicated with the blue dot.

In order to further understand this aspect, we can look at the EM field restricted to the search plane in Figure 6.2. In particular, both the flux lines (in red) and the iso-power lines (in black) are depicted for different instances of d_t and ${}^pR_t$, assuming for simplicity that the transmitter location is ${}^pp_t = [0 \; 0 \; d_t]^\top$. As a matter of fact, ${}^pp^\star = {}^pp_{t/\text{proj}}$ only in the (unlikely to happen) scenarios in which either $d_t = 0$ or ${}^pR_t = I_3$. In all the other cases, $p^\star$ will only be in a neighborhood of $p_{t/\text{proj}}$.

The ARVA signal is received through three antennas directed along the *receiver* frame axes x_r, y_r and z_r, namely along the longitudinal, lateral and vertical direction of the sensor case. The magnetic field sensed at the receiver location, denoted by ${}^ph_m$, is given by

$$
{}^ph_m({}^pp, {}^pR_t, w) = {}^ph({}^pp, {}^pR_t) + {}^pw(t) \tag{6.8}
$$

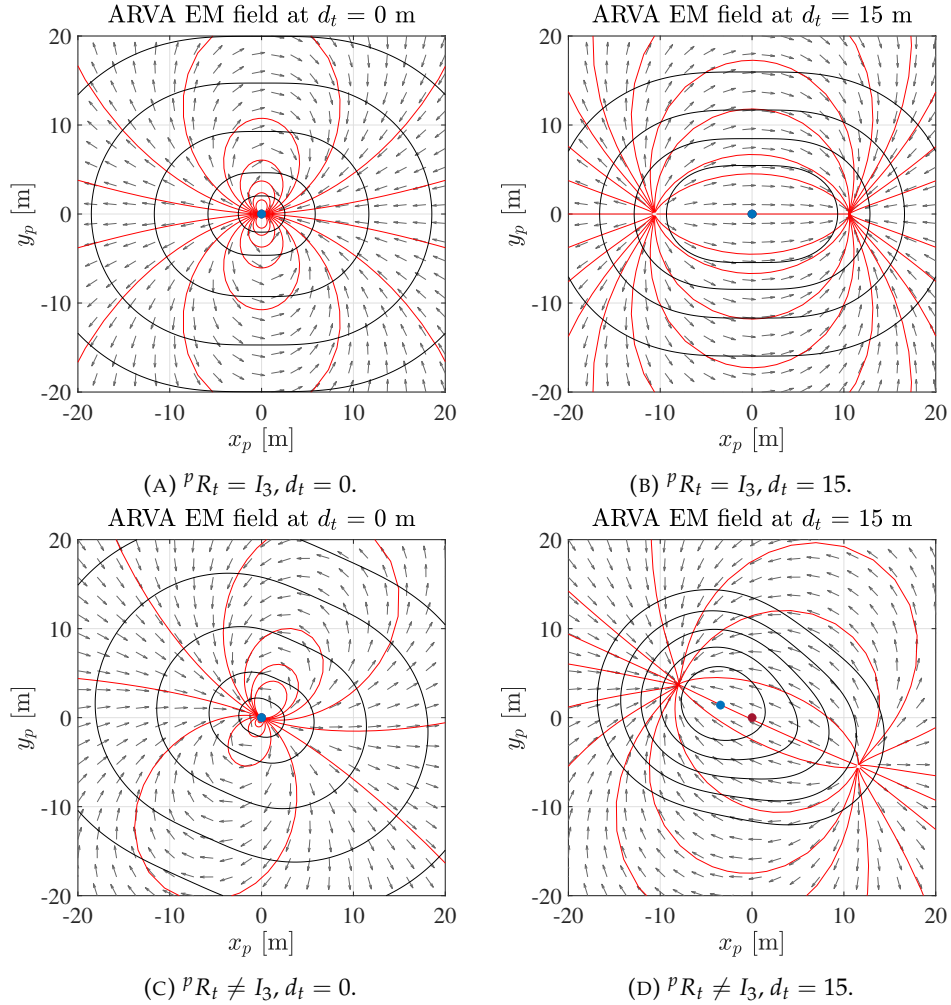where ${}^pw : \mathbb{R} \mapsto \mathbb{R}^3$ indicates the ElectroMagnetic Interferences (EMI) expressed

FIGURE 6.2: ARVA flux lines (in red), EM vector field (arrows), and iso-power lines (in black). The transmitter is located at $^p p_t = [0\,0\,d_t]^\top$, its geometric projection onto the search plane is the red dot $^p p_{t/\mathrm{proj}} = [0\,0\,0]^\top$, while the ARVA EM field maximizer $p^\star$ is the blue dot.

in the search plane frame. There are two sources of EMI, the drone and the environment. Small drones are commonly actuated through electromagnetic brushless motors governed by logic units constituted by switches powered by LiPo batteries. The whole electrical power distribution chain is prone to the emission of EM noises which are sensed by the ARVA receiver. Fortunately, since these interferences can be investigated in dedicated EM testing facilities, the drones under development in (*AerIal RoBotic technologies for professiOnal seaRch aNd rescuE, https://www.airborne-project.eu* 2018) will be equipped with special shields that minimise the on-board generated EMI. On the contrary, the environment clearly cannot be modified to reduce the EM noise. Usually, the environmental electromagnetic field is affected by the presence of power lines, funicular railways, etc. These effects are suitably modeled through signals, namely $^p w(t)$, whose amplitude is bounded and quasi-constant on the avalanche search area, *i.e.* there exists $\overline{w} > 0$ such that $\| ^p w(t) \|_\infty \le \overline{w}$. Finally, it is interesting to notice that the power density of the ideal dipole goes to infinity at the transmitter location and is a strictly decreasing function
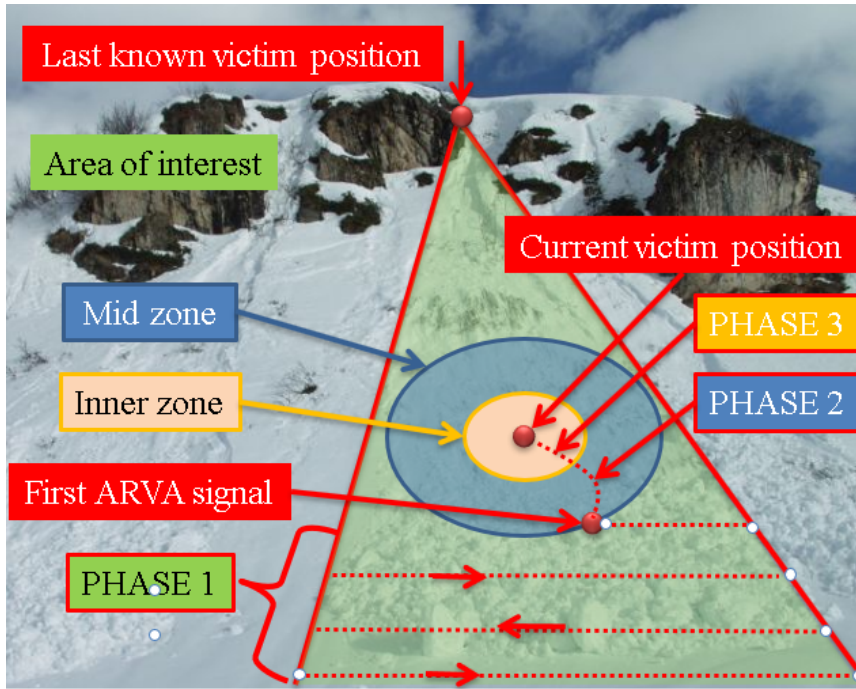
FIGURE 6.3: Rescue scene: area of interest and search phases.

of $\| {}^p p \|$. This, beside the boundedness of ${}^p w$, leads to

$$\lim_{\| {}^p p \| \to \infty} \| {}^p h_m \|_\infty = \bar{w}, \qquad \lim_{\| {}^p p \| \to 0} \| {}^p h_m \|_\infty = \infty \tag{6.9}$$

which will be exploited in Section 6.4.1.

6.3.2 Existing search strategies and problem description

The ARVA-based search strategy is graphically sketched in Figure 6.3. After the definition of the so-called *area of interest*, which is a triangular area starting from the last known victim position and including the avalanche front, the search is divided in three subsequent phases. Starting from the bottom of the area of interest, the *first search phase* consists in following straight parallel lines with an offset of 15-20 meters, with the goal of finding a valid ARVA signal. When sufficiently close to the transmitter (typically around 50 meters), a valid ARVA signal is measured, and the *second search phase* starts. The ARVA receiver displays the EM vector field in terms of magnitude and direction, which actually corresponds to the tangent to the EM field flux line at the operator location. The rescuers are trained to follow the flux line to approach the victim. The *third search phase* begins when the sensed EM field is sufficiently strong, namely the ARVA receiver is sufficiently close to the victim and automatically changes its output modality, providing only the modulus of the EM field at the operator location. The automatic change of modality is thought to inform the rescuers that the flux line approach is no more efficient, and therefore they start searching by iteratively applying a two-step gradient search strategy (which consists in finding maximum EM intensity along orthogonal directions).

Since the first phase does not hide any particular control challenges (it consists of controlling the drone along pre-established trajectories), we mainly focus on the second and the third phases by assuming the availability of a valid ARVA signal. In fact, we merge the second and third search phases in a single one based on the
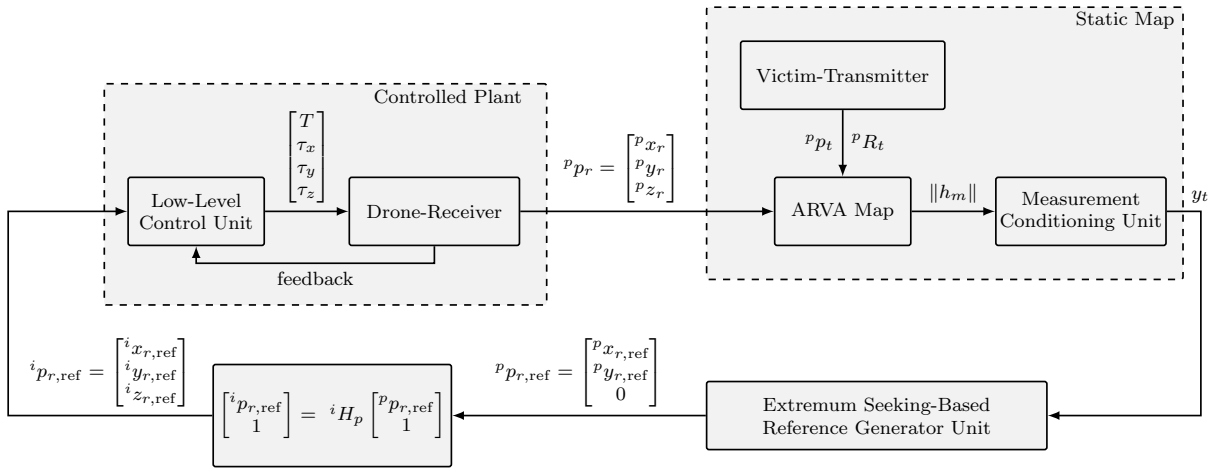
FIGURE 6.4: Overall control scheme.

processing of the ARVA EM intensity and ignoring the geometry of the flux lines typically considered in the second search phase. The flux line following strategy, in fact, has several drawbacks, which could be better understood by looking at Figure 6.2: (i) the search path can be unpredictably long as it depends on the initial position of the receiver with respect to the transmitter; (ii) the search path depends on the initial receiver attitude with respect to the transmitter (the rescuers could follow the flux lines counterclockwise or clockwise thus leading to different search paths); (iii) because of the EMI noise, the measure of the EM directions can be particularly deteriorated.

The envisaged scenario is thus the following. First of all, the area of interest as well as the drone search plane are defined by the rescue team (see Figure 6.1 and Figure 6.3), based on the last known victim position, and the slope of the terrain with respect to the inertial frame. The drone will then take off and reach the search plane, and will start autonomously performing the first search phase to find a valid ARVA signal. At this point, the valid signal indicates that the victim is located at approximately a 50 meters distance from the current position of the drone. Now, in a practice-inspired design philosophy, a search strategy based on a gradient-like policy could lead to the unique extremum on the chosen search plane. Thus, this work aims at designing an automatic control law based on ES, only driven by the intensity of the ARVA EM field, which steers the drone as close as possible to the victim location.

6.4   An Extremum Seeking-based solution

The overall control scheme is sketched in Figure 6.4, where we can distinguish three main units, which are the *measurement conditioning unit*, the *ES-based reference generator unit* and the *low-level control unit*. As already mentioned, we want the ARVA receiver to have only one output modality, that is, to directly provide the intensity of the EM field at the operator location. Therefore, given as inputs the drone-receiver position $^p p_r$, the victim-transmitter position $^p p_t$, and the transmitter orientation $^p R_t$, the *ARVA map* block gives as output $\|h_m\|$, which is the intensity of the measurement (6.8).

6.4.1 Measurement conditioning unit

Being the maximum intensity of (6.8) equal to infinity, any gradient-based algorithm would face with issues in the proximity of the victim. This criticism motivates the following manipulation. The measurement conditioning unit statically processes the ARVA intensity measurement $\|h_m\|$ to create a new intensity map, denoted by y_t, that is continuous and bounded for any $^Pp \in \mathbb{R}^3$, and has a global minimum equal to zero. Specifically, the conditioned measurement y_t is generated as

$$y_t(^Pp, {}^PR_t, {}^Pw) := \frac{1}{\sqrt[3]{\|h_m\|}}. \tag{6.10}$$

Simple computations show that y_t can be approximated by $y_t = {}^Ph_n + v_t$ in which

$$^Ph_n(^Pp, {}^PR_t) := \frac{(4\pi)^{1/3}\|{}^Pp\|}{\sqrt[6]{1 + 3\dfrac{{}^Pp^\top M\,{}^Pp}{\|{}^Pp\|^2}}} \tag{6.11}$$

is the nominal conditioned intensity and

$$v_t(^Pp, {}^PR_t, t) = \Xi_A(^Pp, {}^PR_t)\|{}^Pp\|^3 \, {}^Pw(t) \tag{6.12}$$

is the equivalent additive noise in which $\Xi_A(^Pp, {}^PR_t) \in \mathbb{R}^3$ is a bounded function.

The new output map (6.10) shows some key properties. First, it is well defined because for any $^Pp \in \mathbb{R}^3$

$$0 \le \frac{{}^Pp^\top M\,{}^Pp}{\|{}^Pp\|^2} \le 1. \tag{6.13}$$

In addition, for any fixed $^PR_t \in SO(3)$ the functions $^Ph_n(\,\cdot\,, {}^PR_t)$, $v_t(\,\cdot\,, {}^PR_t, t)$ both have a global minimum at $^Pp = 0$ and are strictly increasing. Furthermore, let the Noise-to-Signal Ratio (NSR) to be defined as

$$\text{NSR}(^Pp, {}^PR_t) := \frac{\|y_t(^Pp, {}^PR_t, t)\|_\infty - |{}^Ph_n(^Pp, {}^PR_t)|}{\|y_t(^Pp, {}^PR_t, t)\|_\infty}. \tag{6.14}$$

This modified ratio belongs to the compact domain $[0, 1]$ and, in particular, for any $^PR_t \in SO(3)$

$$\lim_{^Pp \to 0} \text{NSR}(^Pp, {}^PR_t) = 0, \quad \lim_{^Pp \to \infty} \text{NSR}(^Pp, {}^PR_t) = 1 \tag{6.15}$$

meaning that at the origin $^Pp = 0$ the output is not affected by noise whereas for $^Pp \to \infty$ the nominal signal is annihilated by the noise.

In conclusion, the conditioned map (6.10) can be optimized by means of any (approximate) gradient-based optimization technique. Because of the presence of the noise and the model uncertainty, we do not want to rely on an exact knowledge of the model of y_t, but rather on its convexity property and existence of a minimum. For this reasons, ES is chosen, resulting in a robust and practically implementable control algorithm.

6.4.2 ES-based reference generator unit

The conditioned output map y_t, constrained on the search plane, has a unique extremum (which is a minimum). The optimal position corresponding to the minimum of y_t, clearly coincides with the position relative to the maximum intensity of

the ARVA map without conditioning. Therefore the goal is still that of driving the receiver to the optimal point $^pp^\star$. In fact, $^pp^\star$ now corresponds to the minimum of y_t restricted to the search plane, and is still the blue dot we saw as an example in Figures 6.1 and 6.2.

The reference generator unit and the low-level control unit need to work (and to be designed) in synergy. The ES-based unit processes the conditioned ARVA map y_t, and its role is ideally that of performing a real-time optimization on the search plane, thus driving the drone-receiver position ^pp_r towards the optimal point on the search plane $^pp^\star$. As we do not have direct control on the optimization variable ^pp_r, ES here plays the role of a reference position generator for the drone. A (low-level) reference tracking controller needs to be designed so as to drive the drone position to the generated reference position $^pp_{r,\text{ref}}$, that will be the output of the ES. In this scenario, in order to guarantee proper functioning of the proposed scheme, the controlled plant needs to work on a faster time scale with respect to the ES unit (Ariyur and Krstic, 2003; Tan et al., 2010; Krstic and Wang, 2000). In fact, we do not have a static input-output map to be optimized, but rather the steady-state input-output map of a dynamical system, with input $^pp_{r,\text{ref}}$ and output y_t. Requiring the controlled plant to be way faster than the reference generator, the ES design can be made by considering the controlled plant as if it was a static map, so assuming to have direct control on ^pp_r.

Now, let us define the components of $^pp^\star$ and $^pp_{r,\text{ref}}$ as $^pp^\star = [\,^px^\star \;\, ^py^\star \;\, 0]^\top$ and $^pp_{r,\text{ref}} = [\,^px_{r,\text{ref}} \;\, ^py_{r,\text{ref}} \;\, ^pz_{r,\text{ref}}]^\top$. The following proposition, adapted from (Scheinker and Krstić, 2014), presents the chosen 2-dimensional ES algorithm.

Proposition 6.1. *For any $\delta > 0$, by a sufficiently large choice of $\kappa\alpha$, the point $(^px^\star, ^py^\star)$ is $(1/\omega)$-Semiglobally Practically Uniformly Ultimately Bounded with ultimate bound δ, relative to the system $(^px_{r,\text{ref}}(t), ^py_{r,\text{ref}}(t))$:*

$$
\begin{aligned}
^p\dot{x}_{r,\text{ref}} &= \sqrt{\alpha\omega}\cos(\omega t + \kappa y_t) & ^px_{r,\text{ref}}(0) &= \,^px_r(0) \\
^p\dot{y}_{r,\text{ref}} &= \sqrt{\alpha\omega}\sin(\omega t + \kappa y_t) & ^py_{r,\text{ref}}(0) &= \,^py_r(0).
\end{aligned}
\tag{6.16}
$$

The reference signal $^pp_{r,\text{ref}}$ is obviously completed with $^pz_{r,\text{ref}} = 0$, as we want the drone-receiver to always move on the search plane.

This ES unit processes the conditioned ARVA intensity y_t and generates the reference signals for the drone, expressed in the search plane frame $\mathcal{F}_p$. In particular, (6.16) achieves ES in a practical way, meaning that $(^px_{r,\text{ref}}, ^py_{r,\text{ref}})$ converge to a neighborhood of $(^px^\star, ^py^\star)$, which can be made arbitrarily small by properly choosing the design parameters ω, κ, and α. Moreover, this result is semiglobal as there exists a certain domain of attraction around $(^px^\star, ^py^\star)$, such that, if we start inside this region we can solve the problem. This domain of attraction can be arbitrarily enlarged by properly choosing the design parameters, at the expense of slowing down the convergence speed.

The presented ES scheme works as follows. System (6.16) is evolving in circular trajectories on the $x_p y_p$-plane, where the parameter ω plays the role of the oscillation frequency. In particular, at steady-state the system geometric path is given by a circumference of radius $\sqrt{\alpha\omega}$ around the optimum $(^px^\star, ^py^\star)$, parameterized in time with the frequency ω. In fact, it can be proven (Scheinker and Krstić, 2014) that the trajectories of (6.16) uniformly converge to the trajectories $(^p\bar{x}, ^p\bar{y})$ of the so-called "average" system

$$
\begin{bmatrix} ^p\dot{\bar{x}} \\ ^p\dot{\bar{y}} \end{bmatrix} = -\frac{\kappa\alpha}{2}(\nabla y_t(^p\bar{x}, ^p\bar{y}))^\top, \qquad
\begin{bmatrix} ^p\bar{x}(0) \\ ^p\bar{y}(0) \end{bmatrix} = \begin{bmatrix} ^px_{r,\text{ref}}(0) \\ ^py_{r,\text{ref}}(0) \end{bmatrix},
\tag{6.17}
$$

which exhibits a stable gradient-flow dynamics, with adaptation gain $\kappa\alpha$. Therefore, for any ultimate bound $\delta > 0$, by choosing arbitrarily large values of $\kappa\alpha$ we may ultimately bound $({}^p\bar{x}, {}^p\bar{y})$ within a δ neighborhood of $({}^px^\star, {}^py^\star)$.

Averaging technique (Khalil, 2002, Section 10.4) is always used to analyze ES schemes and shows how the system is evolving, on average, in the gradient-descent direction to seek the minimizer. In particular, in the original coordinates, it is the centre of the circular trajectory which is approaching $({}^px^\star, {}^py^\star)$ in an approximate gradient-descent fashion. The centre of the circular trajectory can be therefore regarded as the current estimate of the optimum. By moving in circular trajectories, we are basically exploring a neighborhood of the current position (i.e. the parameter estimate), to check in which direction the sensed function value is decreasing.

Among all the existing algorithms, this one was chosen for three main reasons. First of all, the generated reference trajectory is guaranteed to be smooth enough to be followed by our UAV. Moreover, this algorithm is called "bounded update rates" ES, as the magnitude of the velocity (which corresponds to the update rate of the estimate) can be a priori chosen as $\|v_r\| = \sqrt{\alpha\omega}$. Finally, this algorithm is easy to be discretized and implemented, and it is also light to be executed on a microcontroller.

The parameters to be tuned are the positive scalars α, ω, and κ. By looking at Proposition 1, they are not difficult to be tuned in general, when we simply have a static map to be optimized. However, in our specific application, we have to consider the noise and the drone. In particular, being the ARVA map noisy, we want to choose κ small. In fact, the reference signal could be significantly deteriorated by κy_t in (6.16). As a consequence, in order to have the learning rate $\kappa\alpha$ sufficiently large (as required by Proposition 1), we have to take a large α. Now, a tradeoff needs to be considered, as we would also like to take ω big, following the fact that $1/\omega$ plays the role of ϵ in the (ϵ, δ)-SPUUB stability result of Proposition 1 (Scheinker and Krstić, 2014). On the other hand, $\sqrt{\alpha\omega}$ corresponds to the maximum speed of the drone, as well as to the radius of the circumference which the drone describes on the search plane. In practice, we will see that a good choice is that of taking α very large and ω quite small such that the maximum allowed speed is respected. In this way, being the frequency of oscillations not very high, while having a big circumference radius, the reference signal will be gentle enough to be followed by the drone in near-hovering condition at all times.

Moreover, we introduce the low-pass filter

$$\dot{\alpha} = -\frac{1}{\lambda}\alpha + \frac{1}{\lambda}\alpha_{\max} \qquad \alpha(0) = 0 \qquad (6.18)$$

resulting in α in (6.16) that approaches the chosen $\alpha_{\max}$ in an arbitrary amount of time (starting from zero). This gives us full authority to impose also the preferred maximum acceleration, so as to ensure a dynamically feasible trajectory. In conclusion, given a maximum velocity and a maximum acceleration, a dynamically feasible reference trajectory can always be guaranteed for our UAV, by an appropriate choice of the parameters in (6.16), (6.18).

As a final part of this unit, we define the homogeneous transformation matrix ${}^iH_p$ such that

$$\begin{bmatrix} {}^ix_{r,\text{ref}} \\ {}^iy_{r,\text{ref}} \\ {}^iz_{r,\text{ref}} \\ 1 \end{bmatrix} = {}^iH_p \begin{bmatrix} {}^px_{r,\text{ref}} \\ {}^py_{r,\text{ref}} \\ 0 \\ 1 \end{bmatrix}. \qquad (6.19)$$

so as to design a low-level controller for the UAV in the more convenient inertial frame $\mathcal{F}_i$.

6.4.3   Low-level Control Unit

The low-level controller aims at driving the drone position to the generated reference position as fast as possible, so as to ensure the time scale separation needed for the proper functioning of the ES unit. A model-based approach based on linearization is followed in the design of the controller as presented next. It must be stressed, though, that any favorite reference tracking controller for UAV can be taken, provided that the time scale separation requirement is fulfilled. However, we choose to develop linearization-based controllers as we only have a reference position to track, without any specific reference for the attitude. This means we can operate the UAV in near-hovering conditions at all times, without requiring a more complicated and computationally heavier controller. This intuition will be supported by the experimental results, where good tracking performance will be achieved, even in hardware-in-the-loop simulations while using a low-cost microcontroller.

As the references are generated by the designed ES optimizer, their model is perfectly known. In particular, we know that *at steady-state* the drone-receiver will be asked to track a biased sinusoidal signal of known frequency ω for each of the position components ^ix_r, ^iy_r, and ^iz_r. This follows by the fact that we are generating a circumference as the geometric path reference on the 2D search plane, which is mapped to an ellipse in the 3D space.

We start by considering the nonlinear dynamical model of vertical take-off and landing aerial vehicles by means of the well-known Newton-Euler rigid body equations (Hua et al., 2013)

$$M\,{}^i\ddot{p}_r = -T\,{}^iR_r e_3 + Mg e_3 \tag{6.20a}$$

$$^i\dot{R}_r = {}^iR_r S({}^r\omega_r) \tag{6.20b}$$

$$J\,{}^r\dot{\omega}_r = -S({}^r\omega_r)J\,{}^r\omega_r + \tau \tag{6.20c}$$

in which $M > 0 \in \mathbb{R}$ and $J = \mathrm{diag}(J_x, J_y, J_z) \in \mathbb{R}^{3\times3}$ are the UAV mass and inertia matrix, respectively, $^ip_r = [{}^ix_r\ {}^iy_r\ {}^iz_r]^\top$ denotes the position of the centre of gravity of the system expressed in the inertial frame, $^r\omega_r = [{}^r\omega_x, {}^r\omega_y, {}^r\omega_z]^\top \in \mathbb{R}^3$ is the angular speed expressed in the drone-receiver frame, $^iR_r(\psi_r, \theta_r, \phi_r) \in SO(3)$ is the rotation matrix from the drone-receiver frame to the inertial frame, while $T > 0 \in \mathbb{R}$ and $\tau = [\tau_x\ \tau_y\ \tau_z]^\top \in \mathbb{R}^3$ are the thrust force and vector of torques, respectively. Finally, recall the definitions of e_3 and the skew-symmetric matrix $S({}^r\omega_r)$ from the Notation, as well as the fact that also the z_r axis of the drone-receiver frame points downwards.

The system (6.20) is then linearized around the *hovering* equilibrium point, namely

$$\begin{cases} ^ip_r^\star & = {}^ip_r^{\mathrm{hov}} \\ ^i\dot{p}_r^\star & = 0_{3\times1} \\ ^iR_r^\star & = I_3 \\ ^r\omega_r^\star & = 0_{3\times1} \end{cases} \qquad \begin{cases} T^\star & = Mg \\ \tau^\star & = 0_{3\times1} \end{cases} \tag{6.21}$$

where $^ip_r^{\mathrm{hov}}$ is any arbitrary hovering position. In a gain scheduling fashion, we linearize online taking $^ip_r^{\mathrm{hov}} = {}^ip_{r,\mathrm{ref}}$. It is well-known that the linearized system results

in four independent systems, namely the *roll*, the *pitch*, the *yaw*, and the *vertical* dynamics. On the four subsystems, the corresponding four inputs are then designed as indicated in the following.

Yaw dynamics and control: The yaw dynamics results in

$$
\begin{bmatrix} \dot{\psi}_r \\ \ddot{\psi}_r \end{bmatrix} = \begin{bmatrix} 0 & 1 \\ 0 & 0 \end{bmatrix} \underbrace{\begin{bmatrix} \psi_r \\ \dot{\psi}_r \end{bmatrix}}_{X_y} + \begin{bmatrix} 0 \\ \dfrac{1}{J_z} \end{bmatrix} \tau_z
\tag{6.22}
$$

and we simply choose to stabilize it with a state-feedback controller of the form $\tau_z = -K_y X_y$, with $K_y \in \mathbb{R}^{1\times 2}$ to be designed such that the resulting closed-loop system is Hurwitz. This choice corresponds to asking the controller to keep the yaw angle to zero (we assume that the yaw is equal to zero when starting the search). As already mentioned, this simple control choice can be made as we do not need to point the receiver towards the transmitter (or in general, towards the direction we are going), but we only need to move the receiver on the search plane, regardless of the "heading" angle.

Roll dynamics and control: We start by defining the error ${}^i e_y := {}^i y_r - {}^i y_{r,\text{ref}}$. The roll dynamics result in

$$
\begin{bmatrix} {}^i \dot{y}_r \\ {}^i \dot{v}_y \\ \dot{\phi}_r \\ \ddot{\phi}_r \end{bmatrix} = \begin{bmatrix} 0 & 1 & 0 & 0 \\ 0 & 0 & g & 0 \\ 0 & 0 & 0 & 1 \\ 0 & 0 & 0 & 0 \end{bmatrix} \underbrace{\begin{bmatrix} {}^i e_y \\ {}^i v_y \\ \phi_r \\ \dot{\phi}_r \end{bmatrix}}_{X_r} + \begin{bmatrix} 0 \\ 0 \\ 0 \\ \dfrac{1}{J_x} \end{bmatrix} \tau_x.
\tag{6.23}
$$

The goal of the control loop is to let the lateral drone position ${}^i y_r$ tracking the reference ${}^i y_{r,\text{ref}}$ computed by the ES-based reference generator system. As previously discussed this reference signal (as well as ${}^i x_{r,\text{ref}}$ and ${}^i z_{r,\text{ref}}$) is a biased sinusoidal signal of unknown amplitude but known frequency ω, coming from (6.16). Thus, in order to drive the regulation error ${}^i e_y$ to zero, we consider an internal model-based regulator (see (Isidori, 2017, Chapter 4)) of the form

$$
\dot{\eta}_r = \underbrace{\begin{bmatrix} 0 & 1 & 0 \\ 0 & 0 & 1 \\ 0 & -\omega^2 & 0 \end{bmatrix}}_{\Phi} \eta_r + \underbrace{\begin{bmatrix} 0 \\ 0 \\ 1 \end{bmatrix}}_{G} {}^i e_y
\tag{6.24}
$$

$$
\tau_x = -K_r X_r - K_{\eta_r} \eta_r
$$

with K_r and K_{η_r} to be designed such that the resulting closed-loop system is Hurwitz.

Pitch dynamics and control: As before, define the error ${}^i e_x := {}^i x_r - {}^i x_{r,\text{ref}}$. The pitch dynamics are given by

$$
\begin{bmatrix} {}^i \dot{x}_r \\ {}^i \dot{v}_x \\ \dot{\theta}_r \\ \ddot{\theta}_r \end{bmatrix} = \begin{bmatrix} 0 & 1 & 0 & 0 \\ 0 & 0 & -g & 0 \\ 0 & 0 & 0 & 1 \\ 0 & 0 & 0 & 0 \end{bmatrix} \underbrace{\begin{bmatrix} {}^i e_x \\ {}^i v_x \\ \theta_r \\ \dot{\theta}_r \end{bmatrix}}_{X_p} + \begin{bmatrix} 0 \\ 0 \\ 0 \\ \dfrac{1}{J_y} \end{bmatrix} \tau_y.
\tag{6.25}
$$

Analogously as before, the internal model-based regulator is

$$\begin{aligned} \dot{\eta}_p &= \Phi\eta_p + G\,{}^i e_x \\ \tau_y &= -K_p X_p - K_{\eta_p}\eta_p \end{aligned} \tag{6.26}$$

with K_p and K_{η_p} to be designed such that the resulting closed-loop system is Hurwitz.

Vertical dynamics and control: Define the error ${}^i e_z := {}^i z_r - {}^i z_{r,\text{ref}}$. The vertical dynamics are given by

$$\begin{bmatrix} {}^i\dot{z}_r \\ {}^i\dot{v}_z \end{bmatrix} = \begin{bmatrix} 0 & 1 \\ 0 & 0 \end{bmatrix} \underbrace{\begin{bmatrix} {}^i e_z \\ {}^i v_z \end{bmatrix}}_{X_v} + \begin{bmatrix} 0 \\ -\dfrac{1}{M} \end{bmatrix}(T - T^\star) \tag{6.27}$$

The internal model-based regulator is given by

$$\begin{aligned} \dot{\eta}_v &= \Phi\eta_v + G\,{}^i e_z \\ T &= -K_v X_v - K_{\eta_v}\eta_v \end{aligned} \tag{6.28}$$

with K_v and K_{η_v} to be designed such that the resulting closed-loop system is Hurwitz.

6.5   Implementation and Results

In order to promote flexibility and encourage usage as well as further improvements, the presented algorithm has been implemented as an extension of the open-source PX4 flight software (Meier, Honegger, and Pollefeys, 2015). Simulations are carried out exploiting the Gazebo-based simulation environment RotorS (Furrer et al., 2016) along with the provided model of the 3DR Iris quadrotor, properly modified to carry the latest available ARVA receiver plugin (Cacace, Mimmo, and Marconi, 2021). The adopted Iris model is also equipped with an essential sensor suite composed of an Inertial Measurement Unit (IMU) and a GPS. Exploiting the PX4 firmware modular structure, we implemented our algorithm combining a new "extremum seeking" PX4 module jointly with a new flight mode called "search", so that we could easily switch to this mode when a first ARVA signal is found and the developed algorithm will autonomously start working. Moreover, slight modifications to the current multicopter control loop have been implemented to admit the new regulator. The already provided PX4 Extended Kalman Filter (EKF) module has been used.

To evaluate the performances of the proposed algorithm, we present two different simulation scenarios that comprise Software-In-The-Loop (SITL) and Hardware-In-The-Loop (HITL) simulations. In order to make the two presented simulation results comparable, the same set-up is used. In particular, the drone-receiver is initially located at ${}^i p_r(0) = [{}^i x_r = 0, {}^i y_r = 0, {}^i z_r = -6]^\top$, corresponding to the position in space where the first ARVA signal has been detected after the first search phase. For simplicity, we also take this starting point as coincident with the origin of the search plane frame.

In order to be compliant with the maximum range of action of commercial ARVA sensors, the victim location has been randomly chosen to be initially approximately 50 meters far from the initial receiver position. We have a distance between the

victim-transmitter and the search plane equal to $d_t = 15$ m. Moreover, the transmitter orientation with respect to the search plane frame ^pR_t has been numerically computed to obtain the worst case scenario in terms of distance between the optimal position on the search plane $p^\star$, and the geometric projection of the victim position on the search plane $p_{t/\text{proj}}$. Therefore we are in a case similar to that of Figure 6.2d. This scenario is of great practical importance because, as victims are usually buried at a distance between 0.5 and 10 meters from the snow plane, the performed simulations really represent a worst case scenario. In fact, the rescuers in charge of the last part of the rescue operations involving digging and finding the victim, are well trained and able to quickly save the victim if they are given an estimate $p^\star$ which is located in a 10 meters radius from the unknown $p_{t/\text{proj}}$ (they perform the digging on the orthogonal direction with respect to the search plane, and thus with respect to the snow plane).

To get closer to real use cases, the Gazebo simulation environment has been shaped to mimic an avalanche scenario, where the drone cannot flight at a fixed altitude with respect to the inertial frame due to the mountain slope, unlike our previous work (Azzollini, Mimmo, and Marconi, 2020). Let the search plane be defined, in inertial coordinates, as:

$$^iz_p = q_p + m_p\,^ix + n_p\,^iy,$$

with q_p, m_p, $n_p \in \mathbb{R}$. Then, the homogeneous transformation between the search plane and the inertial reference frame ^iH_p (from search plane to inertial) is defined as:

$$^iH_p = \begin{bmatrix} ^iR_p & ^iO_p \\ 0 & 1 \end{bmatrix}.$$

In the aforementioned relation, the quantities ^iO_p and ^iR_p are strongly related to the plane parameters q_p, m_p and n_p. In particular, $^iO_p \equiv (0,0,q_p)^T$, while ^iR_p takes the form

$$^iR_p := \begin{bmatrix} \cos(\theta_p)\cos(\psi_p) & -\sin(\psi_p) & \sin(\theta_p)\cos(\psi_p) \\ \cos(\theta_p)\sin(\psi_p) & \cos(\psi_p) & \sin(\theta_p)\sin(\psi_p) \\ -\sin(\theta_p) & 0 & \cos(\theta_p) \end{bmatrix},$$

TABLE 6.1: Simulation parameters.

Victim x-position in inertial coordinates	24.0866
Victim y-position in inertial coordinates	34.0866
Victim z-position in inertial coordinates	-16.8773
Roll angle (transmitter to inertial) ϕ_t	0
Pitch angle (transmitter to inertial) θ_t	0.1745
Yaw angle (transmitter to inertial) ψ_t	2.7052
^iO_p	$[0\ 0\ -6.1268]^\top$
Roll angle (transmitter to search plane) ϕ_p	0
Pitch angle (transmitter to search plane) θ_p	0.6162
Yaw angle (transmitter to search plane) ψ_p	0.7854

(A) Drone trajectory: 3D view.

(D) Drone trajectory: $x_i y_i$-plane view.

(G) Drone trajectory: $x_p y_p$-plane view.

(B) Reference tracking: x-component.

(E) Reference tracking: y-component.

(H) Reference tracking: z-component.

(C) Optimum seeking: x-component.

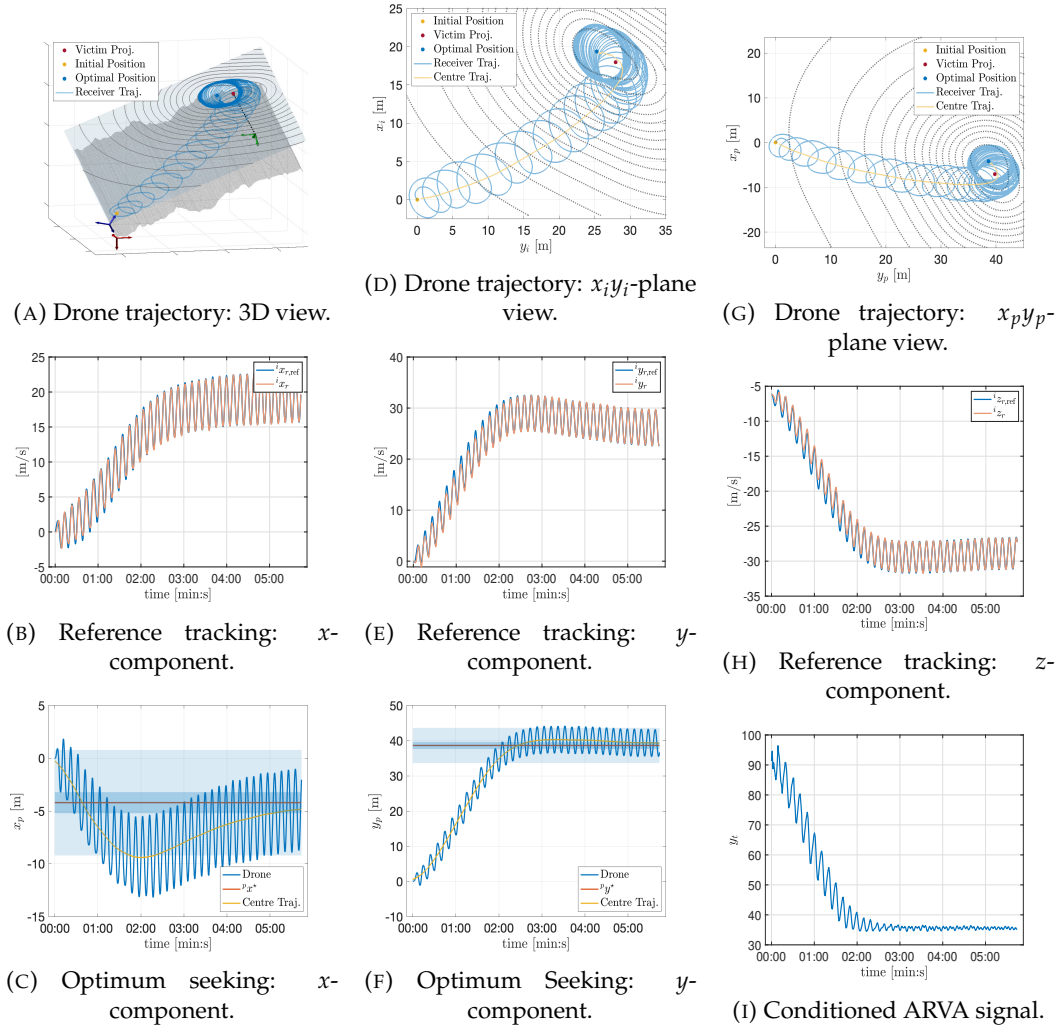(F) Optimum Seeking: y-component.

(I) Conditioned ARVA signal.

FIGURE 6.5: Results of the SITL simulation.

with

$$\theta_p = \arctan\left(-m_p\sqrt{\left(\frac{n_p^2}{m_p^2}+1\right)}\right),$$

$$\psi_p = \arctan\left(\frac{n_p}{m_p}\right).$$

The chosen simulation parameters are summarized in Table 6.1

The proposed algorithm was discretized as follows. The discrete-time low-level controller was obtained by: (i) using the zero-order-hold for discretizing the four plants; (ii) the Tustin's method for discretizing the internal model units; (iii) discrete-time Linear Quadratic Regulation theory to obtain the control gains, so as to force the drone to be in near hovering conditions at all times. The ES algorithm was discretized by means of the simple forward Euler method, while the α-filter was discretized using Tustin's method once again. The low-level controller is designed to work at a fixed frequency of 250 Hz, the ES algorithm runs at 10 Hz while the frequency of the ARVA signals is the lowest, being 1 Hz.

The ES parameters have been carefully designed following the rationale presented at the end of Section 6.4.2, taking into consideration a maximum feasible

(A) Drone trajectory: 3D view.

(D) Drone trajectory: $x_i y_i$-plane view.

(G) Drone trajectory: $x_p y_p$-plane view.

(B) Reference tracking: x-component.

(E) Reference tracking: y-component.

(H) Reference tracking: z-component.

(C) Optimum seeking: x-component.

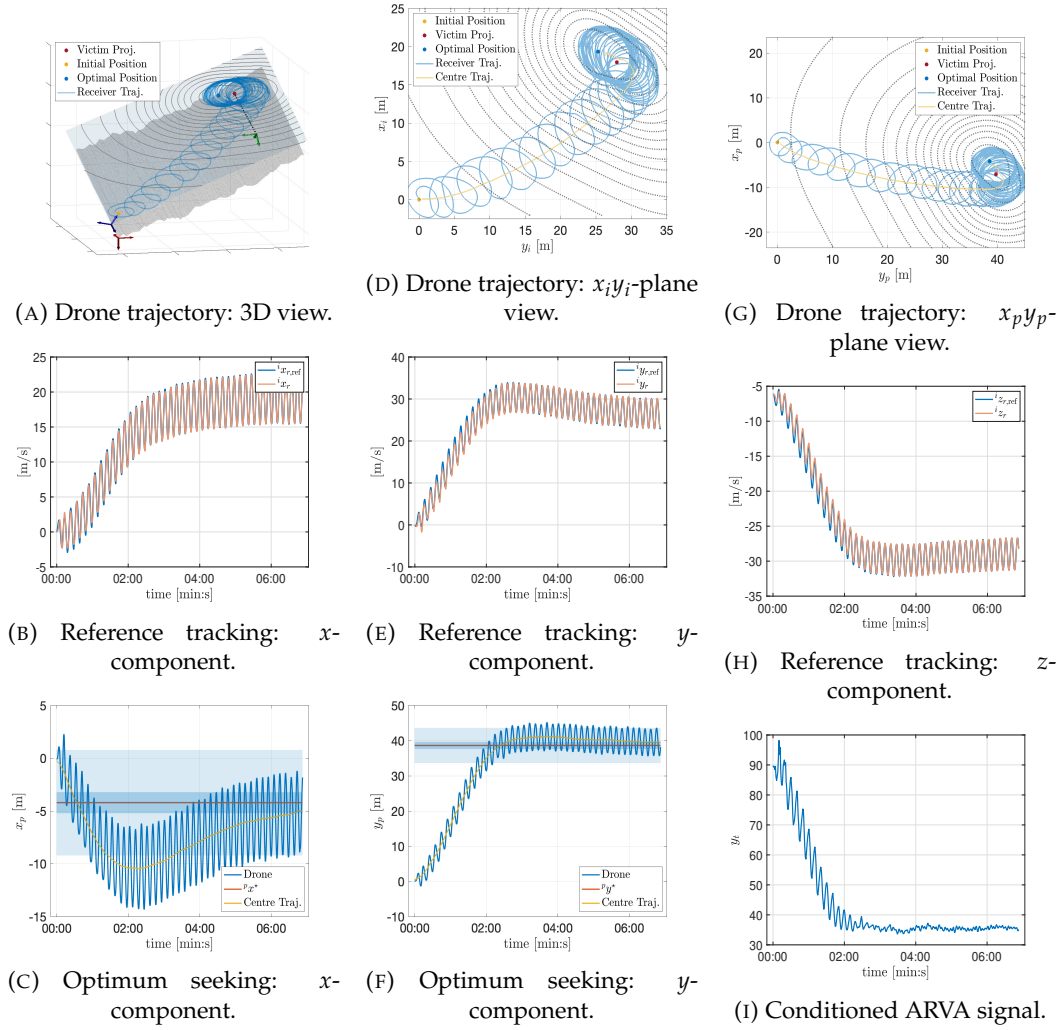(F) Optimum seeking: y-component.

(I) Conditioned ARVA signal.

FIGURE 6.6: Results of the HITL simulation.

velocity of 4 m/s as platform architectural limit. In particular, the best results have been obtained setting $\alpha = 20$, $\kappa = 0.07$ and $\omega = 0.65$, that correspond to a steady-state radius of 3.6 meters and a maximum drone velocity (on the search plane) of 3.6 m/s. Moreover, a low-pass filter has been implemented in order to damp the noise affecting the ARVA signal.

6.5.1 SITL Simulations

SITL simulations have been performed on a PC running Ubuntu 18.04.3 LTS with Intel(R) Core i7-3770K@3.60 GHz CPU and 32 GB RAM. The main results are reported in Figure 6.5. In particular, Figure 6.5c and Figure 6.5f compare the drone trajectories on the search plane (blue line), with both the trajectory of the circumference centre (yellow line) and the position of the ARVA minimizer on the search plane (red line). The dark blue shaded area in Figure 6.5c and Figure 6.5f represents a bounding box of dimensions 1×1 meters around the optimum position, such interval has been chosen as the interval of practical convergence. On the other hand, the light blue shaded area draws a bounding box of dimension 5×5 meters around the optimum, this interval represents the minimum distance required from experienced rescues in order to find a buried victim. From these figures, it is clear that

the practical convergence to the optimum is obtained in approximately 300 seconds, with the loitering circumference centre entering inside the bigger bounding box before 150 seconds. In Figure 6.5a is reported the 3-dimensional drone trajectory (dark blue) on the search plane (light blue) and the iso-power lines of the ARVA function along the search plane (in gray), while in Figure 6.5d and Figure 6.5g the same quantities are projected on the $x_i y_i$-plane and on the search plane, respectively, for better visualization. From the aforementioned figures it is possible to see how the ES algorithm steers the drone-receiver towards the optimum by performing, as expected, a circlular trajectory whose centre follows an approximate gradient descent direction. This behavior is particularly visible in Figure 6.5d and Figure 6.5g, where the yellow line represents the trajectory of the loitering circumference centre. Recall that the sought minimum does not coincide with the projection on the search plane of the victim position. This is visible in Figure 6.5a, Figure 6.5d, and Figure 6.5g, where the red dot represents the victim position projected on the search plane $p_{t/\mathrm{proj}}$, while the blue one is the optimal position (ARVA minimizer) on the same plane $p^\star$. Finally, Figure 6.5i shows the behavior of the ARVA signal, while Figure 6.5b, Figure 6.5e, and Figure 6.5h report the true drone-receiver inertial positions versus the requested ones. Note that, the non-negligible motion of the circles centre, during the transient, causes a mismatch between the adopted internal model and the model of the reference trajectory, leading inevitably to non-zero tracking errors. However, notice that the low-level controller manages to keep the tracking errors very small at all times, thus ensuring the needed time scale separation. Moreover, at steady-state, when the reference signals truly become simply biased sinusoids, the tracking errors are practically zero, thus resulting in a better estimate of the optimum.

6.5.2 HITL Simulations

In order to verify the usability on real applications, the proposed solution has been tested on a low-cost microcontroller with limited capabilities. In particular, HITL simulations have been performed on the *Pixhawk 2 Cube* board, endowed of a STM32F427 Cortex-M4F(R)@168 MHz (252 MIPS) core, with FPU and 256 KB RAM. The obtained results are reported in Figure 6.6, which presents the same images configuration proposed in Figure 6.5, so as to facilitate the comparison. Notice that despite some numerical errors, which induce a degradation of the tracking performance, the practical convergence to the bounding box of 1×1 meters, is still obtained in approximately 390 seconds, while the larger bound is broken after only 180 seconds. Thanks to its lightweight, the developed algorithm is still able to run at a fixed frequency of 250 Hz jointly with the ES module, running at 10 Hz. The source code can be found at https://github.com/casy-lab/PX4_Firmware.

6.6 Conclusions

In this work, we presented a complete control architecture for a UAV which, being equipped with an ARVA receiver, is able to autonomously explore the area of interest and converge as close as possible to the victim-ARVA transmitter.

The scheme presented in Figure 6.4 is general, in the sense that it could be used for any source seeking control problem where a mobile robot needs to be driven towards a source. The particular choice of an ES control algorithm, and of a low-level controller, depends both on the specific application and on the technology at

our disposal. In general, ES should generate a reference trajectory that is dynamically feasible for the specific mobile robot, while the low-level controller should be designed considering both the specific robot and the chosen ES algorithm.

Finally, we extended the well-known PX4 flight stack by creating a new flight mode where our ES reference generator as well as our low-level controller are used. The proposed algorithm performs well even in HITL simulations, converging in a reasonably good amount of time, proving robustness with respect to noise, and providing a very good estimate of the projection of the victim position on the search plane, and thus also on the snow/terrain plane (which is the optimal point from which digging should be performed). The code is available open source to encourage usage as well as possible external contributions.

Concluding Remarks

Several adaptive estimation and control algorithms were presented in this thesis. What all the presented identifiers have in common is that they are robust in an ISS sense, with the trivial exception of the extremum seeking algorithm as it cannot lead to exact convergence, even without disturbances. Anyhow, we could divide the presented works into 2 categories:

- Chapters 3, 5 and 6, in which we develop our algorithms relying on well-known adaptive control tools, thus obtaining "classic" results. By classic we mean that in order to have a robust solution, not surprisingly we had to be able to ensure, or assume, persistency of excitation;

- In Chapters 1, 2, and 4, persistency of excitation would still be related with a correct estimation of the true parameters. Nevertheless, with the proposed designs we formally prove the existence and stability of an optimal steady state (where a cost function - being a function of the estimation or tracking error - is minimized), and robustness with respect to the disturbances in form of input-to-state and input-output stability relative to the unperturbed steady-state trajectories.

In particular, in Chapter 3 PE is simply assumed in Assumption 3.3, and robustness then comes from global exponential stability (which is for free when we have PE and we deal with LTI systems). On the other hand, in Chapter 5 we were able to guarantee PE for the specific trajectories involved in our application, by means of our design choices. We also noticed in Remark 5.1 that this fact should not be taken for granted and does not only depend on the application. In fact, the same straight trajectory that guarantees PE with our design, was not PE for other designs dealing with the same problem. Finally, extremum seeking is a kind of adaptive algorithm which could be easily also seen as an optimization or learning algorithm (are these three worlds so different after all?). In fact, as discussed in Chapter 6, ES algorithm consists in moving in circular trajectories, so as to explore a neighborhood of the current position (or estimate), to check in which direction the sensed function value is decreasing. It is then not surprising that it is a robust estimation algorithm, as it has been proved in the important ES works we mentioned in Section 6.1.2. As a matter of fact, this circular trajectory is nothing but an injection of a sinusoidal signal in the system, which is a PE signal when we have to estimate two parameters (a sinusoid is sufficiently rich of order two, see Chapter 3, where we used this property of sinusoidal signals).

Now, moving to Chapters 1, 2, and 4, it is interesting to notice what they have in common, so as to try to understand whether there could be some underlying principle related to robustness of adaptive systems when PE is not necessarily present (which we formally proved for our specific applications). First of all, in all the aforementioned works we know where to search for the unknown parameters. Accordingly, we define saturation functions in Chapters 1 and 2, while we define a dead-zone-based projection mechanism in Chapter 4, for keeping the parameter estimates

in the desired set. Moreover, the identifiers in Chapters 1 and 2 are stable, in fact the optimal steady state trajectories (related with correct parameter estimation) are proved to be asymptotically stable. On the other hand, the adaptive algorithm in Chapter 4 is given by the union of "classic" adaptive laws (not robust, given by a pure integrator), and the already mentioned dead-zone modification which is a well-known robustification solution. The RLS algorithms are intrinsically robust, while the dead-zone modification guarantees that the estimator in Chapter 6 does not drift by acting only when necessary. In the RLS-based algorithms, in absence of PE, we need a nonzero regularization matrix R (Remark 1.1 and Section 2.5.2). This results in a practical stability result as, what is always guaranteed, is optimality with respect to the chosen cost function[1]. This means that the optimal parameters do not exactly correspond to the true parameters anymore. Anyway, there are several control applications in which we are not interested in exact convergence of the parameters, but in obtaining any asymptotic combination of the parameters such that the estimation error (see Figure 1.5) or tracking error (Chapter 6) are driven as close as possible to zero. In these contexts, robustness of the identifier is much more important than exact convergence to the true parameters as it enables the use of canonical nonlinear control techniques such as small-gain methods, which are key in order to interconnect ISS systems.

We conjecture then that if we choose a stable identifier, and we know a set in which the unknown parameter lies, we could saturate the produced estimates on the desired set and obtain a robust (at least practical) stability result in terms of ISS. The "classic" adaptive control results, relying on PE to achieve robustness, neither consider stable identifiers (in the classic formulation we obtain pure integrators as identifiers), nor they assume that a set in which we are sure to find the parameters is known. In this sense, this is an additional assumption we are requiring with respect to classic approaches (nothing comes for free).

---

[1]Notice that also in classic adaptive control, resulting in the standard "pure integrator" identifier, there is always an underlying cost criterion (Ioannou and Sun, 2012, Section 4.2.1)

Bibliography

Abdessameud, A., A. Tayebi, and I. G. Polushin (2017). "Leader-Follower Synchronization of Euler-Lagrange Systems With Time-Varying Leader Trajectory and Constrained Discrete-Time Communication". In: *IEEE Transactions on Automatic Control* 62.5, pp. 2539–2545.

AerIal RoBotic technologies for professiOnal seaRch aNd rescuE, https://www.airborne-project.eu (2018).

Afri, Chouaib, Vincent Andrieu, Laurent Bako, and Pascal Dufour (2016). "State and parameter estimation: A nonlinear Luenberger observer approach". In: *IEEE Transactions on Automatic Control* 62.2, pp. 973–980.

Arablouei, Reza, Kutluyıl Doğançay, Stefan Werner, and Yih-Fang Huang (2014). "Adaptive distributed estimation based on recursive least-squares and partial diffusion". In: *IEEE Transactions on Signal Processing* 62.14, pp. 3510–3522.

Arcak, Murat and Andrew Teel (2002). "Input-to-state stability for a class of Lurie systems". In: *Automatica* 38.11, pp. 1945–1949.

Ariyur, K. B. and M. Krstic (2003). *Real-time optimization by extremum-seeking control*. John Wiley & Sons.

Azzollini, Ilario A., Nicola Mimmo, and Lorenzo Marconi (2020). "An Extremum Seeking Approach to Search and Rescue Operations in Avalanches using ARVA". In: *IFAC-PapersOnLine* 53.2. 21st IFAC World Congress, pp. 1627–1632.

Azzollini, Ilario A., Michelangelo Bin, Pauline Bernard, and Lorenzo Marconi (2021a). "Robust Frequency Estimation of Multi-Harmonic Signals". In: *2021 European Control Conference (ECC)*, pp. 2633–2638.

Azzollini, Ilario Antonio, Wenwu Yu, Shuai Yuan, and Simone Baldi (2020). "Adaptive leader-follower synchronization over heterogeneous and uncertain networks of linear systems without distributed observer". In: *IEEE Transactions on Automatic Control*.

Azzollini, Ilario Antonio, Nicola Mimmo, Lorenzo Gentilini, and Lorenzo Marconi (2021b). "UAV-Based Search and Rescue in Avalanches using ARVA: An Extremum Seeking Approach". In: *arXiv preprint arXiv:2106.14514*.

Bai, E. and S. Sastry (1987). "Global stability proofs for continuous-time indirect adaptive control schemes". In: *IEEE Transactions on Automatic Control* 32.6, pp. 537–543.

Baldi, S., I. A. Azzollini, and P. A. Ioannou (2020). "A distributed indirect adaptive approach to cooperative tracking in networks of uncertain single-input single-output systems". In: *IEEE Transactions on Automatic Control*, pp. 1–1.

Baldi, S. and P. Frasca (2019). "Leaderless synchronization of heterogeneous oscillators by adaptively learning the group model". In: *IEEE Transactions on Automatic Control*.

Bekker, Mieczyslaw Gregory (1960). "Off-the-road locomotion". In: *Research and development in terramechanics*.

Bergerman, Marcel, Silvio M Maeta, Ji Zhang, Gustavo M Freitas, Bradley Hamner, Sanjiv Singh, and George Kantor (2015). "Robot farmers: Autonomous orchard

vehicles help tree fruit production". In: *IEEE Robotics & Automation Magazine* 22.1, pp. 54–63.

Bernard, Pauline. *Observer design for nonlinear systems*. Springer.

Bevacqua, Giuseppe, Jonathan Cacace, Alberto Finzi, and Vincenzo Lippiello (2015). "Mixed-Initiative Planning and Execution for Multiple Drones in Search and Rescue Missions." In: *ICAPS*, pp. 315–323.

Bin, Michelangelo (2020). *Generalized Recursive Least Squares: Stability, Robustness and Excitation*. Systems and Control Letters. In press.

Bin, Michelangelo, Pauline Bernard, and Lorenzo Marconi (2021). "Approximate Nonlinear Regulation via Identification-Based Adaptive Internal Models". In: *IEEE Trans. Autom. Control* 66.8, pp. 3534–3549.

Bin, Michelangelo and Lorenzo Marconi (2020). *Model identification and adaptive state observation for a class of nonlinear systems*. IEEE Trans. Autom. Control. Early Access.

Bin, Michelangelo, Lorenzo Marconi, and Andrew R Teel (2019). "Adaptive output regulation for linear systems via discrete-time identifiers". In: *Automatica* 105, pp. 422–432.

Bodson, Marc, Jonathan S Jensen, and Scott C Douglas (2001). "Active noise control for periodic disturbances". In: *IEEE Transactions on control systems technology* 9.1, pp. 200–205.

Bosso, Alessandro, Ilario A Azzollini, and Simone Baldi (2019). "Global Frequency Synchronization over Networks of Uncertain Second-Order Kuramoto Oscillators via Distributed Adaptive Tracking". In: *2019 IEEE 58th Conference on Decision and Control (CDC)*. IEEE, pp. 1031–1036.

Bosso, Alessandro, Ilario Antonio Azzollini, Simone Baldi, and Luca Zaccarian (2021a). "A Hybrid Distributed Strategy for Robust Global Phase Synchronization of Second-Order Kuramoto Oscillators". In: *2021 IEEE 60th Conference on Decision and Control (CDC)*. IEEE.

— (Oct. 2021b). "Adaptive Hybrid Control for Robust Global Phase Synchronization of Kuramoto Oscillators". Preprint. URL: https://hal.archives-ouvertes.fr/hal-03372616.

Breschi, Valentina, Alberto Bemporad, and Ilya V Kolmanovsky (2020). "Cooperative constrained parameter estimation by ADMM-RLS". In: *Automatica* 121, p. 109175.

Burke, Michael (2012). "Path-following control of a velocity constrained tracked vehicle incorporating adaptive slip estimation". In: *2012 IEEE International Conference on Robotics and Automation*, pp. 97–102.

Cacace, J., A. Finzi, and V. Lippiello (2016). "Implicit robot selection for human multi-robot interaction in search and rescue missions". In: *2016 25th IEEE International Symposium on Robot and Human Interactive Communication (RO-MAN)*, pp. 803–808.

Cacace, J., N. Mimmo, and L. Marconi (2021). "An ARVA Sensor Simulator". In: *Studies in Computational Intelligence* 895, pp. 233–266.

Cacace, J., A. Finzi, V. Lippiello, M. Furci, N. Mimmo, and L. Marconi (2016). "A control architecture for multiple drones operated via multimodal interaction in search & rescue mission". In: *2016 IEEE International Symposium on Safety, Security, and Rescue Robotics (SSRR)*, pp. 233–239.

Cai, Chaohong and Andrew R Teel (2009). "Characterizations of input-to-state stability for hybrid systems". In: *Systems & Control Letters* 58.1, pp. 47–53.

Cai, H., F. L. Lewis, G. Hu, and J. Huang (2017). "The adaptive distributed observer approach to the cooperative output regulation of linear multi-agent systems". In: *Automatica* 75, pp. 299 –305.

Cai, He and Jie Huang (2016). "Leader-following attitude consensus of multiple rigid body systems by attitude feedback control". In: *Automatica* 69, pp. 87–92.

Carnevale, D, S Galeani, M Sassano, and A Astolfi (2016). "Robust hybrid estimation and rejection of multi-frequency signals". In: *International Journal of Adaptive Control and Signal Processing* 30.12, pp. 1649–1673.

Carnevale, Daniele and Alessandro Astolfi (2009). "Hybrid observer for global frequency estimation of saturated signals". In: *IEEE transactions on automatic control* 54.10, pp. 2461–2464.

Casau, Pedro, Christopher G Mayhew, Ricardo G Sanfelice, and Carlos Silvestre (2019). "Robust global exponential stabilization on the n-dimensional sphere with applications to trajectory tracking for quadrotors". In: *Automatica* 110, p. 108534.

Cattivelli, Federico S, Cassio G Lopes, and Ali H Sayed (2008). "Diffusion recursive least-squares for distributed estimation over adaptive networks". In: *IEEE Transactions on Signal Processing* 56.5, pp. 1865–1877.

Cattivelli, Federico S and Ali H Sayed (2010). "Analysis of spatial and incremental LMS processing for distributed estimation". In: *IEEE Transactions on Signal Processing* 59.4, pp. 1465–1480.

Chen, Boli, Gilberto Pin, Wai M Ng, Chi K Lee, SY Ron Hui, and Thomas Parisini (2014). "An adaptive observer-based switched methodology for the identification of a perturbed sinusoidal signal: Theory and experiments". In: *IEEE Transactions on Signal Processing* 62.24, pp. 6355–6365.

Chen, Boli, Gilberto Pin, Wai M Ng, Shu Yuen Ron Hui, and Thomas Parisini (2017). "An adaptive-observer-based robust estimator of multi-sinusoidal signals". In: *IEEE Transactions on Automatic Control* 63.6, pp. 1618–1631.

Chen, Jianshu and Ali H Sayed (2012). "Diffusion adaptation strategies for distributed optimization and learning over networks". In: *IEEE Transactions on Signal Processing* 60.8, pp. 4289–4305.

Choi, Young-Pil, Seung-Yeal Ha, and Seok-Bae Yun (2011). "Complete synchronization of Kuramoto oscillators with finite inertia". In: *Physica D: Nonlinear Phenomena* 240.1, pp. 32 –44.

Chopra, N. and M. W. Spong (2009). "On Exponential Synchronization of Kuramoto Oscillators". In: *IEEE Transactions on Automatic Control* 54.2, pp. 353–357.

Chun, Wendell H and Nikolaos Papanikolopoulos (2016). "Robot surveillance and security". In: *Springer Handbook of Robotics*. Springer, pp. 1605–1626.

Cochran, J. and M. Krstic (2009). "Nonholonomic source seeking with tuning of angular velocity". In: *IEEE Transactions on Automatic Control* 54.4, pp. 717–731.

Cochran, J., E. Kanso, S. D. Kelly, H. Xiong, and M. Krstic (2009). "Source seeking for two nonholonomic models of fish locomotion". In: *IEEE Transactions on Robotics* 25.5, pp. 1166–1176.

Costley, A. and R. Christensen (2020). "Landmark Aided GPS-Denied Navigation for Orchards and Vineyards". In: *2020 IEEE/ION Position, Location and Navigation Symposium (PLANS)*, pp. 987–995.

Dar, T. M. and R. G. Longoria (2010). "Slip estimation for small-scale robotic tracked vehicles". In: *Proceedings of the 2010 American Control Conference*, pp. 6816–6821.

Daubechies, Ingrid (1992). *Ten Lectures on Wavelets*. SIAM.

De Marco, Simone, Lorenzo Marconi, Tarek Hamel, and Robert Mahony (2016). "Output regulation on the special Euclidean group SE(3)". In: *2016 IEEE 55th Conference on Decision and Control (CDC)*. IEEE, pp. 4734–4739.

Delmerico, J., S. Mintchev, A. Giusti, B. Gromov, K. Melo, T. Horvat, C. Cadena, M. Hutter, A. Ijspeert, D. Floreano, L. Gambardella, R. Siegwart, and D. Scaramuzza

(2019). "The current state and future outlook of rescue robotics". In: *Journal of Field Robotics* 36.7, pp. 1171–1191.

Ding, Z. (2017). "Distributed adaptive consensus output regulation of network-connected heterogeneous unknown linear systems on directed graphs". In: *IEEE Transactions on Automatic Control* 62.9, pp. 4683–4690.

Dörfler, Florian and Francesco Bullo (2011). "On the critical coupling for Kuramoto oscillators". In: *SIAM Journal on Applied Dynamical Systems* 10.3, pp. 1070–1099.

Dorfler, Florian and Francesco Bullo (2012). "Synchronization and transient stability in power networks and nonuniform Kuramoto oscillators". In: *SIAM Journal on Control and Optimization* 50.3, pp. 1616–1642.

Dydek, Zachary T., Anuradha M. Annaswamy, and Eugene Lavretsky (2010). "Adaptive Control and the NASA X-15-3 Flight Revisited". In: *IEEE Control Systems Magazine* 30.3, pp. 32–48.

Elliott, H., R. Cristi, and M. Das (1985). "Global stability of adaptive pole placement algorithms". In: *IEEE Transactions on Automatic Control* 30.4, pp. 348–356.

Endo, Daisuke, Yoshito Okada, Keiji Nagatani, and Kazuya Yoshida (2007). "Path following control for tracked vehicles based on slip-compensating odometry". In: *2007 IEEE/RSJ International Conference on Intelligent Robots and Systems*. IEEE, pp. 2871–2876.

Fedele, Giuseppe and Andrea Ferrise (2011). "Non adaptive second-order generalized integrator for identification of a biased sinusoidal signal". In: *IEEE transactions on automatic control* 57.7, pp. 1838–1842.

— (2014). "A frequency-locked-loop filter for biased multi-sinusoidal estimation". In: *IEEE Transactions on Signal Processing* 62.5, pp. 1125–1134.

Feng, Z., G. Hu, W. Ren, W. E. Dixon, and J. Mei (2018). "Distributed Coordination of Multiple Unknown Euler-Lagrange Systems". In: *IEEE Transactions on Control of Network Systems* 5.1, pp. 55–66.

Ferrara, V. (2015). "Technical survey about available technologies for detecting buried people under rubble or avalanches". In: *WIT Transactions on The Built Environment* 150, pp. 91–101.

Francis, B. A. (1977). "The linear multivariable regulator problem". In: *SIAM Journal on Control and Optimization* 15.3, pp. 486–505.

Furrer, Fadri, Michael Burri, Markus Achtelik, and Roland Siegwart (2016). "RotorS:A modular gazebo MAV simulator framework". In: *Robot operating system (ROS)*. Springer, pp. 595–625.

Ghadiri-Modarres, M. A., M. Mojiri, and H. R. Z. Zangeneh (2017). "New Schemes for GPS-Denied Source Localization Using a Nonholonomic Unicycle". In: *IEEE Transactions on Control Systems Technology* 25.2, pp. 720–727.

Gibson, T. E. (2016). "Adaptation and synchronization over a network: Asymptotic error convergence and pinning". In: *2016 IEEE 55th Conference on Decision and Control (CDC)*, pp. 2969–2974.

Goebel, Rafal, Ricardo G Sanfelice, and Andrew R Teel (2009). "Hybrid dynamical systems". In: *IEEE Control Systems Magazine* 29.2, pp. 28–93.

— (2012). *Hybrid dynamical systems: modeling, stability, and robustness*. Princeton University Press, Princeton, NJ.

Gui, Haichao and Anton HJ de Ruiter (2018). "Global finite-time attitude consensus of leader-following spacecraft systems based on distributed observers". In: *Automatica* 91, pp. 225–232.

Guo, Yufeng, Dongrui Zhang, Zhuchun Li, Qi Wang, and Daren Yu (2021). "Overviews on the applications of the Kuramoto model in modern power system analysis". In: *International Journal of Electrical Power & Energy Systems* 129, p. 106804.

Ha, Seung-Yeal, Taeyoung Ha, and Jong-Ho Kim (2010). "On the complete synchronization of the Kuramoto phase model". In: *Physica D: Nonlinear Phenomena* 239.17, pp. 1692 –1700.

Ha, Seung-Yeal, Myeongju Kang, and Dohyun Kim (2021). "Emergent behaviors of high-dimensional Kuramoto models on Stiefel manifolds". In: *arXiv preprint arXiv:2101.04300*.

Hajimolahoseini, Habib, Mohammad Reza Taban, and Hamid Soltanian-Zadeh (2012). "Extended Kalman filter frequency tracker for nonstationary harmonic signals". In: *Measurement* 45.1, pp. 126–132.

Harfouch, Y. A., S. Yuan, and S. Baldi (2018). "An Adaptive Switched Control Approach to Heterogeneous Platooning With Intervehicle Communication Losses". In: *IEEE Transactions on Control of Network Systems* 5.3, pp. 1434–1444.

Haverkort, A.J. Ancha Srinivasan (ed) (2007). *Handbook of precision agriculture: principles and applications*. The Haworth Press Inc. ISBN: 978-1-56022-945-4.

Hou, Ming (2011). "Parameter identification of sinusoids". In: *IEEE Transactions on Automatic Control* 57.2, pp. 467–472.

Hsu, Liu, Romeo Ortega, and Gilney Damm (1999). "A globally convergent frequency estimator". In: *IEEE Transactions on Automatic Control* 44.4, pp. 698–713.

Hua, M., T. Hamel, P. Morin, and C. Samson (2013). "Introduction to feedback control of underactuated VTOLvehicles: A review of basic control design ideas and principles". In: *IEEE Control systems magazine* 33.1, pp. 61–75.

Huang, J. (2004). *Nonlinear output regulation: theory and applications*. Society for Industrial and Applied Mathematics.

Ioannou, P. and J. Sun (2012). *Robust Adaptive Control*. Dover Publications.

Isidori, A., L. Marconi, and G. Casadei (2014). "Robust output synchronization of a network of heterogeneous nonlinear agents via nonlinear regulation theory". In: *IEEE Transactions on Automatic Control* 59.10, pp. 2680–2691.

Isidori, A., L. Marconi, and A. Serrani (2012). *Robust autonomous guidance: an internal model approach*. Springer Science & Business Media.

Isidori, Alberto (1999). *Nonlinear control systems II*. Springer.

— (2017). *Lectures in feedback design for multivariable systems*. Vol. 3. Springer.

Jenkins, B. M., A. M. Annaswamy, E. Lavretsky, and T. E. Gibson (2018). "Convergence properties of adaptive systems and the definition of exponential stability". In: *SIAM Journal on Control and Optimization* 56.4, pp. 2463–2484.

Jiang, X., S. Li, B. Luo, and Q. Meng (2020). "Source Exploration for an Under-Actuated System: A Control-Theoretic Paradigm". In: *IEEE Transactions on Control Systems Technology* 28.3, pp. 1100–1107.

Jiang, Z-P, Andrew R Teel, and Laurent Praly (1994). "Small-gain theorem for ISS systems and applications". In: *Mathematics of Control, Signals and Systems* 7.2, pp. 95–120.

Karimi-Ghartemani, Masoud and Alireza K Ziarani (2004). "A nonlinear time-frequency analysis method". In: *IEEE Transactions on Signal Processing* 52.6, pp. 1585–1595.

Khalil, H. K. (2002). *Nonlinear Systems*. 3rd. Prentice Hall.

Kreisselmeier, Gerhard (1977). "Adaptive observers with exponential rate of convergence". In: *IEEE transactions on automatic control* 22.1, pp. 2–8.

Krstic, M. and H. Wang (2000). "Stability of extremum seeking feedback for general nonlinear dynamic systems". In: *Automatica* 36.4, pp. 595–601.

Kuramoto, Y. (1984). *Chemical Oscillations, Waves, and Turbulence*. Springer.

Li, Lei, Haiquan Zhao, and Shaohui Lv (2021). "Diffusion recursive total least square algorithm over adaptive networks and performance analysis". In: *Signal Processing* 182, p. 107954.

Li, Z., M. Z. Q. Chen, and Z. Ding (2016). "Distributed adaptive controllers for co-operative output regulation of heterogeneous agents over directed graphs". In: *Automatica* 68, pp. 179–183.

Li, Z., Z. Duan, G. Chen, and L. Huang (2010). "Consensus of multiagent systems and synchronization of complex networks: A unified viewpoint". In: *IEEE Transactions on Circuits and Systems I: Regular Papers* 57.1, pp. 213–224.

Li, Z., W. Ren, X. Liu, and L. Xie (2013). "Distributed consensus of linear multi-agent systems with adaptive dynamic protocols". In: *Automatica* 49.7, pp. 1986–1995.

Liu, Zhaoting, Ying Liu, and Chunguang Li (2014). "Distributed sparse recursive least-squares over networks". In: *IEEE Transactions on Signal Processing* 62.6, pp. 1386–1395.

Ljung, L. (1999). *System Identification - Theory for the User*. Prentice-Hall.

Lopes, Cassio G and Ali H Sayed (2007). "Incremental adaptive strategies over distributed networks". In: *IEEE Transactions on Signal Processing* 55.8, pp. 4064–4077.

— (2008). "Diffusion least-mean squares over adaptive networks: Formulation and performance analysis". In: *IEEE Transactions on Signal Processing* 56.7, pp. 3122–3136.

Lv, Y., Z. Li, Z. Duan, and J. Chen (2016). "Distributed adaptive output feedback consensus protocols for linear systems on directed graphs with a leader of bounded input". In: *Automatica* 74, pp. 308–314.

Maggiore, Manfredi, Mario Sassano, and Luca Zaccarian (2018). "Reduction theorems for hybrid dynamical systems". In: *IEEE Transactions on Automatic Control* 64.6, pp. 2254–2265.

Mahony, Robert, Tarek Hamel, and Jean-Michel Pflimlin (2008). "Nonlinear complementary filters on the special orthogonal group". In: *IEEE Transactions on Automatic Control* 53.5, pp. 1203–1218.

Marconi, L. et al. (2012). "The SHERPA project: Smart collaboration between humans and ground-aerial robots for improving rescuing activities in alpine environments". In: *2012 IEEE International Symposium on Safety, Security, and Rescue Robotics (SSRR)*, pp. 1–4.

Marino, Riccardo and Patrizio Tomei (2002). "Global estimation of n unknown frequencies". In: *IEEE Transactions on Automatic Control* 47.8, pp. 1324–1328.

Markdahl, Johan, Daniele Proverbio, and Jorge Goncalves (2020). "Robust synchronization of heterogeneous robot swarms on the sphere". In: *2020 59th IEEE Conference on Decision and Control (CDC)*. IEEE, pp. 5798–5803.

Mateos, Gonzalo and Georgios B Giannakis (2012). "Distributed recursive least-squares: Stability and performance analysis". In: *IEEE Transactions on Signal Processing* 60.7, pp. 3740–3754.

Mateos, Gonzalo, Ioannis D Schizas, and Georgios B Giannakis (2009). "Distributed recursive least-squares for consensus-based in-network adaptive estimation". In: *IEEE Transactions on Signal Processing* 57.11, pp. 4583–4588.

Mayhew, C. G., R. G. Sanfelice, and A. R. Teel (2008). "Robust source-seeking hybrid controllers for nonholonomic vehicles". In: *2008 American Control Conference*. IEEE, pp. 2722–2727.

Mayhew, Christopher G, Ricardo G Sanfelice, and Andrew R Teel (2011). "Quaternion-based hybrid control for robust global attitude tracking". In: *IEEE Transactions on Automatic control* 56.11, pp. 2555–2566.

— (2012). "On path-lifting mechanisms and unwinding in quaternion-based attitude control". In: *IEEE Transactions on Automatic Control* 58.5, pp. 1179–1191.

Mayhew, Christopher G and Andrew R Teel (2010). "Hybrid control of planar rotations". In: *Proceedings of the 2010 American Control Conference*. IEEE, pp. 154–159.

Mayhew, Christopher G, Ricardo G Sanfelice, Jansen Sheng, Murat Arcak, and Andrew R Teel (2011). "Quaternion-based hybrid feedback for robust global attitude synchronization". In: *IEEE Transactions on Automatic Control* 57.8, pp. 2122–2127.

Meier, L., D. Honegger, and M. Pollefeys (2015). "PX4: A node-based multithreaded open source robotics framework for deeply embedded platforms". In: *2015 IEEE international conference on robotics and automation (ICRA)*. IEEE, pp. 6235–6240.

Menara, Tommaso, Giacomo Baggio, Danielle S Bassett, and Fabio Pasqualetti (2019). "A framework to control functional connectivity in the human brain". In: *2019 IEEE 58th Conference on Decision and Control (CDC)*. IEEE, pp. 4697–4704.

Mengoli, D., R. Tazzari, and L. Marconi (2020). "Autonomous Robotic Platform for Precision Orchard Management: Architecture and Software Perspective". In: *2020 IEEE International Workshop on Metrology for Agriculture and Forestry (MetroAgriFor)*, pp. 303–308.

Menon, P. P., C. Edwards, Y. B. Shtessel, D. Ghose, and J. Haywood (2014). "Boundary tracking using a suboptimal sliding mode algorithm". In: *53rd IEEE Conference on Decision and Control*, pp. 5518–5523.

Modares, H., S. P. Nageshrao, G. A. D. Lopes, R. Babuška, and F. L. Lewis (2016). "Optimal model-free output synchronization of heterogeneous systems using off-policy reinforcement learning". In: *Automatica* 71, pp. 334–341.

Mojiri, Mohsen and Alireza R Bakhshai (2004). "An adaptive notch filter for frequency estimation of a periodic signal". In: *IEEE Transactions on Automatic Control* 49.2, pp. 314–318.

Moosavian, S. A. A. and A. Kalantari (2008). "Experimental slip estimation for exact kinematics modeling and control of a Tracked Mobile Robot". In: *2008 IEEE/RSJ International Conference on Intelligent Robots and Systems*, pp. 95–100.

Moreira, Carolina A. and Marcus A.M. de Aguiar (2019). "Global synchronization of partially forced Kuramoto oscillators on networks". In: *Physica A: Statistical Mechanics and its Applications* 514, pp. 487 –496.

Na, Jing, Juan Yang, Xing Wu, and Yu Guo (2015). "Robust adaptive parameter estimation of sinusoidal signals". In: *Automatica* 53, pp. 376–384.

Nagatani, Keiji, Daisuke Endo, and Kazuya Yoshida (2007). "Improvement of the odometry accuracy of a crawler vehicle with consideration of slippage". In: *Proceedings 2007 IEEE International Conference on Robotics and Automation*. IEEE, pp. 2752–2757.

Nikiforov, VO (1998). "Adaptive non-linear tracking with complete compensation of unknown disturbances". In: *European journal of control* 4.2, pp. 132–139.

Panteley, Elena, Antonio Loria, and Andrew Teel (2001). "Relaxed persistency of excitation for uniform asymptotic stability". In: *IEEE Transactions on Automatic Control* 46.12, pp. 1874–1886.

Pigou, A. C. (1920). *The Economics Of Welfare*. London: Macmillan and Co.

Pin, Gilberto, Boli Chen, and Thomas Parisini (2017). "Robust finite-time estimation of biased sinusoidal signals: A volterra operators approach". In: *Automatica* 77, pp. 120–132.

Pin, Gilberto, Boli Chen, Thomas Parisini, and Marc Bodson (2013). "Robust sinusoid identification with structured and unstructured measurement uncertainties". In: *IEEE Transactions on Automatic Control* 59.6, pp. 1588–1593.

Piniés, P. and J. D. Tardós (2006). "Fast localization of avalanche victims using sum of gaussians". In: *Proceedings 2006 IEEE International Conference on Robotics and Automation*, pp. 3989–3994.

Poveda, J. I., P. N. Brown, J. R. Marden, and A. R. Teel (2017). "A class of distributed adaptive pricing mechanisms for societal systems with limited information". In: *2017 IEEE 56th Conf. Decision Control*, pp. 1490–1495.

Poveda, J. I., M. Benosman, A. R. Teel, and R. G. Sanfelice (2021). "Robust Coordinated Hybrid Source Seeking with Obstacle Avoidance in Multi-Vehicle Autonomous Systems". In: *IEEE Transactions on Automatic Control*, pp. 1–1.

Praly, Laurent, A Isidori, and L Marconi (2006). "A new observer for an unknown harmonic oscillator". In: *Proceedings of the 17th International Symposium on Mathematical Theory of Networks and Systems, Kyoto, Japan*, pp. 24–28.

Qin, Yuzhen, Yu Kawano, Oscar Portoles, and Ming Cao (2021). "Partial Phase Cohesiveness in Networks of Networks of Kuramoto Oscillators". In: *IEEE Transactions on Automatic Control*.

Rajagopalan, V., Ç. Meriçli, and A. Kelly (2016). "Slip-aware Model Predictive optimal control for Path following". In: *2016 IEEE International Conference on Robotics and Automation*, pp. 4585–4590.

Rastegarnia, Amir (2019). "Reduced-communication diffusion RLS for distributed estimation over multi-agent networks". In: *IEEE Transactions on Circuits and Systems II: Express Briefs* 67.1, pp. 177–181.

Rogers-Marcovitz, Forrest, Neal Seegmiller, and Alonzo Kelly (2012). "Continuous Vehicle Slip Model Identification on Changing Terrains". In: *Proceedings of RSS 2012 Workshop on Long-term Operation of Autonomous Robotic Systems in Changing Environments*.

Salaris, P., M. Cognetti, R. Spica, and P. R. Giordano (2019). "Online Optimal Perception-Aware Trajectory Generation". In: *IEEE Transactions on Robotics* 35.6, pp. 1307–1322.

Sanfelice, Ricardo, David Copp, and Pablo Nanez (2013). "A toolbox for simulation of hybrid systems in Matlab/Simulink: Hybrid Equations (HyEQ) Toolbox". In: *Proceedings of the 16th international conference on Hybrid systems: computation and control*, pp. 101–106.

Sayed, Ali H, Sheng-Yuan Tu, Jianshu Chen, Xiaochuan Zhao, and Zaid J Towfic (2013). "Diffusion strategies for adaptation and learning over networks: an examination of distributed strategies and network behavior". In: *IEEE Signal Processing Magazine* 30.3, pp. 155–171.

Scardovi, L., Alain Sarlette, and Rodolphe Sepulchre (2007). "Synchronization and balancing on the N-torus". In: *Systems and Control Letters* 56, pp. 335–341.

Scheinker, A. and M. Krstić (2014). "Extremum seeking with bounded update rates". In: *Systems & Control Letters* 63, pp. 25–31.

Schizas, Ioannis D, Gonzalo Mateos, and Georgios B Giannakis (2009). "Distributed LMS for consensus-based in-network adaptive processing". In: *IEEE Transactions on Signal Processing* 57.6, pp. 2365–2382.

Schmidt, Gerd S., Antonis Papachristodoulou, Ulrich Münz, and Frank Allgöwer (2012). "Frequency synchronization and phase agreement in Kuramoto oscillator networks with delays". In: *Automatica* 48.12, pp. 3008 –3017.

Schoukens, Johan, Rik Pintelon, and Hugo Van Hamme (1992). "The interpolated fast Fourier transform: A comparative study". In: *IEEE Transactions on instrumentation and measurement* 41.2, pp. 226–232.

Sebastian, Bijo and Pinhas Ben-Tzvi (Feb. 2019). "Active Disturbance Rejection Control for Handling Slip in Tracked Vehicle Locomotion". In: *Journal of Mechanisms and Robotics* 11.2. ISSN: 1942-4302.

Serrani, Andrea, Alberto Isidori, and Lorenzo Marconi (2001). "Semi-global nonlinear output regulation with adaptive internal model". In: *IEEE Transactions on Automatic Control* 46.8, pp. 1178–1194.

Siciliano, B., L. Sciavicco, L. Villani, and G. Oriolo (2010). *Robotics: modelling, planning and control*. Springer Science & Business Media.

Sjöberg, J, T McKelvey, and L Ljung (1993). "On the use of regularization in system identification". In: *IFAC Proceedings Volumes* 26.2, pp. 75–80.

Slaughter, DC, DK Giles, and D Downey (2008). "Autonomous robotic weed control systems: A review". In: *Computers and electronics in agriculture* 61.1, pp. 63–78.

Small, Kenneth A. and E. T. Verhoef (2007). *The economics of urban transportation*. New York: Routledge.

Söderström, T. (2007). "Errors-in-variables methods in system identification". In: *Automatica* 43, pp. 939–958.

Sontag, Eduardo D and Yuan Wang (1996). "New characterizations of input-to-state stability". In: *IEEE transactions on automatic control* 41.9, pp. 1283–1294.

Su, Y., Y. Hong, and J. Huang (2013). "A general result on the robust cooperative output regulation for linear uncertain multi-agent systems". In: *IEEE Transactions on Automatic Control* 58.5, pp. 1275–1279.

Su, Y. and J. Huang (2012a). "Cooperative output regulation of linear multi-agent systems". In: *IEEE Transactions on Automatic Control* 57.4, pp. 1062–1066.

— (2012b). "Cooperative output regulation of linear multi-agent systems by output feedback". In: *Systems & Control Letters* 61.12, pp. 1248–1253.

— (2013). "Cooperative adaptive output regulation for a class of nonlinear uncertain multi-agent systems with unknown leader". In: *Systems & Control Letters* 62.6, pp. 461–467.

Tan, Y., D. Nešić, and I. Mareels (2006). "On non-local stability properties of extremum seeking control". In: *Automatica* 42.6, pp. 889–903.

Tan, Y., W. H. Moase, C. Manzie, D. Nešić, and I. Mareels (2010). "Extremum seeking from 1922 to 2010". In: *Proceedings of the 29th Chinese Control Conference*, pp. 14–26.

Tazzari, R., D. Mengoli, and L. Marconi (2020). "Design Concept and Modelling of a Tracked UGV for Orchard Precision Agriculture". In: *2020 IEEE International Workshop on Metrology for Agriculture and Forestry (MetroAgriFor)*, pp. 207–212.

Tazzari, Roberto, Ilario A. Azzollini, and Lorenzo Marconi (2021). "An Adaptive Observer approach to Slip Estimation for Agricultural Tracked Vehicles". In: *2021 European Control Conference (ECC)*, pp. 1591–1596.

Tu, Sheng-Yuan and Ali H Sayed (2012). "Diffusion strategies outperform consensus strategies for distributed estimation over adaptive networks". In: *IEEE Transactions on Signal Processing* 60.12, pp. 6217–6234.

Walters, A. A. (1961). "The Theory and Measurement of Private and Social Cost of Highway Congestion". In: *Econometrica* 29.4, pp. 676–699.

Wang, S. and J. Huang (2019). "Adaptive Leader-Following Consensus for Multiple Euler–Lagrange Systems With an Uncertain Leader System". In: *IEEE Transactions on Neural Networks and Learning Systems* 30.7, pp. 2188–2196.

Wang, S. and J. Huang (2019). "Cooperative output regulation of linear multi-agent systems subject to an uncertain leader system". In: *International Journal of Control*, pp. 1–9.

Wang, X., Y. Hong, J. Huang, and Z. Jiang (2010). "A distributed control approach to a robust output regulation problem for multi-agent linear systems". In: *IEEE Transactions on Automatic Control* 55.12, pp. 2891–2895.

Wang, Y. and F. J. Doyle (2013). "Exponential Synchronization Rate of Kuramoto Oscillators in the Presence of a Pacemaker". In: *IEEE Transactions on Automatic Control* 58.4, pp. 989–994.

Wang, Zifeng, Zheng Yu, Qing Ling, Dimitris Berberidis, and Georgios B Giannakis (2018). "Decentralized RLS with data-adaptive censoring for regressions over large-scale networks". In: *IEEE Transactions on Signal Processing* 66.6, pp. 1634–1648.

Wieland, P., R. Sepulchre, and F. Allgöwer (2011). "An internal model principle is necessary and sufficient for linear output synchronization". In: *Automatica* 47.5, pp. 1068 –1074.

Wong, Jo Yung (2008). *Theory of Ground Vehicles*. 4ᵗʰ. John Wiley & Sons. ISBN: 978-0-470-17038-0.

Wong, J.Y. and Wei Huang (2006). "Wheels vs. tracks â€" A fundamental evaluation from the traction perspective". In: *Journal of Terramechanics* 43.1, pp. 27 –42. ISSN: 0022-4898.

Wu, Biqing and Marc Bodson (2003). "A magnitude/phase-locked loop approach to parameter estimation of periodic signals". In: *IEEE Transactions on Automatic Control* 48.4, pp. 612–618.

Wu, Liang and Haoyong Chen (2020). "Synchronization Conditions for a Third-order Kuramoto Network". In: *2020 59th IEEE Conference on Decision and Control (CDC)*. IEEE, pp. 5834–5839.

Wu, Y., R. Lu, P. Shi, H. Su, and Z. Wu (2017). "Adaptive output synchronization of heterogeneous network with an uncertain leader". In: *Automatica* 76, pp. 183 –192.

Xiang, J., W. Wei, and Y. Li (2009). "Synchronized output regulation of linear networked systems". In: *IEEE Transactions on Automatic Control* 54.6, pp. 1336–1341.

Xie, Siyu and Lei Guo (2018a). "A necessary and sufficient condition for stability of LMS-based consensus adaptive filters". In: *Automatica* 93, pp. 12–19.

— (2018b). "Analysis of distributed adaptive filters based on diffusion strategies over sensor networks". In: *IEEE Transactions on Automatic Control* 63.11, pp. 3643–3658.

— (2018c). "Analysis of normalized least mean squares-based consensus adaptive filters under a general information condition". In: *SIAM Journal on Control and Optimization* 56.5, pp. 3404–3431.

Xie, Siyu, Yaqi Zhang, and Lei Guo (2020). "Convergence of a Distributed Least Squares". In: *IEEE Transactions on Automatic Control*.

Yang, Hai and Haijun Huang (2005). *Mathematical and economic theory of road pricing*. Amsterdam; Boston: Elsevier.

Yang, Hai, Qiang Meng, and Der-Horng Lee (2004). "Trial-and-error implementation of marginal-cost pricing on networks in the absence of demand functions". In: *Transp. Res. B* 38.6, pp. 477–493.

Yi, Jingang, Dezhen Song, Junjie Zhang, and Zane Goodwin (2007). "Adaptive trajectory tracking control of skid-steered mobile robots". In: *Proceedings 2007 IEEE International Conference on Robotics and Automation*. IEEE, pp. 2605–2610.

Yoshida, Kazuya (2009). "Achievements in space robotics". In: *IEEE Robotics & Automation Magazine* 16.4, pp. 20–28.

Yu, Yi, Haiquan Zhao, Rodrigo C de Lamare, Yuriy Zakharov, and Lu Lu (2019). "Robust distributed diffusion recursive least squares algorithms with side information for adaptive networks". In: *IEEE Transactions on Signal Processing* 67.6, pp. 1566–1581.

Yuan, S., B. De Schutter, and S. Baldi (2017). "Adaptive Asymptotic Tracking Control of Uncertain Time-Driven Switched Linear Systems". In: *IEEE Transactions on Automatic Control* 62.11, pp. 5802–5807.

Zhang, C., D. Arnold, N. Ghods, A. Siranosian, and M. Krstic (2007). "Source seeking with non-holonomic unicycle without position measurement and with tuning of forward velocity". In: *Systems & control letters* 56.3, pp. 245–252.

Zhang, Hongwei and Frank L Lewis (2012). "Adaptive cooperative tracking control of higher-order nonlinear systems with unknown dynamics". In: *Automatica* 48.7, pp. 1432–1439.

Zhang, Jinxing and Jiandong Zhu (2019). "Exponential synchronization of the high-dimensional Kuramoto model with identical oscillators under digraphs". In: *Automatica* 102, pp. 122 –128.

Zhang, Yaofeng and Renbin Xiao (2014). "Synchronization of Kuramoto oscillators in small-world networks". In: *Physica A: Statistical Mechanics and its Applications* 416, pp. 33 –40.

Zhou, Bo, Yan Peng, and Jianda Han (2007). "UKF based estimation and tracking control of nonholonomic mobile robots with slipping". In: *2007 IEEE International Conference on Robotics and Biomimetics (ROBIO)*. IEEE, pp. 2058–2063.

Zhu, Lijun and David J Hill (2020). "Synchronization of Kuramoto oscillators: A regional stability framework". In: *IEEE Transactions on Automatic Control* 65.12, pp. 5070–5082.

Zou, Ting, Jorge Angeles, and Ferri Hassani (2018). "Dynamic modeling and trajectory tracking control of unmanned tracked vehicles". In: *Robotics and Autonomous Systems* 110, pp. 102 –111. ISSN: 0921-8890.